Smart Light Therapy Glasses for Sleep, Cognition, and Mental Wellness

by

Lucas Wen Tang

A thesis
presented to the University of Waterloo
in fulfillment of the
thesis requirement for the degree of
Master of Applied Science
in
Mechanical and Mechatronics Engineering

Waterloo, Ontario, Canada, 2025

© Lucas Tang 2025

Author's Declaration

I hereby declare that I am the sole author of this thesis. This is a true copy of the thesis, including any required final revisions, as accepted by my examiners.

I understand that my thesis may be made electronically available to the public.

Abstract

For the past century, people have gradually transitioned to spending their time indoors where, compared with the outdoors, light levels are significantly lower during the day and higher at night. This mismatch of lighting has been associated with related health problems like rising depression rates and sleep issues. As such, bright-light therapy has been established as a treatment for mood and sleep disorders. However, existing devices face major barriers to adoption; light boxes require people to stay in one place for a long time, and wearable products often lack social acceptability. As a result, the research literature has been constrained to short interventions with limited exploration of dose, duration, and individualized understanding of response to light. This thesis presents the design, engineering, and clinical evaluation of a pair of smart light therapy glasses (Lumos glasses) developed to improve convenience, social acceptability, and comfort. The hardware provides the foundational infrastructure for an intelligent, data-driven approach to personalized circadian health. The glasses use a nanotechnology lens with wavelength-based reflection, which allows key light therapy components to be compacted into a classic glasses shape. A hardware-software platform was developed featuring calibrated light therapy optical systems, on-device sensors for reliable wear detection, melanopic ambient light detection, an FCC-approved Bluetooth module with a custom antenna, as well as a compatible cloud-connected mobile app. More than 100 units were manufactured and deployed in a double-blind, randomized, placebo-controlled crossover clinical trial. Participants receiving bright-light showed significant improvements in sleep disturbance (PROMIS) and psychomotor vigilance (PVT) relative to active dim-light control. Stratified analyses revealed that participants with darker eyes generally exhibited more significant improvements under bright-light compared to dim-light control. In contrast, mood (using the Montegomery Asberg Depression Rating Scale) and working memory (word-pair recall) reached statistical significance only after accounting for eye color. Exploratory models also showed that daily use and exposure to ambient light were correlated with improved outcomes, while higher baseline severity strongly predicted room for change. Age and sex contributed smaller, secondary effects. For working memory, dark-eyed participants showed significant Phase 1 gains under bright-light, while other subgroups demonstrated positive associations between daily usage and recall performance. This yielded meaningful insights that adherence and individual pigmentation influence optimal light dosage. This work demonstrates that mobile sensor-driven light therapy can overcome long-standing adherence barriers and enable in-depth research about dose–response and personalization. By combining engineering innovation with clinical validation, the Lumos Smart Glasses provide a foundation for next-generation circadian health technologies that are practical, effective, and scalable.

Acknowledgements

I would like to thank everyone who made this thesis possible. First and foremost, my supervisor Dr. Zhao Pan, who supported this project since my undergraduate days. Thank you for your faith, guidance, and unconditional support.

My sincere thanks to Dr. Jonathan Oakman, Principal Investigator for the clinical component of this thesis and formally recognized as co-supervisor. You consistently mentored my work and modeled thoughtful engagement with the human dimensions of research: communication, emotion, and ethics.

I would like to acknowledge Dr. Jamie Zeitzer for your guidance since joining me in the journey to bring more light to people since 2019. Thank you for openly sharing your decades of cumulated experience in light therapy, circadian rhythms, and sleep health. Your guidance has helped shaped the design of the glasses, the light sources we selected, and Lumos's brand identity as a science focused, responsible company.

I would like to thank Dr. Jeff Hovis, Dr. Dorothy Sit, and Dr. Paul Murphy for being on the data safety and monitoring board. Your combined expertise in eye safety, health, light, and psychology has helped keep our participants safe, and our trial methods scientifically and ethically responsible.

Thanks to Dr. David Sliney for offering guidance on eye safety. Your life's work laid the foundation upon which we can design optical devices to optimize well-being while being considerate of ocular safety.

I would like to acknowledge Felix Xu for supporting the Android version of the clinical app, as well as managing our app and database as the trial monitor while I was in double blind. Your coding expertise and academic integrity has been a backbone for our research.

Thanks to James Ro, for teaching me fundamentals of PCB design, firmware, and working countless hours to design and test our electrical system. I still remember the moment of excitement with our first successful bluetooth connection after debugging for weeks.

I would like to acknowledge all the volunteers who worked on the clinical team for the trial; your dedication to helping people, and caring for our participants left a warm feeling in my heart. I am so glad that our next generation of psychologists and health leaders have people like you to lead the way.

Thank you to all the participants for dedicating your time to this trial. This would have not been possible without you. This data serves as a foundation from which we build our work to help more people across the world.

Thank you to my family and extended family who raised me in an environment where creativity, critical thinking, and the practice of science is encouraged. Thank you for supporting me during my struggles with mental health and sleep problems, and helping me to come out the other side, stronger, wiser, and with a few more patents.

I would also like to acknowledge my late cat Obie and current cat Piper, the trouble-makers who have provided me with so much amusement and comfort through this journey. They have a keen sense of when I'm overworking before I even realize it myself, dragging me out of work for cuddles with their tactical methods like knocking important electrical components off the table. There are also beautiful moments where they relax in front of my light therapy lamps, validating that this work is something that nature needs. (see Figure A.5 and Figure A.6 in the Appendix).

Finally, I would like to acknowledge the use of ChatGPT (GPT-5, OpenAI, 2025), which assisted in language refinement, LaTeX formatting, figure caption drafting, and R code debugging throughout this thesis. The model was used strictly as a technical and editorial aid; all ideas, experimental designs, data analyses, and interpretations are entirely my own and were developed prior to the use of any generative AI tools. All AI-assisted outputs were reviewed, verified, and edited by the author to ensure accuracy and academic integrity, in accordance with the University of Waterloo's guidelines on responsible use of generative AI.

Dedication

I dedicate this thesis to the scientists working in this field, and to those who struggle with mental health and sleep. I hope that this work may help push the field forward, so that your pain may ease, your healing may be faster, and you come out stronger and healthier than before. During my own darkest times with depression and poor sleep, the pain was so excruciating that I would not wish it upon my worst enemy. I came to realize that our emotions are deeply interconnected with those around us, and I prayed for healing both for myself and for everyone facing similar challenges. While light is only one part of the complex landscape of health, I hope that advancing the science in this area may bring a small measure of healing.

Table of Contents

Author's Declaration ii

Abstract iii

Acknowledgements iv

Dedication vi

List of Figures xiv

List of Tables xxi

List of Abbreviations xxvi

Preface 1

1 Introduction 2

1.1 New Paradigm: Socially Acceptable, Convenient Light Therapy 3

1.1.1 Clarifying Blue-Light Safety 6

1.2 Engineering Scope of the Work 7

1.3 Clinical Objectives and Scope of Work 9

2 Engineering Development **11**
2.1 Operating principle . . . 11
2.2 Hardware Evolution and Prototyping . . . 12
2.3 Light Engine Design and Eye Safety . . . 16
2.3.1 Light engine design overview . . . 16
2.3.2 Photobiological Safety Considerations . . . 16
2.3.3 Calibration of the Light Engine . . . 17
2.3.4 Photobiological Safety Testing of Lumos Glasses . . . 18
2.3.5 Optical Simulations . . . 20
2.3.6 Calibration Procedure . . . 21
2.3.7 Time-Dependent Spot Smearing and Boost Mode . . . 25
2.3.8 External Validation with Market-Leading Device . . . 26
2.4 Ambient Light Sensor Design and Calibration . . . 27
2.4.1 Geometric Placement and Orientation . . . 28
2.4.2 Spectral Response and Calibration . . . 29
2.4.3 Circuit Design . . . 29
2.5 User Detection Sensor Iteration . . . 33
2.5.1 Capacitive sensing . . . 33
2.5.2 Infrared proximity sensing . . . 36
2.6 Electrical System . . . 38
2.7 Firmware Architecture (High-Level Summary) . . . 40
2.8 App and Software . . . 43
2.9 Chapter Conclusion . . . 44

3 Clinical Results **46**
3.1 Overview . . . 46
3.2 Methods . . . 47
3.2.1 Design . . . 47

3.2.2 Participants . . . 47
3.2.3 Clinical team . . . 48
3.2.4 Randomization, Allocation Concealment, and Masking . . . 48
3.2.5 Intervention . . . 48
3.2.6 Device Use, Sensing, and Data Capture . . . 49
3.2.7 Measures . . . 49
3.2.8 Sample Size and Power . . . 50
3.2.9 Ethics, Registration, and Data Handling . . . 50
3.3 Results . . . 51
3.3.1 Participant Flow and Sample . . . 51
3.3.2 Baseline Characteristics . . . 52
3.3.3 Device Usage and Light Exposure . . . 54
3.3.4 Outcome: Mood and Depression (MADRS) . . . 57
3.3.5 Mood (MADRS)—Multiple regression (summary) . . . 60
3.3.6 Outcome: Sleep Disturbance (PROMIS) . . . 65
3.3.7 Sleep (PROMIS)—Multiple regression (summary) . . . 68
3.3.8 Outcome: Psychomotor Vigilance (PVT) . . . 74
3.3.9 Psychomotor Vigilance (PVT)—Multiple regression (summary) . . . 77
3.3.10 Outcome: Working Memory (Word Recall) . . . 82
3.3.11 Word-Pair Recall (WORD) and Usage Time . . . 85
3.3.12 Per-participant analysis — Word-Pair Recall (equal-weight endpoint method) . . . 89
3.3.13 Side Effects and Adverse Events . . . 91

4 Discussion **95**
4.1 Overview of Primary Findings . . . 95
4.2 Outcome-Specific Interpretations . . . 95
4.2.1 Mood and Depressive Symptoms (MADRS) . . . 95

4.2.2 Sleep Disturbance (PROMIS) . . . 96
4.2.3 Psychomotor Vigilance (PVT) . . . 96
4.2.4 Working Memory . . . 97
4.3 Moderators of Treatment Response . . . 97
4.4 Cross-Outcome Synthesis . . . 97
4.5 Power and Sensitivity Considerations . . . 98
4.6 Clinically Meaningful Thresholds . . . 99
4.7 Effect Sizes in Context of Bright-Light Therapy . . . 100
4.8 Interpretation in Context . . . 101
4.8.1 Ambient Light in General . . . 103
4.9 Limitations . . . 103
4.10 Implications and Future Work . . . 106

5 Conclusion **108**

References **110**

APPENDICES **121**

A Personal Notes and Behind the Scenes **122**

B Photobiological Safety and Blue-Light Hazard Framework **129**
B.1 Misconceptions About blue-light Hazard . . . 130
B.2 Retinal Damage Mechanisms and Spectrum . . . 130
B.3 IEC 62471 Standard . . . 131
B.4 Radiance Measurement Geometry . . . 132
B.5 Optical Simulations . . . 135
B.6 Time-Dependent Spot Smearing and Boost Mode . . . 139

C Measurement Instruments and Scoring **141**
C.1 Overview . . . 141
C.2 Instrument Summary Table . . . 141
C.3 MADRS-S (Depression) . . . 142
C.4 PROMIS Sleep Disturbance—Short Form . . . 142
C.5 Psychomotor Vigilance Task (PVT) . . . 143
C.6 Paired-Associate Memory (Word-Pair) Test . . . 143
C.7 Administration Platforms . . . 144

D Power Analysis and Sample Size Derivation **145**

E Detailed MADRS Stratified Analyses **147**
E.1 Overview . . . 147
E.2 Light-Eyed Participants (Blue, Green, Hazel) . . . 147
E.3 Brown-Eyed Caucasian Participants . . . 148
E.4 Dark-Eyed Non-Caucasian Participants . . . 148
E.5 Summary . . . 149

F Expanded MADRS Multiple Regression Analyses **150**
F.1 Overview . . . 150
F.1.1 Depression (MADRS) Multiple regression . . . 150
F.1.2 Per-participant analysis (equal-weight endpoint method) . . . 169

G Detailed PROMIS Sleep Analyses **172**
G.1 Overview . . . 172
G.2 Light-eyed participants . . . 172
G.3 Brown-eyed Caucasian participants . . . 173
G.4 Dark-eyed non-Caucasian participants . . . 173

H Detailed PROMIS Sleep Analyses (Multiple Regression) 175
H.1 Overview . . . 175

I Detailed PVT Stratified Analyses 192
I.1 Overview . . . 192
I.2 Dark-eyed non-Caucasians (73.4) . . . 192
I.3 Brown-eyed Caucasians (81.15) . . . 193
I.4 Light-eyed (88.9) . . . 194

J Detailed PVT Multiple Regression Analyses 196
J.1 Overview . . . 196
J.2 Usage time . . . 196
J.3 Ambient Light (lux) Effects — Brown-eyed Caucasian Participants (81.15) 198
J.4 Baseline performance . . . 201
J.5 Age and baseline reaction speed . . . 202
J.6 Rebaselined models and age . . . 203
J.7 Participant-level endpoint analysis . . . 206

K Detailed Working Memory (Word Recall) Analyses by Eye Group 208
K.1 Overview . . . 208
K.2 Light-eyed (88.9) . . . 208
K.3 Brown-eyed Caucasians (81.15) . . . 209
K.4 Dark-eyed (73.4) . . . 210
K.5 Summary . . . 211

L Detailed Word-Pair Recall Usage Analyses 212
L.1 Overview . . . 212
L.2 All participants (all eyes combined) . . . 212
L.3 Light-eyed participants (88.9; Beta arm) . . . 215
L.4 Brown-eyed Caucasian participants (81.15; Beta arm) . . . 216
L.5 Summary . . . 219

M Detailed Word-Pair Recall Covariate Analyses **220**

M.1 Overview 220

M.2 Baseline Performance (WORD) 220

M.3 Age Effects (WORD) 223

M.4 Sex Effects (WORD) 224

N Power and Sensitivity Diagnostics **226**

N.1 Minimum Detectable Partial η^2 Across Outcomes and Strata 226

N.2 Contrasts Near the Detectability Boundary 227

N.3 Full Comparison of Observed vs. Detectable Partial η^2 227

O Third-Party Photobiological Safety Test Report (IEC 62471) **231**

P Study Protocol (Version 18; March 14, 2024) **256**

Glossary **297**

List of Figures

1.1 Comparison of traditional light therapy devices and glasses in the study . . 4
1.2 Demonstration of Lumos light therapy glasses in use 5
1.3 Isometric render of the glasses in the study 6

2.1 Operating principle of the Lumos glasses 11
2.2 Evolution of the prototypes of the Lumos smart light therapy glasses . . . 12
2.3 2021 coating optimizations 14
2.4 Labeled diagram of key components of the Lumos glasses 15
2.5 Basic light engine on PCB 16
2.6 Comparison of radiance measurement geometries 19
2.7 Near-eye optical behavior of the *Lumos* light engine 20
2.8 Lumos calibration fixture and AS72653 spectral response 22
2.9 LED calibration simulation framework 23
2.10 Adjustment of AS72653 D-channel response 24
2.11 AS72653 sensor correlation with TÜV SÜD measurements 25
2.12 Time-dependent retinal averaging 26
2.13 Comparison of calibrated spectral power with a market-leading wearable . 27
2.14 Lumos ambient light sensor (gold rectangular piece). 28
2.15 Lumos ambient light sensor geometry and placement. 29
2.16 Circuit schematic of the Lumos ambient light sensor 30
2.17 Indoor ALS calibration curve 31

2.18 Outdoor ALS calibration curve . . . 32
2.19 Capacitive sensing FPC location in the glasses arm . . . 34
2.20 Capacitive sensing theory of operation . . . 34
2.21 Capacitive sensing signal (left) vs proximity sensor (right) . . . 36
2.22 Concept of proximity sensor sharing the LED window. . . . 37
2.23 Final proximity sensor design integrated with flexible circuit and IR window. 38
2.24 Lumos PCB Layout overview . . . 39
2.25 High-level electrical block diagram of the Lumos system. . . . 39
2.26 Screenshots of the Lumos mobile application (iOS version shown). . . . 43

3.1 Participant flow . . . 51
3.2 Baseline distributions of instruments, x-axis are raw scores, y-axis frequency 53
3.3 Distribution of daily usage hours across all participants. . . . 54
3.4 Distribution of device usage by time of day . . . 55
3.5 Ambient light data by time of day . . . 56
3.6 All participants ΔMADRS score over time . . . 57
3.7 Light-eyed participants: ΔMADRS over time (hinge at Day 56). . . . 59
3.8 Brown-eyed Caucasian participants: ΔMADRS over time (hinge at Day 56). 59
3.9 Dark-eyed non-Caucasian participants: ΔMADRS over time (hinge at Day 56). 60
3.10 MADRS Usage Effects . . . 61
3.11 MADRS Ambient Light Effects . . . 61
3.12 MADRS Baseline Effects . . . 62
3.13 MADRS Per Participant Results . . . 63
3.14 All participants PROMIS score over time . . . 65
3.15 Light-eyed participants: ΔPROMIS over time (hinge at Day 56). . . . 67
3.16 Brown-eyed Caucasian participants: ΔPROMIS over time (hinge at Day 56). 67
3.17 Dark-eyed non-Caucasian participants: ΔPROMIS over time (hinge at Day 56). 68
3.18 **PROMIS usage effects.** 3D graph. . . . 69

3.19 **Ambient light effects (Beta, all eyes).** 3D grapph 69
3.20 **Higher baseline sleep disturbance predicts larger improvement.** . 70
3.21 **Per-participant results (PROMIS, all eyes).** Beta shows larger Phase 1 improvement and a Phase 2 rebound. 71
3.22 **Per-participant results (PROMIS, non–light-eyed).** Beta shows a larger Phase 1 improvement and a Phase 2 rebound, while Alpha remains stable. 72
3.23 **Change in PVT reaction time** (hinge at Day 56). Negative slopes denote faster responses (improvement). 74
3.24 Light-eyed participants: ΔRT over time (hinge at Day 56). 76
3.25 Brown-eyed Caucasian participants: ΔRT over time (hinge at Day 56). . . 76
3.26 Dark-eyed non-Caucasian participants: ΔRT over time (hinge at Day 56). . 77
3.27 **Usage effects (`hours_c`) in Alpha (all eyes).** 3D graph 78
3.28 **Ambient melanopic light effects in brown-eyed Caucasian Alpha participants.** Higher `lux_c` predicts faster reaction times (more negative ΔRT). 78
3.29 **Baseline severity and PVT improvement.** 3D graphs 79
3.30 **Participant-level Δ_1 and Δ_2 reaction time changes by arm.** Negative values denote faster (improved) responses. 80
3.31 Word recall change vs. day: fitted pre-56 (green) and post-56 (blue) slopes for Alpha (left) and Beta (right). 82
3.32 Word recall trajectories (light-eyed, 88.9). Fitted pre-56 (green) and post-56 (blue) slopes for Alpha (left) and Beta (right). 84
3.33 Word recall trajectories (brown-eyed Caucasians, 81.15). Fitted pre-56 (green) and post-56 (blue) slopes. 84
3.34 Word recall trajectories (dark-eyed, 73.4). Fitted pre-56 (green) and post-56 (blue) slopes for Alpha (left) and Beta (right). 85
3.35 Word Recall, Significant stratified usage effects 86
3.36 Word recall baseline effects 88
3.37 Word Recall Significant Per participant analysis Dark-eyed 89

A.1 Piper inspecting Lumos glasses . . . 123
A.2 Prototype nap session . . . 124
A.3 blue-light verification test . . . 125
A.4 Obie and PCB module inspection . . . 126
A.5 Obie under the monitor . . . 127
A.6 Obie relaxing by the light therapy lamp . . . 128

B.1 Blue-light hazard and melanopsin response curves . . . 131
B.2 Lens-based radiance measurement system . . . 133
B.3 Mask-based measurement geometry . . . 133
B.4 Optical simulation showing that pupil size primarily regulates retinal illuminance rather than image focus. . . . 134
B.5 Optical simulation illustrating human eye accommodation. . . . 134
B.6 Comparison of retinal focus for distant and near sources . . . 135
B.7 Retinal focus calibration at 200 mm distance . . . 136
B.8 Retinal irradiance through Lumos optical system . . . 137
B.9 Retinal irradiance using real Lumos LED source . . . 137
B.10 Retinal irradiance at normal eye orientation . . . 138
B.11 Illustration of retinal smearing due to eye movements . . . 139
B.12 Calculation of time-dependent boost mode . . . 140

F.1 **Caucasians with brown eyes — Alpha:** Time + usage (`hours_c`) surface with Day 56 hinge. . . . 152
F.2 **Caucasians with brown eyes — Beta:** Time + usage (`hours_c`) surface with Day 56 hinge. . . . 153
F.3 **Light-eyed — Alpha:** Time + usage (`hours_c`) surface with Day 56 hinge. 154
F.4 Time + centered lux planes for Alpha (left) and Beta (right). Increasing ambient light levels corresponded with greater improvement (lower MADRS). 157
F.5 Time + centered baseline severity planes for Alpha (left) and Beta (right); see Tables F.3 and F.4. . . . 159

F.6 Baseline MADRS and PROMIS scores plotted against age. Regression lines indicate that older participants tended to present with higher baseline scores. 160

F.7 Baseline-normalized analysis for all participants. Green = pre-56; blue = post-56. Beta maintains a steeper improvement and larger rebound than Alpha. 162

F.8 Baseline-normalized analysis for non-light participants (all brown-eyed). Phase-1 Beta improvement remains significant; post-56 difference not significant. . 162

F.9 Baseline-normalized analysis for light-eyed participants. Both pre- and post-56 contrasts remain significant, consistent with the raw model. 163

F.10 Baseline-normalized analysis for brown-eyed Caucasian participants. The Phase-1 between-arm difference remains significant, with a small but significant DiD. 164

F.11 Baseline-normalized analysis for dark-eyed non-Caucasian participants. Between-arm differences are no longer significant, likely due to reduced sample size, though both within-arm hinge effects remain. 164

F.12 Baseline-normalized MADRS with age for brown-eyed Caucasian participants. Alpha (left): older age associated with smaller improvement. Beta (right): older age associated with slightly greater improvement. 166

F.13 Baseline-normalized MADRS with age for dark-eyed non-Caucasian participants. Both Alpha (left) and Beta (right) show reduced improvement with increasing age. 167

F.14 Time + sex regression plane for the Beta group; see Table F.9. A small but significant sex effect was observed ($p = 0.034$), where females showed slightly greater improvement in MADRS. 169

F.15 Non-light (brown-eyed) subgroup: Phase-level MADRS changes by arm under the equal-weight endpoint model. Negative values denote improvement. Significant Phase 1 differences ($p < 0.01$) and Beta rebound after bright-light withdrawal ($p < 0.01$) replicate the main mixed-model findings. . . . 171

H.1 Light-eyed (Alpha): time + usage regression plane for ΔPROMIS. 176

H.2 Brown-eyed Caucasians (Beta): time + usage regression plane for ΔPROMIS. 176

H.3 Beta group (all eyes): time + centered lux regression plane for ΔPROMIS; see Table H.2. 179

H.4 Time + baseline planes for PROMIS in Alpha (left) and Beta (right). . . . 181

H.5 Baseline-normalized analysis of relative change ΔPROMIS/baseline versus day. Lines show fitted pre-56 (green) and post-56 (blue) slopes for Alpha (left) and Beta (right). . . . 183

H.6 Rebaselined PROMIS vs. day with age covariate for Alpha (left) and Beta (right). . . . 185

H.7 Rebaselined PROMIS vs. day with sex covariate for Alpha (left) and Beta (right). . . . 188

H.8 PROMIS endpoint deltas by arm. Left: Phase 1 change Δ_1 (Baseline→Mid). Right: Phase 2 change Δ_2 (Mid→End). Negative values indicate improvement. 189

H.9 **Per-participant results (PROMIS, non–light-eyed).** Beta shows a larger Phase 1 improvement and a Phase 2 rebound, while Alpha remains stable. . . . 190

I.1 PVT reaction time (dark-eyed, 73.4): fitted pre-56 (green) and post-56 (blue) slopes for Alpha (left) and Beta (right). . . . 192

I.2 PVT reaction time (Brown-eyed Caucasians, 81.15): fitted pre- and post-56 slopes. . . . 193

I.3 PVT reaction time (light-eyed, 88.9): fitted pre- and post-56 slopes. . . . 194

J.1 Alpha group: time + centered usage planes for reaction time (REACT). . . . 197

J.2 **Light-eyed participants (Beta):** exploratory Time + usage regression plane for reaction time (PVT). The apparent upward tilt was driven by a few leverage points near the crossover hinge, and no significant effect of usage was detected. . . . 198

J.3 **Brown-eyed Caucasians (Alpha):** Time + lux regression plane for reaction time (PVT). Increasing centered ambient light (`lux_c`) was associated with faster RT (more negative ΔRT), consistent with the significant main effect reported in Table J.2. . . . 199

J.4 **Brown-eyed Caucasians (Beta):** exploratory Time + lux regression plane for reaction time (PVT). The slight positive lux slope ($p \approx 0.08$) appears to arise from a single high-leverage data point near the crossover hinge, and was therefore not included in inferential summaries. . . . 200

J.5 Reaction time with baseline covariate for Alpha (left) and Beta (right); see Table J.3. . . . 202

J.6 Baseline PVT reaction time vs. age. Older participants showed slower baseline speeds, with age explaining a substantial proportion of variance ($R^2 = 0.57$). . . . 203

J.7 Rebaselined reaction time vs. day and age (centered) for Alpha (left) and Beta (right); see Tables J.6 and J.7. . . . 205

J.8 **Participant-level Δ_1 (Baseline→Mid) and Δ_2 (Mid→Final) reaction time changes.** Negative values denote faster (improved) responses. . . . 207

K.1 Word recall (light-eyed, 88.9): fitted pre-56 (green) and post-56 (blue) slopes for Alpha (left) and Beta (right). . . . 209

K.2 Word recall (brown-eyed Caucasians, 81.15): fitted pre-56 (green) and post-56 (blue) slopes. . . . 210

K.3 Word recall (dark-eyed, 73.4): fitted pre-56 (green) and post-56 (blue) slopes for Alpha (left) and Beta (right). . . . 211

L.1 Time + usage regression planes for ΔWORD: Alpha (left) and Beta (right). Alpha shows a weak negative association, while Beta improves with higher daily usage. . . . 214

L.2 Light-eyed participants (Beta arm). Greater daily usage significantly improved recall performance ($p = 1.2 \times 10^{-9}$, $\eta_p^2 = 0.25$). . . . 216

L.3 Brown-eyed Caucasian participants (Beta arm). Increased daily usage improved recall ($p = 0.0056$, $\eta_p^2 = 0.066$). . . . 218

M.1 Time + baseline planes for WORD recall (Alpha left; Beta right). . . . 222

M.2 Time + age planes for WORD (Alpha left; Beta right). . . . 224

M.3 Time + sex plane for the *Beta* arm. . . . 225

List of Tables

2.1 Indoor calibration data for the Lumos ambient light sensor 31

2.2 Outdoor calibration data for the Lumos ambient light sensor 32

3.1 Summary of power analysis assumptions. Detailed derivations in Appendix D. 50

3.2 Baseline characteristics by randomized arm. 53

3.3 Group-level slopes and hinge effects for ΔMADRS (hinge at Day 56). . . . 58

3.4 Primary contrasts for ΔMADRS (per day, hinge at Day 56). 58

3.5 Phase-level summary and hypothesis tests for the non-light (brown-eyed) subgroup under the equal-weight endpoint model. 63

3.6 Summary of significant covariate associations with ΔMADRS. Full coefficients in Appendix F. 64

3.7 Group-level slopes and hinge effects for ΔPROMIS (hinge at Day 56). . . . 66

3.8 Primary contrasts for ΔPROMIS (per day, hinge at Day 56). 66

3.9 Phase-level summary and hypothesis tests for PROMIS under the equal-weight endpoint model (all eyes). 71

3.10 Phase-level summary and hypothesis tests for PROMIS under the equal-weight endpoint model (non–light-eyed). 72

3.11 Summary of significant covariate associations with ΔPROMIS. Full coefficients in Appendix H. 73

3.12 Group-level slopes and hinge effects for ΔRT (hinge at Day 56). 75

3.13 Primary contrasts for ΔRT (ms/day; hinge at Day 56). 75

3.14 Group-level statistics for participant-level reaction time deltas (all eyes). . 80

3.15 Hypothesis tests for participant-level reaction time deltas (all eyes). 80
3.16 Summary of significant covariate associations with ΔRT (ms). Full coefficients in Appendix J. 81
3.17 Group-level slopes and hinge effects for ΔWORD recall (hinge at Day 56). 83
3.18 Primary contrasts for ΔWORD recall (per day; hinge at Day 56). 83
3.19 Group means and standard deviations for ΔWORD (dark-eyed non-Caucasian subgroup). 90
3.20 Hypothesis tests for ΔWORD (dark-eyed non-Caucasian subgroup). 90
3.21 Average weekly side effects reports per participant, by group and phase, with between- and within-group comparisons (all eyes). 91
3.22 Average weekly side-effect reports per participant for dark-eyed participants, by group and phase, with between-arm comparisons. 92
3.23 Average weekly side–effect reports per participant for brown–eyed Caucasian participants, by group and phase, with between–arm comparisons. 92
3.24 Average weekly side-effect reports per participant for light-eyed participants, by group and phase, with between-arm comparisons. 93

4.1 Phase 1 bright-light improvements compared with clinically meaningful thresholds. 100
4.2 Per-participant bright-light effect sizes (Hedges' g and converted Cohen's d) compared with typical bright-light therapy (BLT) effect sizes. 101

C.1 Summary of measurement instruments and key properties. 142

D.1 Detailed planning assumptions and required per-arm sample sizes. 146

E.1 Group-level slopes for ΔMADRS, light-eyed group (hinge = Day 56). . . . 147
E.2 Primary contrasts for ΔMADRS, light-eyed group. 148
E.3 Group-level slopes for ΔMADRS, brown-eyed Caucasian group (hinge = Day 56). 148
E.4 Primary contrasts for ΔMADRS, brown-eyed Caucasian group. 148

E.5 Group-level slopes for ΔMADRS, dark-eyed non-Caucasian group (hinge = Day 56). . . . 149
E.6 Primary contrasts for ΔMADRS, dark-eyed non-Caucasian group. . . . 149

F.1 Time + usage (`hours_c`) models for ΔMADRS with effect sizes. . . . 155
F.2 Time + lux models for ΔMADRS with effect sizes. . . . 156
F.3 Alpha group: time + baseline model for ΔMADRS with updated coefficients and effect sizes. . . . 158
F.4 Beta group: time + baseline model for ΔMADRS with updated coefficients and effect sizes. . . . 158
F.5 Group-level slopes for baseline-normalized ΔMADRS (hinge at Day 56; all participants). . . . 161
F.6 Primary contrasts (per day) for baseline-normalized ΔMADRS (hinge at Day 56; all participants). . . . 161
F.7 Baseline-normalized MADRS with age for brown-eyed Caucasian participants. 165
F.8 Baseline-normalized MADRS with age for dark-eyed non-Caucasian participants. . . . 167
F.9 Time + sex model for ΔMADRS with effect sizes. . . . 168
F.10 Phase-level summary and hypothesis tests for the non-light (brown-eyed) subgroup under the equal-weight endpoint model. . . . 170

G.1 Hypothesis tests for ΔPROMIS — light-eyed participants (per-day contrasts). 172
G.2 Fitted slopes for ΔPROMIS — light-eyed participants (points/day). . . . 172
G.3 Hypothesis tests for ΔPROMIS — brown-eyed Caucasian participants. . . . 173
G.4 Fitted slopes for ΔPROMIS — brown-eyed Caucasian participants (points/day). 173
G.5 Hypothesis tests for ΔPROMIS — dark-eyed non-Caucasian participants. . . 173
G.6 Fitted slopes for ΔPROMIS — dark-eyed non-Caucasian participants (points/day). 174

H.1 Time + usage (`hours_c`) models for ΔPROMIS (significant arms only). . . . 177
H.2 Beta group (all eyes): time + lux model for ΔPROMIS with effect sizes. . . . 178
H.3 Time + baseline models for ΔPROMIS (all eyes) with effect sizes. . . . 180

H.4 Baseline-normalized PROMIS: group-level slopes (hinge at Day 56). 182
H.5 Baseline-normalized PROMIS: primary contrasts with effect sizes. 182
H.6 Rebaselined time + age models for ΔPROMIS (all eyes) with effect sizes. . 184
H.7 Rebaselined time + sex models for ΔPROMIS (all eyes). 187
H.8 Phase-level summary and hypothesis tests for PROMIS under the equal-weight endpoint model (all eyes). 190
H.9 Phase-level summary and hypothesis tests for PROMIS under the equal-weight endpoint model (non–light-eyed). 191

I.1 Group-level slopes and hinge effects for ΔRT, dark-eyed non-Caucasian group (hinge at Day 56). 193
I.2 Dark-eyed (73.4): primary hypothesis tests for PVT (per day; hinge at Day 56). 193
I.3 Group-level slopes and hinge effects for ΔRT, brown-eyed Caucasian group (hinge at Day 56). 194
I.4 Brown-eyed Caucasians (81.15): primary hypothesis tests for PVT (per day; hinge at Day 56). 194
I.5 Group-level slopes and hinge effects for ΔRT, light-eyed group (hinge at Day 56). 195
I.6 Light-eyed (88.9): primary hypothesis tests for PVT (per day; hinge at Day 56). 195

J.1 Alpha group: time + usage model for ΔREACT with effect sizes (all eyes). 197
J.2 Time + lux model for ΔRT, brown-eyed Caucasian participants (hinge at Day 56). 199
J.3 Reaction time (PVT): time + baseline model with effect sizes (all eyes). . . 201
J.4 Rebaselined RT: group-level slopes with hinge at Day 56 (all eyes). 203
J.5 Rebaselined RT: primary contrasts (per day) with effect sizes. 204
J.6 Alpha group: time + age model for rebaselined reaction time with effect sizes (all eyes). 204
J.7 Beta group: time + age model for rebaselined reaction time with effect sizes (all eyes). 204

J.8 Group-level descriptive statistics for participant-level reaction time deltas (all eyes). 206

J.9 Hypothesis tests for participant-level reaction time deltas (all eyes). 206

K.1 Group-level slopes and hinge effects for ΔWORD (light-eyed; hinge at Day 56). 208

K.2 Primary contrasts for ΔWORD (light-eyed; per day, hinge at Day 56). . . 209

K.3 Group-level slopes and hinge effects for ΔWORD (brown-eyed Caucasians; hinge at Day 56). 209

K.4 Primary contrasts for ΔWORD (brown-eyed Caucasians; per day, hinge at Day 56). 210

K.5 Group-level slopes and hinge effects for ΔWORD (dark-eyed; hinge at Day 56). 210

K.6 Primary contrasts for ΔWORD (dark-eyed; per day, hinge at Day 56). . . 211

L.1 Time + usage model for ΔWORD (all eyes combined). 213

L.2 Time + usage model for ΔWORD — light-eyed participants (Beta arm). . . 215

L.3 Time + usage model for ΔWORD — brown-eyed Caucasian participants (Beta arm). 217

M.1 Time + baseline model for ΔWORD with effect sizes. 221

M.2 Time + age model for ΔWORD with effect sizes. 223

M.3 Beta group: time + sex model for ΔWORD. 224

N.1 Minimum detectable partial η^2 (80% power, $\alpha = .05$) across outcomes and eye-pigmentation strata. Smaller values indicate higher statistical sensitivity. 227

N.2 Contrasts where statistical significance did not perfectly align with the power threshold. These effects lie near the detection boundary and are expected in finite-sample studies. 227

N.3 Observed partial η^2 vs. minimum detectable η^2 across all outcomes, strata, and slope contrasts. 228

List of Abbreviations

API Application Programming Interface 44

BLE Bluetooth Low Energy 9, 38–40, 42, 43, 45

FPC Flexible Printed Circuit 37, 39, 45

IPRGC Intrinsically photosensitive retinal ganglion cell 2

IR Infrared 36, 37, 49

LDO Low Dropout Regulator 15, 39

LED Light-Emitting Diode 15–17, 21, 22, 24, 25, 36, 39–41, 139

MADRS Montgomery–Åsberg Depression Rating Scale ix, xi, xv, xviii, xxi–xxiii, 46, 47, 50, 53, 57–62, 64, 104, 108, 142, 144–150, 155–158, 160, 161, 165–169, 171

MADRS-S Montgomery–Åsberg Depression Rating Scale, Self-rated version 49

MCU Microcontroller Unit 38, 39

MDD Major Depressive Disorder 145

nRF52 Nordic Semiconductor nRF52 Bluetooth SoC family 15, 25, 35, 43, 139

PCB Printed Circuit Board 9, 36, 38, 39

PI Principal Investigator 48

PROMIS Patient-Reported Outcomes Measurement Information System Sleep Disturbance Short Form ix, xv, xvi, xviii, xix, xxi, xxiii, xxiv, 46, 49, 50, 53, 65–68, 70–73, 104, 108, 142, 144, 160, 172–191

PSQI Pittsburgh Sleep Quality Index 50, 146

PVT Psychomotor Vigilance Task ix, xvi, xix, xx, xxiv, 9, 39, 40, 45, 46, 50, 53, 74, 77, 108, 143–146, 198–201, 203

PWM Pulse-Width Modulation 40, 41

REB Research Ethics Board 50, 93, 94

SoC System on Chip 38, 40, 43, 45, 297

TÜV SÜD Technischer Überwachungsverein Süd 8, 21–25

WORD Word-Pair Memory Task ix, xiii, xx, xxii, xxv, 83, 85, 87–90, 108, 208–211, 213–215, 217, 220–224

Preface

This thesis represents a continuation of my undergraduate work on the Lumos smart light therapy glasses, an idea I first conceived in 2017 to address my personal struggles with mental health and sleep worsened by insufficient sunlight. In 2018, I took a break from my undergraduate studies to heal, and in that time I invented our core patent to use nano-tech reflective lenses for light therapy. This innovation later convinced Dr. Jamie Zeitzer from Stanford Sleep Sciences to join me as a co-founder in Lumos, a Waterloo-based startup. In 2019, I returned to the University of Waterloo to complete my undergraduate degree, taking on Lumos as my fourth-year design project under the supervision of Dr. Zhao Pan. During that time, I refined the engineering design, including optical simulations, electronic systems, and design for manufacturability. The project received multiple awards and represented the University of Waterloo in both the Ontario and Canadian Engineering Competitions, earning the inaugural Research and Entrepreneurship Award.

The scope of this thesis builds directly on that foundation. I continued the development of Lumos glasses toward a randomized controlled trial (RCT) to study its effects on sleep, mental wellness, and performance. The trial was conducted through the Department of Psychology at the University of Waterloo, with Dr. Jonathan Oakman as principal investigator, myself as student investigator, and Dr. Zhao Pan as engineering supervisor. The project was funded by the Government of Canada through the Mitacs program, with Lumos Health as industry sponsor. The protocol underwent rigorous scientific review and was approved by the University of Waterloo's Research Ethics Board.

This work lies at the intersection of engineering, psychology, and psychiatry. This interdisciplinary space offers opportunities to bridge technological innovation with human-centered science, drawing on engineering design, neurobiology, clinical ethics, and rigorous research methodology. Over the past several years, I've dedicated myself to learning across these fields, and I consider this work to be the beginning of a lifelong endeavor.

Chapter 1

Introduction

Since the invention of the light bulb in the century following the industrial revolution, humanity has moved a majority of activities indoors. Today, the average American spends over 90 percent of their time indoors, where light levels are orders of magnitude lower than in nature. Light is a powerful regulator of human physiology where the Intrinsically photosensitive retinal ganglion cell (IPRGC) modulates circadian rhythms, affecting melatonin, cortisol, serotonin, dopamine, and many other important brain and hormone circuits [62]. However, research and data from this study demonstrate that the median real-world light exposure is often insufficient to robustly engage circadian and melatonin-suppressing pathways [89] [109], and may also contribute to other mood and sleep ailments [25]. This points to a major problem in modern society: the human body has not yet adapted to an indoor lifestyle.

A growing body of research suggests that many modern disturbances in sleep, mood, and general well-being may arise from insufficient exposure to bright-light during the day and excessive exposure to artificial light at night. Studies of preindustrial and hunter-gatherer populations indicate that, in the absence of artificial lighting, individuals experience abundant daytime light and minimal nocturnal light exposure, resulting in more stable circadian rhythms and consistent sleep duration [106, 35, 90]. Building on this, recent population-scale and laboratory studies have demonstrated that greater daytime or outdoor light exposure is associated with improved mood, sleep, and circadian alignment, whereas nighttime light exposure predicts higher risks of depression and other psychiatric conditions [25, 29, 68, 22]. Systematic reviews further emphasize that increasing daytime light exposure and minimizing evening and nighttime illumination constitute effective, non-pharmacological strategies for supporting circadian health and psychological well-being [63, 88]. Together, these findings support the hypothesis that optimal circadian

health may be achieved by mimicking naturalistic light–dark cycles: substantial daylight during waking hours and minimal light after dusk.

For individuals who may have limited access to sufficient bright-light during the day, bright-light therapy has been shown to be an effective frontline treatment for sleep and mood disorders, especially seasonal affective disorder [27], and more recently for non-seasonal depression as well [60, 46]. Extending this line of thinking, longer durations of circadian effective light exposure, particularly those that mimic natural outdoor lighting patterns could yield greater improvements in sleep and mood outcomes.

Some studies suggest that exposure duration may play a more critical role than intensity in producing circadian phase shifts[36], yet longer treatment sessions are often infeasible due to the size, immobility, and comfort limitations of current light therapy devices . As a result, adherence tends to decline as treatment duration increases, and there remains a lack of systematic research examining how duration and intensity interact to influence therapeutic outcomes in depression and sleep improvement. Typical lamp-based treatments require users to remain stationary for 35 to 45 minutes per day, which has been described as a significant time commitment [76], while even wearable implementations report difficulty maintaining one-hour sessions [108]. Systematic reviews have similarly emphasized that adherence and user acceptability require far greater attention in future research [41]. Moreover, incorporating personalized parameters such as eye color, brightness, and dosage timing would necessitate much larger sample sizes to preserve statistical power, further contributing to the scarcity of duration-focused studies. For instance, individuals with lighter-colored eyes may experience stronger effects, as eye pigmentation has been linked to greater light sensitivity and susceptibility to seasonal affective disorder [48, 43].

With rising global rates of depression and sleep problems, it is imperative that the scientific and medical communities advance light therapy research given its significant impact on health outcomes. However, the current form factor of most light therapy devices limits the ability of researchers and clinicians to deliver individualized, targeted treatment and to study its effects under real-world conditions.

1.1 New Paradigm: Socially Acceptable, Convenient Light Therapy

This thesis presents a new paradigm in approaching light therapy with an important component of product design and engineering. A pair of smart light therapy glasses was

designed and engineered to resolve a fundamental issue of convenience, thereby potentially improving user adherence and long term adoption of light therapy in daily routines.

Traditional light boxes can be inconvenient, requiring users to commit a significant amount of their time to sit still in front of a device. And existing light therapy "glasses" on the market resemble headgear from science fiction movies. Figure 1.1 compares a traditional light box, an existing wearable, and the Lumos smart glasses developed in this study.



Figure 1.1: Comparison between (left) a traditional light therapy box, (middle) an existing light therapy wearable, and (right) the Lumos smart glasses prototype developed in this study. (Photos by and of the author.)

Over the past decade, the trajectory of the smart-glasses industry has shown that public adoption is shaped strongly by aesthetics, comfort, and social familiarity. People tend to accept technologies worn on the face only when the device resembles conventional eyewear and feels socially appropriate in everyday environments. This pattern is evident from the contrasting outcomes of earlier consumer smart-glass launches: products that adopted familiar, fashion-aligned eye-wear achieved greater mainstream acceptance, whereas devices with more unconventional designs encountered social friction and privacy-related resistance.

Empirical research supports this observation. Adapa et al. [7] found that perceived image and design were among the strongest predictors of intention to adopt smart wearables, especially glasses-based systems. Kaviani et al. [57] reported that social acceptability, how others perceive the wearer, was one of the most significant barriers to public use of smart glasses. Similarly, Zuidhof et al. [110] identified aesthetics, comfort, and anticipated social reactions as dominant influences on acceptance in healthcare settings. Comprehensive reviews of AR and smart-glasses adoption confirm the same trend: appearance, comfort, and

resemblance to traditional eye-wear are consistently cited as key determinants of real-world uptake [59].

Together, these findings emphasize that the success of technologies worn on the face depends not only on technical performance but also on their alignment with social norms, aesthetic expectations, and familiar visual identities.

Therefore, to let light therapy have the best chance at becoming more widely adopted and reach greater adherence, significant research and development was devoted to designing smart light therapy glasses that combine advanced photonics, ergonomics, and nano-fabrication. One of the first outcomes of this work was granted the U.S. patent *US12364874B2* [93], covering the novel optical delivery and integration design.

As shown in Figure 1.2, the Lumos glasses were designed to resemble regular eye-wear, allowing users to incorporate light therapy seamlessly into daily routines, whether during focused work sessions or relaxed leisure time. This visual and social familiarity plays a crucial role in promoting adherence.



Figure 1.2: Demonstration of Lumos light therapy glasses in use during day and evening settings. The photographs feature models with signed release forms: Madeline Della Mora (left), Christopher John, Victor Shijie Wu (center), and Aman Lohia (right).

The external appearance and product geometry are further illustrated in Figure 1.3, which shows the overall form factor designed for comfort and everyday usability. The design prioritizes balance, weight distribution, and aesthetic subtlety while integrating the electronics discreetly within the temple arms. Each arm houses a custom light engine optimized for spectral power distribution and eye-safety compliance, as discussed later in the *Eye Safety* section. The lenses employ proprietary nano-coatings to shape the spectral profile while minimizing glare and reflection artifacts.



Figure 1.3: Isometric render of the Lumos glasses showing the exterior frame and overall form factor designed for daily wear. The operating principle is illustrated in Figure 2.1, and the internal components are labeled in Figure 2.4.

Further research is underway to refine the form factor, improve comfort, and enhance both aesthetic and social acceptability, expanding the boundaries of interdisciplinary innovation that merges optics, neuroscience, and wearable design. Additional patent applications are currently under examination to protect these ongoing advancements.

1.1.1 Clarifying Blue-Light Safety

Public concern about "blue-light" has grown in recent years, shaped in part by the widespread marketing of blue-light–blocking eye-wear. Many of these products use a very faint blue tint that selectively reflects or absorbs a small portion of short-wavelength light. Although advertised for retinal protection or relief from digital eye strain, studies show that these faint tints attenuate very little blue-light and do not provide a consistent benefit for ocular health or comfort [85]. This marketing trend has contributed to the perception that typical blue-light exposure from screens and indoor LEDs is inherently harmful.

Scientific evidence paints a different picture. The CIE, the American Academy of Ophthalmology, and several recent reviews report that blue-light from consumer lighting and electronic displays remains well below established retinal safety thresholds and is often lower than natural daylight exposure [52, 11, 32]. The actual blue-light hazard refers to a retinal photochemical mechanism that becomes relevant only under high-radiance conditions. Everyday exposures fall far below these levels. The governing exposure limits are formalized in IEC 62471, which defines the action spectrum, radiance metrics, and standardized geometry used to assess photobiological safety [53].

In contrast to the faint-tint category, visibly tinted blue-blocking lenses such as yellow, amber, or orange filters have clear physiological relevance. These lenses meaningfully reduce melanopic stimulation in the evening, and controlled studies show that they can support circadian regulation and improve sleep, particularly in light-sensitive individuals or those taking photosensitizing medications [24, 47]. Their use has also been popularized through public science communication [77], helping translate circadian-lighting research into practical recommendations.

The Lumos optical system incorporates comparable short-wavelength reduction when the device is worn without illumination. Although this is not the primary therapeutic mechanism, the coating provides evening melanopic attenuation similar to these physiologically targeted tinted lenses, offering circadian-friendly support during non-therapy use.

A detailed examination of photobiological safety, including retinal damage mechanisms, blue-light hazard functions, exposure limits, and radiance measurement geometry, is presented in Appendix B. This framework establishes the quantitative basis for ensuring that the Lumos system remains within established ocular safety margins while delivering effective circadian stimulation.

1.2 Engineering Scope of the Work

The first major component of this thesis is the engineering and system design of the Lumos wearable light therapy glasses, presented in Chapter 2. That chapter details the operating principle, hardware evolution and prototyping, light engine and eye-safety validation, ambient-light sensing and calibration, user-detection sensing, electrical architecture, firmware, and mobile software. These subsystems collectively support the goal of developing a comfortable, socially acceptable, and clinically reliable light-therapy device capable of personalized data collection for circadian and mental-health research.

Operating principle. This section explains the fundamental operating principle and key invention that allow Lumos glasses to achieve a slim, eye-wear-like form factor, as described in the author's patent US 12,364,874 B2 [93]. A wavelength-selective nano-coated lens reflects melanopsin-activating light from an embedded light engine back toward the eyes while transmitting other wavelengths for natural vision. This configuration enables a visually comfortable, targeted illumination system within the profile of standard glasses.

Hardware evolution and prototyping. This section outlines the development history of the Lumos glasses leading up to the current design. Beginning with a 2019 proof of concept (3D-printed frame, dichroic insert, simple LED–resistor circuit), the design progressed through a 2020 CES pilot build (custom nanocoating, CNC aluminum frame, rechargeable PCB) and evolved from 2021 onward toward mass manufacturability, clinical robustness, and user comfort. Coating variants (high-melanopic vs. comfort) were tested, and the stainless steel *Citizen* frame was selected via user surveys. The frame accommodates swappable lenses, while TR-90 polymer arms house the electronics. The nRF52-based PCB integrates LED driving, power management and charging, sensing, antenna matching, and button input.

Light engine design and eye safety. This section details the light engine's design and calibration to optimize output while maintaining ocular safety. The engine consists of a PCB-mounted emitter array that projects light toward the coated lens. Calibration was performed by correlating readings from a spectral sensor (AS72653) with Bentham reference spectroradiometer measurements conducted by Technischer Überwachungsverein Süd (TÜV SÜD), determining an optimal LED brightness via PWM control. The device meets the IEC 62471 standard and is classified as Exempt (RG0) at 200 mm [53]. Additional near-eye safety considerations beyond the standard were addressed by specifying angular TEL,309 measurements to TÜV SÜD and conducting optical simulations to apply conservative engineering safety factors for close-range exposure [49].

Ambient light sensor design and calibration. This section describes the design and calibration of the melanopic lux ambient light sensor integrated into the glasses. A custom optical filter was placed over a standard sensor to match the human melanopic spectral sensitivity curve. The sensor was calibrated under representative usage conditions using reference measurements from a f.luxometer. The logging system saturates at 14,000 melanopic lux, exceeding the light level required for melatonin suppression and circadian phase shift [109].

User detection sensor iteration. This section presents the iterative design of the user detection sensor. Early capacitive-sensing prototypes exhibited insufficient signal-to-noise ratio for smaller head sizes. The final design uses infrared proximity sensing implemented on flexible Printed Circuit Boards (PCBs) with an IR-transmissive window and synchronous ambient-light rejection, achieving reliable wear detection across a wide range of users.

Electrical system. This section provides a high-level overview of the electrical system and presents a block diagram of the primary electronics comprising the smart light therapy glasses.

Firmware architecture. This section summarizes the embedded firmware implementation on the Bluetooth-enabled microcontroller. The firmware handles Bluetooth Low Energy (BLE) communication, sensor polling (ALS, proximity, and battery), interrupt and button logic, calibration data storage and editing, and a minimal Psychomotor Vigilance Task (PVT) routine utilizing the glasses' button and light engine.

App and software. This section describes the cloud-connected mobile software that interfaces with the Bluetooth-enabled glasses. The app enforces wear verification before light activation, manages time-of-day and ambient-light logic, and records usage for adherence tracking. Data synchronize to Firebase (authentication, storage, offline persistence); Qualtrics surveys are integrated via Zapier; and an administrator view enables participant monitoring.

Production for study. With these subsystems finalized, over one hundred units were assembled, calibrated, and quality-checked for deployment in the double-blind, placebo-controlled clinical trial.

1.3 Clinical Objectives and Scope of Work

The **primary objective** of the clinical trial was to evaluate the therapeutic potential of the Lumos glasses in a *double-blind, placebo-controlled* setting using standardized psychological, cognitive, and sleep assessments. The goal was to determine whether a novel,

eye-directed light-delivery mechanism could be used safely and effectively to improve mood, sleep quality, and attentional performance.

The **secondary, exploratory objective** was to examine how real-world behavioral and environmental factors (including usage duration, ambient melanopic lux, baseline symptom severity, and demographic moderators such as eye pigmentation, age, and sex) were associated with treatment response. By leveraging onboard sensors and continuous logging, the system enabled high-resolution characterization of dose–response relationships that are typically inaccessible in controlled laboratory settings.

To support these clinical aims, the trial underwent full protocol refinement and approval by the University of Waterloo Research Ethics Board, and was conducted using a randomized, double-blind, placebo-controlled crossover design with clearly defined inclusion and exclusion criteria. Mood, sleep, and cognition were evaluated longitudinally using mixed-effects models, with exploratory regressions assessing the influence of usage, ambient light, and demographic moderators.

Together, the **engineering scope of work** (device invention, prototyping, optical calibration, and system integration) and the **clinical scope of work** (trial design, execution, and statistical analysis) provide an end-to-end evaluation pipeline for wearable light therapy. This thesis therefore integrates device engineering, applied psychophysiology, and clinical psychiatry to address insufficient circadian-effective light exposure in daily environments.

Chapter 2

Engineering Development

2.1 Operating principle

The operating principle of the Lumos glasses is illustrated in Figure 2.1.

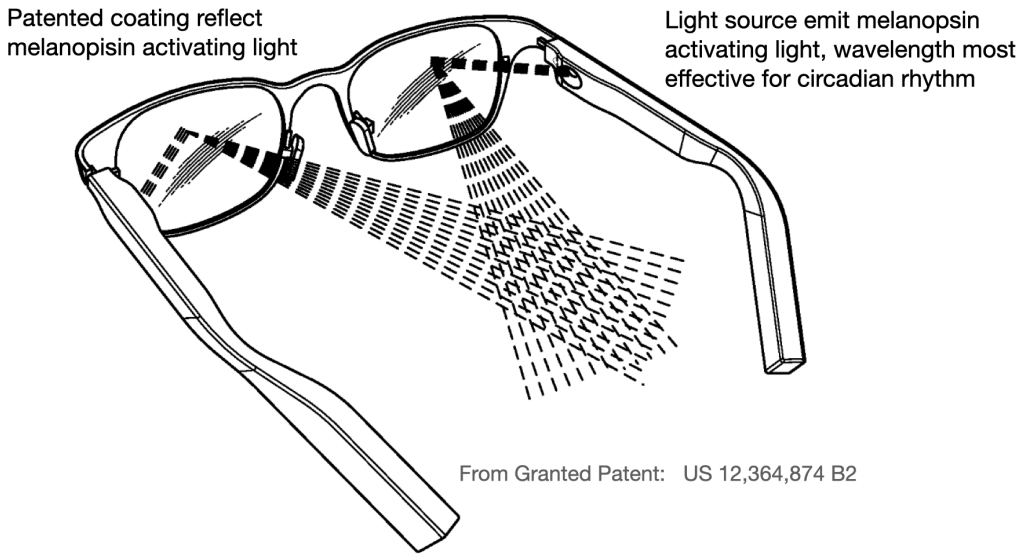


Figure 2.1: Operating principle of the Lumos glasses. Adapted from US [93]

In 2017, early development work was initiated to design a pair of light-therapy glasses

with the appearance and comfort of conventional eye-wear. Evaluation of available optical and electronic technologies at the time revealed significant limitations. These challenges prompted a shift toward a photonics-driven solution, leading to the development and subsequent patenting of a wavelength-selective light-delivery system (U.S. Patent No. 12,364,874 B2). This technology forms the foundation of the first generation of Lumos smart light-therapy glasses examined in the present study. Figure 2.1 illustrates how the operating principle employs a wavelength-selective light engine integrated within the eye-wear arms to emit melanopsin-stimulating light centered near 480 nm. The emitted light is directed onto a lens with a specialized nanocoating that reflects this specific spectral band toward the user's eyes while transmitting other wavelengths to maintain natural visual perception. This enables a compact, glasses-like form that delivers targeted, comfortable light therapy suitable for daily wear. Given the fact that the lenses reflect melanopsin activating light, when the lights are not on, it doubles as blue-light blocking glasses to aid with evening melatonin production.

2.2 Hardware Evolution and Prototyping

Figure 2.2 shows a history of the development of the Lumos glasses.



Figure 2.2: Evolution of the prototypes of the Lumos smart light therapy glasses

Hardware evolution and prototyping. This section outlines the development history of the Lumos glasses leading up to the current design. The first prototype was completed in 2019 using 3D-printed frames, acrylic CNC mock lenses, and a ThorLabs optical-grade dichroic insert. Electronics consisted of a single LED–resistor pair powered by a fishing-float battery and controlled by a slide switch. While bulky, this prototype demonstrated the feasibility of the wavelength-selective illumination concept and provided the confidence to proceed with subsequent engineering development.

During 2020, a second-generation prototype was created for the CES demonstration and pilot study. This version introduced a custom lens fabricated using a novel nanocoating process, a black anodized CNC-aluminum frame, and a rechargeable system powered by a custom printed circuit board with integrated charging circuitry. The CES prototype received favorable early evaluations, including recognition in several technology and vision-care publications. Reviewers described the system as "the best-looking, most-likely-to-be-worn light therapy wearable we've seen yet" [33], and the device was featured in the *Las Vegas Review-Journal* [81], *Vision Monday* [2], and healthcare-technology roundups such as Hucu.ai's "Eye-Catching Innovations for Healthcare at CES" [1].

The engineering work underlying these prototypes was also evaluated through competitive academic forums. The system formed the basis of the author's fourth-year capstone project, which won the Waterloo Engineering Competition and subsequently represented the University of Waterloo at the Ontario Engineering Competition. It then advanced to the Canadian Engineering Competition, where it received the inaugural Research and Entrepreneurship Award for technical innovation and translational potential [3]. Continued development of the technology also contributed to the author's recognition with the provincial *Rising Star: Minister of Colleges and Universities' Award of Excellence* in 2022 for contributions to engineering innovation and student research leadership [6, 4, 5].

The nano-technology lens system was one of the most critical components of the device and underwent continuous refinement throughout development. The earliest prototypes used a dichroic insert embedded in CNC-machined acrylic lenses. This approach was later improved by depositing the coating onto a flat glass substrate, followed by transition to a curved PMMA resin lens that provided better impact resistance and enabled compliance with the FDA's impact-resistant lens requirement for eyeglasses and sunglasses as a Class I medical device [97].

Building on this foundation, multiple coating formulations were explored to balance optical subtlety, user comfort, and circadian effectiveness, as illustrated in Figure 2.3.

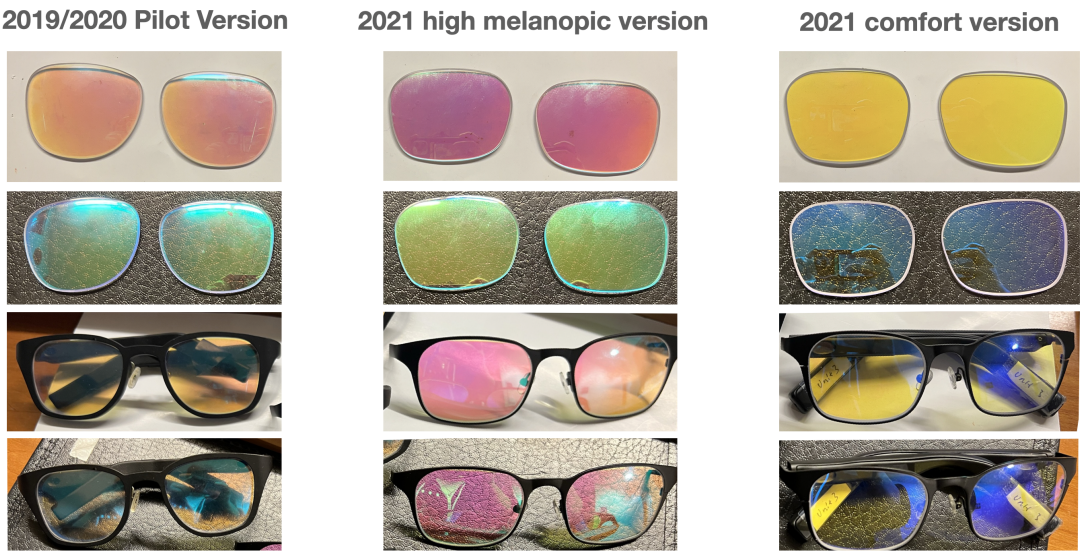


Figure 2.3: 2021 coating optimizations

The 2019–2020 pilot version employed a baseline coating intended primarily for proof-of-concept validation. Building on insights from that study, a high-melanopic variant was developed in 2021 to enhance circadian stimulus delivery while maintaining acceptable visible transparency. Although this formulation improved melanopic efficacy, it introduced noticeable color distortion. To address this, a comfort-optimized coating was produced later in 2021, substantially reducing color distortion while preserving optical performance. This comfort-optimized formulation was ultimately selected for scaled production and used in the clinical trials. During and after the trials, additional coating iterations were developed to further improve subtlety, reliability, manufacturability, and overall user experience.

The lens coating also reflects melanopic blue light from the environment when the therapy LEDs are off, providing effective evening blue-light reduction. In this mode, photopic transmission remains above 75%, allowing safe nighttime driving while attenuating melanopic components of headlights and ambient lighting that could otherwise disrupt sleep.

The mechanical design of the glasses allowed for a swappable front frame with all electronics packed inside the side arms. The front frame of the glasses is stainless steel stamped sheet metal, with V grooves to house the lenses. This design allows for the ability to interchange lenses with a small screwdriver. The front frame has brazed spring hinges on them, which connect to the TR-90 arms through a slot and screw. The arms are made

of two pieces: a housing and a cover, which holds the main circuit board, peripheral sensor flexible circuits, a push button, and battery.

The printed circuit board is designed using Fusion360, formerly Eagle CAD, and uses the Nordic Semiconductor nRF52 Bluetooth SoC family (nRF52) chip as its main microprocessor. It houses the Light-Emitting Diode (LED), processor, ambient light sensor, proximity sensor, antenna, push button switch, microusb charging port, battery charging circuit, Low Dropout Regulator (LDO) voltage control circuit, reset circuit, antenna tuning networks, LED transistor amplifier circuit, ambient light sensor detection circuit, and other supporting circuitry to ensure stable usage.

A diagram of the clinical and commercial version of the glasses is shown in Figure 2.4.

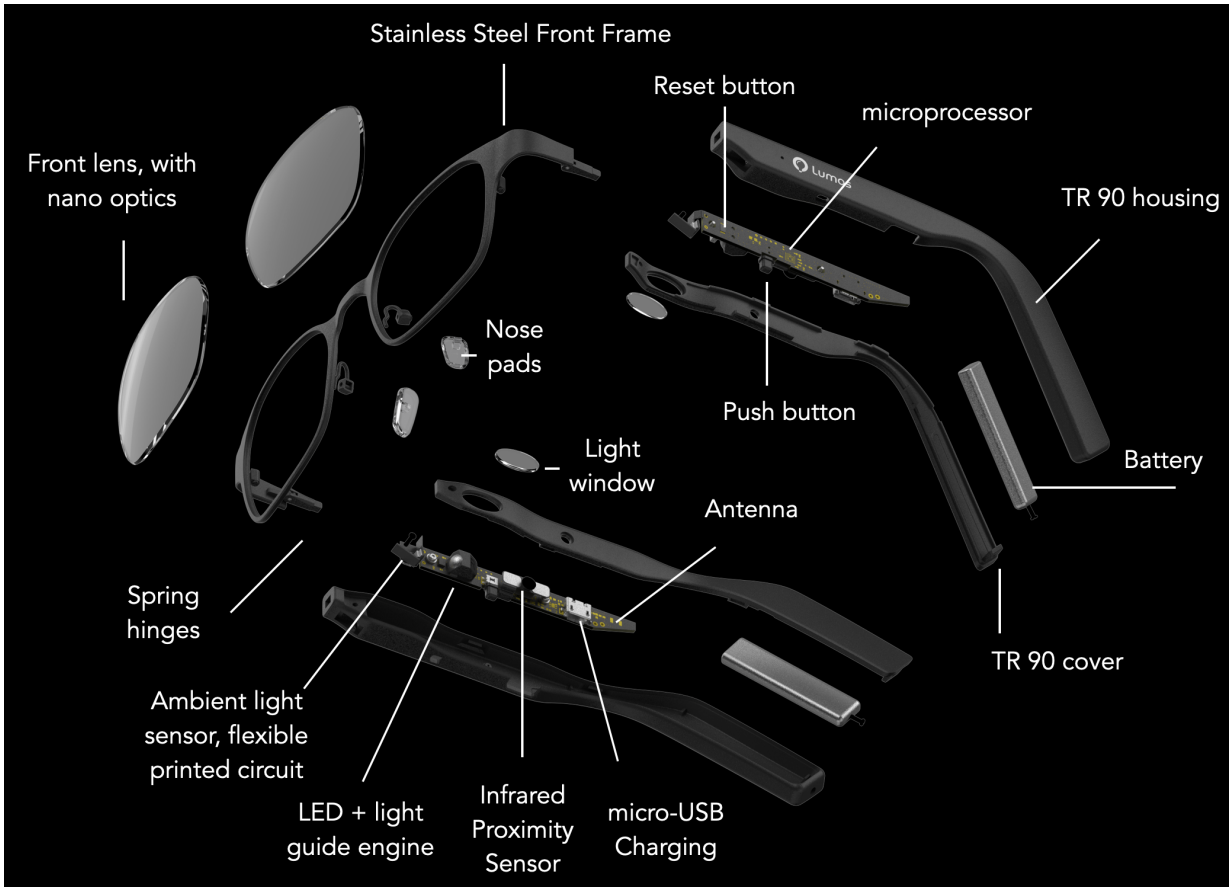


Figure 2.4: Labeled diagram of key components of the Lumos glasses

2.3 Light Engine Design and Eye Safety

2.3.1 Light engine design overview

The light engine shown in Figure 2.5 is one of the most critical and well optimized systems inside the glasses. Its primary function is to gather and shape light from the LED into a controlled beam towards the lenses. It is done through a custom optical-mechanical part mounted to the printed circuit board through two holes made for heat stake riveting.

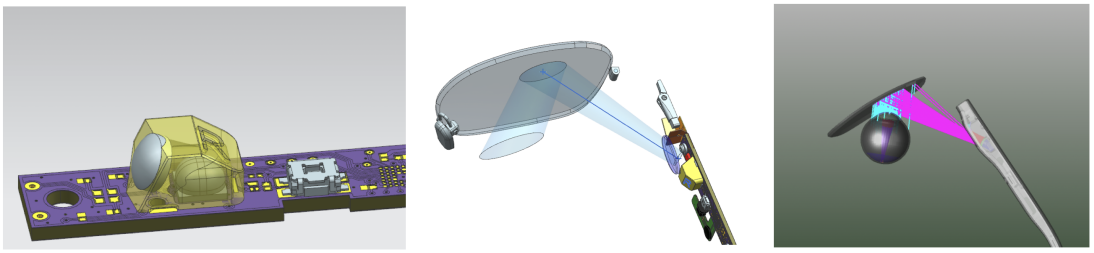


Figure 2.5: Basic light engine on PCB

The light engine housing could be made from plastic or metal. If made of plastic, its mounting method uses the heat stake rivets; ifmetal, it is soldered onto the PCB. Plastic housing can be injection molded in mass production, but offers slightly lower light efficiency. A metal housing allows for more internal reflections, which increases light efficiency at the cost of more stray light and scattering, as well as increased cost in mass production. For the clinical trial and commercial version, the plastic housing was chosen for its mass production benefits.

2.3.2 Photobiological Safety Considerations

While the Introduction outlines the general context of blue-light safety and public misconceptions, the engineering assessment of the Lumos light engine requires a more formal photobiological framework. The relevant safety criteria are defined by the retinal photochemical exposure limits in IEC 62471, which rely on the blue-light hazard function $B(\lambda)$, the blue-light–weighted radiance L_B, and cumulative radiance dose under a standardized 200 mm measurement geometry.

Because the device delivers circadian-effective short-wavelength light directly toward the lens region, its optical design, drive parameters, and viewing geometry were calibrated to ensure that all operating modes remain within these exposure limits. Although circadian stimulation is maximized near 480 nm and the blue-light hazard function peaks closer to 440 nm, there is a region of partial spectral overlap. For this reason, the spectral output, angular distribution, and radiance of the light engine were carefully controlled to achieve circadian efficacy while maintaining compliance with the photochemical exposure limits defined in IEC 62471.

The supporting technical material, including retinal damage mechanisms, hazard-weighting functions, exposure-limit derivations, and radiometric measurement procedures, is provided in Appendix B. This appendix establishes the quantitative basis for the safety evaluations applied throughout this chapter.

2.3.3 Calibration of the Light Engine

Individual LED components can vary significantly in brightness, forward voltage, dominant wavelength, and other electro-optical properties. Even within the same manufacturing bin, the optical output can differ by a factor of two. To ensure consistent dosing and maintain compliance with the eye-safety limits defined in IEC 62471, each unit must therefore be calibrated so that its optical output remains within the permitted radiance range while still delivering sufficient circadian-effective light.

A practical complication is that IEC 62471 was originally developed for lamps and displays viewed at distances beyond the minimum human accommodation distance of approximately 200 mm. The standard therefore assumes exposure geometry typical of everyday lighting. Near-eye systems, including modern smart glasses, fall outside these assumptions. When a source is positioned close to the eye, or when optical elements shape the beam toward the retina, the effective retinal irradiance can increase relative to the 200 mm reference measurement. Horton et al. [49] demonstrated that a source classified as safe at 200 mm may exceed safe limits if brought significantly closer.

For this reason, the calibration process for Lumos incorporated both the standard radiance limits and additional geometric considerations specific to near-eye use. Simulation studies, detailed review of the relevant sections of IEC 62471, and consultation with leading experts in photobiological safety were used to define safe operating ranges and to guide the selection of drive currents and duty cycles. These considerations are summarized in Appendix B, which provides the technical foundation for the safety constraints applied during calibration.

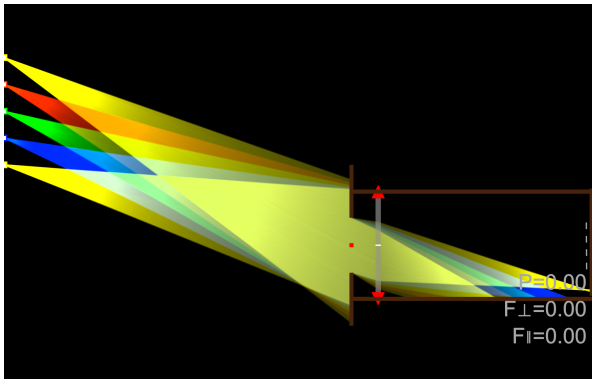
2.3.4 Photobiological Safety Testing of Lumos Glasses

The Lumos glasses were evaluated for photobiological safety in accordance with IEC 62471 at the standard evaluation distance of 200 mm. Even at maximum output, the product met all photobiological safety requirements and was classified as **Risk Group 0 (Exempt)**. This indicates that even if a user were to hold the glasses away from the face and look directly into the reflected emission, the radiance would remain below the blue-light hazard limits. The full third-party test results and certification are provided in Appendix O (TÜV SÜD Canada IEC 62471 Test Report No. 7169009669-000).

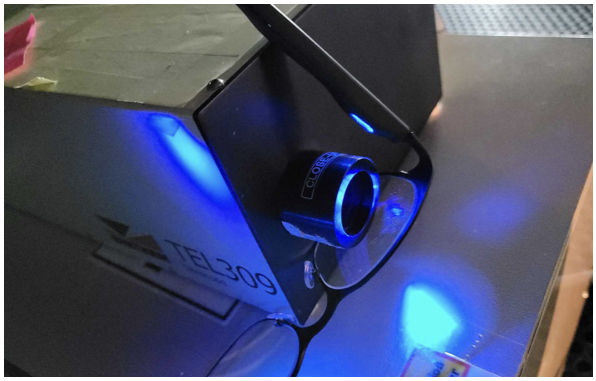
With wearable systems, however, the light source is positioned much closer to the eye, and the geometry of illumination differs from that assumed by the standard. Although the eye cannot form a sharply focused image of the emitting region, a sufficiently high luminous flux distributed across the pupil can still pose a photochemical or thermal hazard. Horton et al. [49] showed through simulation that sources positioned closer than 200 mm may produce higher effective retinal exposure than predicted from standard-distance measurements. Consequently, a source that meets the limits at 200 mm may not remain within safe exposure levels if moved substantially closer to the eye.

One might expect that placing the radiance telescope of an instrument such as the TEL,309 at the nominal eye location would reproduce near-eye conditions. In practice, this approach introduces geometric and optical challenges. Because the human eye generally views forward, a telescope placed in the same orientation would not intercept the Lumos emission, which enters from an oblique angle. Since the detector sits at the rear focal plane of the telescope, off-axis light would not be properly imaged onto the sensor, producing invalid radiance measurements. This limitation is illustrated in Figure 2.6a.

A practical solution is to orient the TEL,309 telescope directly toward the emitting region, as shown in Figure 2.6b. This alignment allows accurate radiance measurement while a cosine correction factor is applied to approximate the typical forward gaze of the eye during long-duration use.



(a) Geometric limitation of using the standard radiance measurement configuration at the eye location while viewing forward. Off-axis emission cannot be properly focused onto the detector.



(b) Angular radiance measurement with the TEL 309. The telescope is rotated to directly face the emitting region, with a cosine correction applied to represent typical forward gaze.

Figure 2.6: Comparison of radiance measurement geometries for near-eye sources. The forward-viewing geometry (left) fails to capture off-axis light, whereas the angled telescope configuration (right) provides accurate radiance measurement.

The TEL,309 instrument employs an averaging field of view of 11 mrad due to hardware limitations. This is conservative, since IEC 62471 specifies that for long-duration exposures relevant to Risk Group 0 (Exempt) classification, radiance should be averaged over an effective 100 mrad field to account for natural eye movements during normal visual tasks. With the smaller 11 mrad aperture, localized intensity peaks within the emission pattern remain unaveraged, which leads to an overestimation of the potential hazard. This limitation, observed even with equipment from a leading safety certification agency, highlights the current lack of radiometric instrumentation optimized for near-eye wearable systems.

The 11 mrad measurement was therefore used with the understanding that it represents a conservative assessment. If this value were interpreted as though it had been obtained with a 100 mrad averaging field, the resulting radiance would still overestimate the true retinal hazard. Consequently, realistic evaluation of near-eye illumination systems requires complementing empirical measurements with optical simulations that account for image defocus, pupil geometry, and dynamic eye motion.

2.3.5 Optical Simulations

Near-eye light sources produce a fundamentally different retinal image than the sharp focal spot assessed under the IEC 62471 reference geometry at 200 mm. To characterize this difference, non-sequential optical simulations were performed using a calibrated Zemax human eye model. As illustrated in Figure 2.7, a distant collimated source forms a highly concentrated focal spot, whereas the Lumos near-eye optical system produces a broad 2–4 mm diffuse footprint due to geometric defocus, oblique incidence, and natural eye-motion averaging. This spreading greatly reduces peak retinal irradiance compared to the worst-case conditions assumed in photobiological safety limits. Full simulation and explanation details are provided in section B.5.

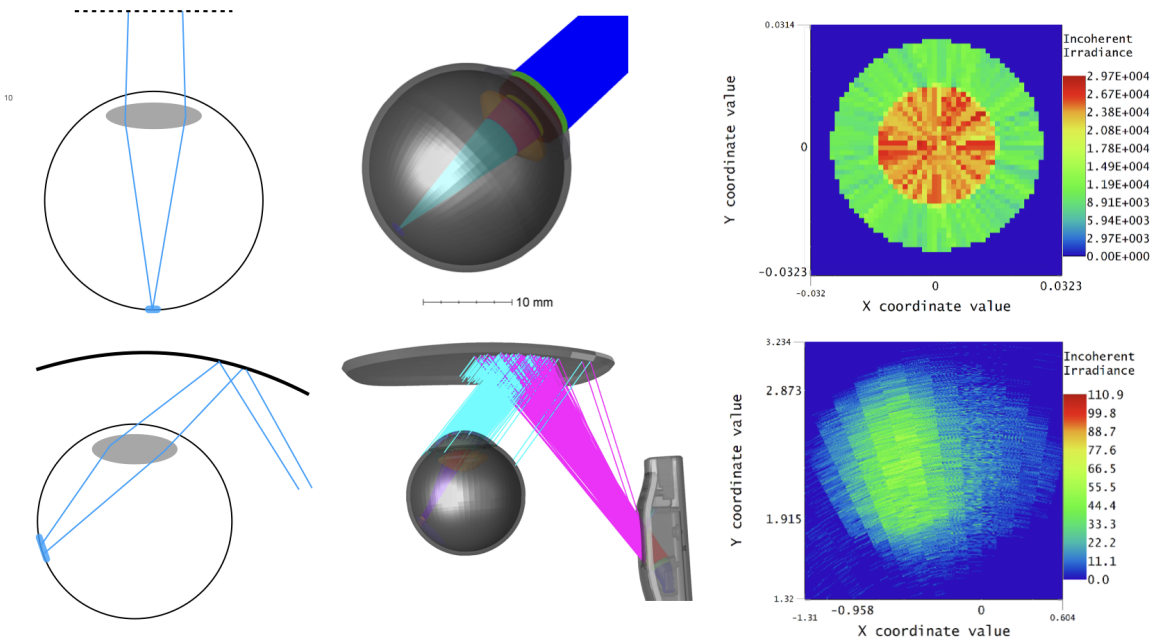


Figure 2.7: Comparison of retinal image formation for a distant 200 mm source (top row) versus the near-eye Lumos optical system (bottom row). Left: conceptual ray diagrams and Zemax ray-trace geometry. Right: simulated retinal irradiance maps. The near-eye configuration produces a large, diffuse 2–4 mm retinal footprint, significantly reducing peak irradiance relative to the scenario defined in IEC 62471.

Design safety factor It is common in engineering practice to add an extra safety factor (SF) at the product level. For optical radiation, however, the applicable exposure limits deriving from IEC 62471 already embed a substantial margin below observed damage thresholds.[53] In particular, Schulmeister et al. (ILSC 2019) note that the blue-light photochemical exposure limits sit *on the order of 10–20*× below ophthalmoscopically visible retinal lesion thresholds reported in rhesus monkeys.[80]

Implication for this device. Because the standard's limits already include this margin, it is generally *not necessary* to apply an additional arbitrary SF on top of a compliant assessment. Instead, we reserve extra margin only where justified by measurement uncertainty, worst-case geometries, or prolonged exposures specific to our use case. Our safety evaluation therefore reports compliance against IEC 62471 exposure limits and documents device-specific uncertainties, rather than stacking an additional blanket SF.

From this exercise, it is apparent that the IEC 62471 standards have met a lot of limitations when it comes to near eye display, and it may be beneficial to develop a new set of measurement techniques. Furthermore, more research and testing should be done on the spatial and temporal effects of light damage on the retina, ideally testing the sensitivity to damage of different spots over long period exposure.

2.3.6 Calibration Procedure

A calibration method was developed to correlate LED output measurements obtained from standard spectrometric sensors with reference measurements performed by TÜV SÜD using the Bentham IDR300-PSL Photobiological Safety Spectroradiometer [17]. It was impractical for TÜV SÜD to test every manufactured unit using the standardized IEC 62471 measurement setup given the extensive configuration and measurement time required, so an alternative per-device calibration process was implemented. This procedure began by capturing spectral and power data from each device using an off-the-shelf spectrometer (AS72653), which is then correlated against the reference measurements obtained by TÜV SÜD. The calibration station and sensor response characteristics are shown in Figure 2.8.

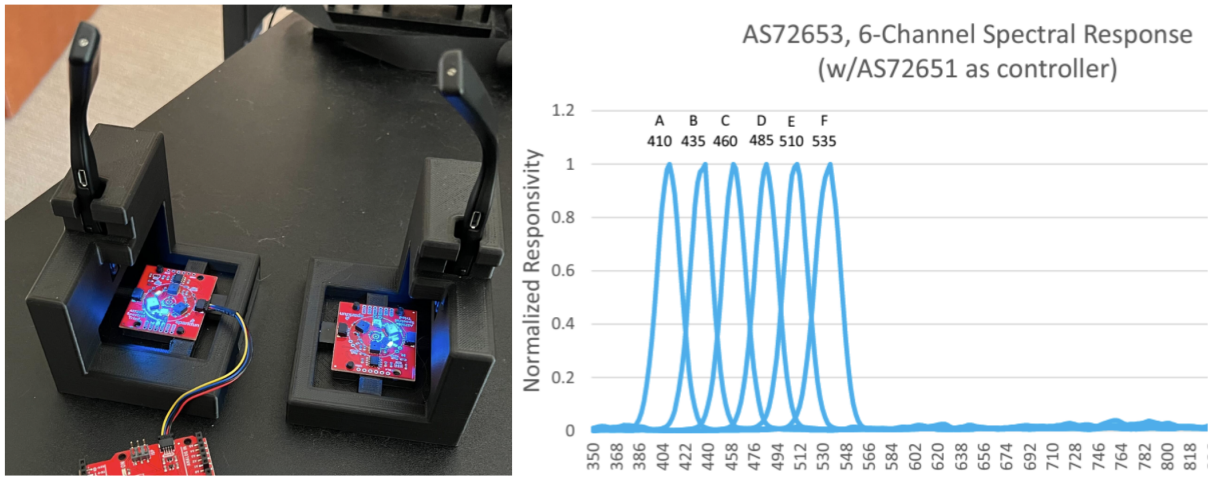


Figure 2.8: Lumos calibration fixture with the AS72653 spectrometer used for per-device spectral characterization. Reference calibration data were obtained using a Bentham IDR300-PSL Photobiological Safety Spectroradiometer.

Based on manufacturer specifications and established principles of LED fabrication, individual emitters can exhibit notable variation in both luminous intensity and dominant wavelength, whereas batch-to-batch variation in emission bandwidth (full width at half maximum, FWHM) tends to be relatively small [64, 94, 34, 74]. This behavior has been attributed to variations in epitaxial layer thickness and composition, which influence the peak emission wavelength, while the bandwidth is determined by material properties and remains stable across operating conditions and production batches.

These trends are consistent with internal measurements of the LEDs used in the Lumos system. Accordingly, an LED population may be reasonably characterized by its center wavelength and peak optical power, with the dominant wavelength modeled as a normally distributed variable having a standard deviation of approximately 11 nm.

As a next step, a simulation framework was developed to evaluate how accurately dominant wavelength and peak power could be extracted from the AS72653 sensor, which measures light at six discrete spectral channels spaced at 25 nm intervals. The goal was to correlate these sparse measurements with the high-fidelity reference spectra obtained from TÜV SÜD at 5 nm resolution. To achieve this, the spectral response of each AS72653 channel was digitized from its datasheet and modeled as a normal distribution. Simulated LED sources were then generated as normal distributions with arbitrary dominant wavelengths and peak powers, sampled at 5 nm intervals to match the reference data resolution.

For each simulated source, the spectral emission curve was multiplied by each channel's responsivity function and numerically integrated, producing six predicted sensor outputs (channels A–F corresponding to 410, 435, 460, 485, 510, and 535 nm). Shown in Figure 2.9.

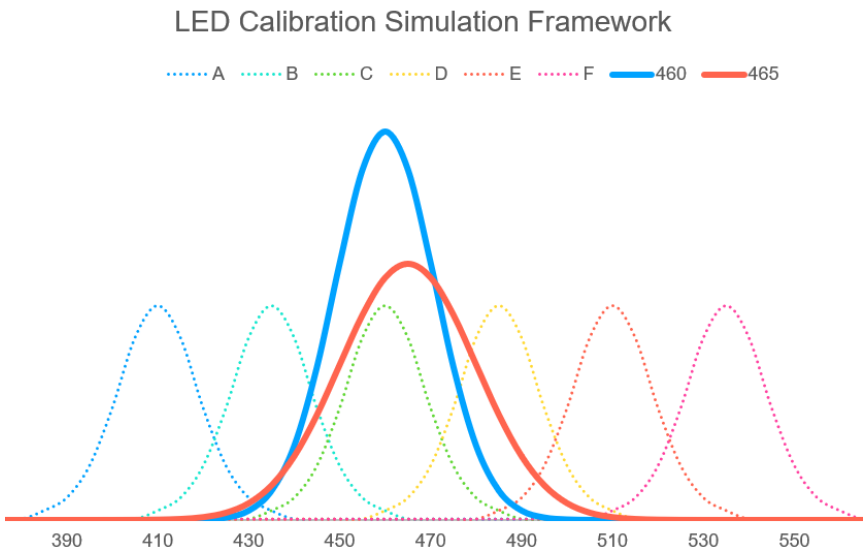


Figure 2.9: Simulation of LED calibration framework showing the modeled spectral responsivity of the AS72653 sensor channels (A–F) and two simulated LED sources with dominant wavelengths of 460 nm and 465 nm, respectively.

Several algorithms were evaluated for estimating the dominant wavelength from these six measurements. The best-performing method was the *center-of-mass* approach, in which each sensor's reading was treated as a mass and its central wavelength as a positional weight. The weighted mean wavelength was then computed as the effective center of mass. Across simulations spanning dominant wavelengths from 460–500 nm, this method achieved sub-nanometer precision, with a max error 0.05 nm.

Peak optical power was estimated by summing all six sensor readings and correlating the result with simulated peak intensity. This approach yielded errors within 0.6% at three standard deviations, demonstrating that the center-of-mass method for dominant wavelength and summation method for peak power provide high theoretical accuracy for the AS72653 configuration.

As a next step, measurements from the AS72653 sensor were correlated with the corresponding TÜV SÜD reference spectra sampled at 5 nm intervals. The center-of-mass method yielded highly consistent results for one sensor, but in another channel—the D

receptor, nominally centered at 485 nm—an offset was observed. To achieve proper correlation, the peak wavelength of the D channel was adjusted from 485 nm to 475 nm, compensating for a tolerance shift in the AS72653's internal optical filter. This adjustment is conservative; by shifting the peak toward shorter wavelengths, the sensor's sensitivity moves closer to the maximum of the blue-light hazard weighting function near 440 nm, thereby biasing results toward a more stringent safety margin. After calibration, this corrected spectral response was applied to the right-arm sensor configuration of the Lumos system. The adjustment and its effect on spectral alignment are illustrated in Figure 2.10.

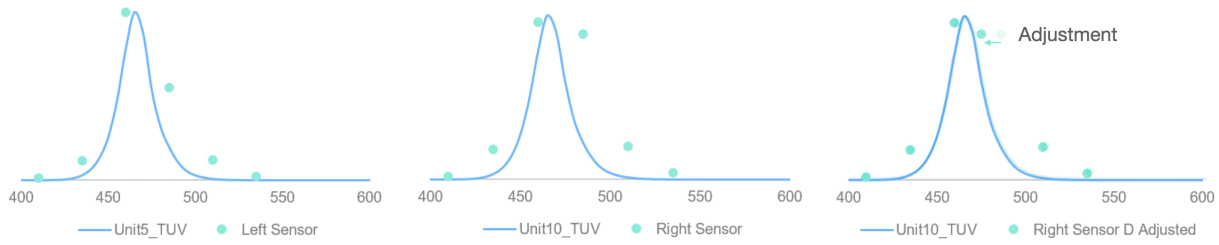


Figure 2.10: Comparison between raw AS72653 sensor readings and TÜV SÜD reference data. (Left) Unadjusted calibration for Unit 5 showing strong alignment. (Center) Unit 10 data revealing a wavelength offset in the D channel (nominally 485 nm). (Right) Adjustment of the D-channel peak to 475 nm restores alignment with the reference spectrum, indicating a minor filter-tolerance shift within the sensor.

After this adjustment, dominant wavelength accuracy resolved to be around 2 nm when compared with TUV SUD measurements.

The peak power correlation exhibited slightly greater variance, primarily due to measurement geometry constraints and variations in battery voltage that influence the LED drive circuitry. Although the system employs a low-dropout (LDO) regulator to maintain a 3.3 V supply, operation near the regulator's dropout threshold can introduce small output fluctuations, as the device remains operational slightly below 3.3 V.

TÜV SÜD confirmed that all safety certification measurements were performed with fully charged devices. However, to establish a conservative calibration model, AS72653 readings were recorded at nominal, low, and high charge states for the same device and included in the regression. This approach ensures that potential measurement variability—such as a unit being tested at reduced charge—is inherently accounted for in the calibration model.

A linear regression model (Figure 2.11) was fitted to the dataset to correlate the summed

AS72653 sensor readings with the reference peak power values obtained from TÜV SÜD. The resulting calibration function provides a predictive relationship for estimating LED output power directly from sensor data.

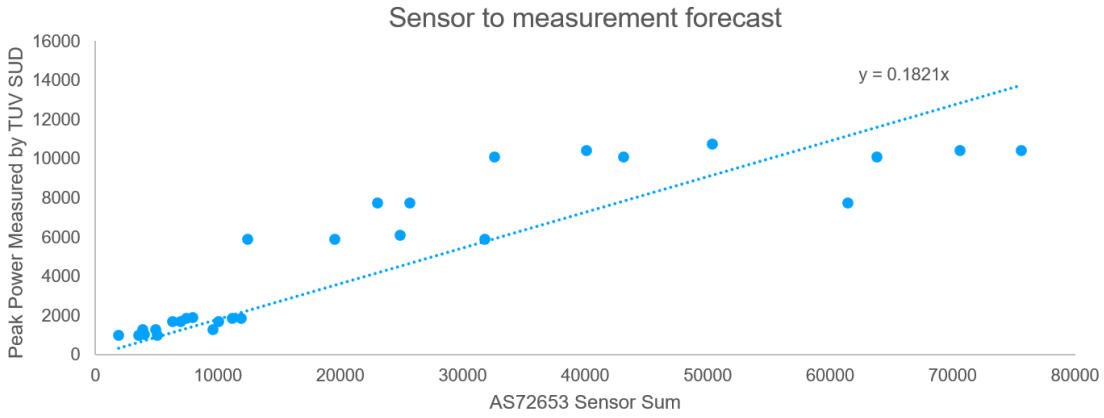


Figure 2.11: Linear regression between the summed AS72653 sensor readings and peak power measured by TÜV SÜD. The regression equation ($y = 0.1821x$) establishes a predictive relationship for estimating output power from sensor data, incorporating measurements across different device charge states to ensure a conservative calibration.

With the peak optical power and dominant wavelength now accurately estimated, the calibrated AS72653 sensor can reconstruct a detailed emission spectrum that closely emulates the Bentham reference measurements. This reconstructed spectrum is subsequently integrated with the blue-light hazard weighting function to compute the weighted radiance value. Applying the cosine correction and source-area adjustment factors yields the final photobiological hazard metric as defined in IEC 62471. To ensure that this value remains within the 100 $\mathrm{W\,m^{-2}\,sr^{-1}}$ limit prescribed by the standard, the LED output is automatically fine-tuned through pulse-width modulation (PWM), which maintains a strictly linear relationship with optical power. The finalized calibration parameters are then stored in the non-volatile flash memory of the nRF52 microcontroller, allowing each unit to maintain its safety-compliant light output across operating conditions.

2.3.7 Time-Dependent Spot Smearing and Boost Mode

The IEC 62471 blue-light hazard limit scales with exposure duration, permitting higher radiance for shorter viewing times. However, at short durations the effective retinal averaging

area also decreases, since eye and head movements contribute less to spatial smearing. To capture this effect, a time-dependent angular subtense model was derived and aligned with optical simulation results, linking exposure duration to an effective retinal spot size. As illustrated in Figure 2.12, short exposures produce a smaller averaging region, whereas long exposures smear the retinal footprint to approximately 4 mm, reducing peak irradiance. The full mathematical formulation, simulation workflow, and boost-mode derivation are included in section B.6.

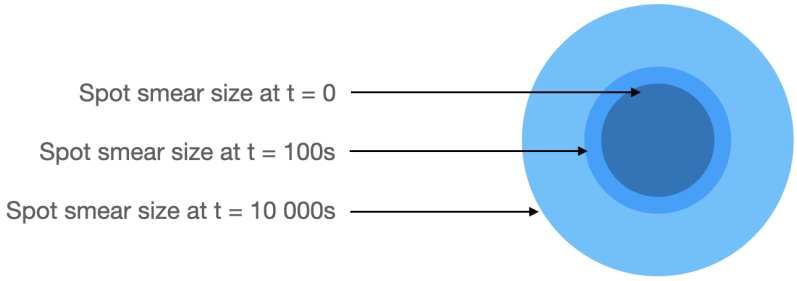


Figure 2.12: Conceptual illustration of IEC 62471 time-dependent spot smearing. Short exposures retain the ∼2 mm optical footprint, while long exposures smear to ∼4 mm due to physiological eye motion.

Although a dynamic boost mode would comply with the time-dependent radiance limits of IEC 62471, it was not implemented during the clinical trial to reduce complexity and preserve the integrity of the double-blind design.

2.3.8 External Validation with Market-Leading Device

As a validation step, a f.luxometer spectroradiometric system [42] was used to measure the calibrated spectral power output of the Lumos glasses and compare it with a commercially available light therapy wearable currently positioned as a market leader. The results indicated comparable irradiance levels between the two devices. Notably, the Lumos emission spectrum is slightly shifted toward green, with a dominant wavelength closer to 480 nm. This spectral design enables higher melanopsin activation efficiency while simultaneously reducing potential blue-light hazard risk, which peaks near 440 nm. A comparison of the measured spectra is shown in Figure 2.13.

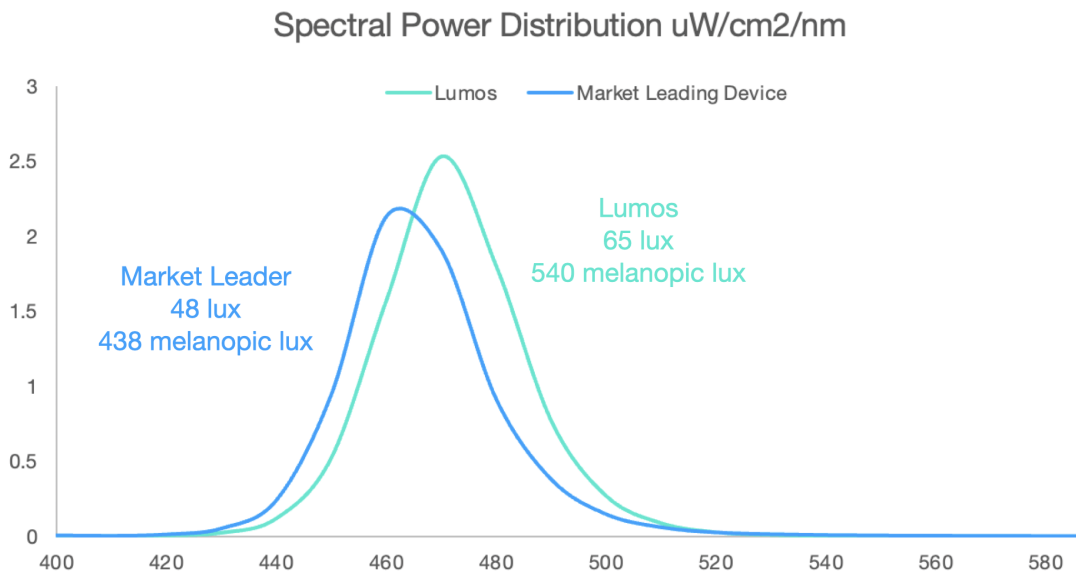


Figure 2.13: Comparison of the Lumos glasses spectral power distribution (green-shifted, $\lambda_{\text{dom}} \approx 490$ nm) and a representative market-leading light therapy wearable, after calibration. Both devices show similar irradiance levels under equivalent operating conditions.

2.4 Ambient Light Sensor Design and Calibration

The ambient light sensing modules on the Lumos glasses are another important component of the system, as they enable real-time tracking of the user's environmental light exposure. This allows for quantitative analysis of how everyday lighting conditions interact with light therapy and influence wellness outcomes. The ambient light sensor (Figure 2.14) was designed with several considerations to approximate the human melanopsin response as closely as possible, including its geometric placement, angular orientation, and spectral sensitivity.



Figure 2.14: Lumos ambient light sensor (gold rectangular piece).

2.4.1 Geometric Placement and Orientation

A primary advantage of mounting the ambient light sensor directly on the glasses is its proximity to the eyes. Many existing studies rely on wrist-mounted ambient light sensors, which are susceptible to clothing occlusion and misalignment with the natural angle of light incidence [19, 101, 100]. Integrating the sensor into the glasses eliminates these issues and leverages the platform's existing optical geometry for more accurate measurement of the light reaching the eyes.

Humans typically maintain a slight downward gaze during most visual tasks [84, 56, 58]. To approximate this eye orientation, the sensor was mounted with a small downward angle. This placement also enabled the sensor to be housed within the glasses' arms rather than the front frame, preserving a thin and modular front design while maintaining proper exposure to the incident light field. The mechanical design and placement of the sensor are illustrated in Figure 2.15.

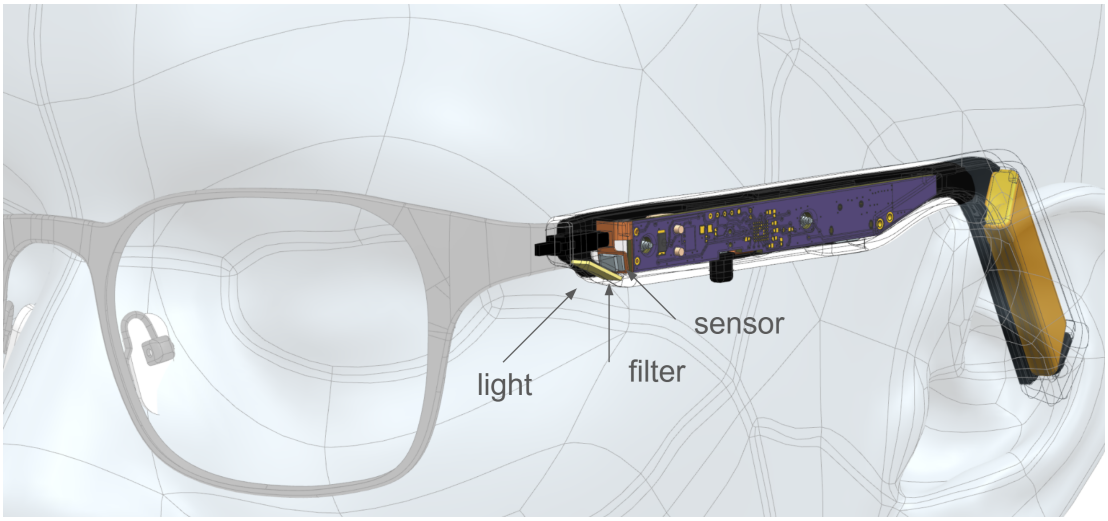


Figure 2.15: Lumos ambient light sensor geometry and placement.

2.4.2 Spectral Response and Calibration

A spectral filter was positioned in front of the sensor so that, when combined with the sensor's native spectral response, the resulting sensitivity curve closely matched the human melanopsin action spectrum. This modification enables a standard broadband ambient light sensor to more accurately represent light exposure relevant to circadian and sleep physiology. It improves accuracy under lighting conditions dominated by warm (amber) sources or when viewing displays with enabled night-shift modes.

2.4.3 Circuit Design

A silicon NPN epitaxial planar phototransistor was used as the sensor. Its output current at the emitter is converted through a resistor network into a measurable analog voltage signal (ALS_SIG), which is read by the microcontroller's ADC with a max input voltage of 3.3V. A transistor-controlled digital switch (ALS_SWITCH) allows the circuit to change resistor values dynamically, thereby extending its range for high-brightness environments due to the ADC's max voltage reading of 3.3V. This enables accurate detection from low indoor illuminance levels to bright outdoor sunlight conditions. The ambient light sensing circuit is shown in Figure 2.16.

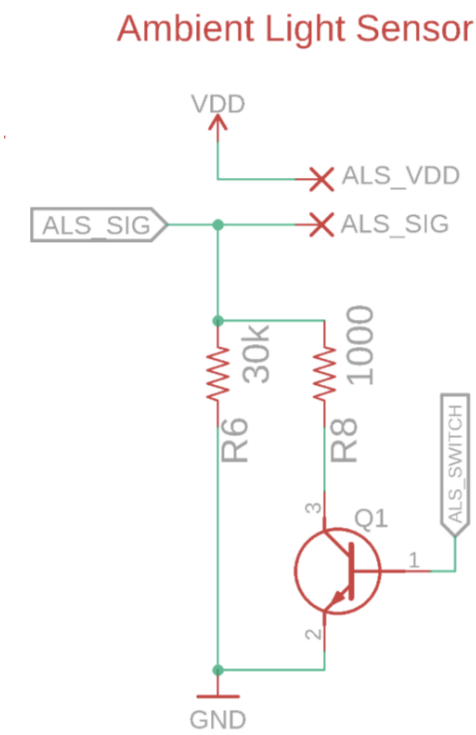


Figure 2.16: Circuit schematic of the Lumos ambient light sensor. ALS_SIG is connected to the sensor emitter, ALS_VDD connected to sensor collector. The transistor switch (Q1) dynamically adjusts the resistor divider to extend measurable range under high illuminance conditions.

The combined filter–sensor system was calibrated using a ground-truth spectroradiometric instrument, the *f.luxometer* [42], across a range of representative indoor and outdoor conditions. Indoor measurements were used to verify linearity across typical lighting levels, while outdoor tests established the sensor's behavior under saturation conditions. Representative calibration data are summarized in Table 2.1 and Table 2.2, showing sensor voltage readings and corresponding reference melanopic lux values obtained from the *f.luxometer*. Regression analyses for both indoor and outdoor datasets are shown in Figure 2.17 and Figure 2.18.

Table 2.1: Measured output of the Lumos ambient light sensor across representative indoor lighting scenarios, showing sensor voltage and corresponding reference melanopic lux values measured by the *f.luxometer*.

Indoor Scenario	**Sensor Voltage (mV)**	**Illuminance (m-lux)**
Room fluorescent lights	5	30
Looking directly at fluorescent lights	80	129
Looking at Wyze bulb (max brightness)	250	400
Looking out window from room	680	3,400
Common room, facing inward	120	338
Common room, facing window	600	2,200
Common room, facing outside	1,500	6,500
Common room, facing outside near exit	2,500	11,000

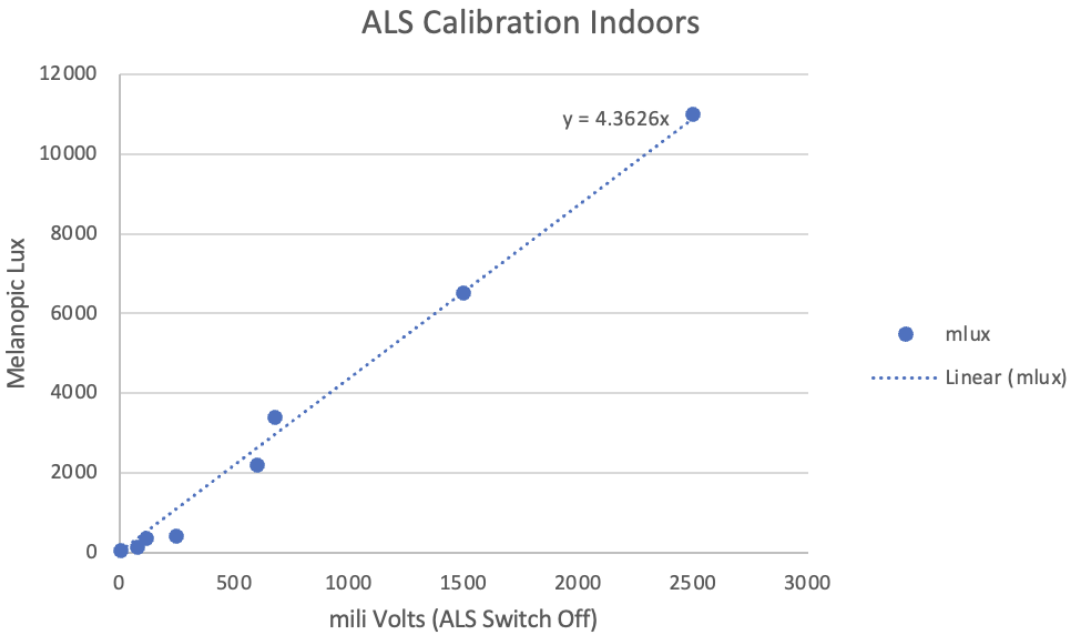


Figure 2.17: Calibration results for the Lumos ambient light sensor under indoor lighting conditions, showing a strong linear correlation between sensor voltage and melanopic lux.

Table 2.2: Measured output of the Lumos ambient light sensor across representative outdoor lighting scenarios, showing sensor voltage and corresponding reference melanopic lux values measured by the *f.luxometer*.

Outdoor Scenario	**High Voltage (mV)**	**Illuminance (m-lux)**
Facing the lake	211	22,000
On rooftop (facing upward)	800	45,000
Facing trees	55	4,500
Facing the sun	1,460	55,000
On outdoor couch	80	12,000
Lying on ground	400	24,000
On the deck, looking at sky	3,000	38,000

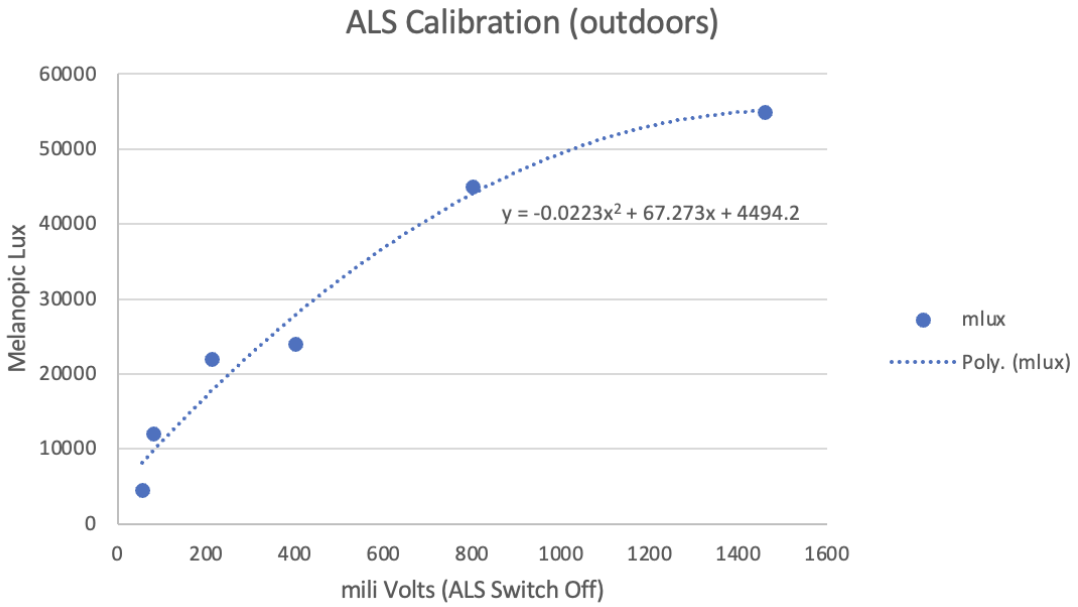


Figure 2.18: Outdoor calibration results for the Lumos ambient light sensor showing a second-order polynomial fit ($y = -0.0223x^2 + 67.273x + 4494.2$) due to partial saturation of the photodiode at high illuminance levels.

As shown in Table 2.1 and Figure 2.17, the photodiode produced currents high enough to saturate the analog-to-digital conversion path. This necessitated the digital switching mechanism in Figure 2.16, which allowed the circuit to dynamically lower the transimpedance resistance when high illumination levels were detected.

In the final clinical-trial configuration, this switching feature was disabled to reduce routing complexity near the critical antenna region. As a result, the sensor saturates at approximately 14,000 melanopic lux, a level that typically indicates outdoor exposure and is far above the roughly 1,000-lux threshold associated with maximal melatonin suppression [109].

Summary. The Lumos ambient light sensor, optimized for melanopsin-weighted response, demonstrated strong linearity under indoor conditions and predictable nonlinear behavior under bright outdoor conditions. The inclusion of a filter, optimized geometry, and calibration against the *f.luxometer* ensures reliable measurement of physiologically relevant light levels, enabling accurate quantification of real-world melanopic exposure in both research and clinical contexts.

2.5 User Detection Sensor Iteration

Reliable user detection is essential for determining when the glasses are actively being worn. This capability is particularly important because adherence to light therapy outside controlled settings is difficult to verify using self-report alone. In a pilot study of bright-light therapy for seasonal affective disorder, self-reported daily lamp usage was found to be unrelated to the actual duration recorded by the device's built-in meter, indicating that patient logs substantially overestimated true exposure time [65]. A robust on-device wear sensor therefore enables accurate, automatic usage logging and provides an objective measure of adherence that can support both clinical research protocols and real-world therapeutic use. The following sections describe the iterative development of the user detection sensor and the design considerations that informed its final implementation.

2.5.1 Capacitive sensing

Capacitive sensing was selected as the first user-detection approach because it is low-power, inexpensive, and selective to conductive objects (e.g., skin), minimizing false positives from fabric or plastics. A diagram of the capacitive sensor is shown in Figure 2.19. The

capacitive sensor features a flexible printed circuit board laminated to the inside surface of the arm's lid.

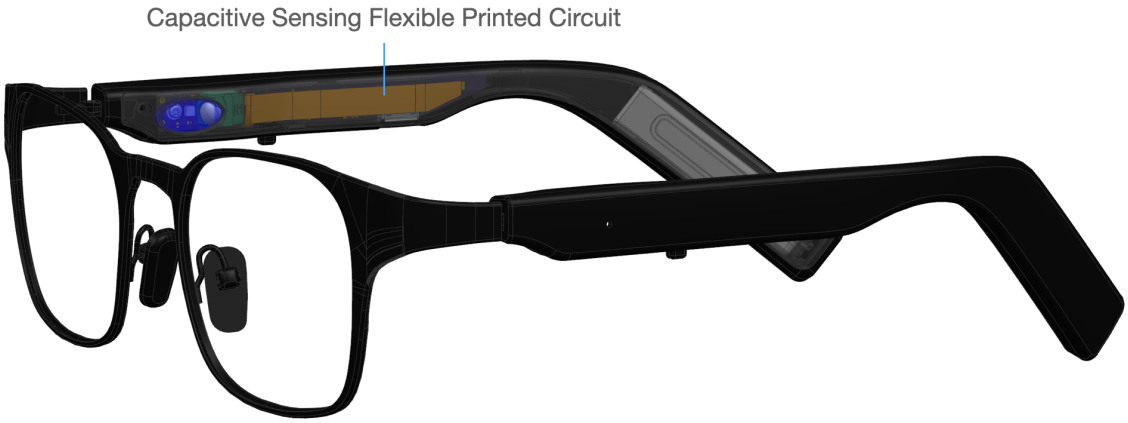


Figure 2.19: Prototype implementation of the capacitive user-detection sensor. A flexible printed circuit (FPC) electrode runs along the inner surface of the temple; the wearer's skin forms the return electrode via body capacitance. The theory of operation of the capacitive sensor is shown in Figure 2.20 below.

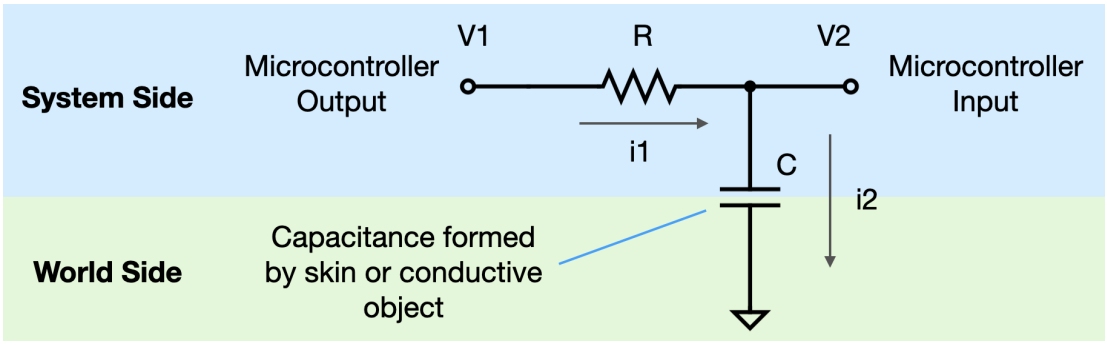


Figure 2.20: Conceptual RC topology for capacitive sensing: the microcontroller drives the sensing node through a resistor R, the skin-dependent capacitance C charges toward the drive voltage, and the sampled node voltage is used to estimate C.

The flexible PCB on the device acts as one side of the capactiro electrode, while the human body provides the complementary plate through parasitic body–ground capacitance. When the temple is worn, the effective capacitance increases; when removed, it decreases.

The measurement uses the RC topology shown in Fig. 2.20: a series resistor R and unknown capacitor C are driven from a logic output and observed by an ADC input.

By Kirchhoff's current law, the currents through the resistor and capacitor are equal:

$$i_1 = i_2, \tag{2.1}$$

where

$$i_1 = \frac{V_1 - V_2}{R} \qquad \text{and} \qquad i_2 = C\,\frac{dV_2}{dt}. \tag{2.2}$$

Equating these yields the first-order differential equation

$$\frac{V_1 - V_2}{R} = C\,\frac{dV_2}{dt}, \tag{2.3}$$

which, for a constant step input V_1, has the standard solution

$$V_2(t) = V_1\big(1 - e^{-t/RC}\big)\,. \tag{2.4}$$

The time constant $\tau = RC$ defines the 63% rise time. By timing the interval required for the sense node to reach a fixed threshold voltage, C can be inferred for a known R. A larger capacitance produces a slower rise, enabling a threshold on τ to classify the *worn* and *not worn* states.

In the firmware implementation, the standard Arduino *CapacitiveSensor* library [15] performs this measurement by cycling the source and sense pins at high frequency and estimating the relative capacitance from timing differences. Since the library is not directly compatible with the nRF52 architecture, the algorithm was ported and optimized for the Lumos firmware to ensure clean, low-noise measurements under the same timing principle.

Selectivity. Since the sensor responds primarily to conductive bodies, everyday non-conductive coverings (hair, most fabrics, plastics) do not spuriously trigger the *worn* state. This material selectivity, combined with the electrode's placement along the temple, provided reliable wear detection in bench and field tests and a foundation for subsequent adherence analytics.

Temperature, humidity, and other factors can cause signal noise for the capacitive sensor, and after building the prototype, it was determined that while it was a reliable sensor for the author's head, the capacitive sensor does not have enough signal-to-noise ratio sufficient to cover a broad range of head sizes. Capacitive sensing works well for very close distances, such as touch sensors with only a thin piece of plastic in between the

inner device plate and the finger. However, when a person has a smaller head, the distance between the temple and the plate becomes too large to induce a sufficient signal for basic algorithms to capture. Figure 2.21 shows that proximity sensing has significantly better signal-to-noise ratio than capacitive sense, which is important for reliability. It is worth noting that Apple's AirPods also use an infrared proximity sensor for user detection, while reserving capacitive touch sensing for controls [50].

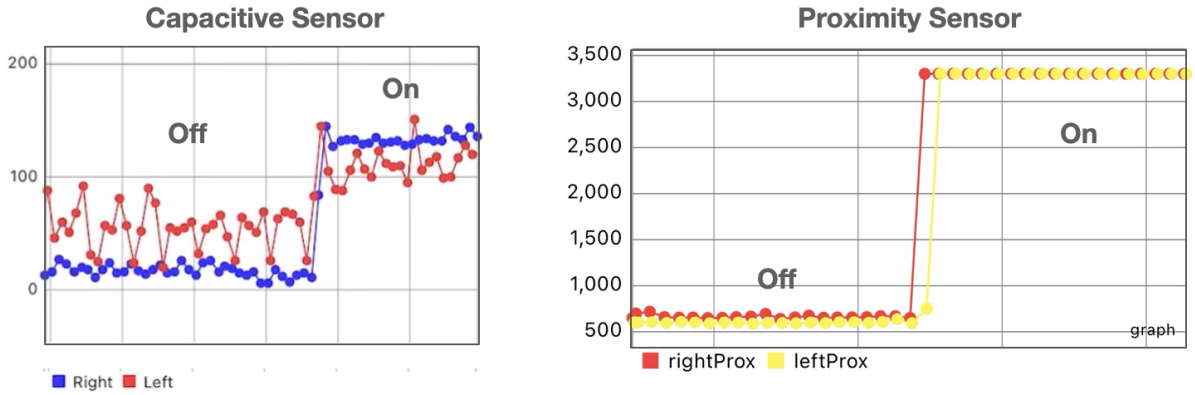


Figure 2.21: Capacitive sensing signal (left) vs proximity sensor (right)

2.5.2 Infrared proximity sensing

The proximity sensor relies on the reflection of infrared (Infrared (IR)) light. It consists of two main parts: an IR emitter and an IR ambient light sensor. The sensor detects light from the emitter reflecting off a nearby surface. Typically, the closer a surface is to the sensor, the more light reflected resulting in a higher signal. This principle is widely used in smartphones to detect when the phone is held close to a user's ear, automatically switching audio output to the receiver.

Given that the proximity sensor demonstrated better performance than capacitive sensing, and to minimize mechanical redesigns and avoid mold or tooling rework, an attempt to integrate the proximity sensor through the existing LED window occurred. In this configuration, the sensor is mounted directly on the PCB in front of the light engine and positioned to emit and receive light through the same optical window. This approach required minimal design modifications, involving only an additional component on the PCB. The board was fabricated and tested for performance. see Figure 2.22 for the initial tested location of the sensor.

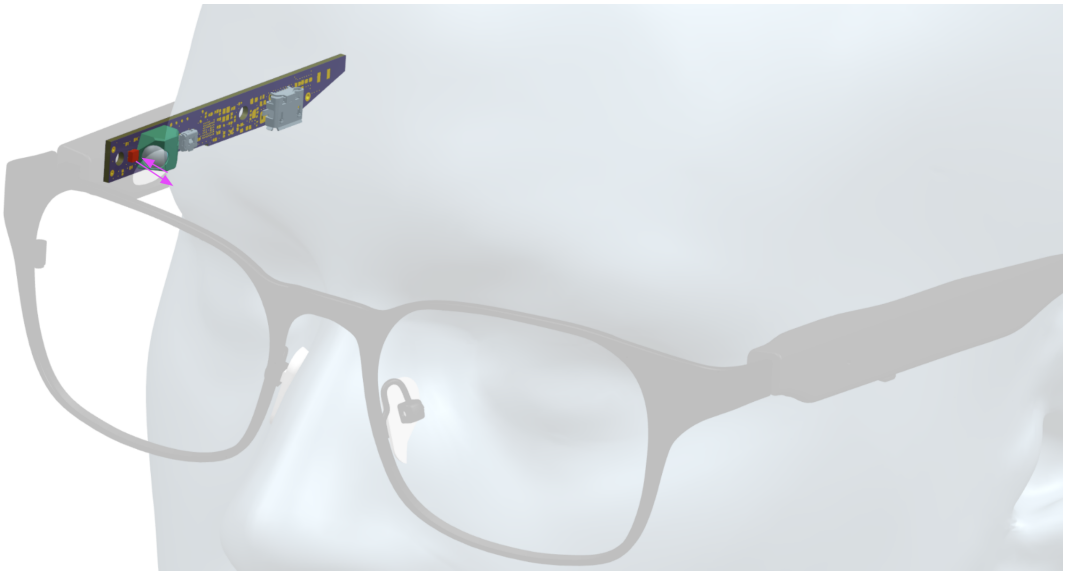


Figure 2.22: Concept of proximity sensor sharing the LED window.

Experimental testing confirmed that this method functioned as intended; however, the signal-to-noise ratio decreased significantly for users with smaller head sizes. Therefore, it was necessary to reposition the proximity sensor closer to the actual contact region of the frame with an additional set of flexible printed circuit boards (Flexible Printed Circuits (FPCs)). These circuits housed the proximity sensor, supporting electronics, and adhesive tapes and foams to secure the assembly against the inner housing. Furthermore, a dedicated optical window was added to the arm of the glasses, allowing infrared transmission in the sensor's operating wavelength. A schematic of the final design is shown in Figure 2.23.

One challenge was false triggering caused by ambient infrared light, especially under sunlight. To mitigate this, a time-sequential measurement approach was implemented in firmware. The IR emitter is first turned off to record the ambient IR baseline, followed by a second measurement taken immediately after the emitter is activated. The difference between these two readings isolates the reflected component from the proximity emitter, effectively rejecting ambient interference. This technique substantially improved sensor reliability under varying lighting conditions.

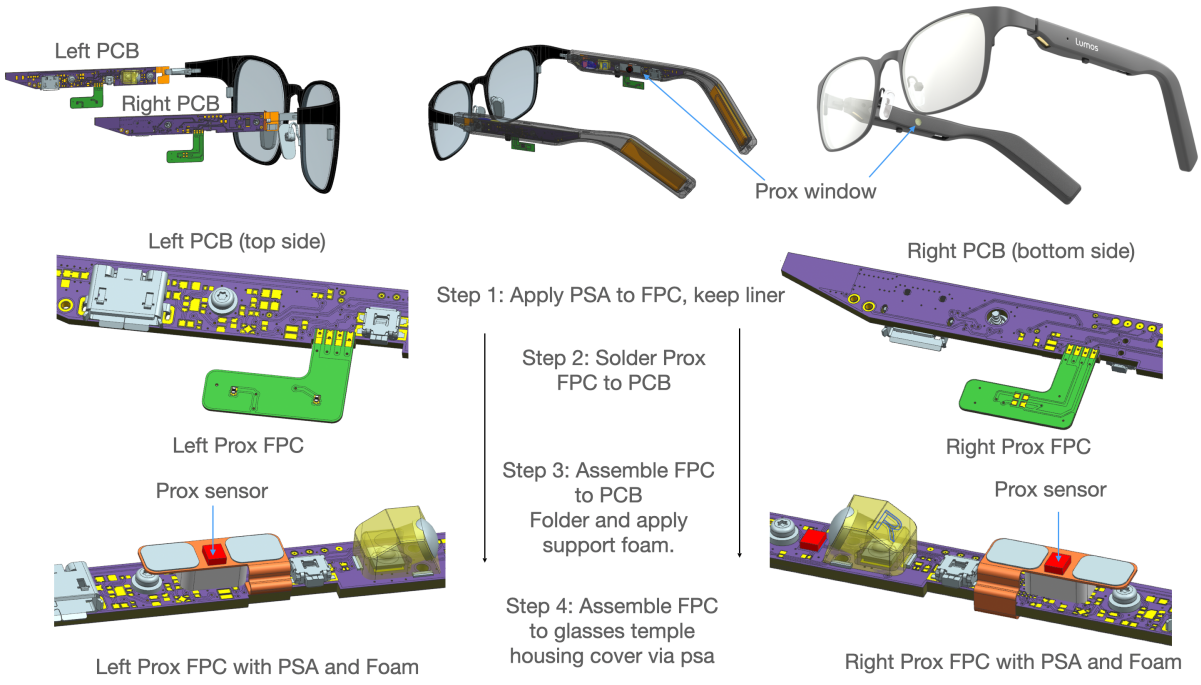


Figure 2.23: Final proximity sensor design integrated with flexible circuit and IR window.

2.6 Electrical System

The electrical subsystem of the Lumos glasses integrates sensing, control, and power management circuits into a compact printed circuit board (PCB) designed by the author. The initial hardware architecture and early board layouts were developed by James Ro, the author's founding teammate at Lumos Health, establishing the foundation for component selection and signal routing. Building upon this foundation, the author took over the design in 2021, adding the proximity sensor, improving system integration and manufacturability, and optimizing antenna performance. The design work was conducted in Autodesk Eagle and later migrated to *Fusion 360 Electronics* for enhanced 3D visualization and seamless integration with the mechanical enclosure. The final board layout is shown in Figure 2.24, and a high-level block diagram of the system architecture is provided in Figure 2.25.

The central component of the system is the *Nordic Semiconductor nRF52832* microprocessor, a low-power System on Chip (SoC) that integrates a 64 MHz ARM Cortex-M4 CPU, BLE radio, and multiple peripheral interfaces. The Microcontroller Unit (MCU) interfaces with the proximity sensor and ambient light sensor through flexible printed circuits

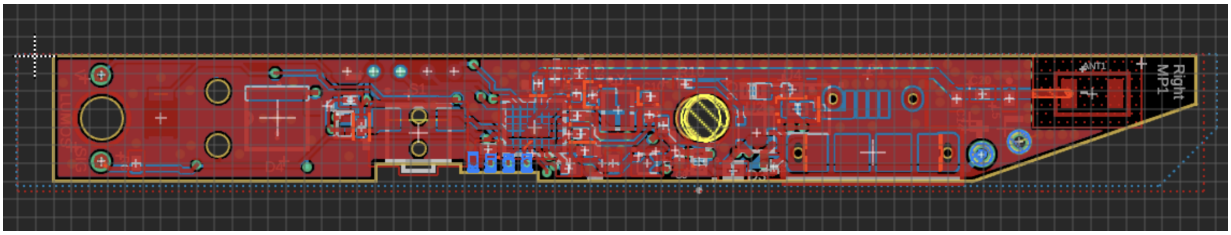


Figure 2.24: Top view of the Lumos main PCB layout, showing compact routing of sensing, logic, and power sections.

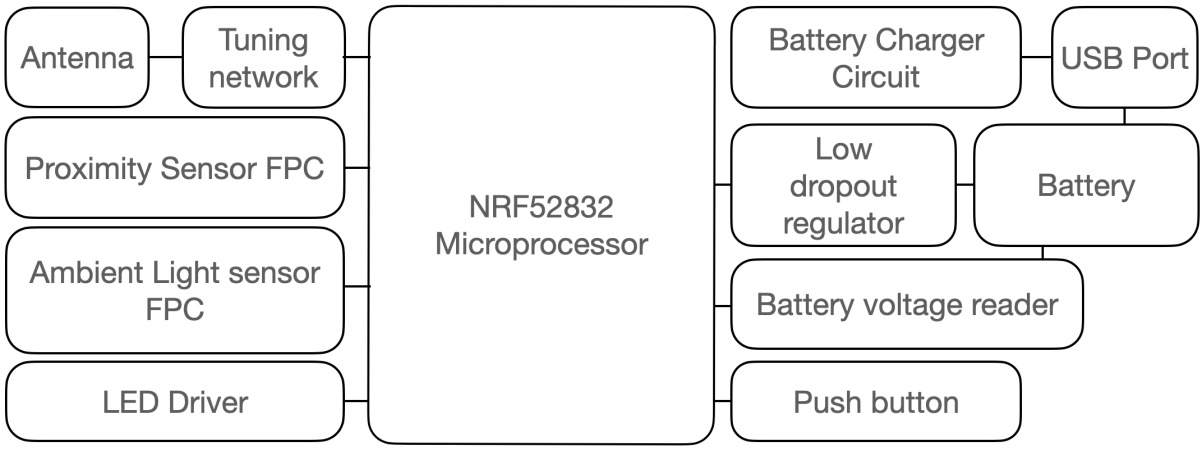


Figure 2.25: High-level electrical block diagram of the Lumos system.

(FPCs) connected to dedicated I/O pins. The microcontroller also controls the therapy LED driver which regulates the light output used for circadian rhythm and light therapy.

A rechargeable lithium-polymer battery powers the system. The battery is charged through a dedicated constant current constant voltage charging circuit connected to the onboard USB port. Once charged, the battery supplies power to the rest of the circuitry through a low-dropout voltage regulator (LDO), which ensures a stable supply voltage to the MCU and associated sensors. A voltage divider circuit continuously monitors the battery level, allowing the firmware to track charge status and transmit it to the companion smartphone application via BLE.

The board also includes a tactile push button for user input, enabling activation of the therapy light, interaction with the PVT, and execution of other control functions. A Matching Network was implemented to optimize the BLE antenna impedance and radiation efficiency, with validation and technical support provided by engineers at *Nordic Semicon-*

ductor [82].

Throughout the design, careful consideration was given to isolating analog and digital noise domains, optimizing the placement of power decoupling components, and maintaining consistent ground return paths. The resulting design achieves a high degree of integration and robustness within the mechanical constraints of the slim glasses arm, enabling reliable sensing, communication, and power performance in a wearable form factor.

2.7 Firmware Architecture (High-Level Summary)

The author developed the firmware for the left module of the Lumos glasses which runs on the *Nordic Semiconductor nRF52832* SoC. It implements Bluetooth Low Energy (BLE) communication, sensing, actuation of the therapy light, and safety/control features needed for both clinical and commercial operation. To protect proprietary details, this section presents a high-level summary without disclosing state diagrams, register maps, or unique identifiers.

System Overview

At a high level, the firmware coordinates five functions:

1. **Wireless Communication:** A custom BLE service exposes characteristics for light control, proximity readings, ambient light values, battery telemetry, calibration, and a PVT interaction channel.

2. **Sensing:** Periodic polling of the proximity and ambient light sensors produces filtered measurements used for wear detection and context-aware behavior.

3. **Light Engine Control:** A hardware-Pulse-Width Modulation (PWM) path drives the therapy LED, with duty cycle and effective frequency chosen for optical safety and perceptual comfort.

4. **Power and Reliability:** A watchdog timer, adaptive polling based on client subscriptions, and idle behaviors help reduce current draw while preserving responsiveness.

5. **Calibration and Modes:** Non-volatile storage (Flash Memory) holds calibration constants and mode flags; a clinical mode enforces app-supervised usage, while a user mode allows limited stand-alone operation.

BLE Service Model

The device operates as a peripheral with a single custom service. Characteristics (names only, no UUIDs shown) include:

- **Light Control:** Read/write of light state and intensity parameters; notifications used to reflect state to connected clients.
- **Proximity / ALS Telemetry:** Read/notify for proximity and ambient light values. When a client subscribes (CCCD write), the firmware increases the corresponding polling rate to improve responsiveness.
- **Battery Telemetry:** Read/notify for battery voltage to support app-side state of charge estimation and user feedback.
- **Calibration and Configuration:** Read/write of persistent calibration constants (e.g., maximum safe intensity, proximity thresholds) and an operational mode flag (clinical vs. user).
- **PVT Game Channel:** A lightweight command/notify pathway to coordinate trial rounds (start signal and per-round result codes).

Sensing and Wear Detection

Wear detection relies on proximity sensing at both temples; both sides must exceed a threshold to classify the device as "worn," mitigating false positives when the frame is folded. The firmware also samples ambient light to support app logic (e.g., day/evening behaviors) and adapts sensor polling intervals based on client subscriptions to conserve power.

Therapy Light Control

The therapy LED is driven by PWM with:

- A calibrated ceiling that enforces eye-safety constraints stored in Flash Memory.
- Adjustable frequency and duty cycle to accommodate clinical and user modes.
- Smooth ramps on connect/disconnect and mode changes to avoid abrupt transitions.

Calibration, Persistence, and Modes

Calibration constants and mode flags are stored in internal Flash Memory. Key items include:

- **Safety Intensity Limit:** Upper bound for duty cycle, used as a ceiling across modes.
- **Proximity Thresholds:** Baselines and deltas that support robust wear detection across users.
- **Clinical/User Mode Flag:** In clinical mode, light activation requires an active app connection and a valid wear state; in user mode, the button may toggle light locally within safety limits.

Values can be updated over BLE by authorized tooling.

Power, Timing, and Reliability

A hardware watchdog periodically resets the system if the main loop stalls. Polling periods for sensors and telemetry are longer by default and automatically shorten when a client subscribes to notifications (CCCD set), balancing power with responsiveness. Advertising packets include manufacturer data for device classification; connect/disconnect events update the light state and timers to provide user feedback and manage timeouts.

Psychomotor Vigilance Task (PVT)

A minimal embedded loop supports a single-round PVT for research workflows. Upon a start command from the app, the device presents a simple reaction-time stimulus using the light and records the user's button response. The result is encoded and notified back to the app for storage and analysis. Detailed timing constants, scaling functions, and admissibility rules are withheld.

Safety and Confidentiality

The firmware enforces an intensity ceiling, app-gated activation in clinical workflows, and wear detection checks prior to light enable. To protect proprietary methods, the following

are intentionally omitted: unique identifiers (e.g., UUIDs), pin assignments, register settings, state machine diagrams, timing constants, filter parameters, and file formats. The description above is sufficient for scientific reproducibility of study logic while preserving commercial confidentiality.

2.8 App and Software

The Lumos mobile application serves as the central hub of the system. It interfaces with the glasses via BLE, provides user authentication and control, presents a graphical interface, and manages data transfer with the cloud. Screenshots of the iOS version are shown in Figure 2.26.

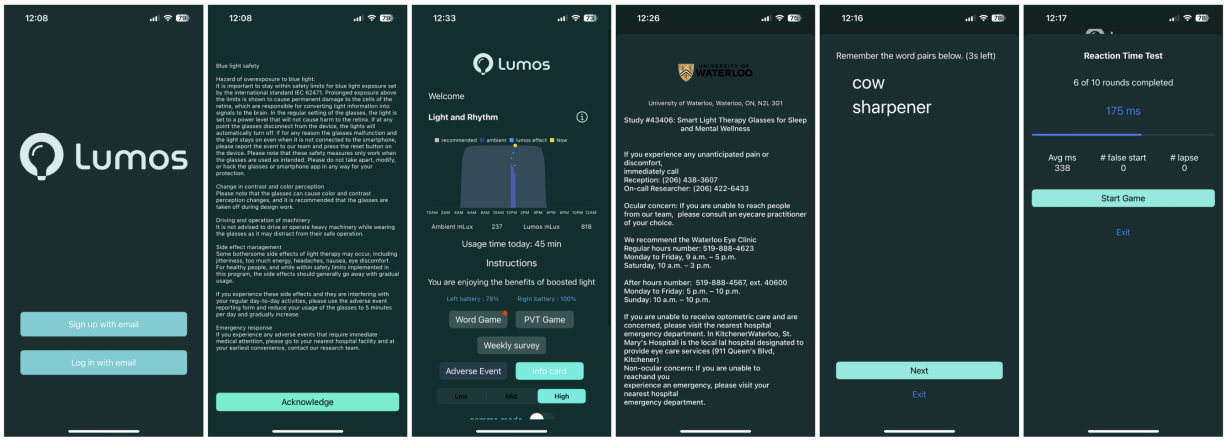


Figure 2.26: Screenshots of the Lumos mobile application (iOS version shown).

Using data transmitted from the BLE firmware, the app records the total light-therapy duration and determines when the glasses are being worn.

Wear detection is based on proximity-sensor data from both the left and right arms of the glasses. Both sensors must exceed a defined threshold to classify the device as being worn. This logic prevents false positives that could occur in the folded state, where one arm may occlude the other. Multiple rounds of testing across diverse head sizes were performed to determine the optimal threshold values that reliably distinguish between worn and folded conditions.

Because the nRF52 SoC provides limited onboard Flash Memory, the app plays an essential role in cloud synchronization. During the clinical trial, the light engine could be

activated only when the app verified that the user was wearing the glasses. This ensured that all therapy usage data were accurately tracked and uploaded to the cloud database.

In addition, the app calculates the appropriate light schedule based on the time of day and ambient-light measurements to determine whether the therapy light should be on and what feedback to deliver to the user.

The app's backend infrastructure is powered by Google Firebase, which provides Application Programming Interfaces (APIs) for user authentication, permission management, password resets, and secure data storage. Firebase also supports data persistence, allowing offline operation and automatic synchronization once connectivity is restored.

To integrate with the University of Waterloo research workflow, Firebase is linked to Qualtrics (a research-grade survey platform) via Zapier, an automation service that ensures survey responses are automatically synchronized with participant records in the cloud.

An administrator-facing version of the app enables real-time participant monitoring, and allows clinical staff to review usage adherence, detect potential adverse events, and follow up with participants as required.

Finally, Firebase stores a custom hash representing each participant's group allocation. This hash determines whether the glasses operate in bright-light (treatment) or dim-light (placebo) mode. The decoding key for this hash was held exclusively by the sponsor monitor, Jianping (Felix) Xu, ensuring that neither the author nor the research team could access treatment assignments during the trial or preliminary analysis, preserving the integrity of the double-blind design.

The iOS application and the core architecture of the Android version were developed by the author. The final Android clinical release and the administrator-facing app were completed by Jianping (Felix) Xu, who served as the sponsor monitor for the study.

2.9 Chapter Conclusion

This chapter presented the engineering development of the Lumos wearable light–therapy system from operating principle and hardware evolution to electrical design, firmware architecture, and the companion mobile application. The core invention centers on a wavelength-selective light engine and nanocoating that enable a slim, eyewear-like form factor delivering melanopsin-targeted illumination while preserving natural vision. Iterative prototyping from early proofs-of-concept to production-ready hardware established a

manufacturable, durable platform with swappable lenses and TR-90 arms that house the electronics.

On the electronics side, the nRF52832-based main board integrates sensing, power management, and wireless connectivity with an antenna Matching Network validated in collaboration with Nordic Semiconductor. The system transitioned from capacitive user detection to infrared proximity sensing on flexible FPCs, paired with synchronous ambient rejection for robust wear classification across head sizes. A melanopsin-weighted ambient light sensor was designed and calibrated against a reference spectroradiometric system, enabling physiologically meaningful exposure tracking in real-world settings.

Eye safety and calibration were addressed through a combined measurement–simulation framework aligned with IEC 62471. Third-party testing confirmed an Exempt (RG0) classification at 200 mm, while optical modeling of near-eye geometry and time-dependent retinal averaging informed conservative operating margins. A per-unit calibration pipeline (using onboard sensing correlated to reference spectra) sets a device-specific PWM ceiling and stores parameters in non-volatile memory to maintain safety compliance over operating conditions.

Firmware running on the SoC provides BLE services, sensor polling, interrupt and button handling, safe light control, and a minimal PVT pathway. The mobile application controls light activation on verified wear detection, manages time-of-day and ambient-light logic, and synchronizes usage data to Firebase. Research surveys integrated via Zapier and an administrator view (developed and maintained by Jianping (Felix) Xu) enables participant monitoring. Treatment assignment is controlled via a hashed code to preserve double-blind conditions.

Together, these subsystems form a cohesive, clinically deployable platform that balances optical efficacy, user comfort, safety, and data integrity. The engineering decisions documented here directly support the study's scientific aims. The next chapter describes the clinical protocol, measurement endpoints, and analysis methods that build on this engineering foundation to evaluate the Lumos system's effects on circadian and mental-health outcomes.

Chapter 3

Clinical Results

3.1 Overview

This chapter presents the implementation and results of the Lumos smart light therapy glasses evaluated in a double-blind, randomized, placebo-controlled crossover clinical trial. The study was conducted over sixteen weeks, with participants crossing over between treatment conditions at week 8.

The primary hypotheses were that daily use of the Lumos glasses delivering high-intensity, circadian-effective light would significantly reduce depressive symptoms and sleep-disturbance scores compared with low-intensity (placebo) exposure, and that these benefits would be accompanied by improvements in psychomotor vigilance and working-memory performance. Secondary hypotheses proposed that individual factors, particularly daily usage time, ambient light exposure, baseline symptom severity, and eye pigmentation, would moderate treatment response. Age and sex were also expected to exert smaller but measurable influences on outcome variability.

Primary endpoints included changes in depressive symptoms (Montgomery–Åsberg Depression Rating Scale (MADRS)), sleep disturbance (Patient-Reported Outcomes Measurement Information System Sleep Disturbance Short Form (PROMIS) Short Form), psychomotor vigilance (reaction time, Psychomotor Vigilance Task (PVT)), and associative memory (Word-Pair accuracy). Secondary analyses examined how adherence (usage hours), ambient melanopic light levels, and demographic factors influenced these outcomes. Adverse events were recorded weekly to assess tolerability and safety.

Overall, we found that bright-light exposure produced measurable improvements in

mood and sleep relative to dim-light control consistent with the primary hypotheses. However, the aggregate MADRS effect did not reach statistical significance until the data were stratified by eye-color group, revealing strong subgroup-specific patterns. Dark-eyed participants (brown-eyed Caucasian and non-Caucasian groups) exhibited clear Phase-1 improvement under bright-light. Conversely, participants with light-colored eyes (blue, green, hazel) showed greater initial improvement under dim-light control, suggesting a differential response linked to iris pigmentation. This finding is further addressed in the Discussion section 4.1, where correlations between eye color, light transmission, and potential differences in iris melanopsin sensitivity are considered as possible explanatory mechanisms.

Both daily usage time and ambient light exposure (melanopic lux) moderated outcomes, with higher exposure associated with greater improvements in several subgroups. Psychomotor vigilance improved robustly across all participants regardless of eye color, while the Word-Pair memory test showed the least clear pattern until usage time is accounted for. Adverse events were generally mild and infrequent across the study, and the Lumos glasses were well tolerated overall. Notably, light-eyed participants reported more discomfort when bright-light was administered first, with persistence after crossover, whereas darker-eyed groups reported more headaches in the dim-light condition. Full protocol details are provided in Appendix P.

3.2 Methods

3.2.1 Design

Participants ($n = 73$) were randomized to one of two groups (Alpha, Beta) that alternated between *active* and *low-light* (placebo). For the first 8 weeks, the Beta group ($n = 36$) received bright-light active treatment while the Alpha group ($n = 37$) received low-light control. After week 8, the groups crossed over, with the Alpha group receiving active treatment and the Beta group receiving low-light control. Masking was maintained for participants and study staff, including the author and research team. The app enforced allocation, phase timing, and blinded crossover, with the encryption key held by the study monitor and the Data Safety and Monitoring Board.

3.2.2 Participants

Adults ($\geq$18 years) with access to a smartphone, who experienced at least minor mood or sleep symptoms, and spent on average less than two hours outdoors per day were

eligible for the study. Exclusions included severe depression requiring urgent intervention, ocular disease that could affect light safety, photosensitizing medications, and night shift work. Recruitment, consent, and baseline assessments were performed via Qualtrics survey, followed by a verification and consent call from the clinical team.

3.2.3 Clinical team

The clinical team was led by the Principal Investigator (PI), Dr. Jonathan Oakman, a licensed psychologist in Ontario; the student investigator, Lucas Tang; and volunteer research coordinators from the psychology department at the University of Waterloo. The team was responsible for participant intake, monitoring, and follow up. Adverse events were handled by Lucas Tang, Dr. Oakman, and the Data Safety and Monitoring Board, who worked with the Research Ethics Boards to report each incident.

3.2.4 Randomization, Allocation Concealment, and Masking

Participants were assigned to **Alpha** or **Beta** via slot-based randomization with concealed mapping; allocation and crossover were automated in the app/cloud to preserve masking. No unmasking events occurred due to unforeseen events, and all unmasking followed the standard protocol. A partial unmasking was done for data analysis where Alpha and Beta groups were disclosed without revealing which group received treatment first. This allowed for an unbiased analysis. Before full unmasking, the author presented initial assessment of the data to the Data Safety and Monitoring Board with strong evidence that the Beta group received treatment first. At this point permission was granted for full unmasking, where the study monitor confirmed that Beta indeed received treatment first. Analysis then continued for secondary findings and multiple regression with the unmasked data.

3.2.5 Intervention

During *active* phases, the glasses delivered bright-light targeted for high melanopic effectiveness, around 500 to 700 melanopic lux. During *low-light* phases, output was minimized to maintain device perception while limiting physiological dose. Due to the hardware limitation of this version, the low-light was set to a value around one tenth of the bright dosage, around 50 to 70 melanopic lux. This meant that the low-light intervention may have some minor effect, and could be considered active control. Participants with no prior knowledge of the light levels would find it difficult to tell if they were in the treatment or

control group, allowing for a good placebo. It is possible that the proximity sensors emitted sufficient infrared light to the user to have a minor effect present in both groups. As such, the placebo group may have had some minor treatment effects through low dose blue-light and infrared therapy, as well as being able to use the glasses as a blue-light blocker in the evenings. In a sense, this can be considered an active control group.

3.2.6 Device Use, Sensing, and Data Capture

Wear detection (Infrared (IR) proximity) and ambient light sensor were streamed via Bluetooth to the smartphone and uploaded to the secure cloud database. The glasses were considered on the user when both arms' sensors crossed a detection threshold, and only then would the light turn on. This ensured that if the user wanted to receive light therapy, they must be connected to the smartphone, and have the glasses on properly. Proximity sensor data is sent multiple times a second to the smartphone via Bluetooth low energy. Each glasses' temples also have an ambient light sensor which streams data multiple times a second to the smartphone. To conserve internet use for participants, the data is first aggregated on a minute per minute basis, measuring number of seconds used for that minute, as well as the average ambient light in that minute, and uploaded to the cloud.

3.2.7 Measures

Each week, participants completed four short assessments through the Lumos app to track mood, sleep, alertness, and memory. These instruments were selected to capture both emotional and cognitive effects of light exposure while keeping the testing experience simple and consistent across participants. A brief overview is provided below, with detailed scoring procedures, reliability statistics, and psychometric references in Appendix C.

- **Mood (Montgomery–Åsberg Depression Rating Scale, Self-rated version (MADRS-S)).** Participants rated their mood and related symptoms using the self-rated version of the Montgomery–Åsberg Depression Rating Scale. This short questionnaire covered aspects such as sadness, motivation, and sleep, providing a weekly measure of overall depression severity.
- **Sleep Quality (Patient-Reported Outcomes Measurement Information System Sleep Disturbance Short Form (PROMIS) Sleep Disturbance).** This brief survey asked about sleep quality, depth, and restfulness over the past week. It offered an easy way to track perceived changes in sleep patterns over time.

- **Alertness and Reaction Time (PVT).** A quick in-app reaction test measured how fast participants responded to a light signal from the glasses. Slower reaction times indicated reduced alertness or fatigue.
- **Memory (Word-Pair Recall Test).** Participants studied short word pairs and later recalled the second word when shown the first. The number of correct recalls provided a simple measure of working memory and focus.

3.2.8 Sample Size and Power

Power analysis was conducted during study planning to ensure adequate sensitivity for detecting meaningful changes in mood, sleep, alertness, and memory outcomes. This section provides a brief overview, and the full calculation details, assumptions, and references are presented in Appendix D.

The analysis compared two treatment conditions at the week 8 crossover point, using a two-sample test on means ($\alpha = 0.05$, power $= 0.80$). While the preliminary protocol (Appendix P) used averaged standard deviations, the final power estimates were updated using the corrected pooled variance method. Sample size requirements were derived from published light-therapy studies on comparable outcomes. Across endpoints, a minimum of 25 participants per arm was sufficient to achieve 80% power; the final design used $n = 48$ per arm ($N = 96$) to account for attrition and enable subgroup analyses.

Table 3.1: Summary of power analysis assumptions. Detailed derivations in Appendix D.

Endpoint	Reference Study	Required n/arm (two-sided)
Depression (MADRS)	Lam et al., 2016 [60]	25
Sleep (PSQI) proxy for PROMIS	Akyar & Akdemir, 2014 [8]	9
Vigilance (PVT)	Rosa et al., 2018 [78]	9
Memory (Word-Pair)	Bersani et al., 2008 [18]	34

3.2.9 Ethics, Registration, and Data Handling

This study was reviewed and received ethics clearance through the University of Waterloo Research Ethics Board (REB) (`43406`). The approved protocol (Version 18; March 14, 2024) is provided in Appendix P. All data were de-identified and stored on secure servers. The study was also registered on *ClinicalTrials.gov* [98] (Identifier: NCT07168954).

3.3 Results

3.3.1 Participant Flow and Sample

Participants were first automatically filtered for eligibility through an online questionnaire via Qualtrics. If they qualified, a member on the clinical team reached out to confirm eligibility and informed consent via phone or video call. Afterwards, participants were then encoded to a unique encrypted ID, the database for blinding control, and glasses were shipped to them. Once they connected the glasses to the app, the app would pull the encrypted ID from the database, decrypt it for the treatment arms, and begin treatment. The participant flow is shown in Figure 3.1 below.

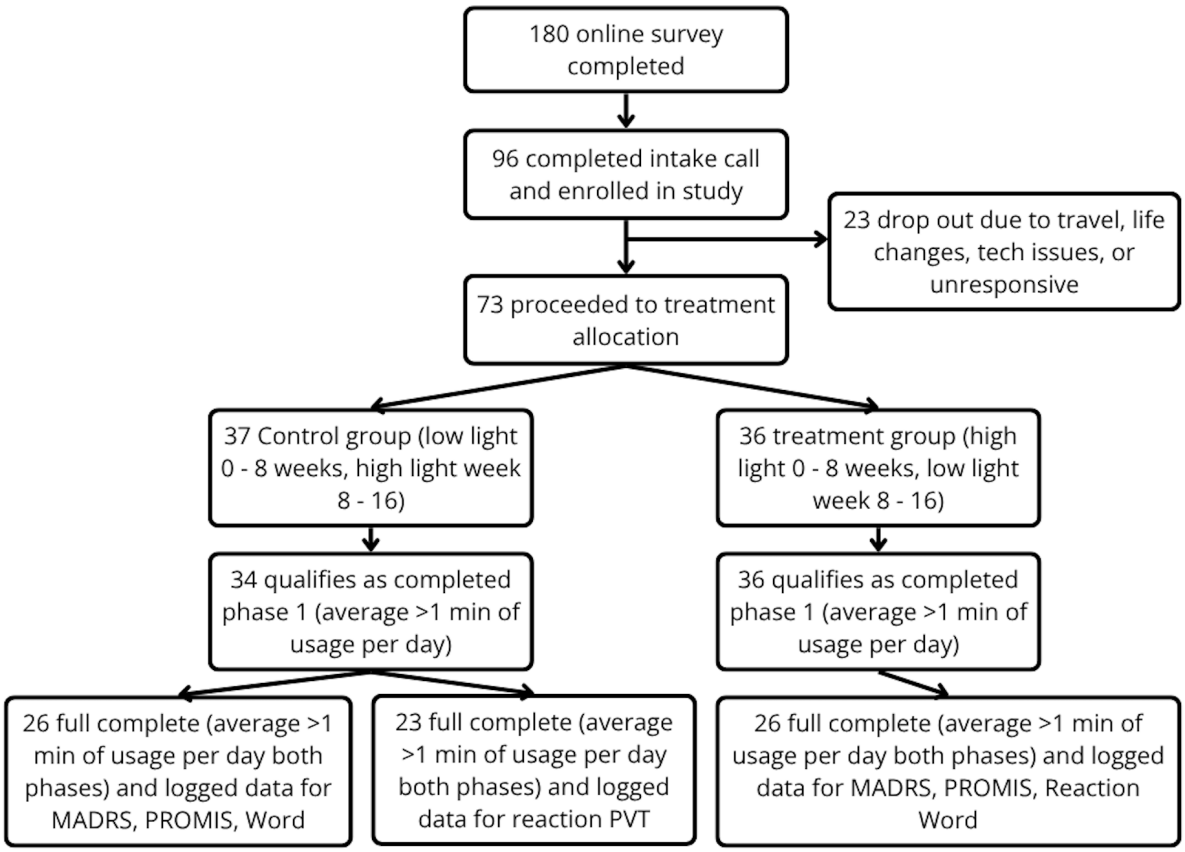


Figure 3.1: Participant flow

3.3.2 Baseline Characteristics

Baseline estimation method. As some participants waited several days to weeks before receiving their glasses and completing device setup, the baseline score is not necessarily the score recorded at study intake. To correct for this delay, all participants were baseline-aligned to the date their light-therapy glasses were first connected (*Day 0* ($t = 0$)).

For each participant i and outcome variable (MADRS or PROMIS), a baseline value B_i was estimated using the nearest available measurement before ($v_{\text{pre}}, t_{\text{pre}} < 0$) and after ($v_{\text{post}}, t_{\text{post}} > 0$) Day 0, where v is the score and t is the number of days from the connection date. If a measurement existed exactly on Day 0 , that value was used directly:

$$B_i = v_0.$$

Otherwise, B_i was estimated as a weighted average of the closest pre- and post-Day 0 measurements:

$$B_i = \frac{w_{\text{pre}}\, v_{\text{pre}} + w_{\text{post}}\, v_{\text{post}}}{w_{\text{pre}} + w_{\text{post}}}.$$

Weights were designed to (a) emphasize measurements closer to Day 0 and (b) down-weight post-treatment scores if they were taken long after device activation. Specifically,

$$w_{\text{pre}} = \frac{1}{|t_{\text{pre}}|}, \qquad w_{\text{post}} = \frac{1}{t_{\text{post}}}\, 2^{-\frac{t_{\text{post}}}{T_{\text{post}}}},$$

where T_{post} is the post-side half-life constant (set to three days in this analysis). The $1/|t|$ term serves as a *proximity factor*, giving greater influence to visits temporally close to Day 0, while the exponential term attenuates the contribution of post-Day 0 scores to mitigate early treatment effects.

For the reaction time and word-pair tests, baseline scores were determined directly from the first measurements recorded through the smartphone application. As both tasks were administered via the app, participants were required to complete the smartphone setup before taking these tests. App setup instructions were provided around the time participants received their light-therapy glasses, meaning these initial scores occurred close to the start of treatment. Therefore, the first recorded test result was taken as each participant's baseline score. Note there are very few cases of word and reaction time scores recorded a few days prior to the official start date as it is possible that a participant completed these tasks before the glasses completed a full connection on the database and recorded usage time. In these cases, the baseline score stilled remained to be the first score registered, and were assigned to be Day 0. The summary of starting scores at baseline is shown in Table 3.2.

Table 3.2: Baseline characteristics by randomized arm.

Characteristic	Alpha ($N_{\text{rand}} = 37$)	Beta ($N_{\text{rand}} = 36$)
Age, years, mean (SD) [n]	35.4 (13.1) [n=37]	34.9 (11.9) [n=36]
Sex at birth, female, n/N (%)	27/37 (73%)	30/36 (83%)
MADRS (baseline), mean (SD) [n]	20.9 (8.4) [n=37]	22.3 (9.4) [n=36]
PROMIS Sleep (baseline), mean (SD) [n]	25.1 (6.7) [n=37]	26.5 (5.1) [n=36]
PVT mean RT (ms), mean (SD) [n]	318.2 (70.6) [n=32]	329.7 (75.1) [n=35]
Word-Pair correct (0–30), mean (SD) [n]	1.5 (1.4) [n=37]	1.7 (1.9) [n=36]

Notes: Values are mean (SD) [n] unless stated otherwise. For categorical variables, values are n/N (%). Denominators vary due to metric eligibility and some missed baseline assessments. Distributions of the scores are shown in Figure 3.2.

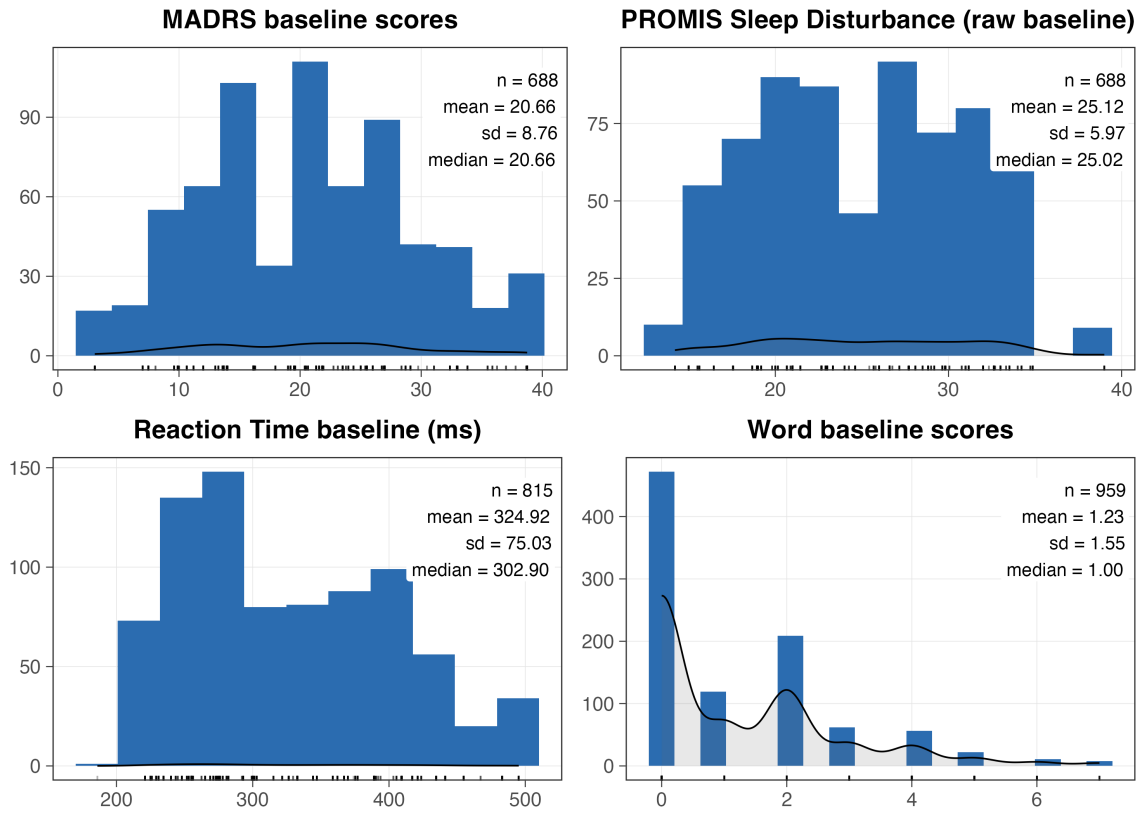


Figure 3.2: Baseline distributions of instruments, x-axis are raw scores, y-axis frequency

3.3.3 Device Usage and Light Exposure

The following section summarizes device usage patterns and ambient light exposure recorded by the glasses during the study. A total of 245,457 one-minute epochs (245,457 minutes of data) were included in this analysis. Figure 3.3 illustrates the distribution of total daily usage duration of the Lumos light therapy glasses across all participants and study phases. In the study protocol, participants are asked to wear the glasses with light therapy for at least 20 minutes per day, while suggesting that longer usage may lead to more improvements. Note that the glasses can also be used as blue-light blockers in the evenings, which contributed to the usage time if worn in the evenings while connected to the smartphone.

The histogram reveals a highly right-skewed pattern with the majority of daily sessions lasting less than one hour. A smaller subset of participants achieved extended usage durations, producing a long tail of higher daily totals. Some participants wore the glasses for over 10 hours on some days, demonstrating that the device can be comfortably used for extended durations, a central goal of the engineering and design.

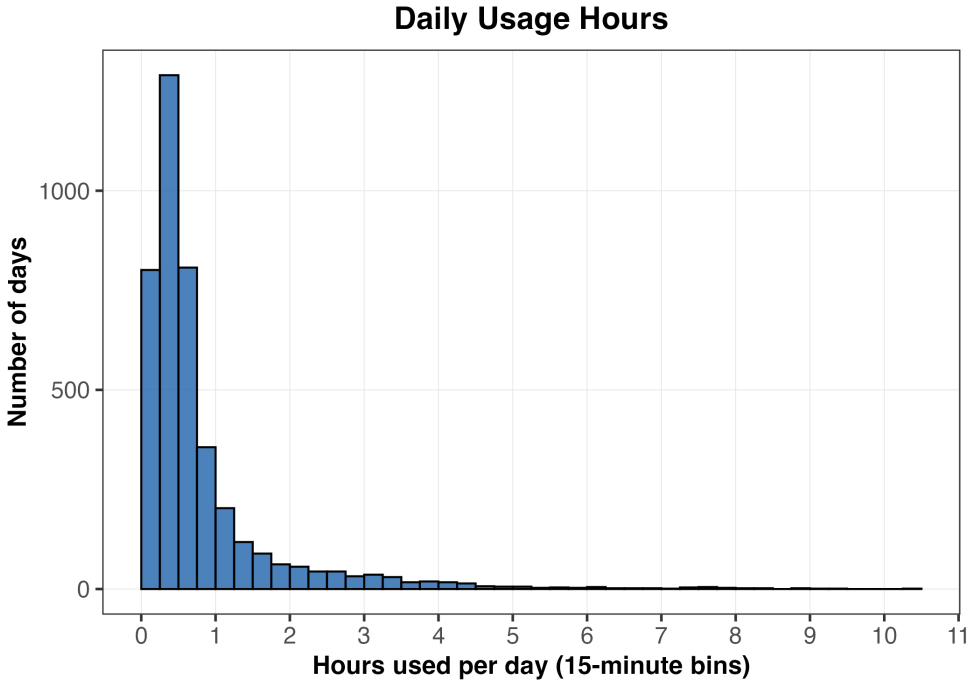


Figure 3.3: Distribution of daily usage hours across all participants.

Time-of-day usage. Figure 3.4 shows the temporal distribution of device usage throughout the 24-hour day, aggregated across all participants. Usage predominantly occurred during daylight hours (5 AM–5 PM; blue), corresponding to the prescribed light therapy period. Evening and nighttime usage (5 PM–5 AM; orange) represents instances when the light therapy mode was turned off and the glasses functioned as blue-light–blocking eye-wear. However, it should be noted that some participants may have used the glasses for blue-blocking without an active Bluetooth connection to the smartphone app, and thus such sessions would not be captured in this dataset. Consequently, the observed evening usage may underestimate the true extent of blue-blocking behaviour. Given this uncertainty, subsequent analyses focus primarily on daytime light therapy usage, where session duration and timing could be reliably verified through app-connected data.

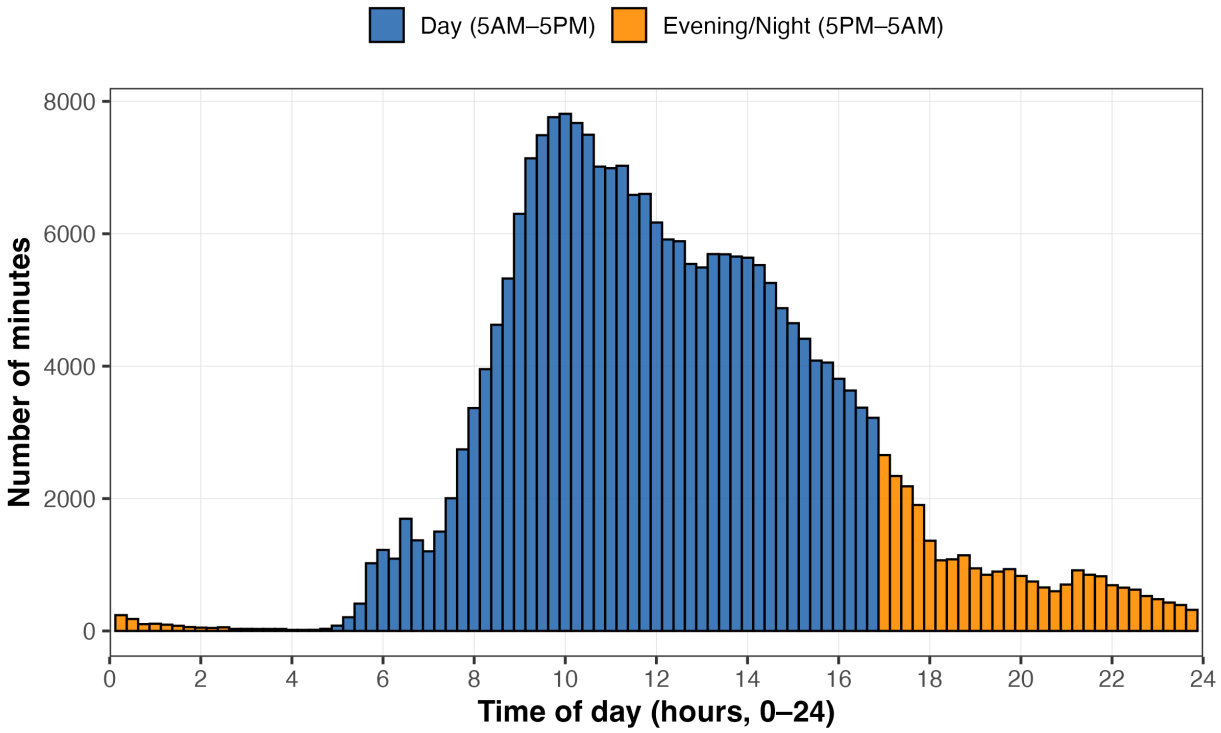


Figure 3.4: Distribution of device usage by time of day. Daytime usage (5 AM–5 PM; blue) dominated, while evening and nighttime usage (5 PM–5 AM; orange) occurred less frequently.

Ambient melanopic lux. Figure 3.5 shows the ambient melanopic lux recorded by the on-device sensors across the day. Exposure generally peaked between 10 a.m. and 2 p.m., with lower levels in the early morning and evening. The median daytime exposure was approximately 50–100 melanopic lux, on the lower end of the range associated with effective circadian stimulation in typical indoor environments [21, 89]. A subset of participants nonetheless experienced higher values, reflecting periods spent in brighter environments or near windows.

For context, Figure 3.5 includes two reference lines: a daytime target of 250 melanopic lux (5 a.m.–5 p.m.) and an evening/night target of 10 melanopic lux. These values, consistent with the ranges discussed in prior light-exposure studies [21, 89], should be interpreted as broad guidelines rather than strict thresholds, as individual sensitivity varies widely. Even so, most participants received far less than 250 melanopic lux during the day and substantially more than 10 melanopic lux in the evening. This pattern of low daytime and elevated nighttime exposure provides important context for interpreting treatment outcomes and understanding variability in circadian light environments across participants.

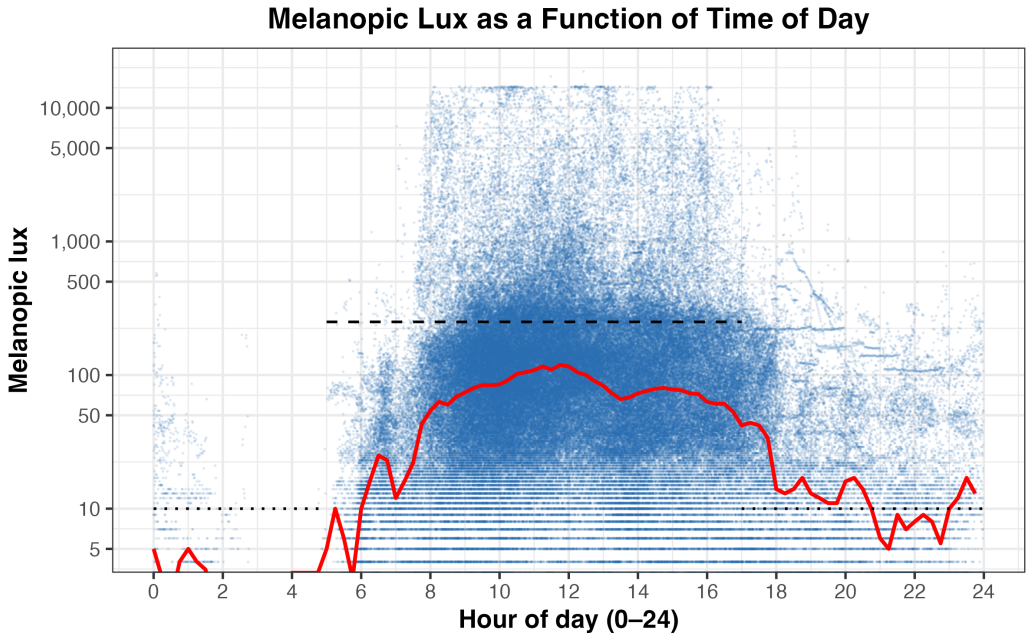


Figure 3.5: Ambient melanopic lux by clock hour. The red line indicates the median melanopic illuminance per 15-minute interval. Dashed and dotted lines show daytime (250 melanopic lux) and nighttime (10 melanopic lux) reference targets.

3.3.4 Outcome: Mood and Depression (MADRS)

Summary Across the study, participants showed significant reductions in depressive symptoms, with clear but individualized responses patterns. In Phase 1, both treatment arms improved, though darker-eyed participants benefited more from bright-light (Beta) and light-eyed participants improved more under dim-light (Alpha). After crossover, most Beta participants rebounded toward baseline, whereas Alpha trajectories were more heterogeneous. Multiple regression analyses showed that usage duration, ambient melanopic exposure, and baseline severity further moderated these patterns.

Assessment method Mood symptoms were assessed weekly using the self-rated MADRS-S scale via Qualtrics links integrated within the app. Since not all participants completed surveys at regular intervals, temporal trends were modeled using a piecewise linear regression linear regression with a hinge at Day 56 (the crossover point):

$$\Delta\text{MADRS} = \beta_1\,\text{day} + \beta_2\,\text{after56} + \varepsilon, \qquad \text{after56} = \max\{0,\ \text{day} - 56\}.$$

Only participants with sufficient data in both phases (>1 min/day average usage) were included ($n = 26$ per arm). Results are presented in Figure 3.6, with group-level coefficients summarized in Table 3.3 and corresponding hypothesis tests in Table 3.4.

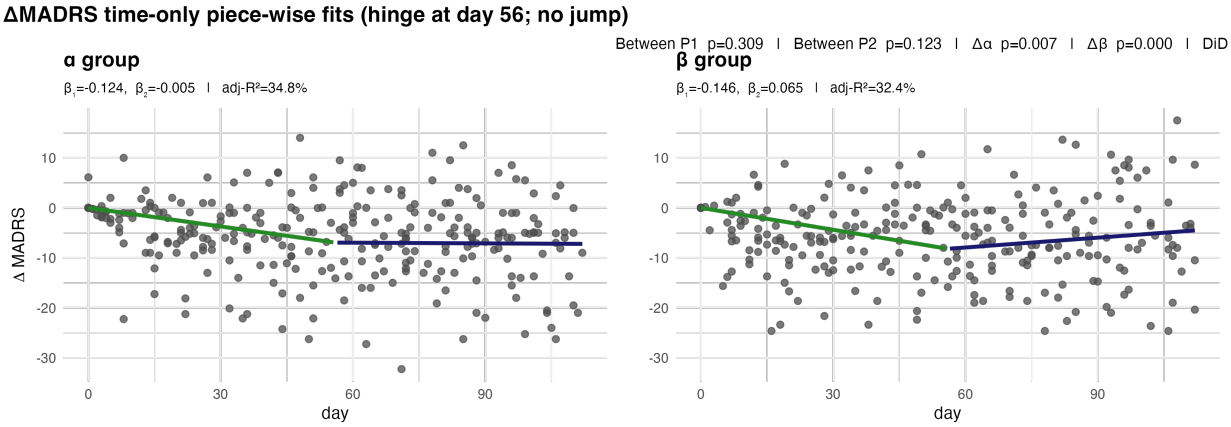


Figure 3.6: Change in MADRS over time, (hinge at Day 56). Negative values indicate improvement from baseline.

Table 3.3: Group-level slopes and hinge effects for ΔMADRS (hinge at Day 56).

Group	Pre-56 slope	p	η^2	Δ_{56}	p_Δ	η^2_Δ	Post-56 slope
Alpha	−0.124	4.7×10^{-15}	0.19	+0.120	0.0065	0.025	−0.005
Beta	−0.146	2.9×10^{-18}	0.24	+0.212	4.9×10^{-6}	0.072	+0.065

Table 3.4: Primary contrasts for ΔMADRS (per day, hinge at Day 56).

Contrast	Estimate	t	df	p	partial η^2
Between groups: pre-56	+0.022	1.02	281	0.31	0.004
Between groups: post-56	−0.070	−1.55	281	0.12	0.008
Within Alpha: change at 56	+0.120	2.74	291	0.0065	0.025
Within Beta: change at 56	+0.212	4.66	281	4.9×10^{-6}	0.072

Aggregate findings Both groups showed significant improvement during the first eight weeks, with the Beta arm (bright-light first) exhibiting a steeper rate of change. However, the between-group difference was not significant ($p = 0.31$) when all participant data were analyzed in aggregate. After crossover, Alpha slopes flattened while Beta rebounded toward baseline. The within-arm hinge effects were significant for both Alpha ($p = 0.0065$) and Beta ($p < 0.001$), indicating meaningful phase-specific changes following the treatment switch. Overall, the model explained moderate variance ($R^2_{adj} = 0.30$–0.42). Importantly, stratifying the analysis by eye color revealed strong differential effects that were not apparent in the aggregate results; these subgroup findings are presented below as a primary outcome.

Stratified Analyses by Eye Color

To evaluate whether responses varied by eye pigmentation, analyses were stratified by self-reported eye color/ethnicity: light (blue/green/hazel), brown-eyed Caucasian, and dark-eyed non-Caucasian participants. While the aggregate analysis showed a non-significant trend toward faster Beta improvement ($p = 0.31$), stratification revealed opposing patterns across pigmentation groups. Light-eyed participants exhibited a reversed effect (greater improvement under dim-light control) whereas both brown- and dark-eyed groups showed larger gains under bright-light treatment, each with significant hinge shifts. Only summary figures are shown below; full tables of slopes and contrasts are provided in Appendix E.

Light-eyed participants (Alpha: $n = 11$, Beta: $n = 11$) improved significantly under dim-light in Phase 1 ($p_{\text{pre}} = 0.018$). In Phase 2, Beta (bright $\rightarrow$ dim) showed a significant rebound ($p_{\text{hinge}} = 0.003$), whereas Alpha (dim $\rightarrow$ bright) flattened but continued improving. The between-group difference in Phase 2 was also significant ($p_{\text{pre}} = 0.033$) (see Figure 3.7).

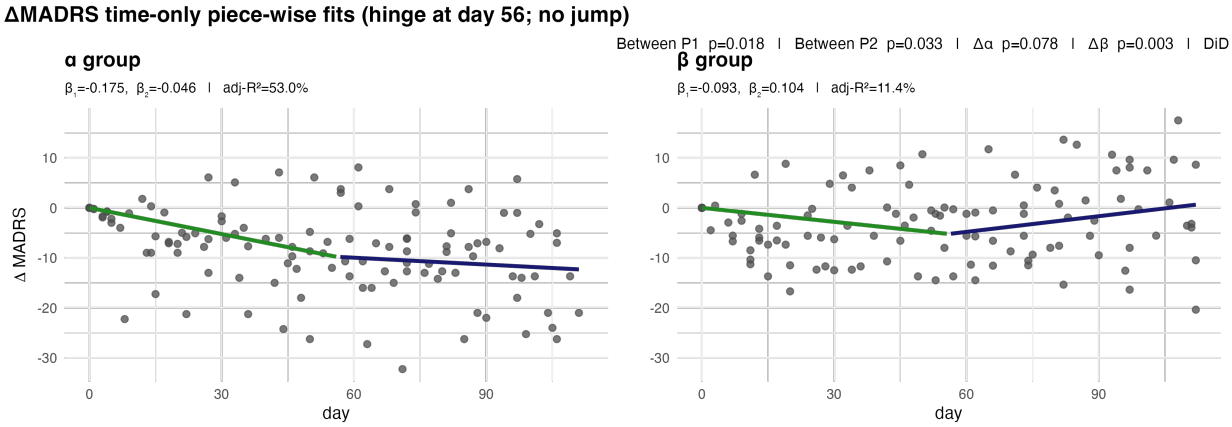


Figure 3.7: Light-eyed participants: ΔMADRS over time (hinge at Day 56).

Brown-eyed Caucasian participants (Alpha: $n = 8$, Beta: $n = 7$) showed the expected pattern. In Phase 1, they improved significantly more under bright-light ($p_{\text{pre}} = 0.007$). In Phase 2, Alpha (dim $\rightarrow$ bright) improved faster while Beta flattened, though Phase 2 and hinge effects did not reach significance. (see Figure 3.8).

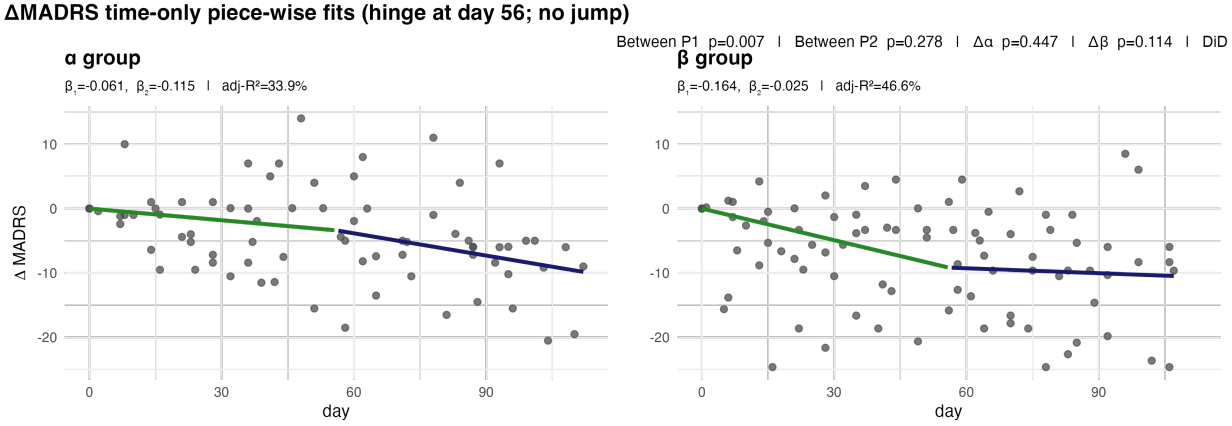


Figure 3.8: Brown-eyed Caucasian participants: ΔMADRS over time (hinge at Day 56).

Dark-eyed non-Caucasian participants (Alpha: $n = 7$, Beta: $n = 8$) showed the strongest Phase 1 improvement under bright-light ($p_{\text{pre}} = 0.013$). In Phase 2, both groups regressed with a large hinge effect (see Figure 3.9).

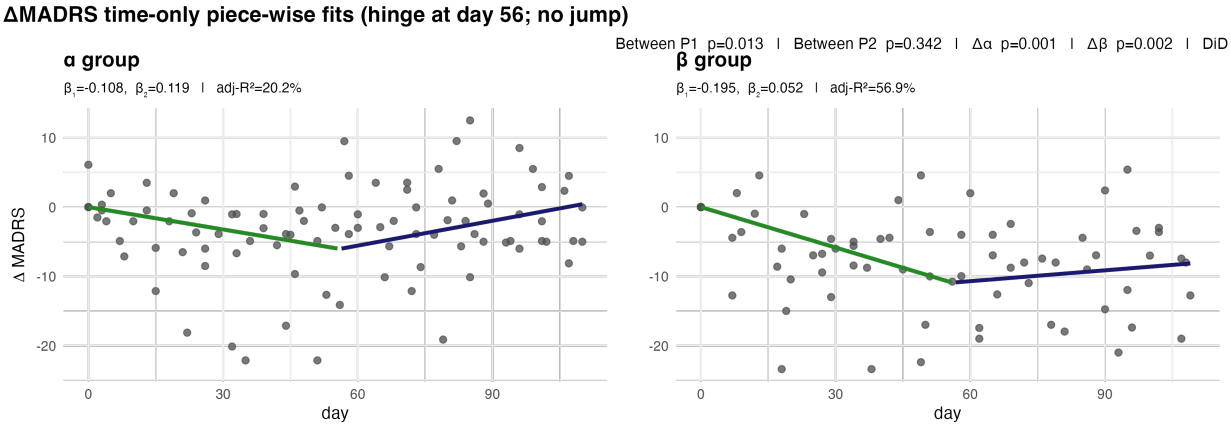


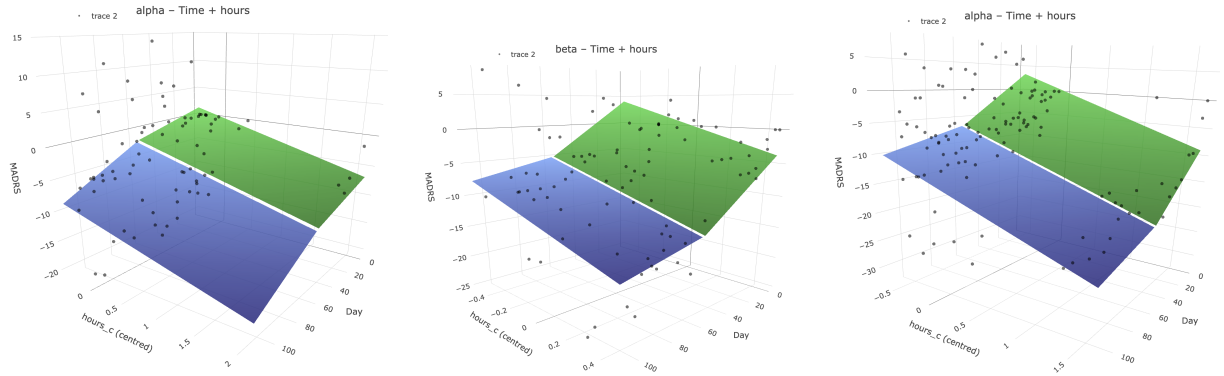
Figure 3.9: Dark-eyed non-Caucasian participants: ΔMADRS over time (hinge at Day 56).

Together, these findings show that while aggregate differences were modest, stratified analyses revealed distinct response patterns by eye pigmentation. This highlights that individual photic sensitivity, mediated by iris pigmentation, can modulate mood responses to bright-light therapy.

3.3.5 Mood (MADRS)—Multiple regression (summary)

This section evaluated whether usage duration, ambient melanopic light, baseline severity, age, and sex were associated with changes in MADRS. Models extended the time–hinge specification with centered covariates (e.g., `hours_c`, `lux_c`) to aid interpretation. Detailed model forms, full coefficients, surfaces, and subgroup tables are provided in Appendix F.

Usage time (`hours_c`): Significant dose–response improvements (more negative ΔMADRS) were observed in brown-eyed Caucasians (Alpha and Beta) and light-eyed Alpha (Appendix Tables F.1A–B), where higher daily usage corresponded to greater improvement. Because participants tended to maintain similar usage patterns across phases, usage-time effects were modeled across the full trajectory rather than phase-specific slopes. Figure 3.10 summarizes these three subgroups, and Table 3.6 reports the corresponding effects, p values, and effect sizes alongside other covariates.



(a) Brown-eye Cauc. — Alpha (b) Brown-eye Cauc. — Beta (c) Light-eyed — Alpha

Figure 3.10: **MADRS usage effects.** Time + usage (`hours_c`) planes for subgroups with significant usage effects. Higher `hours_c` was associated with greater improvement (more negative ΔMADRS).

Ambient light (`lux_c`) : Higher melanopic exposure was associated with greater improvement; effects were significant in both arms shown in Figure 3.11 and robust across subgroups except light-eye Alpha. (Details in Appendix Table F.2).

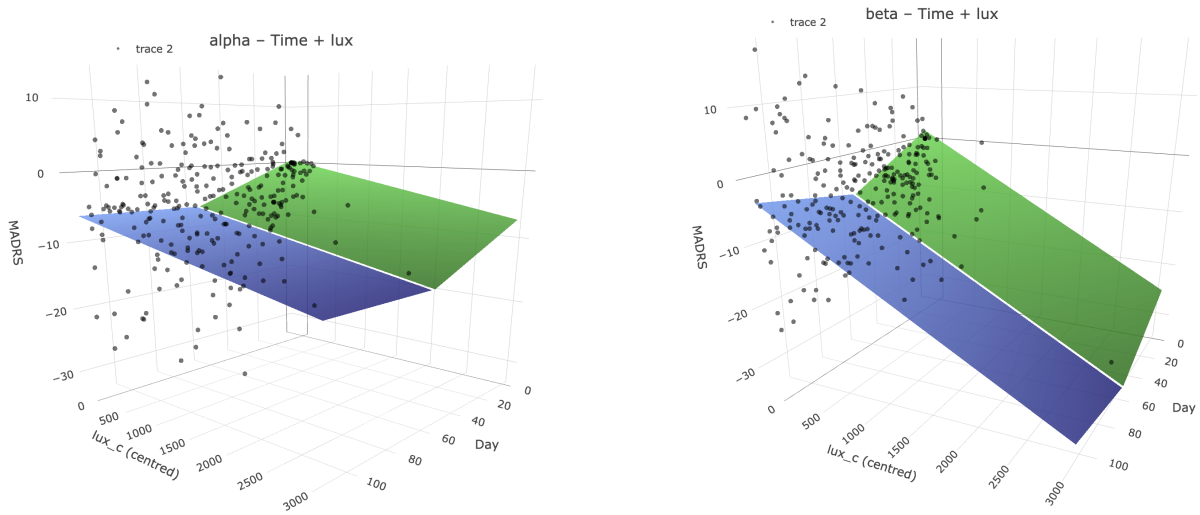
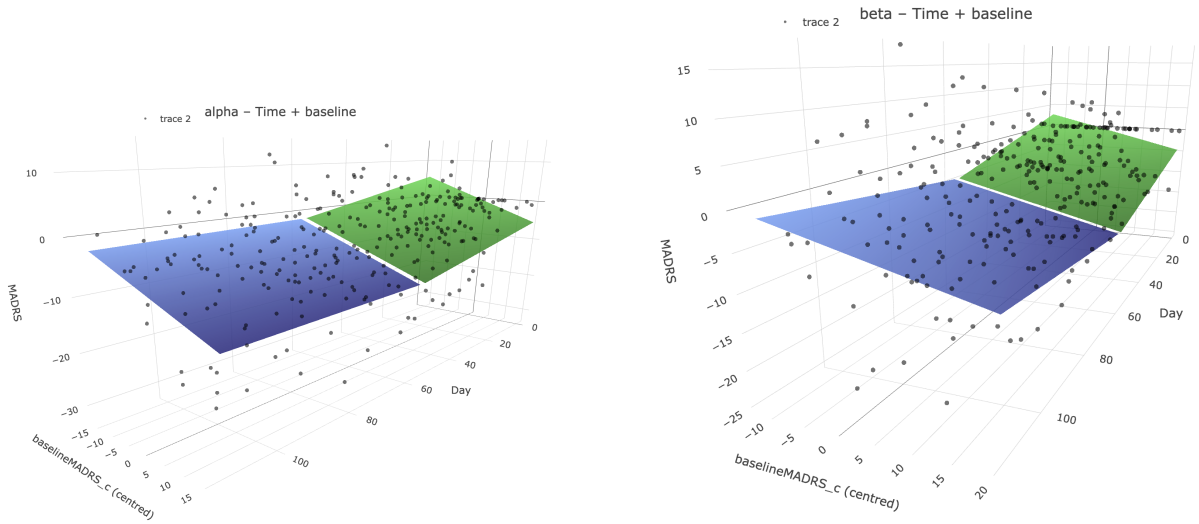


Figure 3.11: Time + centred lux planes for Alpha (left) and Beta (right). Increasing ambient light levels corresponded with greater improvement (lower MADRS).

Baseline severity : Higher baseline MADRS predicted larger subsequent reductions (Alpha: medium effect; Beta: small–medium; Appendix Tables F.3–F.4).



(a) Time + baseline — Alpha

(b) Time + baseline — Beta

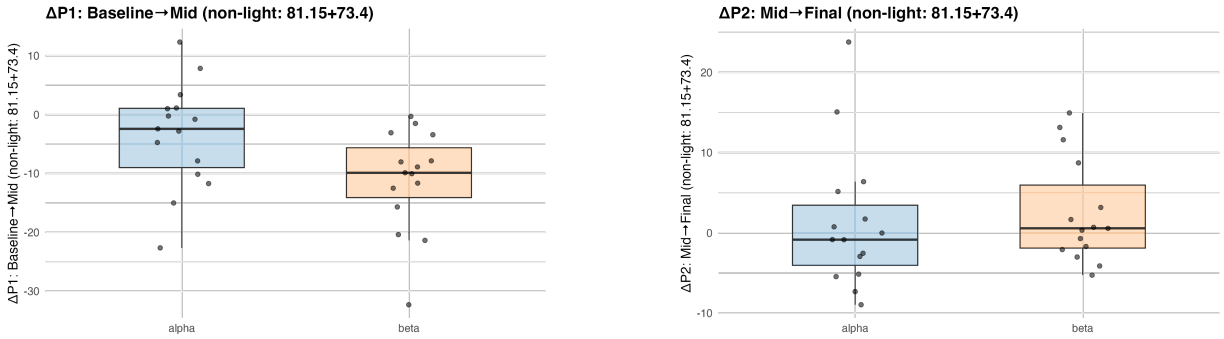
Figure 3.12: **Higher baseline severity predicts larger improvement.** Corresponding coefficients are in Appendix Tables F.3–F.4.

Sensitivity analysis. Baseline severity strongly influenced observed changes, so regression models were re-run using baseline-normalized scores for all primary outcomes. This adjustment accounted for minor baseline differences between the Beta and Alpha groups and confirmed that the main findings were robust to baseline scaling. The direction and significance of the principal effects were retained after normalization (see Appendix F.1.1).

Age (baseline-normalized models). Because age was modestly correlated with baseline severity—older participants tended to start with higher MADRS scores (Figure F.6)—age effects were examined after re-baselining. This analysis revealed small but significant associations whose direction varied by subgroup, as summarized in Table 3.6 and detailed in Appendix Tables F.7–F.8.

Sex. Sex showed a small effect only in the Beta arm, where females improved slightly more; this is summarized in Table 3.6 and reported in detail in Appendix Table F.9.

Per-participant analysis. To complement the mixed-effects model, an equal-weight per-participant regression was performed. It produced similar patterns overall, with the strongest significant effects in the combined non-light (brown-eyed) subgroup. As shown in Figure 3.13 and Table F.10, Beta showed faster Phase 1 improvement and a post-crossover rebound, while Alpha remained comparatively stable.



(a) Phase 1 change (Δ_1)

(b) Phase 2 change (Δ_2)

Figure 3.13: **Per-participant results (non-light/brown-eyed).** Beta shows larger Phase 1 improvement and rebound post-crossover ($p < 0.01$). Results in Table F.10

Table 3.5: Phase-level summary and hypothesis tests for the non-light (brown-eyed) subgroup under the equal-weight endpoint model.

Group	**Phase 1 mean ± SD**	**Phase 2 mean ± SD**
Alpha	-3.52 ± 8.94	$+1.25 \pm 8.64$
Beta	-11.13 ± 8.55	$+2.53 \pm 6.47$

Contrast / Phase	t	**df**	p	**Effect size**	**Interpretation**
Between groups (Phase 1)	2.38	27.95	0.024	$g = 0.85$	large
Between groups (Phase 2)	-0.46	25.93	0.651	$g = -0.16$	n.s.
Within Alpha (Δ_2 vs. Δ_1)	1.16	14	0.264	$d_z = 0.30$	small
Within Beta (Δ_2 vs. Δ_1)	4.26	14	0.0008	$d_z = 1.10$	large

Notes. Negative values denote improvement (reduction in MADRS score). Effect sizes are reported as Hedges' g (between groups) and Cohen's d_z (within groups). n.s. = not significant.

Overall summary. This study demonstrates that individual response to bright-light therapy is shaped by multiple interacting factors, including usage duration, ambient melanopic light exposure, baseline symptom severity, and demographic characteristics. The summary table is shown in Table 3.6 below. These variables not only predicted overall treatment response but also moderated effects within specific subgroups defined by eye pigmentation and age. Together, the results highlight that both behavioral adherence (usage and light exposure) and biological sensitivity (baseline severity and pigmentation) contribute to variability in antidepressant outcomes, underscoring the need for personalized light-therapy approaches.

Table 3.6: Summary of significant covariate associations with ΔMADRS. Full coefficients in Appendix F.

Covariate	**Subgroup / Arm**	**Effect**	p	**Effect size**
Usage	Brown-eyed Cauc. (Alpha)	Improves	0.010	Small
Usage	Brown-eyed Cauc. (Beta)	Improves	0.0067	Small
Usage	Light-eyed (Alpha)	Improves	1.45×10^{-8}	Medium
Ambient light	Alpha	Improves	0.028	Small
Ambient light	Beta	Improves	7.2×10^{-7}	Medium
Baseline severity	Alpha	Improves	2.7×10^{-9}	Medium
Baseline severity	Beta	Improves	5.0×10^{-5}	Small–med.
Age (re-based)	Brown-eyed Cauc. (Alpha)	Declines	0.012	Small
Age (re-based)	Brown-eyed Cauc. (Beta)	Improves	0.021	Small
Age (re-based)	Dark-eyed non-Cauc. (Alpha)	Declines	0.020	Small
Age (re-based)	Dark-eyed non-Cauc. (Beta)	Declines	0.031	Small
Sex	Beta	Female improves	0.034	Small

3.3.6 Outcome: Sleep Disturbance (PROMIS)

Summary. Participants showed clear reductions in sleep disturbance across the study, with distinct patterns across phases and eye-pigmentation groups. In Phase 1, both arms improved, with the bright-light (Beta) group showing significantly steeper improvement. After crossover, Beta participants exhibited a mild rebound whereas Alpha trajectories flattened. Stratified analyses revealed that darker-eyed participants benefited most from bright-light, whereas light-eyed participants improved comparably, or occasionally more, under dim-light. Multiple regression showed that usage duration, ambient melanopic exposure, baseline severity, and demographics contributed additional explanatory power.

Assessment method. Sleep disturbance was assessed weekly using the PROMIS Sleep Disturbance—Short Form [72], via Qualtrics links integrated within the app. As surveys were not always completed at fixed intervals, temporal trends were modeled using a piecewise linear regression linear regression with a hinge at Day 56 (the crossover point):

$$\Delta\text{PROMIS} = \beta_1\,\text{day} + \beta_2\,\text{after56} + \varepsilon, \qquad \text{after56} = \max\{0,\,\text{day} - 56\}.$$

Only participants with sufficient data in both phases (>1 min/day average usage) were included ($n = 26$ per arm). Results are presented in Figure 3.14, with group-level coefficients summarized in Table 3.7 and corresponding hypothesis tests in Table 3.8.

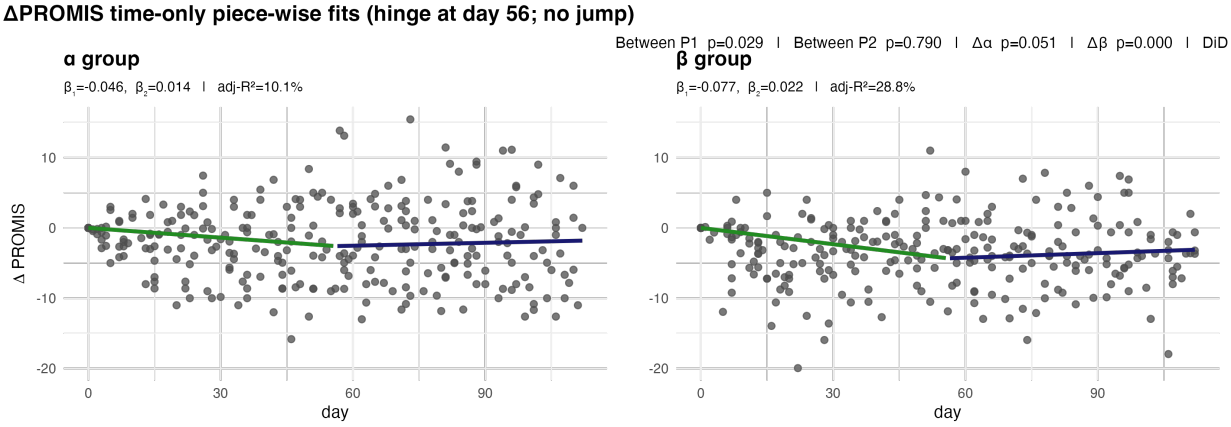


Figure 3.14: **Change in PROMIS sleep disturbance over time** (hinge at Day 56). Negative values indicate improvement (lower sleep disturbance).

Table 3.7: Group-level slopes and hinge effects for ΔPROMIS (hinge at Day 56).

Group	Pre-56 slope	p	η^2	Δ_{56}	p_Δ	η^2_Δ	Post-56 slope
Alpha	−0.0462	1.6×10^{-5}	0.062	+0.0601	0.0511	0.013	+0.0139
Beta	−0.0773	1.6×10^{-14}	0.205	+0.0991	4.0×10^{-4}	0.044	+0.0218

Table 3.8: Primary contrasts for ΔPROMIS (per day, hinge at Day 56).

Contrast	Estimate	t	df	p	partial η^2
Between groups: pre-56	+0.0311	2.19	281	0.0295	0.017
Between groups: post-56	−0.0079	−0.27	281	0.790	0.0003
Within Alpha: change at 56	+0.0601	1.96	291	0.051	0.013
Within Beta: change at 56	+0.0991	3.58	281	4.0×10^{-4}	0.044

Aggregate findings. Both groups showed improvements during the first eight weeks, with the Beta arm (bright-light first) exhibiting a steeper decline in sleep disturbance. The Phase 1 between-arm contrast was significant ($p = 0.0295$), indicating faster improvement in Beta. After crossover, Alpha slopes flattened while Beta rebounded slightly, consistent with treatment withdrawal. The hinge effect was marginal in Alpha ($p = 0.051$) and significant in Beta ($p = 4.0 \times 10^{-4}$), while post-56 between-group differences were not significant ($p = 0.79$). Overall, the model explained moderate temporal variance ($R^2_{adj} = 0.30$–0.42). As with MADRS, aggregate results obscured meaningful subgroup differences, motivating stratified analyses.

Stratified Analyses by Eye Color

To evaluate whether sleep outcomes varied by eye pigmentation, analyses were stratified by self-reported eye color/ethnicity: light (blue/green/hazel), brown-eyed Caucasian, and dark-eyed non-Caucasian participants. While aggregate results showed an overall Beta advantage during Phase 1, stratification revealed distinct subgroup patterns similar to those observed for mood outcomes.

Light-eyed participants (Alpha: $n = 11$, Beta: $n = 11$) showed comparable pre-56 improvement in both arms ($p_{\text{pre}} = 0.105$), with significant hinge effects in Alpha ($p = 0.005$) and Beta ($p = 0.012$). After crossover, both arms flattened, and post-56 differences were non-significant. (see Figure 3.15).

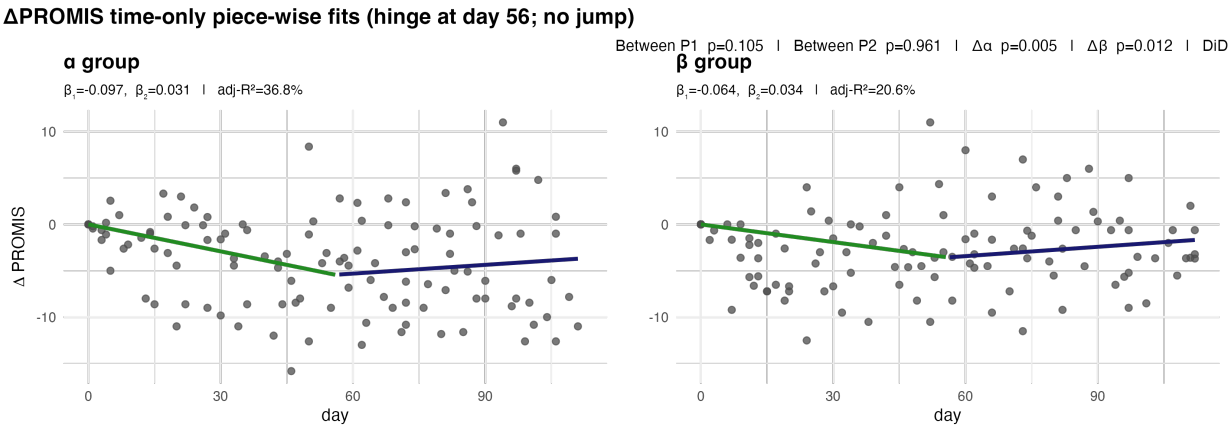


Figure 3.15: Light-eyed participants: ΔPROMIS over time (hinge at Day 56).

Brown-eyed Caucasian participants (Alpha: $n = 8$, Beta: $n = 7$) again showed patterns most consistent with the hypothesized bright-light advantage, with modest Phase 1 differences favoring Beta ($p = 0.046$). In Phase 2, Alpha (dim $\rightarrow$ bright) showed a slight increase in improvement, whereas Beta (bright $\rightarrow$ dim) showed a mild regression; however, neither the Phase 2 between-group contrast nor the hinge effects reached significance ($p > 0.3$) (see Figure 3.16).

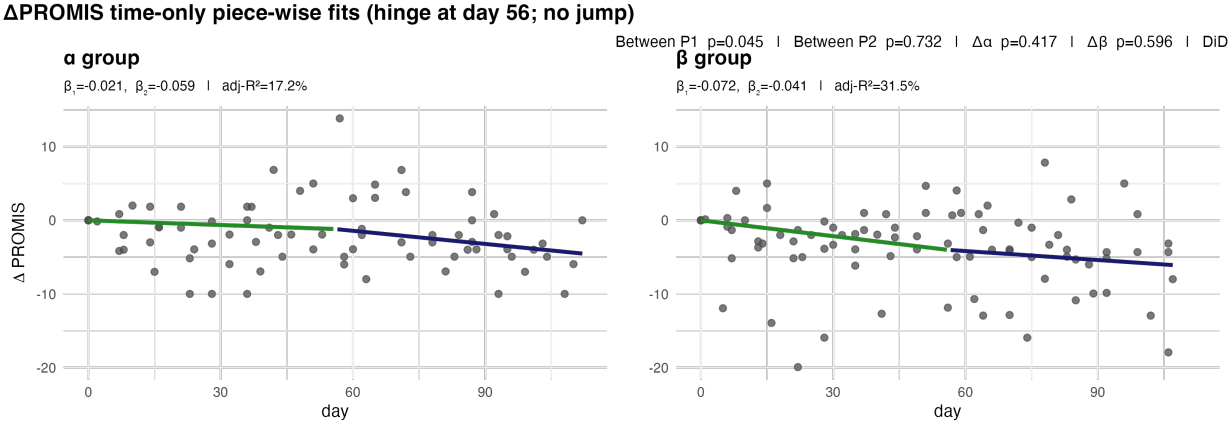


Figure 3.16: Brown-eyed Caucasian participants: ΔPROMIS over time (hinge at Day 56).

Dark-eyed non-Caucasian participants (Alpha: $n = 7$, Beta: $n = 8$) demonstrated the strongest Phase 1 response to bright-light ($p = 2.3 \times 10^{-4}$, $\eta_p^2 = 0.17$) and a significant

Beta hinge effect ($p = 0.003$. While for the Alpha group, improvements remained flat in both phase with no significant differences within. (see Figure 3.17).

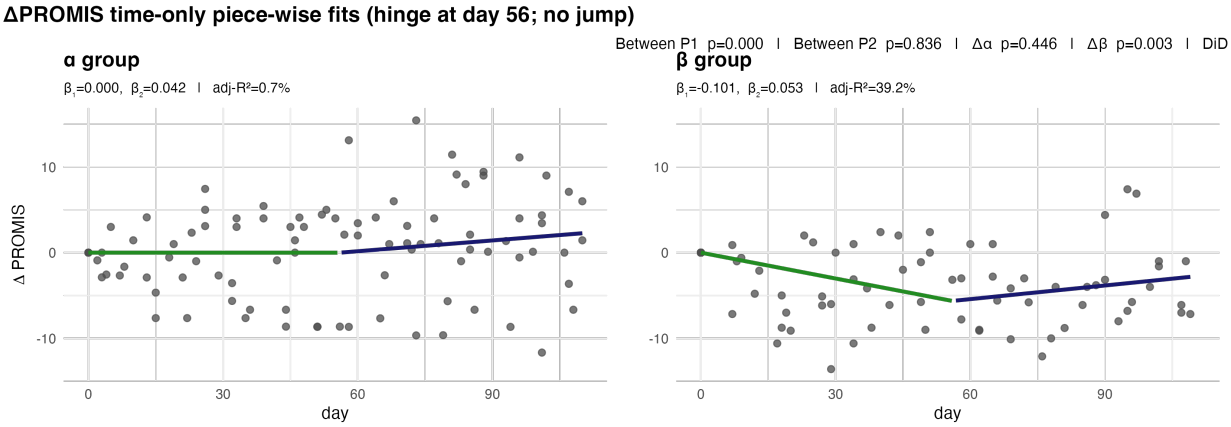


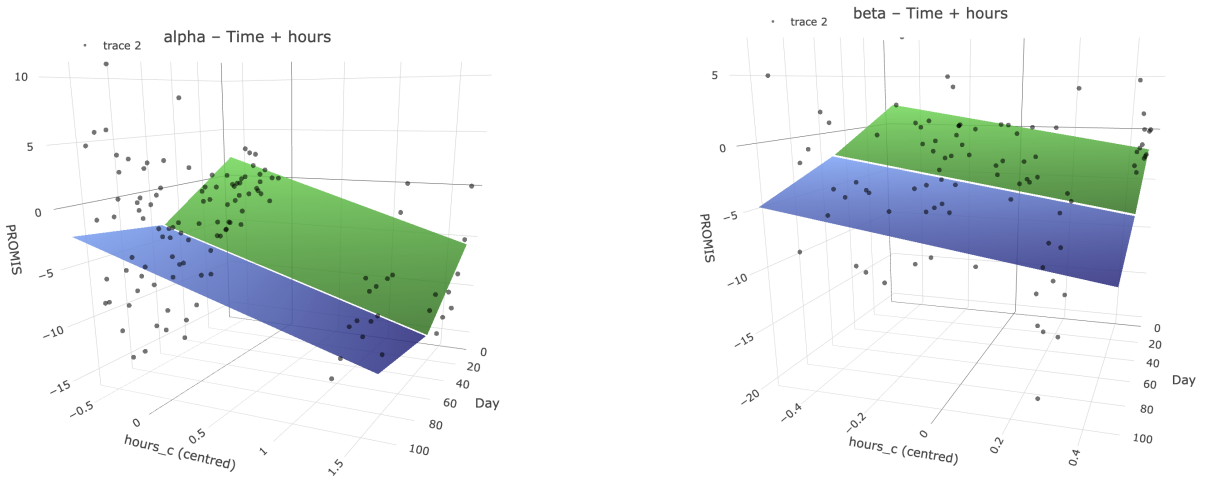
Figure 3.17: Dark-eyed non-Caucasian participants: ΔPROMIS over time (hinge at Day 56).

Together, these findings echo the MADRS results, showing that bright-light exposure produced faster initial improvements, particularly among darker-eyed participants, followed by mild rebound or plateau effects after crossover. This supports a shared pattern across mood and sleep outcomes, where light sensitivity and pigmentation appear to moderate treatment response. Full tables of slopes and contrasts are provided in Appendix G.

3.3.7 Sleep (PROMIS)—Multiple regression (summary)

This section evaluated whether usage duration, ambient melanopic light, baseline sleep severity, age, and sex were associated with changes in PROMIS. Models extended the time–hinge specification with centered covariates (e.g., `hours_c`, `lux_c`, `baselinePROMIS_c`, `age_c`, `sex_c`). Detailed model forms, full coefficients, surfaces, and subgroup tables are provided in Appendix H.

Usage time (`hours_c`). Significant dose–response improvements (more negative ΔPROMIS) were observed in *Light eyes (Alpha)* and *Brown-eyed Caucasians (Beta)* (Appendix Table H.1). Higher daily usage was associated with greater improvement across the full trajectory rather than phase-specific slopes. Figure 3.18 illustrates these two subgroups.



(a) Usage (Light-eyed (Alpha)

(b) Usage (Brown-eyed Caucasians (Beta)

Figure 3.18: **PROMIS usage effects.** 3D graph.

Ambient light (`lux_c`). Higher ambient melanopic exposure predicted greater improvement in the Beta arm (Appendix Table H.2), consistent with light-driven reductions in sleep disturbance. Figure 3.19 shows the fitted time–lux surfaces for Beta.

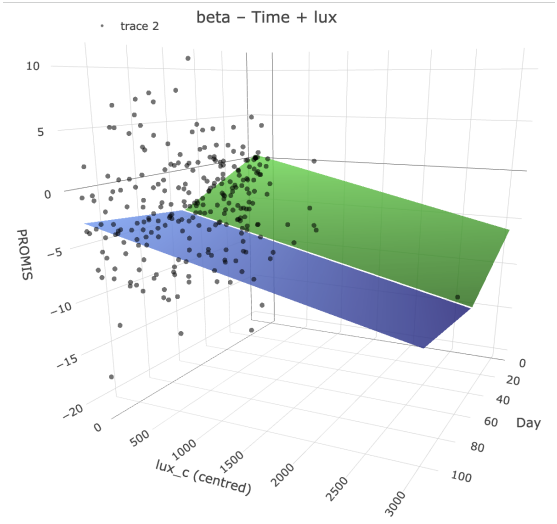
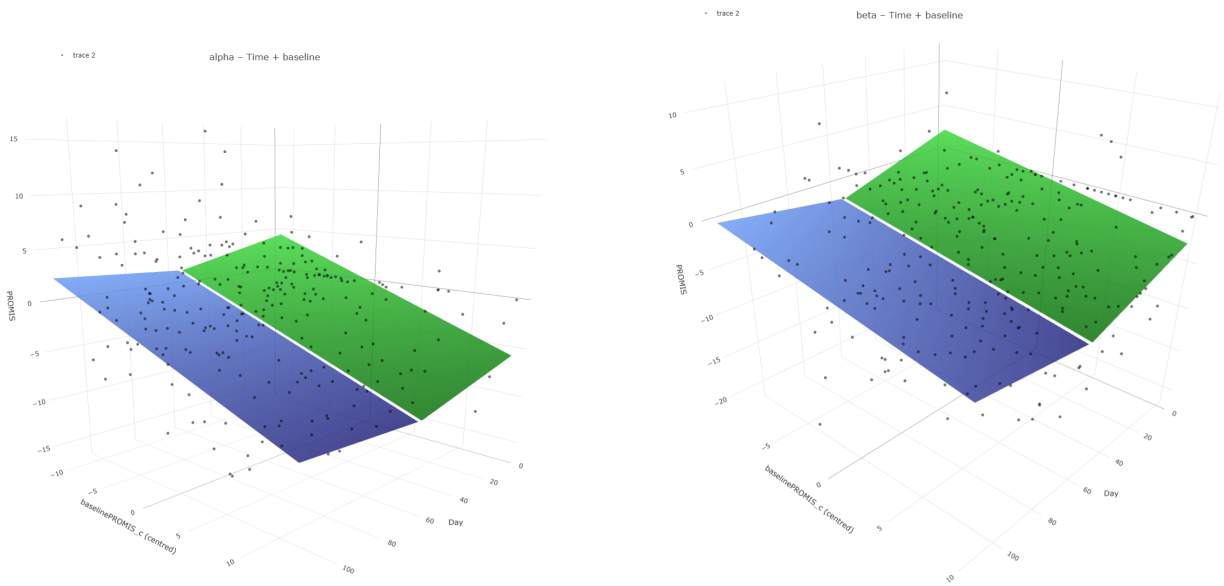


Figure 3.19: **Ambient light effects (Beta, all eyes).** 3D grapph

Baseline severity. Higher baseline PROMIS scores predicted larger reductions across both arms (Appendix Table H.3). Figure 3.20 shows the fitted time–baseline planes.



(a) Time + baseline — Alpha

(b) Time + baseline — Beta

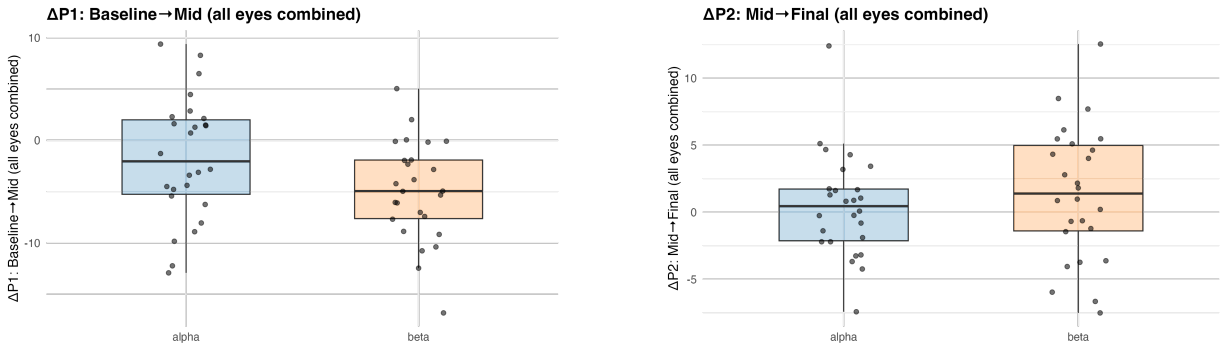
Figure 3.20: **Higher baseline sleep disturbance predicts larger improvement.**

Sensitivity analysis. Because baseline severity strongly influenced observed change, all PROMIS models were re-run using baseline-normalized scores. This accounted for minor baseline differences between Alpha and Beta and confirmed that the main findings were robust to normalization. The direction and significance of usage, ambient light, and baseline effects were preserved (Appendix H.1).

Age (baseline-normalized models). Age showed small but significant associations in both arms (Appendix Tables H.6), with older participants generally experiencing slightly larger reductions in sleep disturbance after re-baselining. Effects were consistent in direction across subgroups.

Sex. Sex showed small but significant effects in both arms, with females improving slightly more in Beta and male in Alpah group after controlling for baseline severity (Appendix Table H.7). The effect size was small.

Per-participant analysis. To complement the mixed-effects model, an equal-weight per-participant analysis was performed. As shown in Figure 3.21 and Table H.8, Beta showed larger Phase 1 improvement and a significant post-crossover rebound, whereas Alpha remained comparatively stable.



(a) Phase 1 change (Δ_1)

(b) Phase 2 change (Δ_2)

Figure 3.21: **Per-participant results (PROMIS, all eyes).** Beta shows larger Phase 1 improvement and a Phase 2 rebound.

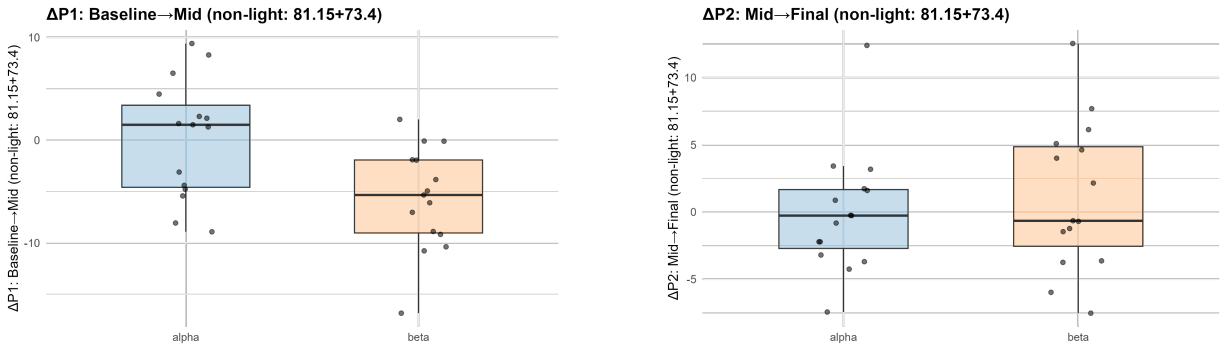
Table 3.9: Phase-level summary and hypothesis tests for PROMIS under the equal-weight endpoint model (all eyes).

Group	**Phase 1 mean±SD**	**Phase 2 mean±SD**
Alpha	-1.75 ± 7.82	$+0.43 \pm 8.10$
Beta	-4.94 ± 8.41	$+1.42 \pm 6.88$

Contrast / Phase	t	df	p	Effect size	Interpretation
Between groups (Phase 1)	2.12	48.1	0.039	$g = 0.58$	medium
Between groups (Phase 2)	-0.80	47.2	0.43	$g = -0.22$	n.s.
Within Alpha	1.35	25	0.19	$d_z = 0.30$	n.s.
Within Beta	3.88	25	0.0007	$d_z = 1.10$	large

Notes. Negative values denote improvement (reduction in sleep disturbance). Effect sizes: Hedges' g (between groups) and Cohen's d_z (within groups). n.s. = not significant.

Per-participant analysis (non–light-eyed). An equal-weight per-participant analysis was also performed for non–light-eyed participants. As shown in Figure H.9 and Table H.9, the Beta group exhibited a markedly larger improvement during Phase 1 and a significant rebound after crossover, whereas Alpha remained comparatively stable across phases.



(a) Phase 1 change (Δ_1)

(b) Phase 2 change (Δ_2)

Figure 3.22: **Per-participant results (PROMIS, non–light-eyed).** Beta shows a larger Phase 1 improvement and a Phase 2 rebound, while Alpha remains stable.

Table 3.10: Phase-level summary and hypothesis tests for PROMIS under the equal-weight endpoint model (non–light-eyed).

Group	**Phase 1 mean±SD**	**Phase 2 mean±SD**
Alpha	$+0.18 \pm 5.74$	-0.07 ± 4.55
Beta	-5.69 ± 5.00	$+1.16 \pm 5.51$

Contrast / Phase	t	df	p	Effect size	Interpretation
Between groups (Phase 1)	2.99	27.49	0.0058	$g = 1.06$	large
Between groups (Phase 2)	-0.67	27.02	0.511	$g = -0.24$	n.s.
Within Alpha	-0.11	14	0.911	$d_z = -0.03$	n.s.
Within Beta	2.98	14	0.0099	$d_z = 0.77$	large

Notes. Negative values denote improvement (reduction in sleep disturbance). Effect sizes: Hedges' g (between groups) and Cohen's d_z (within groups). n.s. = not significant.

Overall summary. Promis sleep outcomes were shaped by multiple interacting factors, including usage duration, ambient melanopic exposure, baseline sleep severity, and small demographic effects. These variables predicted both overall improvement and subgroup-specific patterns, closely paralleling the MADRS findings. Together, the results indicate that behavioral adherence (usage and ambient light exposure) and biological sensitivity (baseline severity and pigmentation) jointly influence sleep-related response to bright-light therapy.

Table 3.11: Summary of significant covariate associations with ΔPROMIS. Full coefficients in Appendix H.

Covariate	**Subgroup / Arm**	**Effect**	p	**Effect size**
Usage	Light eyes (Alpha)	Improves	8.51×10^{-9}	Medium
Usage	Brown-eyed Cauc. (Beta)	Improves	0.0408	Small
Ambient light	Beta (all eyes)	Improves	0.007	Small–med.
Baseline severity	Alpha (all eyes)	Improves	4.46×10^{-16}	Large
Baseline severity	Beta (all eyes)	Improves	6.43×10^{-5}	Small–med.
Age (re-based)	Alpha (all eyes)	Improves	0.0198	Small
Age (re-based)	Beta (all eyes)	Improves	0.0100	Small
Sex (re-based)	Alpha (all eyes)	Male improves	0.012	Small
Sex (re-based)	Beta (all eyes)	Female improves	0.019	Small

3.3.8 Outcome: Psychomotor Vigilance (PVT)

Summary. Psychomotor vigilance improved substantially over the course of the trial, with both arms showing faster reaction times in Phase 1 and a pronounced advantage for the bright-light (Beta) group. After crossover, Beta participants slowed following treatment withdrawal, whereas Alpha trajectories largely flattened. Unlike mood and sleep, these vigilance benefits were observed across all eye-pigmentation subgroups, with no reversal among light-eyed participants.

Assessment method. Psychomotor vigilance was assessed weekly using an on-device PVT test that measured average reaction time (RT) in milliseconds. To standardize across participants, lapses and false starts were recoded as 500 ms and averaged with trial-level RTs to yield an adjusted RT, which served as the primary outcome. Temporal trends were modeled using a piecewise linear regression linear regression with a hinge at Day 56 (the crossover point):

$$\Delta\mathrm{RT} = \beta_1\,\mathrm{day} + \beta_2\,\mathrm{after56} + \varepsilon, \qquad \mathrm{after56} = \max\{0,\ \mathrm{day} - 56\}.$$

Participants with sufficient data in both phases (>1 min/day average usage) were included ($n = 26$ per arm). Results are presented in Figure 3.23, with group-level coefficients summarized in Table 3.12 and corresponding hypothesis tests in Table 3.13.

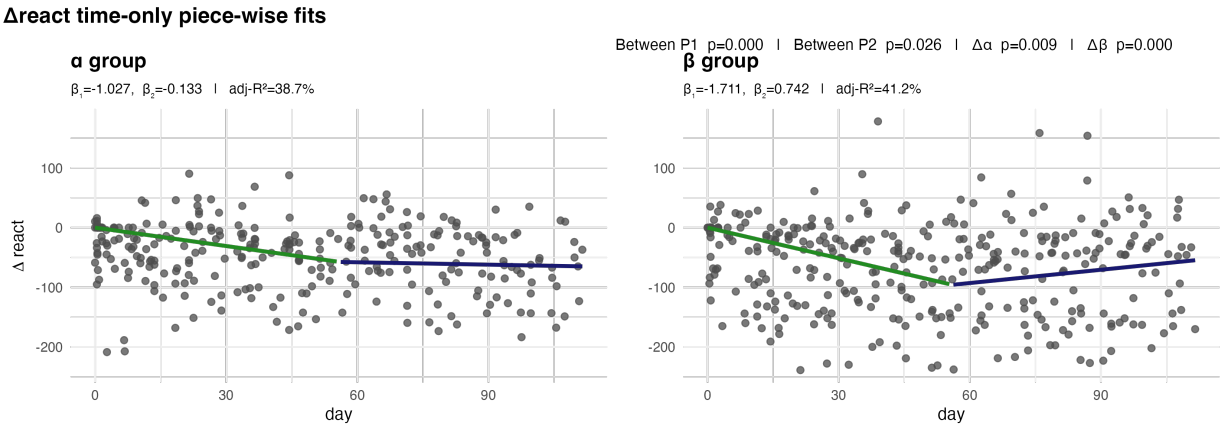


Figure 3.23: **Change in PVT reaction time** (hinge at Day 56). Negative slopes denote faster responses (improvement).

Table 3.12: Group-level slopes and hinge effects for ΔRT (hinge at Day 56).

Group	Pre-56 slope	p	η^2	Δ_{56}	p_Δ	η^2_Δ	Post-56 slope
Alpha	-1.027	1.06×10^{-17}	0.219	$+0.894$	9.11×10^{-3}	0.0226	-0.133
Beta	-1.711	1.78×10^{-29}	0.308	$+2.453$	6.89×10^{-9}	0.0928	$+0.742$

Table 3.13: Primary contrasts for ΔRT (ms/day; hinge at Day 56).

Contrast	Estimate	t	df	p	partial η^2
Between groups: pre-56	$+0.684$	3.84	298	1.48×10^{-4}	0.047
Between groups: post-56	-0.875	-2.23	298	0.026	0.017
Within Alpha: change at 56	$+0.894$	2.63	298	9.1×10^{-3}	0.023
Within Beta: change at 56	$+2.453$	5.94	345	6.9×10^{-9}	0.093

Aggregate findings. Both arms showed marked improvement in Phase 1, with a highly significant between-arm contrast favoring Beta (steeper decline; $p = 1.5 \times 10^{-4}$). At crossover, Alpha slopes flattened ($p = 0.009$), whereas Beta exhibited a large positive hinge ($p < 10^{-8}$), consistent with slowing after bright-light withdrawal. Post-56 between-arm differences remained significant but smaller ($p = 0.026$), indicating partial convergence rather than complete loss of the Beta advantage.

Stratified Analyses by Eye Color

To evaluate whether vigilance responses varied by eye pigmentation, analyses were stratified by self-reported eye color/ethnicity: light (blue/green/hazel), brown-eyed Caucasian, and dark-eyed non-Caucasian participants. Across all strata, Phase 1 slopes were negative, indicating faster responses over time, and the Beta arm generally improved more than Alpha. This pattern contrasts with MADRS (subsection 3.3.4) and PROMIS (subsection 3.3.6), where light-eyed participants sometimes fared better under dim-light.

Light-eyed participants (Alpha: $n = 9$, Beta: $n = 11$) improved in both arms, with a significant Phase 1 advantage for Beta ($p_{\text{pre}} = 0.037$) and a robust hinge effect in Beta ($p_{\text{hinge}} = 1.1 \times 10^{-4}$; Appendix Table I.6).

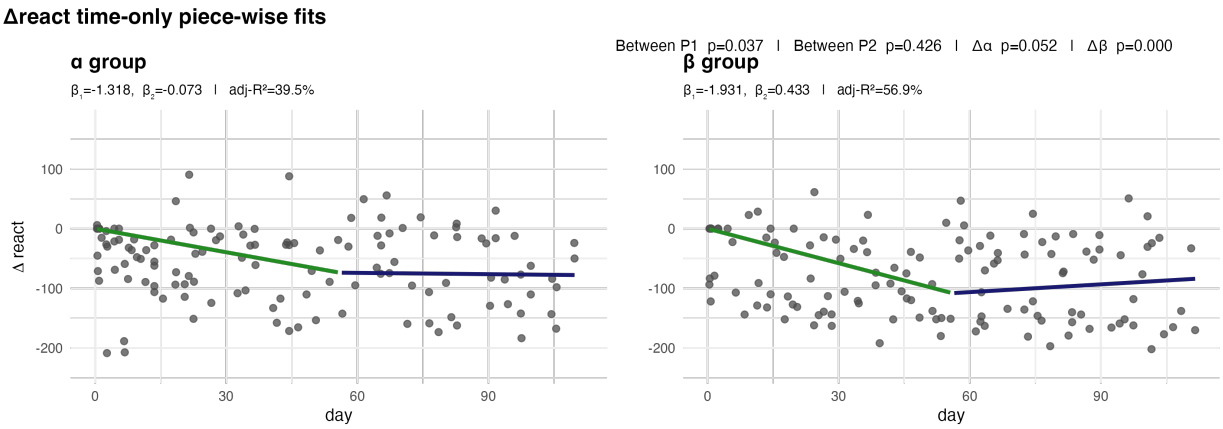


Figure 3.24: Light-eyed participants: ΔRT over time (hinge at Day 56).

Brown-eyed Caucasian participants (Alpha: $n = 8$, Beta: $n = 7$) showed the strongest Phase 1 difference favoring Beta ($p_{\text{pre}} = 1.8 \times 10^{-4}$) and a significant hinge effect ($p_{\text{hinge}} = 5.3 \times 10^{-4}$; Appendix Table I.4), indicating pronounced slowing after crossover.

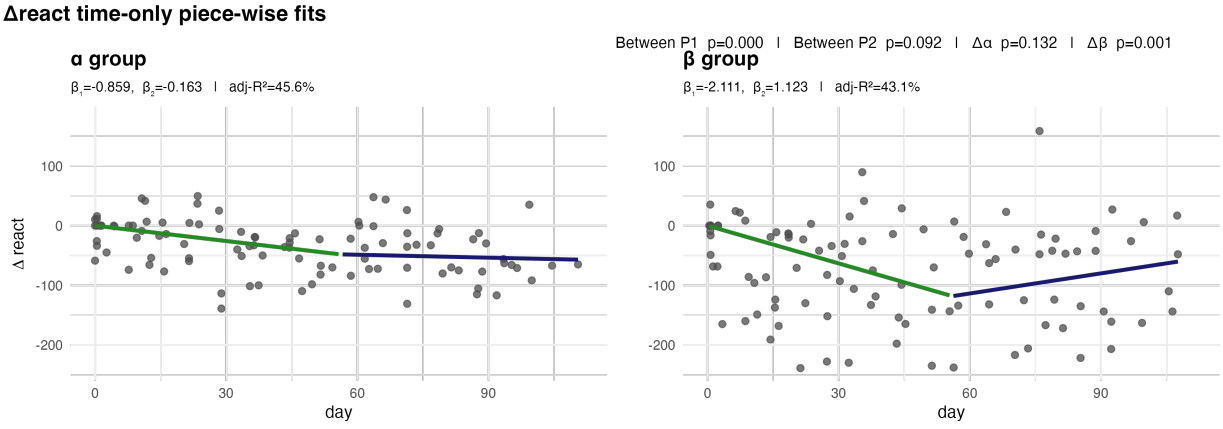


Figure 3.25: Brown-eyed Caucasian participants: ΔRT over time (hinge at Day 56).

Dark-eyed non-Caucasian participants(Alpha: $n = 6$, Beta: $n = 8$) exhibited a moderate Beta benefit, with negative Phase 1 slopes in both arms but a non-significant between-arm Phase 1 contrast ($p_{\text{pre}} = 0.40$). The Beta hinge remained significant ($p_{\text{hinge}} = 0.007$; Appendix Table I.2), reflecting measurable post-crossover slowing after strong early gains.

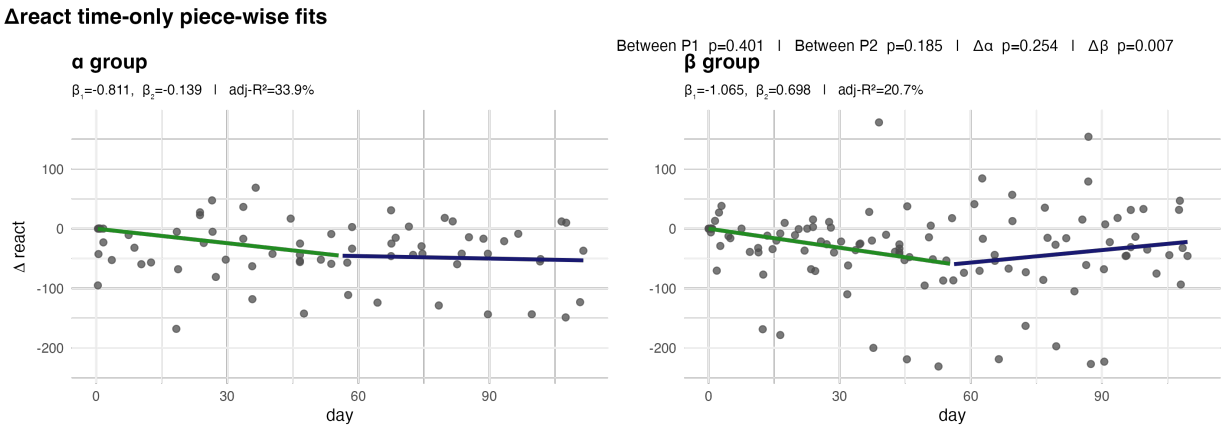


Figure 3.26: Dark-eyed non-Caucasian participants: ΔRT over time (hinge at Day 56).

Together, these stratified patterns show that, unlike mood and sleep, PVT performance consistently benefited from bright-light across eye-pigmentation groups.

3.3.9 Psychomotor Vigilance (PVT)—Multiple regression (summary)

This section evaluated whether usage duration, ambient melanopic light, baseline reaction time, and age were associated with changes in ΔRT. All models used a hinge-at-Day 56 specification with centered covariates (`hours_c`, `lux_c`, `baselineReact_c`, `age_c`). Detailed coefficients, block tests, and regression surfaces are provided in Appendix J.

Usage time (`hours_c`). Greater daily usage predicted faster RT improvement in the Alpha arm (all eyes; $p = 0.012$; Appendix Table J.1). Participants who wore the glasses longer each day showed larger reductions in reaction time over the full trajectory.

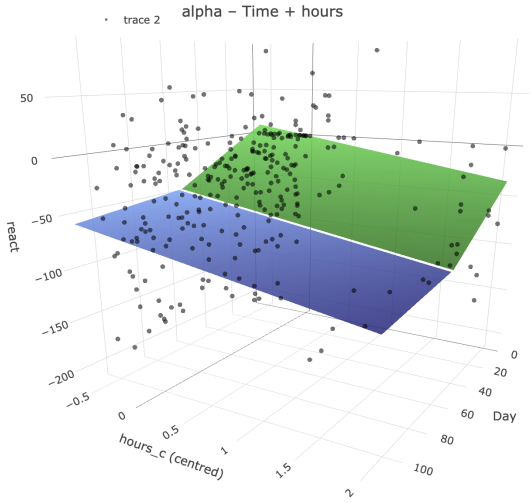


Figure 3.27: **Usage effects (`hours_c`) in Alpha (all eyes).** 3D graph

Ambient light (`lux_c`). In the brown-eyed Caucasian Alpha subgroup, higher ambient melanopic illuminance was associated with faster responses ($p = 0.037$; Appendix Table J.2). This suggests that, beyond the on-device treatment, background light exposure further enhanced vigilance in this subgroup.

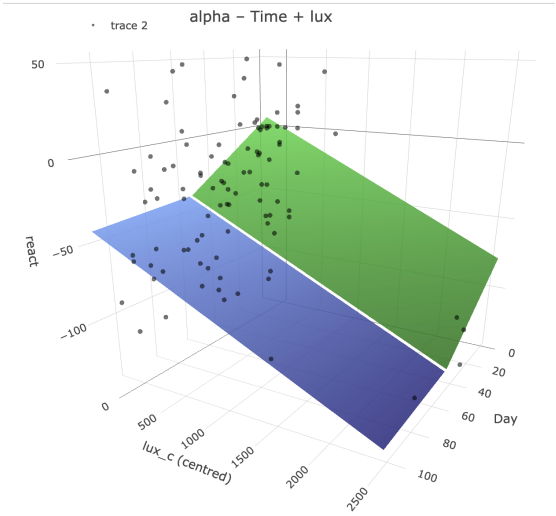
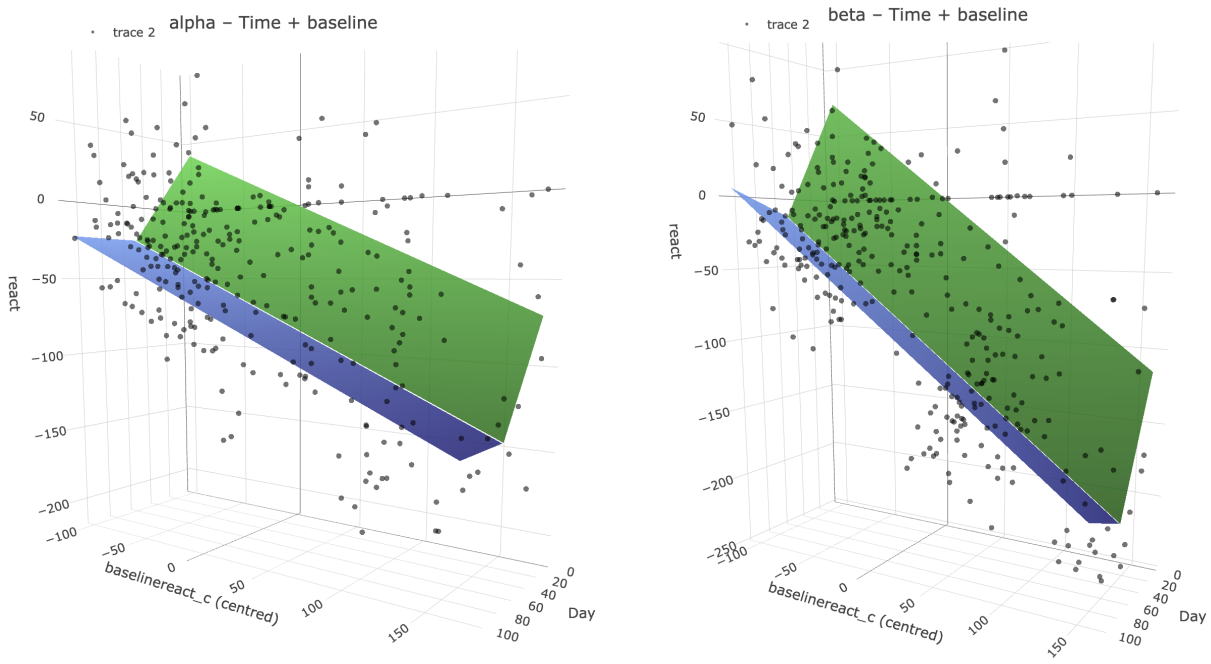


Figure 3.28: **Ambient melanopic light effects in brown-eyed Caucasian Alpha participants.** Higher `lux_c` predicts faster reaction times (more negative ΔRT).

Baseline reaction time. Baseline performance had a strong influence on subsequent change: slower initial RT predicted larger improvements in both Alpha and Beta ($p < 10^{-5}$; Appendix Table J.3).



(a) Baseline RT — Alpha

(b) Baseline RT — Beta

Figure 3.29: **Baseline severity and PVT improvement.** 3D graphs

Sensitivity analysis. Because baseline RT strongly influenced observed change, PVT models were also re-run using baseline-normalized scores. This adjustment confirmed that the main effects of usage, baseline performance, and ambient light were robust to normalization (Appendix J.5).

Age (baseline-normalized models). From our data, age was significantly correlated with baseline RT, see Appendix J.5. After re-baselining to account for initial RT differences, age showed small but significant associations in both arms ($p = 0.03$–0.05; Appendix Tables J.6–J.7), with older participants exhibiting slightly larger relative gains. Effect sizes were small, and no dedicated age figure is shown.

Per-participant analysis. To complement the mixed-effects models, a participant-level endpoint analysis was performed using modeled midpoints (Day 56) and endpoints (Day 112) derived from individual hinge fits ($react \sim 0 + \text{day} + \text{after56}$; no jump). Phase 1 ($\Delta_1$) represents the change from baseline to midpoint, and Phase 2 (Δ_2) represents the change from midpoint to final measurement. Negative values indicate faster (improved) reaction times.

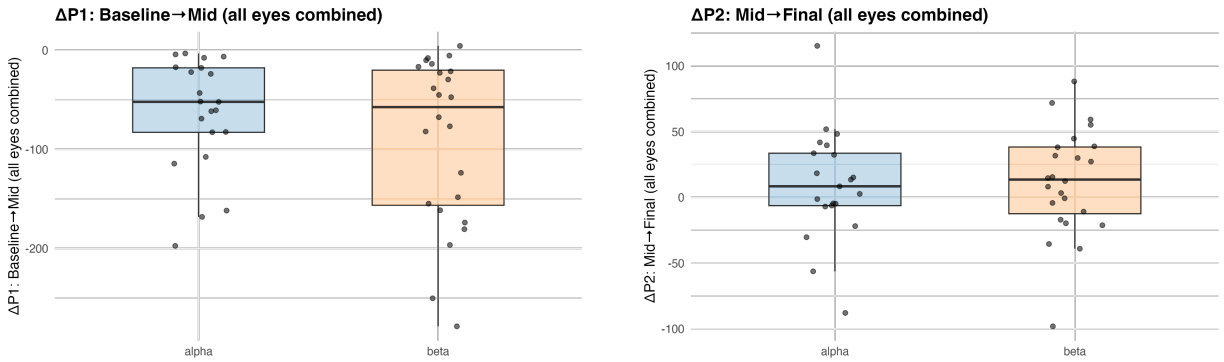


Figure 3.30: **Participant-level Δ_1 and Δ_2 reaction time changes by arm.** Negative values denote faster (improved) responses.

Table 3.14: Group-level statistics for participant-level reaction time deltas (all eyes).

Group	Phase	n	Mean (ms)	SD (ms)
Alpha	Phase 1 (baseline→mid)	21	−64.5	57.2
Alpha	Phase 2 (mid→final)	21	+9.5	41.9
Beta	Phase 1 (baseline→mid)	24	−89.5	84.0
Beta	Phase 2 (mid→final)	24	+12.2	40.6

Table 3.15: Hypothesis tests for participant-level reaction time deltas (all eyes).

Contrast	t	df	p	Effect size	Interpretation
Between arms: Δ_1 (Phase 1)	1.18	40.7	0.25	$g = 0.34$	small, n.s.
Between arms: Δ_2 (Phase 2)	−0.22	41.8	0.83	$g = -0.06$	none, n.s.
Within Alpha: $\Delta_2 - \Delta_1$	3.83	20	0.0010	$d_z = 0.84$	large rebound
Within Beta: $\Delta_2 - \Delta_1$	4.63	23	1.17×10^{-4}	$d_z = 0.95$	large rebound

Overall summary. Taken together, PVT outcomes complement the mood and sleep results. Bright-light exposure produced robust improvements in vigilance during Phase 1 across all eye-pigmentation groups, followed by measurable slowing after crossover, particularly in Beta. Usage, ambient light, baseline performance, and age all contributed to variability in response, underscoring the importance of both behavioral adherence and baseline cognitive status for understanding vigilance outcomes.

Table 3.16: Summary of significant covariate associations with ΔRT (ms). Full coefficients in Appendix J.

Covariate	**Subgroup / Arm**	**Effect (faster = negative)**	p	**Effect size**
Usage (`hours_c`)	Alpha (all eyes)	Faster RT with higher usage	0.012	small–med. f^2=0.09
Ambient light (`lux_c`)	Brown-eyed Cauc. (Alpha)	Higher illuminance ⇒ faster RT	0.037	small–med. f^2=0.04
Baseline RT	Alpha (all eyes)	Worse baseline ⇒ larger gain	3.9×10^{-6}	medium
Baseline RT	Beta (all eyes)	Worse baseline ⇒ larger gain	7.1×10^{-7}	medium
Age (re-based)	Alpha (all eyes)	Older ⇒ slightly greater rel. gain	0.049	small
Age (re-based)	Beta (all eyes)	Older ⇒ slightly greater rel. gain	0.031	small

3.3.10 Outcome: Working Memory (Word Recall)

Summary. Working-memory performance improved modestly over time, with clear Phase 1 learning effects in both arms and small overall treatment differences. Stratified results showed that light- and brown-eyed Caucasian participants often improved more quickly under dim-light early on, while dark-eyed participants showed stronger gains under bright-light. Usage-time analyses further revealed that Caucasian participants improved more when they used the bright-light condition for longer each day. Combined with the raw dark-eyed results, these findings strongly suggest that bright-light exposure supports better working-memory performance across all pigmentation groups.

The word-pair recall task was analyzed using the same piecewise linear model with a hinge at Day 56. Scores were normalized to each participant's baseline performance to control for individual variability:

$$\Delta\text{Word} = \beta_1\,\text{day} + \beta_2\,\text{after56} + \varepsilon, \qquad \text{after56} = \max(0,\ \text{day} - 56).$$

Trajectory. Figure 3.31 shows the fitted pre-56 (green) and post-56 (blue) trajectories for both arms. Both *Alpha* and *Beta* groups exhibited modest gains during Phase 1 (Weeks 0–8), followed by a flattening after crossover. Results and hypothesis tests shown in Table 3.17 and Table 3.18.

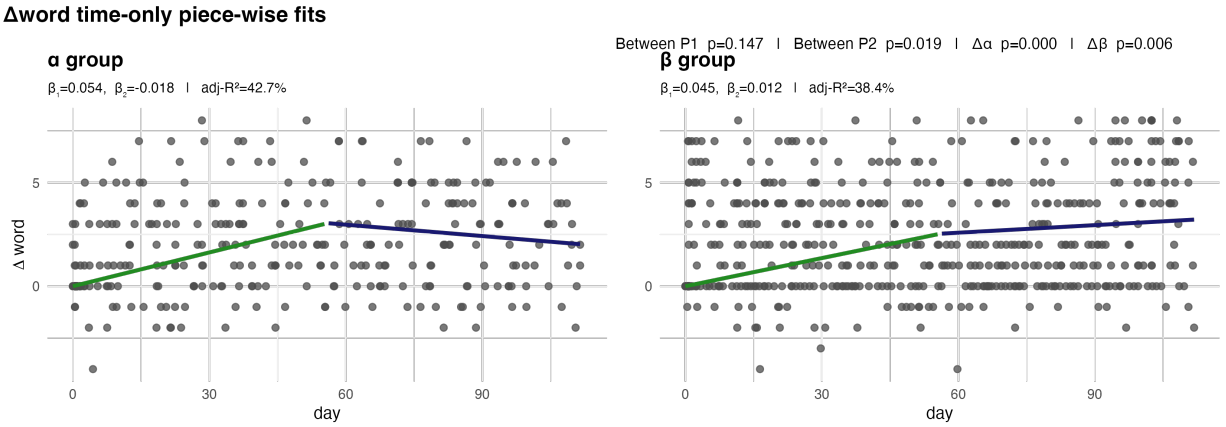


Figure 3.31: Word recall change vs. day: fitted pre-56 (green) and post-56 (blue) slopes for Alpha (left) and Beta (right).

Table 3.17: Group-level slopes and hinge effects for ΔWORD recall (hinge at Day 56).

Group	Pre-56 slope	p	η^2	Δ@56	p_Δ	η^2_Δ	Post-56 slope
Alpha	+0.0543	1.07×10^{-26}	0.301	−0.0726	1.77×10^{-7}	0.0818	−0.0183
Beta	+0.0452	2.78×10^{-24}	0.184	−0.0330	0.00618	0.0146	+0.0122

Table 3.18: Primary contrasts for ΔWORD recall (per day; hinge at Day 56).

Contrast	Estimate	t	df	p	partial η^2
Between groups: pre-56	+0.00910	1.45	320	0.147	0.0066
Between groups: post-56	−0.0305	−2.35	320	0.0194	0.0170
Within Alpha: change at 56	−0.0726	−5.34	320	1.77×10^{-7}	0.0818
Within Beta: change at 56	−0.0330	−2.75	509	0.00618	0.0146

Interpretation. Both groups improved modestly during Phase 1, with no significant between-group difference ($p = 0.47$). Post-crossover, both trajectories flattened or declined slightly, more noticeably in *Alpha* ($p = 0.014$) than in *Beta* ($p = 0.041$). Between-arm contrasts remained small ($\eta_p^2 < 0.02$).

Working Memory (Word Recall) — Stratified by eye group

The piecewise model (hinge at Day 56) was re-fit within each eye-color subgroup to examine whether working-memory performance varied with pigmentation. Figure summaries are presented below; detailed regression coefficients, hinge terms, and effect sizes are reported in Appendix K.

Light-eyed (88.9). As shown in Figure 3.32, both arms exhibited significant Phase 1 improvement (*Alpha* $p < 10^{-15}$, *Beta* $p < 10^{-6}$), consistent with a strong learning effect. *Alpha* displayed a larger pre-56 slope and a significant hinge reduction ($p = 5.2 \times 10^{-5}$), indicating that recall gains slowed after crossover. *Beta* showed a smaller hinge ($p = 0.085$), suggesting continued mild improvement. Between-group contrasts were significant for the pre-56 phase ($p = 0.004$; $\eta_p^2 = 0.056$), but not for post-56 performance, implying faster initial gains under dim-light.

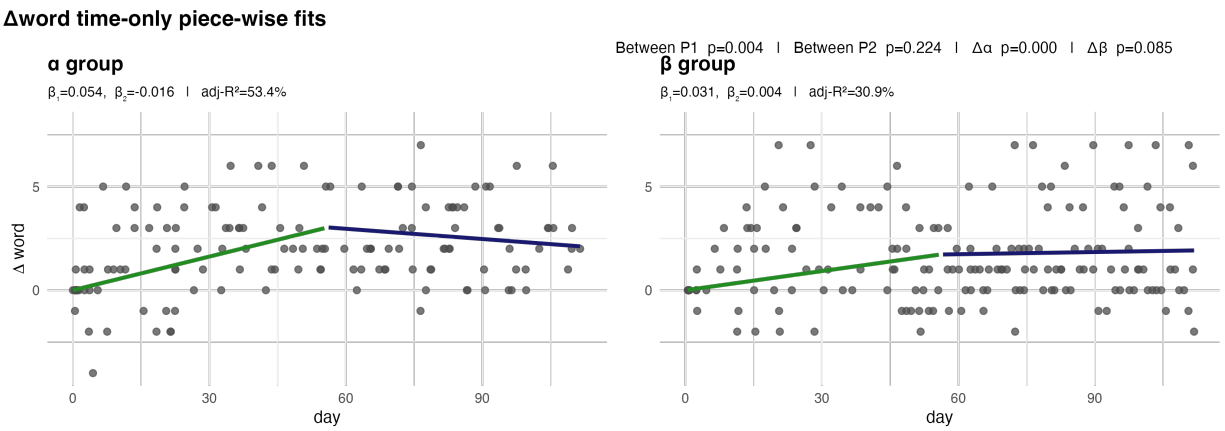


Figure 3.32: Word recall trajectories (light-eyed, 88.9). Fitted pre-56 (green) and post-56 (blue) slopes for Alpha (left) and Beta (right).

Brown-eyed Caucasians (81.15). Figure 3.33 shows robust Phase 1 improvement in both arms. *Alpha* exhibited a markedly steeper pre-56 slope ($p < 10^{-11}$) and a strong hinge decline ($p < 10^{-4}$), while *Beta* improved more gradually ($p < 10^{-5}$) and plateaued post-56. The between-group pre-56 difference was large and significant ($p = 6.9 \times 10^{-4}$; $\eta_p^2 = 0.135$), confirming faster early gains under dim-light. However, *Alpha*'s post-crossover drop led to a significant group-by-phase interaction ($p = 0.011$), whereas *Beta* maintained its performance, suggesting better retention under bright-light in later weeks.

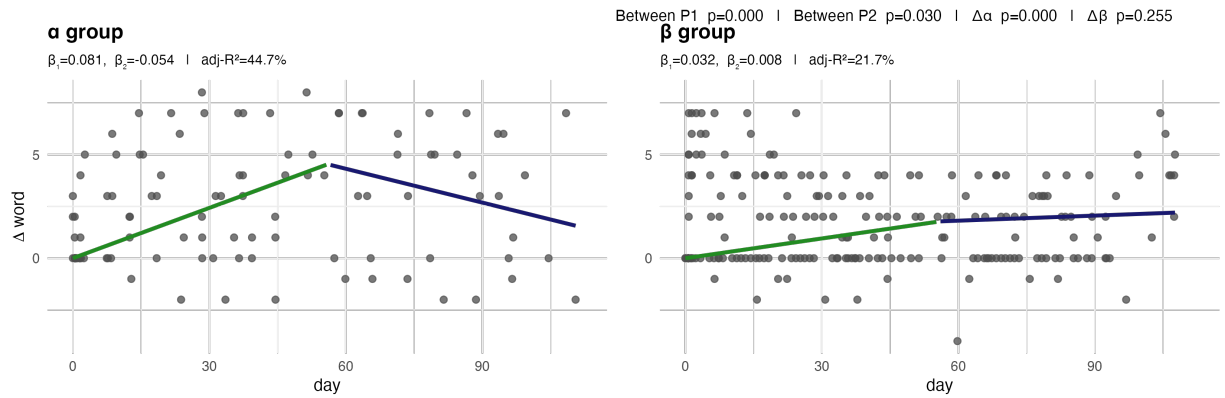


Figure 3.33: Word recall trajectories (brown-eyed Caucasians, 81.15). Fitted pre-56 (green) and post-56 (blue) slopes.

Dark-eyed (73.4). As shown in Figure 3.34, both arms improved during Phase 1, but with striking between-group differences. *Beta* participants exhibited a substantially faster pre-56 slope ($p < 10^{-20}$) and a significant hinge reduction ($p = 2.5 \times 10^{-5}$), whereas *Alpha* showed only a mild Phase 1 trend ($p = 0.008$) and no detectable hinge change ($p = 0.887$). Between-group contrasts confirmed a large pre-56 difference favoring bright-light ($p < 10^{-8}$; $\eta_p^2 = 0.37$), indicating that participants with darker eyes benefited most from bright-light exposure.

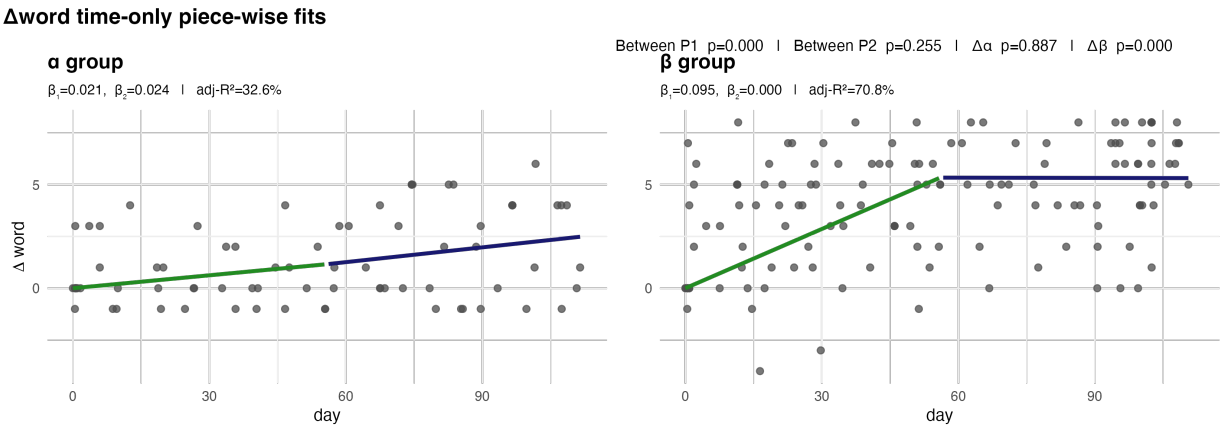


Figure 3.34: Word recall trajectories (dark-eyed, 73.4). Fitted pre-56 (green) and post-56 (blue) slopes for Alpha (left) and Beta (right).

Summary. Across all pigmentation subgroups, participants improved during Phase 1, likely reflecting learning effects. Among brown- and light-eyed Caucasians, *Alpha* displayed slightly stronger early gains, while in dark-eyed non-Caucasians, *Beta* showed markedly greater Phase 1 improvement and better post-crossover stability. Interpretation is limited, however, as confounding factors—such as English proficiency, cultural familiarity with verbal tasks, and the smartphone-based testing format—may have introduced variability and reduced precision compared with standardized verbal assessments. These aspects are revisited in the discussion section.

3.3.11 Word-Pair Recall (WORD) and Usage Time

Overview. To clarify whether daily usage intensity contributed to the observed gains in working-memory performance, a centered usage term ($\text{hours}_c = \text{hours} - \overline{\text{hours}}$) was

added to the hinge model. Full coefficients, adjusted R^2, and diagnostics are presented in Appendix L. In the non-stratified (all-eyes) analysis, usage effects were small and only marginally significant; however, the stratified models revealed *highly significant and subgroup-specific* dose–response relationships. These stratified results therefore provide the clearest evidence that usage time meaningfully influenced word-pair recall performance.

Stratified results. Figure 3.35 summarizes the key findings by eye-color subgroup. In the bright-light condition (*Beta* arm), both light- and brown-eyed Caucasian participants showed clear, dose–response improvements with higher daily usage, whereas the dim-light (*Alpha*) arm and non-Caucasian participants displayed flat or nonsignificant slopes. These stratified results reinforce the aggregate regressions, demonstrating that the relationship between usage and recall performance is not uniform but strongly moderated by eye pigmentation.

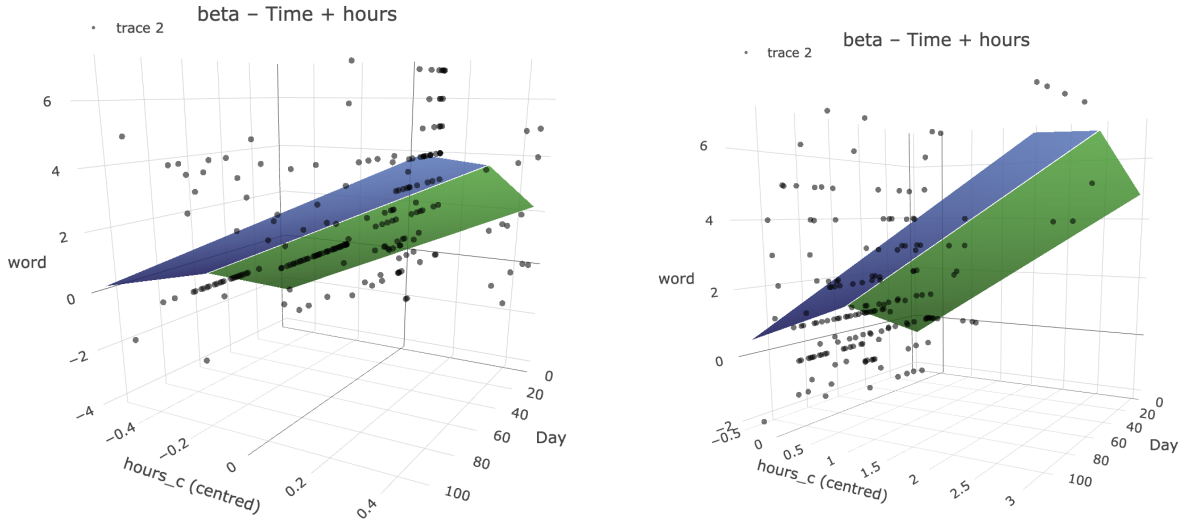


Figure 3.35: Stratified usage effects in the bright-light (*Beta*) arm: brown-eyed Caucasians (left) and light-eyed participants (right). Both subgroups exhibit significant positive relationships between daily usage and word-pair recall, confirming the subgroup-specific pattern seen in the raw regressions.

Summary and interpretation. Taken together, the stratified usage analyses clarify several ambiguities that appeared in the raw mixed-effects models. Although the non-stratified trajectories suggested that *Alpha* improved slightly faster than *Beta* within the

Caucasian subgroups, the strong dose–response effects observed here, particularly in the light-eyed and brown-eyed Caucasian participants, indicate that this pattern may be offset by differential usage intensity rather than true treatment superiority. In contrast, non-Caucasian participants already demonstrated a clear Phase 1 advantage in the *Beta* arm in the raw time model, and the stratified usage regression further supports this directionality by showing that additional daily bright-light exposure reliably improved performance in these groups as well.

Overall, these findings suggest that bright-light, when actually used, exerts a measurable influence on short-term working-memory performance, with effect magnitude moderated by ocular pigmentation and usage adherence. At the same time, interpretation should be tempered by the limitations of the smartphone-based recall test—potentially less precise than standardized verbal protocols—and by possible intercultural differences in verbal memory performance. Nonetheless, the convergence across stratified models provides a compelling signal of cognitive benefit under bright-light exposure and motivates further targeted investigation.

Covariate Effects: Baseline, Age, and Sex

Overview. Baseline performance, age, and sex were added as centered covariates to the hinge model to assess whether individual characteristics moderated changes in WORD recall. Full coefficient tables and diagnostics are provided in Appendices M.2, M.3, and M.4. Here, we highlight the most interpretable covariate effect (baseline) with summary figures, while age and sex results are described succinctly.

Baseline performance. Across both arms, higher baseline recall strongly predicted smaller subsequent gains, consistent with a ceiling effect. Baseline contributed substantial explanatory power in both Alpha and Beta models ($\Delta R^2_{\text{adj}} \approx 0.10$), indicating that initial memory capacity was the dominant covariate influencing recall trajectories. Shown in Figure 3.36.

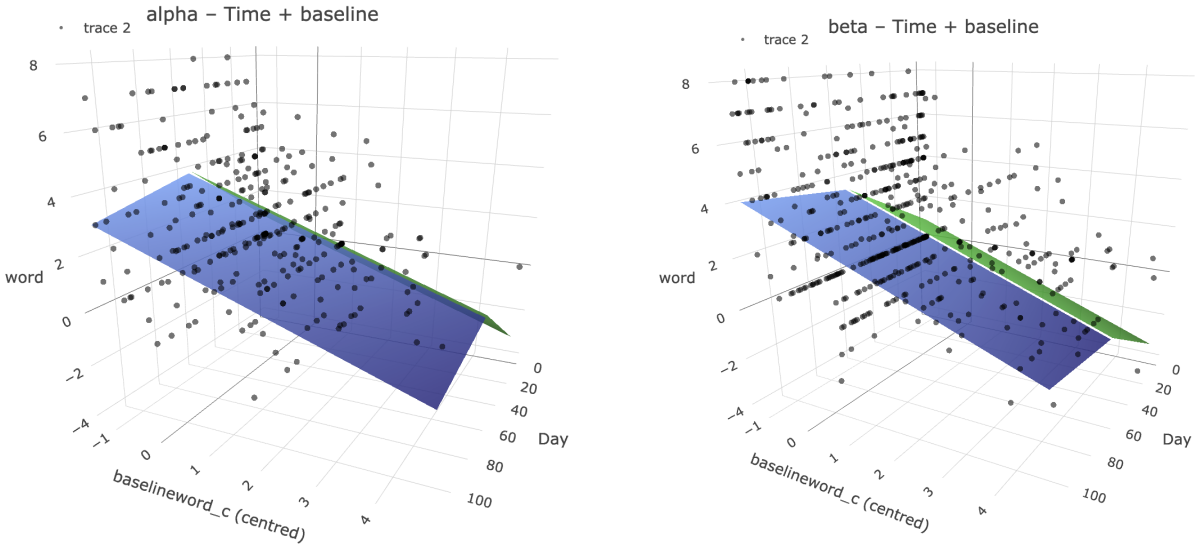


Figure 3.36: Time + baseline regression planes for WORD recall in Alpha (left) and Beta (right). Higher baseline performance corresponds to smaller subsequent improvements, consistent with ceiling effects. Full statistics in Appendix M.2.

Age effects. Age showed a small but consistent negative association with recall improvement: older participants exhibited slightly smaller gains across both phases. Effects were statistically significant but modest in magnitude. Full results appear in Appendix M.3.

Sex effects. A small sex effect was present only in the bright-light (*Beta*) arm, where male participants showed slightly smaller improvements than females. This effect was weak but directionally consistent across phases. Full results are provided in Appendix M.4.

Summary. Covariate analyses reveal that Word-Pair Recall is strongly shaped by baseline memory performance, with smaller but consistent influences of age and sex. These results contextualize the usage findings (Section 3.3.11), emphasizing that baseline ability explains the majority of between-subject variability, while sustained bright-light usage remains a significant modulator of short-term memory improvement.

3.3.12 Per-participant analysis — Word-Pair Recall (equal-weight endpoint method)

Using the same per-participant endpoint model (requiring at least two data points in each phase), the WORD scores were analyzed to estimate individual Phase 1 (Δ_1) and Phase 2 (Δ_2) changes. Each participant's midpoint and final predicted values were used to derive phase deltas, assigning equal weight to all individuals regardless of observation count.

Results (dark-eyed non-Caucasian subgroup). When stratified by eye color, a significant between-arm difference emerged only among dark-eyed non-Caucasian participants (Fig. 3.37). During Phase 1, the **Beta** arm demonstrated greater improvements in word-pair recall compared with **Alpha** ($p < 0.01$), suggesting a positive effect of bright-light exposure on short-term verbal-memory consolidation. After crossover (Phase 2), Beta participants exhibited a modest decline ($p < 0.05$), whereas Alpha remained largely stable. No significant phase effects were observed for light- or white-brown–eyed groups.

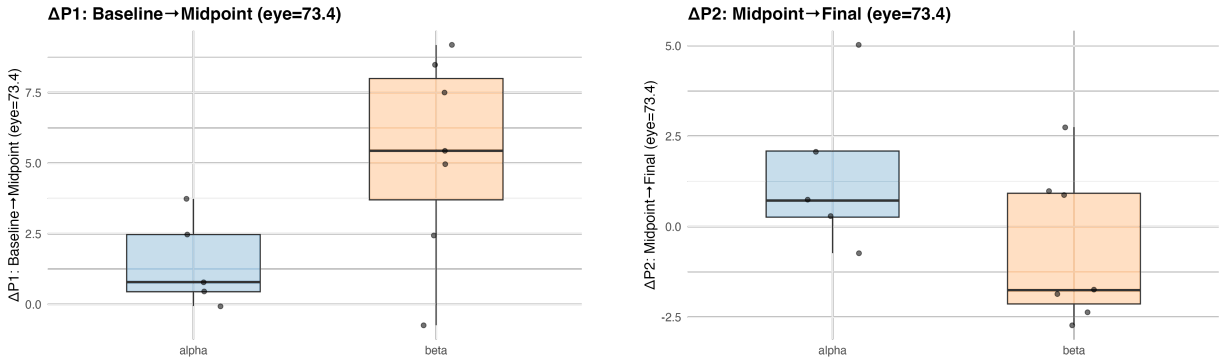


Figure 3.37: Dark-eye (non-Caucasian) subgroup: participant-level Word-Pair Recall phase changes. Left: Phase 1 (Δ_1), showing greater improvement in Beta vs. Alpha ($p < 0.01$). Right: Phase 2 (Δ_2), showing partial regression in Beta ($p < 0.05$) with stable Alpha responses.

Table 3.19: Group means and standard deviations for ΔWORD (dark-eyed non-Caucasian subgroup).

Phase	Group	n	Mean (pts)	SD
Phase 1 (Δ_1)	Alpha	8	+1.47	1.29
	Beta	9	+5.33	2.14
Phase 2 (Δ_2)	Alpha	8	+1.10	1.34
	Beta	9	−1.03	1.87

Notes. Values represent per-participant mean phase changes derived from hinge-fit endpoints. Positive numbers indicate improvement relative to baseline.

Table 3.20: Hypothesis tests for ΔWORD (dark-eyed non-Caucasian subgroup).

Contrast	t	df	p	Effect size	Interpretation
Between arms: Phase 1 (Δ_1)	3.34	14.9	0.003	$g = 1.12$	large
Between arms: Phase 2 (Δ_2)	−2.24	15.6	0.039	$g = -0.79$	small–medium
Within Beta: $\Delta_2 - \Delta_1$	−2.91	8	0.010	$d_z = 0.97$	large rebound
Within Alpha: $\Delta_2 - \Delta_1$	−0.53	7	0.600	$d_z = 0.19$	n.s.

Notes. Welch's t-tests compare Alpha and Beta arms for each phase; within-arm paired tests compare Δ_1 and Δ_2. Hedges' g and Cohen's d_z denote between- and within-group standardized effect sizes.

Interpretation. The per-participant endpoint patterns broadly mirror the raw piecewise-regression results but should be viewed as descriptive. Only in the dark-eyed (73.4) subgroup does the larger Phase-1 advantage for the *Beta* (bright-light) arm from the time-slope model also appear in the equal-weight Δ_1/Δ_2 endpoints, with a modest post-crossover softening. For the light- and brown-eyed groups, endpoint contrasts did not reach significance despite similar directional trends, which is likely due to limited sample size and residual variability in the smartphone-based endpoint (e.g., measurement noise, practice and language effects).

3.3.13 Side Effects and Adverse Events

Weekly survey data were used to evaluate the frequency and severity of adverse events across treatment arms. Table 3.21 summarizes average weekly side-effect reports per participant for the full sample, while Tables 3.22, 3.23 and 3.24 present stratified analyses by eye-color subgroup to explore whether ocular pigmentation influenced tolerability.

Table 3.21: Average weekly side effects reports per participant, by group and phase, with between- and within-group comparisons (all eyes).

	Phase	n	Headache	Jitter	Nausea	Eyestrain	Vision changes
Alpha	Phase 1 (mean ± SD)	37	0.6 ± 0.7	0.1 ± 0.2	0.2 ± 0.5	0.7 ± 0.9	0.3 ± 0.6
	Phase 2 (mean ± SD)	29	0.7 ± 0.8	0.1 ± 0.2	0.1 ± 0.4	0.6 ± 0.9	0.3 ± 0.9
Beta	Phase 1 (mean ± SD)	36	0.5 ± 0.8	0.1 ± 0.2	0.2 ± 0.4	0.8 ± 0.9	0.3 ± 0.7
	Phase 2 (mean ± SD)	27	0.4 ± 0.8	0.1 ± 0.4	0.3 ± 0.9	1.0 ± 1.6	0.5 ± 1.0
Between groups p (Phase 1)			0.224	0.280	0.447	0.400	0.410
Between groups p (Phase 2)			0.149	0.163	0.170	0.130	0.201
Within Alpha p			0.42	0.48	0.31	0.39	0.47
Within Beta p			0.40	0.28	0.22	0.21	0.19

Notes. No comparisons reached significance at the $p < 0.05$ level. Absolute frequencies were low (< 1 report per week).

Eye-color stratification. To assess whether ocular pigmentation influenced sensitivity to bright or dim-light exposure, side effects were next stratified into dark-eyed, brown-eyed Caucasian, and light-eyed groups. The following tables provide these subgroup summaries: Table 3.22 (dark-eyed), Table 3.23 (brown-eyed Caucasian), and Table 3.24 (light-eyed participants).

Table 3.22: Average weekly side-effect reports per participant for dark-eyed participants, by group and phase, with between-arm comparisons.

	Phase	n	Headache	Jitter	Nausea	Eyestrain	Vision changes
Alpha	Phase 1 (mean ± SD)	11	0.9 ± 0.7	0.1 ± 0.3	0.1 ± 0.2	1.2 ± 0.9	0.1 ± 0.2
	Phase 2 (mean ± SD)	8	0.9 ± 0.8	0.1 ± 0.2	0.1 ± 0.3	0.9 ± 0.9	0.2 ± 0.3
Beta	Phase 1 (mean ± SD)	12	0.4 ± 0.7	0.0 ± 0.1	0.1 ± 0.2	0.6 ± 0.9	0.0 ± 0.1
	Phase 2 (mean ± SD)	9	0.3 ± 0.6	0.0 ± 0.1	0.1 ± 0.2	1.0 ± 2.0	0.0 ± 0.1
Between-group p (Phase 1)			**0.05**	0.17	0.21	0.07	0.20
Between-group p (Phase 2)			0.07	0.33	0.36	0.44	0.14

Notes. Headache incidence was marginally higher in Alpha during Phase 1 ($p = 0.05$). All other comparisons were non-significant. Absolute frequencies were low.

Table 3.23: Average weekly side–effect reports per participant for brown–eyed Caucasian participants, by group and phase, with between–arm comparisons.

	Phase	n	Headache	Jitter	Nausea	Eyestrain	Vision changes
Alpha	Phase 1 (mean ± SD)	10	0.7 ± 0.7	0.1 ± 0.2	0.3 ± 0.6	0.6 ± 0.8	0.4 ± 0.8
	Phase 2 (mean ± SD)	9	1.0 ± 1.0	0.1 ± 0.3	0.3 ± 0.6	0.8 ± 1.2	0.6 ± 1.6
Beta	Phase 1 (mean ± SD)	10	0.2 ± 0.3	0.1 ± 0.2	0.1 ± 0.4	0.5 ± 0.5	0.0 ± 0.0
	Phase 2 (mean ± SD)	7	0.2 ± 0.3	0.3 ± 0.7	0.3 ± 0.8	0.6 ± 1.0	0.0 ± 0.0
Between–group p (Phase 1)			**0.04**	0.40	0.26	0.35	0.08
Between–group p (Phase 2)			**0.02**	0.27	0.48	0.38	0.12

Notes. Brown–eyed Caucasian participants showed significantly higher headache reports in Alpha vs. Beta during Phase 1 ($p = 0.04$) and Phase 2 ($p = 0.02$). All other symptom comparisons were non–significant. Absolute event frequencies remained low (< 1/week).

Table 3.24: Average weekly side-effect reports per participant for light-eyed participants, by group and phase, with between-arm comparisons.

	Phase	n	Headache	Jitter	Nausea	Eyestrain	Vision changes
Alpha	Phase 1 (mean ± SD)	15	0.4 ± 0.7	0.0 ± 0.0	0.2 ± 0.5	0.4 ± 0.7	0.3 ± 0.7
	Phase 2 (mean ± SD)	11	0.2 ± 0.4	0.0 ± 0.0	0.0 ± 0.1	0.3 ± 0.7	0.1 ± 0.2
Beta	Phase 1 (mean ± SD)	14	0.7 ± 1.0	0.1 ± 0.3	0.3 ± 0.6	1.1 ± 1.1	0.7 ± 0.9
	Phase 2 (mean ± SD)	11	0.7 ± 1.1	0.1 ± 0.2	0.5 ± 1.4	1.3 ± 1.6	1.2 ± 1.3
Between-group p (Phase 1)			0.11	**0.05**	0.26	**0.03**	0.09
Between-group p (Phase 2)			0.11	**0.04**	0.12	**0.04**	**0.01**

Notes. Light-eyed Beta participants reported significantly higher jitter, eyestrain, and vision changes, and a trend-level difference in nausea across phases (Phase 1 jitter/eyestrain $p \leq 0.05$; Phase 2 jitter, eyestrain, and vision changes $p \leq 0.04$). Although absolute symptom levels remained low (< 1/week), this pattern may indicate heightened sensitivity to bright-light exposure or possible carryover effects.

Summary. Across all subgroups, adverse events were generally mild and infrequent (< 1 report per week), with no clinically meaningful safety concerns. Dark-eyed participants showed a marginally higher Phase 1 headache rate in the Alpha group (Table 3.22), and brown-eyed Caucasian participants reported significantly more headaches in Alpha during both phases (Table 3.23). Because Alpha participants received the *dim-light control* condition, these patterns suggest that headaches in darker- and brown-eyed individuals were unlikely to be driven by bright-light exposure. Instead, they may reflect device-related comfort factors or individual susceptibility—points elaborated in the discussion section.

The clearest and most consistent pattern emerged in the light-eyed subgroup (Table 3.24). Here, the Beta arm reported elevated jitter, nausea, eyestrain, and vision-change symptoms in Phase 1 and—strikingly—these symptoms persisted into Phase 2 *despite the switch to dim-light exposure*. This persistence suggests a combination of heightened photic sensitivity and possible carryover or expectation effects following initial bright-light exposure. Such discomfort could plausibly blunt mood improvements in this group, aligning with the attenuated MADRS benefit observed in light-eyed participants.

Overall, adverse events remained low in frequency and severity across all groups.

Serious Adverse Events In terms of serious adverse events, two reports were filed with REB. A case of psychosis was observed and confirmed to be not related to the protocol; the

participant received aid from their therapist and was able to manage the symptoms and wished to continue with the study. An adverse event report was filed to the REB. A case of eye hemorrhage was observed that was also confirmed to not be related to the protocol. The participant continued with the study after receiving care and permission from their physician. An adverse event report was filed to the REB.

Chapter 4

Discussion

4.1 Overview of Primary Findings

Across mood (MADRS), sleep disturbance (PROMIS), psychomotor vigilance (PVT), and working memory, bright-light exposure delivered through the Lumos smart glasses produced measurable benefits relative to dim-light control. However, the magnitude and direction of these effects varied across ocular pigmentation, usage behavior, ambient light exposure, and baseline symptom severity. These findings indicate that individual photobiological response profiles shape treatment efficacy and highlight the importance of personalized light-dosing strategies.

4.2 Outcome-Specific Interpretations

4.2.1 Mood and Depressive Symptoms (MADRS)

MADRS displayed the strongest pigmentation-dependent effects. Participants with darker irides responded most robustly to bright-light, and their regression after crossover reflects a withdrawal of melanopic stimulus rather than an adverse reaction. This pattern is consistent with the idea that greater ocular pigmentation reduces retinal transmittance and may require higher melanopic doses to produce comparable biological effects.

Light-eyed participants showed a different pattern. They improved more under dim-light and exhibited muted or unstable responses once bright-light was introduced. Their

higher retinal transmittance likely increases the effective melanopic dose for a given intensity, which makes lower intensities sufficient or even preferable, as discussed further in Section 4.8. Their higher rate of brightness-related discomfort supports this explanation and may help account for the inverted dose response observed in their mood outcomes.

Some unexpected reversals, especially among dark-eyed non-Caucasian participants, suggest that psychological and motivational factors also played a role. Participants who benefited little during Phase 1, or who sensed that they were receiving the dim-light condition, may have reduced their engagement or altered their symptom ratings, which would blunt Phase 2 trajectories.

Overall, these findings indicate that ocular pigmentation interacts with subjective comfort and treatment expectations. Personalized melanopic dosing appears especially important for mood-related outcomes.

4.2.2 Sleep Disturbance (PROMIS)

Sleep disturbance outcomes paralleled the pigmentation effects seen in MADRS but showed a more physiologically stable pattern. bright-light produced faster improvement overall, and darker-eyed participants experienced the largest Phase 1 benefits. Light-eyed participants showed a slight preference for dim-light in Phase 1, although the differences were smaller than those for mood.

After crossover, Beta participants showed clear rebound effects when bright-light was withdrawn. Alpha participants showed more variable Phase 2 responses, shaped by pigmentation and usage patterns. These responses suggest that sleep reflects both circadian physiology and a moderate influence of subjective comfort, although less than is seen for mood.

4.2.3 Psychomotor Vigilance (PVT)

PVT was the most objective and physiologically driven outcome. bright-light consistently improved vigilance across all pigmentation groups, and dimming the light produced reliable regressions after crossover. Light-eyed participants responded strongly to bright-light, which indicates that the melanopsin-mediated alertness pathway operates effectively regardless of pigmentation when the outcome measure is fully objective.

The stability of PVT responses and their close alignment with crossover expectations suggest that this outcome depends mainly on direct melanopic stimulation. Subjective comfort and expectancy effects appear to have minimal influence.

4.2.4 Working Memory

Working memory performance showed clear practice effects but still displayed treatment-related patterns. Dark-eyed participants improved under bright-light during Phase 1. Some light-eyed or Caucasian subgroups showed modest early gains under dim-light, which may reflect a mixture of learning effects and pigmentation-related sensitivity. Participants who used the glasses consistently showed clearer cognitive benefits, which suggests that adherence strengthens working-memory improvements, especially under bright-light conditions.

4.3 Moderators of Treatment Response

Usage behavior was one of the strongest moderators across outcomes. Longer daily wear amplified improvements in mood, sleep, and cognition, particularly in subgroups that showed weaker baseline responsiveness under dim-light. This pattern suggests that consistent melanopic dosing enhances treatment effects even when group-level patterns are modest.

Ambient melanopic light predicted improvement in several models. Participants who received more total melanopic light across the day, whether from the environment or the device, showed greater reductions in symptoms. This result aligns with substantial evidence that daytime light exposure improves mood, sleep quality, and circadian alignment.

Baseline symptom severity consistently predicted improvement, indicating greater headroom for change among more symptomatic participants. Age and sex produced statistically detectable but small effects, which suggests secondary roles compared with pigmentation, usage, and melanopic exposure.

4.4 Cross-Outcome Synthesis

The outcomes form a coherent gradient linking subjective, mixed, and objective processes. Mood was the most sensitive to subjective comfort, expectancy, and motivation. Sleep reflected both physiological circadian mechanisms and moderate psychological influence. PVT showed a direct physiological response that was consistent across all pigmentation groups. Working memory reflected both light exposure and practice effects.

These gradients map onto the biological and psychological components inherent in each outcome. Outcomes with stronger subjective components, such as mood, exhibited larger

pigmentation-dependent differences. Outcomes with stronger physiological drivers, such as PVT, followed the hypothesized pattern more consistently.

A unifying interpretation is that ocular pigmentation modulates the effective melanopic dose, which influences both subjective comfort and treatment sensitivity. Those with darker eyes benefit more from higher intensities, whereas lighter-eyed may require moderated intensities to avoid overstimulation. Usage behavior and ambient light exposure further shape dose accumulation and treatment effectiveness.

4.5 Power and Sensitivity Considerations

Because the trial was powered primarily for the aggregate sample rather than for multiple pigmentation-based strata, it was important to evaluate the statistical sensitivity of the analyses. For each outcome (MADRS, PROMIS sleep disturbance, psychomotor vigilance, and word-pair recall), a post hoc sensitivity analysis was performed to determine the minimum partial η^2 detectable with 80% power at $\alpha = .05$ under the two-sample slope-contrast framework used throughout the study.

The full-sample ("All Eyes") analyses showed the highest sensitivity, with minimum detectable partial η^2 values of approximately 0.014 for MADRS and PROMIS, 0.020 for psychomotor vigilance, and 0.015 for word-pair recall. These correspond to small effect sizes, indicating that the aggregate analyses were well powered. In contrast, pigmentation-stratified analyses required medium or larger effects (minimum detectable partial η^2 ranging from 0.03 to 0.05) due to the smaller subgroup sizes.

Across all outcomes and strata, every statistically significant contrast exhibited a partial η^2 that exceeded the detectable threshold for its stratum, indicating that these effects were adequately powered. Conversely, most non-significant subgroup contrasts had partial η^2 values below their respective thresholds, meaning that these null findings should be viewed as inconclusive rather than as evidence of no treatment effect. This pattern occurs because power reflects the probability of detecting effects of a given magnitude; when the minimum detectable effect is relatively large, smaller effects will routinely produce non-significant results even if they are real.

Only three contrasts across all analyses showed mild inconsistencies between statistical significance and detectability. These "oddball" cases all arose near the detection boundary and are expected in finite-sample studies:

- **Psychomotor vigilance (All Eyes, Between-Post):** $p = .026$ but partial η^2 was

slightly below threshold. This reflects a small but statistically detectable effect that would not be consistently detected across repeated samples.

- **Psychomotor vigilance (Exclude light eyes, Within-Alpha):** $p = .051$ but partial η^2 exceeded the detectable threshold. This represents a borderline, trend-level effect that narrowly missed significance but is unlikely to be a null effect.
- **Word-pair recall (All Eyes, Within-Beta):** $p = .006$ with partial η^2 essentially equal to (but slightly below) the detection threshold. This indicates a very small effect that reached significance because of the large full-sample size, a well-known phenomenon where trivial effects become statistically significant in large datasets.

These cases do not undermine the overall findings. Instead, they illustrate three statistically expected behaviors: (1) small significant effects occurring just below the 80% power boundary, (2) borderline effects that narrowly miss significance despite being detectable, and (3) large-sample detection of very small effects that may have limited practical relevance.

Together, the power and sensitivity diagnostics demonstrate that the study was well powered to detect small effects in the aggregate analyses and medium or larger effects within pigmentation strata. This framework provides a principled interpretation of both statistically significant findings and null or borderline results. Detailed numerical comparisons and the full effect-size tables are provided in Appendix N.

4.6 Clinically Meaningful Thresholds

To interpret the practical significance of the findings, Phase 1 improvements were compared against published clinically meaningful thresholds for each outcome. Phase 1 was used because it reflects each participant's initial treatment assignment prior to crossover, providing the clearest estimate of the treatment-specific dose–response effect. For each outcome, the subgroup showing the clearest bright-light responsiveness was selected: non–light-eyed participants for MADRS and PROMIS, the full sample for PVT, and the dark-eyed subgroup for Word-Pair recall. The estimated Phase 1 slope (β_1) from the piecewise time model was multiplied by 56 days to obtain the total expected change from baseline:

$$\Delta_{\text{Phase 1}} = \beta_1 \times 56.$$

These bright-light deltas were then compared with established clinically or practically meaningful thresholds identified in the literature. As shown in Table 4.1, the bright-light

improvements in mood and sleep exceeded widely accepted minimal clinically important differences for MADRS and PROMIS. PVT changes exceeded operational thresholds used in vigilance and fatigue research by a wide margin, and the Word-Pair recall gains were substantially larger than typical practice-adjusted cognitive improvements.

Table 4.1: Phase 1 bright-light improvements compared with clinically meaningful thresholds.

Outcome	**Meaningful Threshold**	**Δ Phase 1**	**Meaningful?**
MADRS (non-light)	3–6 pts [38, 40]	−9.97	Yes
PROMIS Sleep Dist. (non-light)	2–3 T-score pts [26, 107]	−4.76	Yes
PVT Reaction Time (all eyes)	20–30 ms [16, 37]	−95.8 ms	Yes
Word-Pair Recall (dark eyes)	≥2 items [70, 75]	+5.32 items	Yes

Taken together, these results demonstrate that the effects of bright-light exposure delivered through the Lumos glasses were not only statistically significant but also clinically and practically meaningful across mood, sleep, vigilance, and memory domains. The magnitudes of these Phase 1 improvements are consistent with, and in some cases exceed, effect sizes reported in established bright-light therapy and cognitive-performance literature.

4.7 Effect Sizes in Context of Bright-Light Therapy

To evaluate the practical significance of the findings, per-participant effect sizes (Hedges' g, approximately equivalent to Cohen's d at the sample sizes used here) were compared with typical effect sizes reported in the bright-light therapy (BLT) literature. Table 4.2 summarizes the Phase 1 bright-light effect sizes in this study alongside established BLT benchmarks for depression, sleep disturbance, alertness, and cognition.

Across outcomes, the bright-light effects observed in this study were comparable to or larger than those typically reported for BLT. For depression (MADRS), the non–light-eyed subgroup showed a moderate-to-large effect ($g \approx 0.85$), consistent with the upper range of BLT effects in nonseasonal depression trials [44, 60]. The PROMIS Sleep Disturbance effect ($g \approx 1.06$) exceeded the small-to-moderate effects commonly reported for BLT in sleep outcomes [26, 107]. Improvements in psychomotor vigilance ($g \approx 0.34$) aligned with established light-induced alertness effects [16]. Finally, the Word-Pair recall effect in dark-eyed participants was very large ($g \approx 1.12$), surpassing the modest cognitive effect sizes typically

observed in light or sleep-intervention studies [70, 75]. These comparisons demonstrate that the bright-light intervention delivered through the Lumos glasses produced clinically and practically meaningful improvements across multiple domains.

Table 4.2: Per-participant bright-light effect sizes (Hedges' g and converted Cohen's d) compared with typical bright-light therapy (BLT) effect sizes.

Outcome	**Hedges' g**	**Cohen's d**	**Typical BLT d**	**Comparison**
MADRS (non-light)	0.85	0.85	0.5–0.8 [44, 60]	Matches upper BLT
PROMIS SD (non-light)	1.06	1.06	0.3–0.6 [26, 107]	Much larger
PVT RT (all eyes)	0.34	0.34	0.3–0.5 [16]	Within BLT range
Word Recall (dark eyes)	1.12	1.12	0.2–0.4 [70, 75]	Far larger

4.8 Interpretation in Context

One important finding from this study is the moderating role of eye color in determining light therapy response and, by extension, vulnerability to light-related mood disorders. Anatomically, the amount of light reaching the retina is influenced not only by pupil diameter but also by the transmission and scattering of light through the iris and adjacent ocular tissues. Van den Burg et al. demonstrated that for light blue eyes with a 4 mm pupil, approximately 5–17% of incident light can reach the retina through peri-iris and stromal pathways. In contrast, transmission in dark brown irides is nearly two orders of magnitude lower, with Caucasian brown eyes falling between these extremes [99]. Because the pupil can constrict to 2–4 mm under bright conditions, the proportion of extra-pupillary light entering the retina may become even greater in lighter eyes. These physiological differences provide a mechanistic basis for the varying responses to bright-light therapy observed across pigmentation groups.

The optical origin of blue eye color further supports this interpretation. Blue irides do not contain blue pigment; rather, their color arises from light scattering in the low-melanin anterior stroma, a phenomenon related to the Tyndall effect. This structural coloration implies reduced pigment-based absorption and therefore limited shielding of incident light. Several reviews describe this process clearly [91, 51, 102, 10]. The paucity of stromal melanin in blue eyes is consistent with the higher retinal transmission reported in physiological measurements.

Epidemiological and clinical evidence aligns with these anatomical considerations. Individuals with lighter-colored eyes show lower susceptibility to seasonal affective disorder and reduced depressive symptom severity compared with those with darker eyes [105, 43]. These findings suggest that lower stromal and peri-iris transmittance in darker irides may reduce retinal illuminance during short winter photoperiods, increasing the likelihood of circadian and mood dysregulation in susceptible populations.

However, differences in iris transmission cannot fully explain variability in light responsiveness. Retinal physiology, particularly the photoreceptor-level conversion of light into neural signals, also contributes meaningfully. Lavoie et al. reported that individuals with seasonal affective disorder show reduced cone electroretinogram (ERG) amplitude during the winter depressive state, which normalizes following four weeks of bright-light therapy [61]. This suggests that light therapy may restore retinal responsivity in addition to influencing central circadian pathways. Earlier work by Terman [95] found that SAD patients exhibited heightened photopic and scotopic sensitivity during winter, with normalization after treatment. These seemingly opposing results likely reflect different aspects of visual adaptation. Reduced physiological response amplitude at the photoreceptor level may coexist with increased perceptual sensitivity downstream. Together, these findings support the hypothesis that SAD involves dysregulation in both retinal gain control and higher-order light-processing mechanisms.

Inter-individual differences in light processing extend beyond circadian and affective domains. Classic psychophysical studies report that darker-eyed individuals tend to exhibit faster visual reaction times than lighter-eyed individuals [69]. This may reflect evolutionary trade-offs between neural response speed and light sensitivity, mediated by pigment-dependent differences in retinal or cortical responsiveness. Such findings help explain the moderation of psychomotor vigilance by eye color observed in the present study and suggest that ocular pigmentation modulates not only affective responses but also cognitive performance in response to light.

Taken together, these results support a coherent multi-level model. Anatomical pigmentation shapes retinal light transmittance. Retinal physiology determines the gain and adaptation of photoreceptor responses. These factors interact with central neural circuits governing mood, sleep, and vigilance. Understanding the layered interplay among pigmentation, retinal physiology, and neural adaptation is essential for optimizing light therapy dosage, timing, and spectral composition for individuals with different eye colors and light sensitivities.

4.8.1 Ambient Light in General

A consistent finding across the broader circadian, environmental, and occupational-health literature is the importance of access to natural daylight. Studies have shown that exposure to daylight and access to windows in office environments are associated with better sleep quality, reduced depressive symptoms, improved cognitive performance, and greater overall well-being [23, 12, 96, 103]. These effects appear across diverse settings, including workplaces, urban residences, and real-world environments, suggesting that daylight is a fundamental regulator of human physiological and psychological functioning.

The present study closely echoes these findings. Ambient melanopic light exposure emerged as a significant moderator of mood, sleep, and reaction time, independent of the bright-light intervention delivered by the Lumos glasses. Participants who received higher total daily melanopic exposure, whether through windows, outdoor light, or well-lit environments, tended to show greater improvements across multiple domains. This supports a cumulative-light model in which environmental illumination and device-delivered illumination jointly influence circadian alignment and neurobehavioral outcomes.

However, these results also highlight a key issue of social inequity. Access to windows and natural light in workplaces is often unequally distributed, typically favoring individuals in higher management positions, while many employees in lower-ranked or interior roles work in spaces with little or no daylight. Given the well-established health benefits of daylight exposure, such disparities may contribute to unequal sleep, mood, and cognitive outcomes across socioeconomic strata.

A core motivation for this research is the belief that the health and well-being benefits of adequate light exposure should be accessible to all individuals, regardless of their occupational or socioeconomic status. Technologies such as the Lumos smart glasses may help mitigate these disparities by providing biologically meaningful light exposure to those who lack consistent access to natural light due to workplace design, environmental constraints, or socioeconomic factors.

These findings also align with other large-scale observational and mechanistic studies that link natural or high–melanopic content light environments to improved mental health, better sleep patterns, and more stable circadian rhythms [25, 29, 68, 22, 106, 35, 90].

4.9 Limitations

One limitation of the present study is its modest sample size. Although the original design targeted 96 participants, only 73 began the study, 66 completed Phase 1, and 50

completed both phases. This sample was sufficient to detect the primary findings that bright-light therapy significantly improves mood, sleep, and reaction time compared with dim-light active control. It also allowed for the discovery of meaningful secondary patterns involving usage time, eye pigmentation, and ambient light exposure. However, several subgroup effects, particularly those involving age, sex, and pigmentation-specific reversals, were small and would benefit from validation in a larger cohort.

The paired word-recall task also illustrates the implications of sample size and measurement constraints. Although this cognitive outcome did yield some meaningful treatment-related findings, especially when accounting for daily usage time, the overall effects were modest and partly constrained by ceiling effects and the limited range of performance in a mobile-based testing format. A larger sample size would allow finer resolution of cognitive effects, improve power to detect pigmentation and demographic moderators, and help disentangle psychological contributors to the reversal patterns observed in mood outcomes.

Importantly, the current study demonstrates that the Lumos glasses and accompanying app infrastructure are well suited for large-scale deployments. Because the intervention is portable, low burden, and instrumented with continuous usage and light-exposure logging, future studies can recruit substantially larger and more diverse samples while capturing detailed behavioral and environmental data. This scalability is one of the key advantages of the Lumos platform and will enable more definitive testing of individual differences, including age, sex, pigmentation, usage behavior, and psychological factors, that were only partly observable within the current dataset.

Test instruments, such as self reported MADRS[40], PROMIS [72] uses standard proven metrics, and was administered through the Qualtrics survey portal. While these tests are solid, they are also bundled with a large number of quality of life and adverse events questions, which may make the weekly survey cumbersome. There is a tradeoff with the study, where longer surveys using more sensitive instruments could lead to more accurate results, but risk compliance issues as surveys get too long.

Another limitation concerns baseline timing and the alignment of survey responses with actual device usage. In the initial design, many participants experienced a delay between completing their intake survey and receiving their glasses, which meant their first scheduled weekly survey did not always correspond to their true pre-treatment state. This issue was addressed analytically through a global rebaselining method, which helped ensure that treatment effects were not conflated with timing irregularities. However, this approach is still an approximation and may not fully capture each participant's true baseline, especially for those who began using the glasses or completing surveys later than intended. A practical improvement for future studies would be to require a baseline assessment immediately

upon receipt of the glasses and prior to any device use. Implementing a mandatory in-app baseline checkpoint would eliminate ambiguity in baseline timing, reduce the need for post hoc adjustment, and strengthen internal validity for all subsequent outcome trajectories.

A further limitation relates to unequal measurement density across participants. In the original piecewise regression framework, individuals who completed more weekly surveys exerted proportionally greater influence on the estimated slopes and breakpoints, whereas participants with sparse data contributed less to the model fit. This issue was largely resolved by using endpoint regression methods, which reduce sensitivity to uneven sampling and mitigate weighting biases. However, participants with very few data points still provide less robust estimates, and their trajectories remain more uncertain. Future studies can address this by implementing more convenient and engaging survey workflows within the app, thereby increasing compliance and reducing missingness. Improving survey adherence would strengthen the reliability of both individual-level trajectories and group-level inferences, and would support the application of more sophisticated statistical approaches such as bootstrapping or multilevel modeling with equal participant weighting.

For reaction time, the industry standard Psychomotor Vigilance Test was referenced [16], and made with some modifications to test 10 reactions and a custom metric where mean reaction is averaged with lapses and false starts penalized as a 500 ms reaction time. This was done to keep the test short and reduce strain for participants. To also reduce risk of participant phone differences, the core calculations of the test are administered inside the glasses' hardware and firmware, allowing a solid reference.

The word paired test was not administered in an ideal manner, as standard testing is ideally done with 10 words for 3 sets, verbally with an administrator. With text- and app-based testing in this study, participants may have many other factors that could influence their performance, such as smartphone compatibility, screen brightness, font size, and potential for taking screenshots or photos.

This study used the 2024 generation of the coating on PMMA lenses, which offers a good balance of blue-light blocking, as well as reflection for treatment. It does have some light leakage out the front, where people can observe a glowing light at certain angles, which may contribute to lower compliance or likelihood of wearing it in public. There is a newer generation of the lenses in 2025 that dramatically improves subtleness through advancements on material and coating formula, while improving reflection and blue blocking all together. It would be interesting to see how this may affect compliance rates.

Another limitation relates to the hardware form factor. This study used a medium-sized frame with overextension hinges, which accommodated most participants but did not

provide an optimal fit for all head shapes and facial structures. Suboptimal fit may influence comfort, stability, and willingness to wear the glasses for longer durations, which in turn can affect usage-dependent outcomes such as mood, sleep, and cognitive performance. A next-generation design, now available, includes three frame sizes and an adjustable screw-based mechanism to improve fit and comfort. Incorporating these updated frames in future studies may reduce variability introduced by physical fit, enhance adherence, and provide a more accurate estimate of the device's treatment effects.

In addition, there are other methods of analysis that may yield even more meaningful results. For example, when taking account of average time when a participant started treatment, it didn't yield results alone. However, it may be possible that the time along with the duration, as well as intensity would yield a result. A more robust analysis method may be applied, such as the Functional Principle Component Analysis which represents the time-based data into meaningful eigenfunction scores. The study collected 245457 minutes of usage data, along with the average melanopic lux in that minute for each participant; a significant amount of data that a more robust analysis can help decipher additional information.

A final limitation involves the participants who only wore the glasses for a short duration in the day, therefore missing data for the remaining hours where ambient light exposure was not collected. A method would need to be devised to gauge scores with missing data.

4.10 Implications and Future Work

All in all, the study is able to show significant improvement of bright-light compared with dim-light control via the Lumos smart light therapy glasses with the reflective coating technology. It also demonstrated insights where usage time, eye color, baseline scores, ambient light can significantly affect outcomes in certain groups, and indicate a potential correlation of age and sex on outcomes. The paired word test did not show significant outcomes due to poorly designed testing method and sample size limitations.

One immediate task would be to apply more advanced analysis methods and algorithms towards the data from this study. For example, using Functional Principle Component Analysis, fractal analysis, machine learning, or informed metrics based on a combination of ambient light and usage data may yield more results without completing a new study.

A future study could simply repeat this study with a better designed paired word test, more polished study flow, latest generation of the glasses, and a much larger sample size. A recommended sample size could range from 300 to 2000 depending on regulatory and

insurance compliance. Perhaps an even more interesting method is to do a continuous field study as the glasses become commercially available later in 2025. Users and buyers of the glasses can optionally join a study where they complete quick surveys and tasks to track their mood, sleep, reaction time, cognition, and other parameters as they use it. This particular method can be scalable as the total number of users who consent to join the field study can provide a massive data set where deeper insights can be drawn. Future generations of the glasses may also include the effect of different wavelengths and frequency of light, and integrate combination therapy and sound therapy.

From a hardware perspective, adding in additional sensors or integration with health apps can also yield better results. For example, participants can be given a smart band that tracks sleep through inertial motion unit data, activity, body temperature, and heart rate. One key missing data point in this study is the ambient light exposure of the participant when they are not wearing the glasses. One key challenge for Lumos is to make glasses comfortable enough to be worn all day in order to yield the best benefits and data collection. It is possible other hardware can collect this ambient light data; regardless, advances in engineering, design, and technology can continue to enhance this scientific endeavor.

Beyond intensity and duration, several emerging dimensions of light stimulation offer promising pathways for improving interindividual tailoring of light therapy. These include wavelength-specific tuning across multiple spectral bands, temporal modulation such as pulsed or frequency-structured light (e.g., 40 Hz stimulation), and spatially targeted illumination of distinct retinal regions (temporal vs. nasal, superior vs. inferior), which may differentiate biological responses based on ipRGC distribution and downstream neural circuitry. Additionally, the timing of exposure relative to circadian phase, exercise, autonomic state, heart rate, and thermal regulation may shape an individual's responsiveness more strongly than previously recognized. Integrating these dimensions with continuous data on ambient light history, behavior, and physiology would enable adaptive dosing algorithms that learn each user's unique response profile. Such advances point toward a future of personalized light therapy that is multispectral, temporally structured, spatially optimized, and informed by real-time physiological context.

Chapter 5

Conclusion

Traditional light therapy devices have struggled with adherence and practicality. For example, stationary light boxes are inconvenient, most wearable products lack social acceptability or engineering refinements are needed for sustained use. The literature acknowledges these limitations by questioning longer durations, dose–response, and how individual factors such as age, eye color, and baseline severity shape outcomes. This gap has limited both clinical adoption and scientific understanding.

This thesis addresses this gap with the design, engineering, and clinical validation of the Lumos Smart Glasses. The engineering effort delivered a patented optical system, calibrated light engines, on-board ambient and proximity sensors, and integrated software to ensure both safety and verifiable adherence. The result was a platform that provided bright circadian-effective light in a glasses-like form factor and captured usage data with high fidelity.

The clinical trial showed that these glasses significantly improved mood, sleep, and cognition compared with an active dim-light control. In Phase 1, the Beta group experienced large gains that regressed when treatment was withdrawn, confirming efficacy. The Alpha group, once switched to active treatment, also benefited in some groups, though adherence issues partly muted the effects. While PROMIS and PVT both showed clear and significant improvements under bright-light, the MADRS outcome reached statistical significance only after accounting for eye color. Stratified analyses revealed that participants with darker eyes showed stronger mood improvements under bright-light, whereas those with lighter eyes (blue, green, or hazel) achieved comparable benefits under dimmer light exposure. This suggests that optimal therapeutic intensity may depend on individual differences in ocular pigmentation. WORD results also showed that significant improvements

are observed in the bright-light group after accounting for usage time. Exploratory models further identified important moderators: higher usage time and higher ambient light were associated with greater improvements across outcomes, and higher baseline severity predicted more room for change. These findings point to the value of personalization and the importance of considering individual and environmental factors in light therapy.

In summary, this work demonstrates that wearable, sensor-driven light therapy can overcome the long-standing limitations of older devices. The Lumos Smart Glasses make it possible to study dose, duration, and demographic differences in ways that were previously impractical, and to deliver circadian-effective light in daily life. While MADRS and word paired effects were only significant after analyzing stratified results and some secondary effects (e.g., age, sex) were small, the overall evidence strongly supports that mobile light therapy can improve mental health outcomes that opens new directions for more personalized studies.

In conclusion, the Lumos platform represents a step forward: taking light therapy from static devices toward a practical, everyday wearable. By merging engineering innovation with clinical validation, it lays the groundwork for future more effective, personalized and widely adopted circadian health technologies.

References

[1] Eye-catching innovations for healthcare at ces, 2020. Accessed: 2025-11-18.

[2] Innovative vision tech abounds at ces 2020, January 2020. Accessed: 2025-11-18.

[3] Raising the bar: Waterloo engineering students capture top spots at provincial and national competitions, 2020. Accessed: 2025-11-18.

[4] Graduate student receives minister of colleges and universities' award of excellence, 2022. Accessed: 2025-11-18.

[5] Minister's award of excellence announcement, 2022. Accessed: 2025-11-18.

[6] Provincial recognition for exceptional contributions, 2022. Accessed: 2025-11-18.

[7] S. Adapa, J. Nandhakumar, and P. Reddy. Factors influencing the adoption of smart wearable devices: An empirical study. *Journal of Retailing and Consumer Services*, 43:157–169, 2018.

[8] I. Akyar and N. Akdemir. The effect of light therapy on the sleep quality of the elderly: An intervention study. *Australian Journal of Advanced Nursing*, 31(3):31–38, 2014.

[9] Allied Market Research. Blue light blocking glasses market size, share & trends, 2034 – global opportunity analysis and industry forecast, 2024–2034. https://www.alliedmarketresearch.com/blue-light-blocking-glasses-market-A65843, 2024. Report Code: A65843.

[10] American Academy of Ophthalmology. Your blue eyes are not really blue. https://www.aao.org/eye-health/tips-prevention/your-blue-eyes-arent-really-blue, 2020. Accessed: 2025-12-03.

[11] American Academy of Ophthalmology. Should you be worried about blue light? https://www.aao.org/eye-health/tips-prevention/should-you-be-worried-about-blue-light, 2024. Accessed: 2025-10-30.

[12] Mihyang An, Stephen M. Colarelli, Kimberly O'Brien, and Melanie E. Boyajian. Why we need more nature at work: Effects of natural elements and sunlight on employee mental health and work attitudes. *PLOS ONE*, 11(5):e0155614, 2016.

[13] Ansys Zemax. How to use osram led data with opticstudio, 2023. Accessed: 2025-11-02.

[14] Ansys Zemax. Opticstudio models of the human eye, 2023. Accessed: 2025-11-02.

[15] Arduino Project. *CapacitiveSensor Library Documentation*, 2024. Accessed: 2025-11-03.

[16] Mathias Basner and David F. Dinges. Maximizing sensitivity of the psychomotor vigilance test (pvt) to sleep loss. *Sleep*, 34(5):581–591, 2011.

[17] Bentham Instruments Ltd. Idr300-psl photobiological safety spectroradiometer, 2024. Accessed: 2025-11-02.

[18] G. Bersani, D. Marconi, L. Limpido, E. Tarolla, and E. Caroti. Pilot study of light therapy and neurocognitive performance of attention and memory in healthy subjects. *Psychological Reports*, 102(1):299–304, 2008.

[19] Surabhi Bhandari, Stephen W. Cain, and Andrew J.K. Phillips. Wearable sensors for measurement of viewing behavior, light exposure, and sleep. *Sensors*, 21(21):7096, 2021. Demonstrates that wrist-worn devices underestimate illuminance compared to temple-mounted sensors.

[20] Katharina Blatter, Patricia Graw, Mirjam Münch, Vera Knoblauch, Anna Wirz-Justice, and Christian Cajochen. Gender and age differences in psychomotor vigilance performance during 40 h of sleep deprivation. *Neurobiology of Aging*, 27(5):789–796, 2006.

[21] Christina Blume, Corrado Garbazza, and Manuel Spitschan. Effects of light on human circadian rhythms, sleep and mood. *Somnologie*, 23(3):147–156, 2019.

[22] M. Boubekri, M. S. Rea, M. G. Figueiro, and R. Kuller. Association between sunlight exposure and mental health: Evidence from population data. *Frontiers in Public Health*, 11:1173492, 2023.

[23] Mohamed Boubekri, Ivy N. Cheung, Kathryn J. Reid, Chia-Hui Wang, and Phyllis C. Zee. Impact of windows and daylight exposure on overall health and sleep quality of office workers: a case-control pilot study. *Journal of Clinical Sleep Medicine*, 10(6):603–611, 2014.

[24] Kathleen Burkhart and Jeffrey R. Phelps. Amber lenses to block blue light and improve sleep: a randomized trial. *Chronobiology International*, 26(8):1602–1612, 2009.

[25] Angus C. Burns, Daniel P. Windred, Martin K. Rutter, Patrick Olivier, Céline Vetter, Richa Saxena, Jacqueline M. Lane, Andrew J. K. Phillips, Sean W. Cain, et al. Day and night light exposure are associated with psychiatric disorders: an objective light study in >85,000 people. *Nature Mental Health*, 1:853–862, 2023.

[26] Daniel J. Buysse, Lan Yu, Douglas E. Moul, Anne Germain, Angela Stover, Nathan E. Dodds, Kelly L. Johnston, Melissa A. Shablesky-Cade, and Paul A. Pilkonis. Development and validation of patient-reported outcome measures for sleep disturbance and sleep-related impairments. *Sleep*, 33(6):781–792, 2010.

[27] P. D. Campbell and P. J. Murphy. Bright light therapy: Effectiveness and mechanisms in sleep and mood disorders. *Therapeutic Advances in Psychopharmacology*, 7(5):193–205, 2017.

[28] Philip D. Campbell, Ann M. Miller, and Mary E. Woesner. Bright light therapy: Seasonal affective disorder and beyond. *Einstein Journal of Biology and Medicine*, 32:E13–E25, 2017. PMC Free Article.

[29] Manman Chen, Yuankai Zhao, Qu Lu, Zichen Ye, Anying Bai, Zhilan Xie, Daqian Zhang, and Yu Jiang. Artificial light at night and risk of depression: a systematic review and meta-analysis. *Environmental Health and Preventive Medicine*, 29:73, 2024. Meta-analysis showing positive associations of both outdoor and indoor ALAN exposure with depression risk.

[30] S. F. Cleary and G. A. Flamme. Laser-induced acoustic transients in the mammalian eye. *The Journal of the Acoustical Society of America*, 46(4B):1037–1044, 1969. Published October 1969.

[31] Cognitive Market Research. Why google glass failed: An analysis of technology adoption and social acceptance. https://www.cognitivemarketresearch.com/blog/google-glass, 2023. Accessed: 2025-10-26.

[32] Audrey Cougnard-Grégoire, Bénédicte M. J. Merle, Tariq Aslam, Johanna M. Seddon, Isabelle Aknin, Caroline C. W. Klaver, Gerhard Garhöfer, Alfredo Garcia Layana, Angelo Maria Minnella, Rufino Silva, and Cécile Delcourt. Blue light exposure: Ocular hazards and prevention—a narrative review. *Ophthalmology and Therapy*, 12(2):755–788, 2023. Open Access; PMCID: PMC9938358.

[33] Ben Davis. Ces 2020 sleep tech roundup, January 2020. Accessed: 2025-11-18.

[34] J. L. Davis et al. Initial benchmarks of uv leds and comparison with white leds. Technical report, LED Systems Reliability Consortium, U.S. Department of Energy, 2021. Accessed: 2025-11-02.

[35] H. O. de la Iglesia, E. Fernández-Duque, D. A. Golombek, N. Lanza, J. F. Duffy, C. A. Czeisler, and C. R. Valeggia. Access to electric light is associated with shorter sleep in a traditionally hunter–gatherer community. *Journal of Biological Rhythms*, 30(4):342–350, 2015.

[36] Karuna Dewan, Susan Benloucif, Kathryn J. Reid, Lisa F. Wolfe, and Phyllis C. Zee. Light-induced changes of the circadian clock of humans: Increasing duration is more effective than increasing light intensity. *Sleep*, 34(5):593–599, 2011.

[37] David F. Dinges and John W. Powell. Microcomputer analyses of performance on a portable, simple visual rt task. *Behavior Research Methods, Instruments, & Computers*, 17(6):652–655, 1985.

[38] Güler Duru and Bruno Fantino. The clinical relevance of changes in the montgomery–åsberg depression rating scale using the minimum clinically important difference approach. *Current Medical Research and Opinion*, 24(10):2729–2735, 2008.

[39] J. S. Emens, A. J. Lewy, R. A. Bernert, A. Ohsawa, and T. Tomita. Effect of light and melatonin and other melatonin receptor agonists on human circadian physiology. *Journal of Clinical Sleep Medicine (Review)*, 11(10), 2015.

[40] Bruno Fantino and Nicholas Moore. The self-reported montgomery-åsberg depression rating scale is a useful evaluative tool in major depressive disorder. *BMC Psychiatry*, 9(1):26, 2009.

[41] Sally Faulkner, Derk-Jan Dijk, Richard Drake, and Penny Bee. Adherence and acceptability of light therapies to improve sleep in intrinsic circadian rhythm sleep disorders and neuropsychiatric illness: A systematic review. *Sleep Health*, 6(6):690–701, 2020.

[42] f.luxometer. f.luxometer – handheld spectroradiometer for light therapy, 2024. Accessed: 2025-11-03.

[43] Namni Goel, Michael Terman, and Jiuan Su Terman. Depressive symptomatology differentiates subgroups of patients with seasonal affective disorder. *Depression and Anxiety*, 15(1):34–41, 2002.

[44] Robert N. Golden, Bradley N. Gaynes, Richard D. Ekstrom, Richard M. Hamer, Frederick M. Jacobsen, Trisha Suppes, Katherine L. Wisner, and Charles B. Nemeroff. The efficacy of light therapy in the treatment of mood disorders: A systematic review and meta-analysis of the evidence. *American Journal of Psychiatry*, 162(4):656–662, 2005.

[45] William T. Jr. Ham, Harold A. Mueller, and David H. Sliney. Retinal sensitivity to damage from short wavelength light. *Nature*, 260:153–155, 1976.

[46] Harvard Health Publishing. Light therapy: Not just for seasonal depression? https://www.health.harvard.edu/mind-and-mood/light-therapy-not-just-for-seasonal-depression, 2022. Accessed: 2025-10-26.

[47] Landon Hester, Deanna Dang, Christopher J. Barker, Michael Heath, Sidra Mesiya, Tekenari Tienabeso, and Kevin Watson. Evening wear of blue-blocking glasses for sleep and mood disorders: a systematic review. *Chronobiology International*, 38(10):1375–1383, 2021. Systematic review of evening blue-blocking glasses for sleep and mood outcomes.

[48] S. Higuchi, Y. Motohashi, K. Ishibashi, and T. Maeda. Influence of eye colors of caucasians and asians on suppression of melatonin secretion by light. *American Journal of Physiology - Regulatory, Integrative and Comparative Physiology*, 292(6):R2352–R2356, 2007.

[49] Nicholas G. Horton, Kevin L. Pollock, Edward T. Fei, and Erwin K. Lau. Retinal hazard analysis for laser and led illumination for close-in, long duration exposure. In *International Laser Safety Conference (ILSC) 2019 Proceedings*, Orlando, FL, USA, 2019. Laser Institute of America. Paper 1204.

[50] iFixit. Airpods teardown, 2016. Accessed November 7, 2025.

[51] P. D. Imesch, I. H. Wallow, and D. M. Albert. The color of the human iris: A study of melanin in the stroma and pigment epithelium. *Archives of Ophthalmology*, 115(3):384–389, 1997.

[52] International Commission on Illumination. Position statement on the blue light hazard, 2019. Accessed: 2025-08-07.

[53] International Electrotechnical Commission. Iec 62471: Photobiological safety of lamps and lamp systems, 2006. Standard.

[54] Investopedia. How and why google glass failed. https://www.investopedia.com/articles/investing/052115/how-why-google-glass-failed.asp, 2015. Accessed: 2025-10-26.

[55] Imene Jaadane, Gloria Villalpando Rodriguez, Pierre Boulenguez, Samuel Carré, Irene Dassieni, Cécile Lebon, Sabine Chahory, Francine Behar-Cohen, Christophe Martinsons, and Alicia Torriglia. Retinal phototoxicity and the evaluation of the blue light hazard of a new solid-state lighting technology. *Scientific Reports*, 10:6733, 2020. Open Access.

[56] C. A. Johnson and J. K. Keltner. Incidence of normal visual-field test results with downward gaze. *Investigative Ophthalmology & Visual Science*, 24(2):176–181, 1983.

[57] P. Kaviani, A. Williamson, P. de Souza, et al. Exploring social perceptions of everyday smartglass use in australia. *PLOS ONE*, 19(7):e0313001, 2024.

[58] Jan J. Koenderink and Andrea J. van Doorn. Facts on optic flow. *Biological Cybernetics*, 28(4-5):239–248, 1978.

[59] G. Koutromanos, G. Styliaras, and P. Avgeriou. Augmented reality smart glasses use and acceptance: A systematic review. *Computers and Education: Artificial Intelligence*, 4:100106, 2023.

[60] Raymond W. Lam, Anthony J. Levitt, Robert D. Levitan, Murray W. Enns, Robert Morehouse, Erin E. Michalak, and Edwin Tam. Efficacy of bright light treatment, fluoxetine, and the combination in patients with nonseasonal major depressive disorder. *JAMA Psychiatry*, 73(1):56–63, 2016.

[61] Marie-Pierre Lavoie, Raymond W. Lam, Geneviève Bouchard, Geneviève Murray, Pierre Blier, Chantal Mërette, Anne-Marie Gagné, Jean Tremblay, and Diane B. Boivin. Evidence of a biological effect of light therapy on the retina of patients with

seasonal affective disorder. *Biological Psychiatry*, 66(3):253–258, 2009. Demonstrated reduced cone ERG amplitude in SAD, normalizing after light therapy.

[62] Tara A. LeGates, Diego C. Fernandez, and Samer Hattar. Light as a central modulator of circadian rhythms, sleep and affect. *Nature Reviews Neuroscience*, 15(7):443–454, 2014. Highly cited review on ipRGCs, circadian rhythms, and mood regulation.

[63] R. J. Lucas, S. N. Peirson, T. M. Brown, et al. Lights should support circadian rhythms: Evidence-based scientific recommendations. *PLOS Biology*, 20(3):e3001571, 2022.

[64] Kwong Man and Ian Ashdown. Accurate colorimetric feedback for rgb led clusters. *LEUKOS*, 3(2):121–138, 2006.

[65] Erin E. Michalak, Greg Murray, Clare Wilkinson, Chris Dowrick, and Raymond W. Lam. A pilot study of adherence with light treatment for seasonal affective disorder. *Psychiatry Research*, 149(1–3):315–320, 2007.

[66] Stuart A. Montgomery and Marie Åsberg. A new depression scale designed to be sensitive to change. *The British Journal of Psychiatry*, 134(4):382–389, 1979.

[67] Raymond P. Najjar, Luzian Wolf, Jacques Taillard, Luc J. M. Schlangen, Alex Salam, Christian Cajochen, and Claude Gronfier. Chronic artificial blue-enriched white light is an effective countermeasure to delayed circadian phase and neurobehavioral decrements. *PLOS ONE*, 9(7):e102827, 2014. Open access, distributed under CC BY.

[68] K. Obayashi, K. Saeki, and N. Kurumatani. Time spent in outdoor light is associated with mood, sleep, and circadian-related outcomes: A population-based study. *Chronobiology International*, 39(6):783–793, 2022.

[69] R. J. Pellegrini, A. G. Schauss, and A. Ryan. Eye color and reaction time to visual stimuli. *Perceptual and Motor Skills*, 52(1):127–130, 1981. Reported darker-eyed individuals exhibit faster reaction times to visual stimuli.

[70] Corinne Pettigrew and Anja Soldan. Cantab paired associates learning detects early cognitive changes in preclinical alzheimer's disease. *Neuropsychology*, 35(3):248–260, 2021.

[71] Power and Sample Size. Power and sample size calculator. http://powerandsamplesize.com. Accessed: 2025-11-09.

[72] PROMIS Health Organization (PHO) and PROMIS Cooperative Group. PROMIS Sleep Disturbance—Short Form (Adult), DSM-5 Level 2—Sleep Disturbance—Adult measure, 2008. Copyright © 2008–2012 PROMIS Health Organization (PHO) and PROMIS Cooperative Group. Instructions and scoring © 2013 American Psychiatric Association.

[73] PROMIS® Health Measures. *PROMIS® Sleep Disturbance Scoring Manual (Adult)*, 2021. T-score interpretation and conversion tables for PROMIS Sleep Disturbance short forms.

[74] Encyclopedia Pub. Temperature-sensitive optical parameters, 2022. Accessed: 2025-11-02.

[75] Craig W. Ritchie et al. Recommended cognitive outcomes in preclinical alzheimer's disease trials. *Alzheimer's & Dementia*, 13(2):186–195, 2017.

[76] Kathryn A. Roecklein, Julie A. Schumacher, Megan A. Miller, and Natalie C. Ernecoff. Cognitive and behavioral predictors of light therapy use. *PLOS ONE*, 7(6):e39275, 2012.

[77] ROKA. Huberman wind down™ collaboration – roka. https://www.roka.com/pages/huberman, 2025. Accessed: 2025-10-30.

[78] João Paulo P. Rosa, Ana Silva, Daniel F. Rodrigues, Marcos A. Simim, Fernando V. Narciso, Sergio Tufik, and Marco T. de Mello. Effect of bright light therapy on delayed sleep/wake cycle and reaction time of athletes participating in the rio 2016 olympic games. *Chronobiology International*, pages 1–9, 2018.

[79] Alexandre Sasseville et al. Blue blocker glasses impede the capacity of bright light to suppress melatonin production. *Journal of Pineal Research*, 41(1):73–78, 2006.

[80] Karl Schulmeister, John O'Hagan, and David H. Sliney. Lamp and led safety – classification vs. realistic exposure analysis. In *International Laser Safety Conference (ILSC) 2019 Proceedings*, pages 174–183, Orlando, FL, USA, 2019. Laser Institute of America. Paper 801; March 18–21, 2019.

[81] Michael Lyle Seeman. Dr. oz says we need more sleep; these devices can help, January 2020. Accessed: 2025-11-18.

[82] Nordic Semiconductor. Empowering wireless innovation, n.d.

[83] Ari Shechter et al. Blocking nocturnal blue light for insomnia: A randomized controlled trial. *Journal of Psychiatric Research*, 2018. Epub 2017.

[84] James E. Sheedy. Design considerations for computer eyewear. *Optometry and Vision Science*, 82(7):513–522, 2005.

[85] Sumeer Singh, Peter R. Keller, Ljoudmila Busija, Patrick McMillan, Eve Makrai, John G. Lawrenson, Christopher C. Hull, and Laura E. Downie. Blue-light filtering spectacle lenses for visual performance, sleep, and macular health in adults. *Cochrane Database of Systematic Reviews*, (8):CD013244, 2023. Systematic review showing little to no consistent benefit of blue-light filtering lenses on eye strain, visual performance, or sleep outcomes.

[86] David H. Sliney. Ocular thermal injury from intense light. Technical report, USAF School of Aerospace Medicine, Brooks Air Force Base, TX, 1982. Technical Report SAM-TR-82-21.

[87] David H. Sliney, Rolf Bergman, and John O'Hagan. Photobiological risk classification of lamps and lamp systems—history and rationale. *LEUKOS*, 12(4):213–234, 2016.

[88] K. C. H. J. Smolders and Y. A. W. de Kort. The effect of light on well-being: A systematic review and meta-analysis. *Sleep Health*, 10(2):123–137, 2024.

[89] Oliver Stefani, Reto Marek, Jürg Schwarz, Sina Plate, Johannes Zauner, and Björn Schrader. Wearable light loggers in field conditions: Corneal light characteristics, user compliance, and acceptance. *Clocks & Sleep*, 6(4):619–634, 2024. Field measurements show discrepancy between mean and median mEDI; median mEDI = 51 lx_mEDI.

[90] E. R. Stothard and R. G. Foster. Circadian entrainment to the natural light–dark cycle. *Current Biology*, 27(12):R681–R702, 2017.

[91] Richard A. Sturm and Mats Larsson. Genetics of human iris colour and patterns. *Pigment Cell & Melanoma Research*, 22(5):544–562, 2009.

[92] P. Svanborg and M. Åsberg. A new self-rating scale for depression and anxiety states based on the comprehensive psychopathological rating scale. *Acta Psychiatrica Scandinavica*, 89(1):21–28, 1994.

[93] Lucas Wen Tang, Xin Yao, and Wei Zhang. Ophthalmic devices for light therapy (u.s. patent no. 12,364,874 b2). U.S. Patent and Trademark Office, 2025. Assignee: Lumos Health Inc. Filed Mar. 27, 2024. Published Jul. 22, 2025. Priority Apr. 1, 2022.

[94] E. Taylor. Colourimetry and efficiency of white leds: Spectral width and colour shift. *physica status solidi (a)*, 209(11):2133–2140, 2012.

[95] Jay S. Terman and Michael Terman. Photopic and scotopic light detection in patients with seasonal affective disorder and control subjects. *Biological Psychiatry*, 46(2):164–170, 1999. Found seasonally altered cone/rod sensitivity in SAD, normalizing with morning light therapy.

[96] David Trilling. Daylight, windows and workers' well-being: Research review. Journalist's Resource, Harvard Kennedy School, 2017.

[97] U.S. Food and Drug Administration. 21 cfr 801.410 – use of impact-resistant lenses in eyeglasses and sunglasses. https://www.ecfr.gov/current/title-21/chapter-I/subchapter-H/part-801/subpart-H/section-801.410, 2025. Accessed: 2025-12-01.

[98] U.S. National Library of Medicine. Lumos smart glasses and their effects of light therapy duration on mood, sleep and cognition. *ClinicalTrials.gov*, Identifier: NCT07168954, 2024. Available at https://clinicaltrials.gov/study/NCT07168954 (Accessed: 2025-11-09).

[99] T. van den Berg. Dependence of intraocular straylight on pigmentation and light transmission through the ocular wall. *Vision Research*, 31(8):1455–1462, 1991.

[100] J. van Duijnhoven, R. Müller, K. C. H. J. Smolders, and Y. A. W. de Kort. Measuring light exposure in daily life: A review of wearable loggers. *Building and Environment*, 259:111013, 2025. Reviews wearable light-loggers and highlights limitations of wrist-mounted sensors such as occlusion and angular misalignment.

[101] Guang Wen, Melissa A. St. Hilaire, Steven W. Lockley, and Shadab Rahman. Effect of mount location on the quantification of light intensity from wearable devices. *Frontiers in Neuroscience*, 17:1200981, 2023. Shows that temple- or spectacle-mounted sensors better represent eye-level exposure than wrist-mounted ones.

[102] Adriana R. Wielgus and Tadeusz Sarna. Melanin in human irides: Biophysical properties and their implications. *Photochemical & Photobiological Sciences*, 4:1087–1092, 2005.

[103] May Woo, Piers MacNaughton, Jaewook Lee, Brandon Tinianov, Usha Satish, and Mohamed Boubekri. Access to daylight and views improves physical and emotional wellbeing of office workers: A crossover study. *Frontiers in Sustainable Cities*, 3:690055, 2021.

[104] Lance Workman, Nathalie Akçay, Michael Reeves, and Sandie Taylor. Blue eyes keep away the winter blues: Is blue eye pigmentation an evolved feature to provide resilience to seasonal affective disorder? *Open Access Journal of Behavioural Science & Psychology*, 1(1):180002, 2018. Open access, published May 7, 2018.

[105] Lance Workman, Louisa Chilvers, Catherine Price, Denise Gibbs, and John Maltby. Blue eyes keep away the winter blues: Is blue eye pigmentation an evolved feature to provide resilience to seasonal affective disorder? *Medical Hypotheses*, 132:109379, 2019. Proposes lighter eye pigmentation as evolutionary adaptation reducing SAD susceptibility.

[106] G. Yetish, H. Kaplan, M. Gurven, B. Wood, H. Pontzer, P. R. Manger, C. Wilson, R. McGregor, and J. M. Siegel. Natural sleep and its seasonal variations in three pre-industrial societies. *Current Biology*, 25(21):2862–2868, 2015.

[107] Lan Yu, Daniel J. Buysse, Anne Germain, Douglas E. Moul, Angela Stover, Nathan E. Dodds, Kelly L. Johnston, Melissa A. Shablesky-Cade, and Paul A. Pilkonis. Development of short forms from the promis™ sleep disturbance and sleep-related impairment item banks. *Behavioral Sleep Medicine*, 10(1):6–24, 2012.

[108] Alyson K. Zalta, Kimberly Bravo, Zoey Valdespino-Hayden, Mark H. Pollack, and Helen J. Burgess. A placebo-controlled pilot study of a wearable morning bright light treatment for probable ptsd. *Depression and Anxiety*, 36(9):866–875, 2019.

[109] Jamie M. Zeitzer, Derk-Jan Dijk, Richard E. Kronauer, Emery N. Brown, and Charles A. Czeisler. Sensitivity of the human circadian pacemaker to nocturnal light: melatonin phase resetting and suppression. *Journal of Physiology*, 526(Pt 3):695–702, 2000.

[110] R. Zuidhof, M. Wouters, E. de Korte, et al. Perspectives on the acceptance and use of smart glasses in healthcare: A qualitative focus group study. *Frontiers in Digital Health*, 2:285492376, 2024.

APPENDICES

Appendix A

Personal Notes and Behind the Scenes

This appendix celebrates the small, personal moments that accompanied the development of this work, from early prototypes to the quiet company of the two cats who helped ensure I never worked too long without a break.

My late cat **Obie** and my current cat **Piper** have been unexpected collaborators throughout this journey. Both possessed an uncanny sense of when I was overworking and would intervene, sometimes gently and sometimes with tactical chaos, such as walking across keyboards or knocking critical circuit boards off the desk. Their presence brought balance, humor, and perspective to long nights of research and writing.

The Companions

Both of them provided invaluable emotional feedback throughout this project, reminding me that science and compassion can coexist, and that sometimes, progress means stepping away for a cuddle.

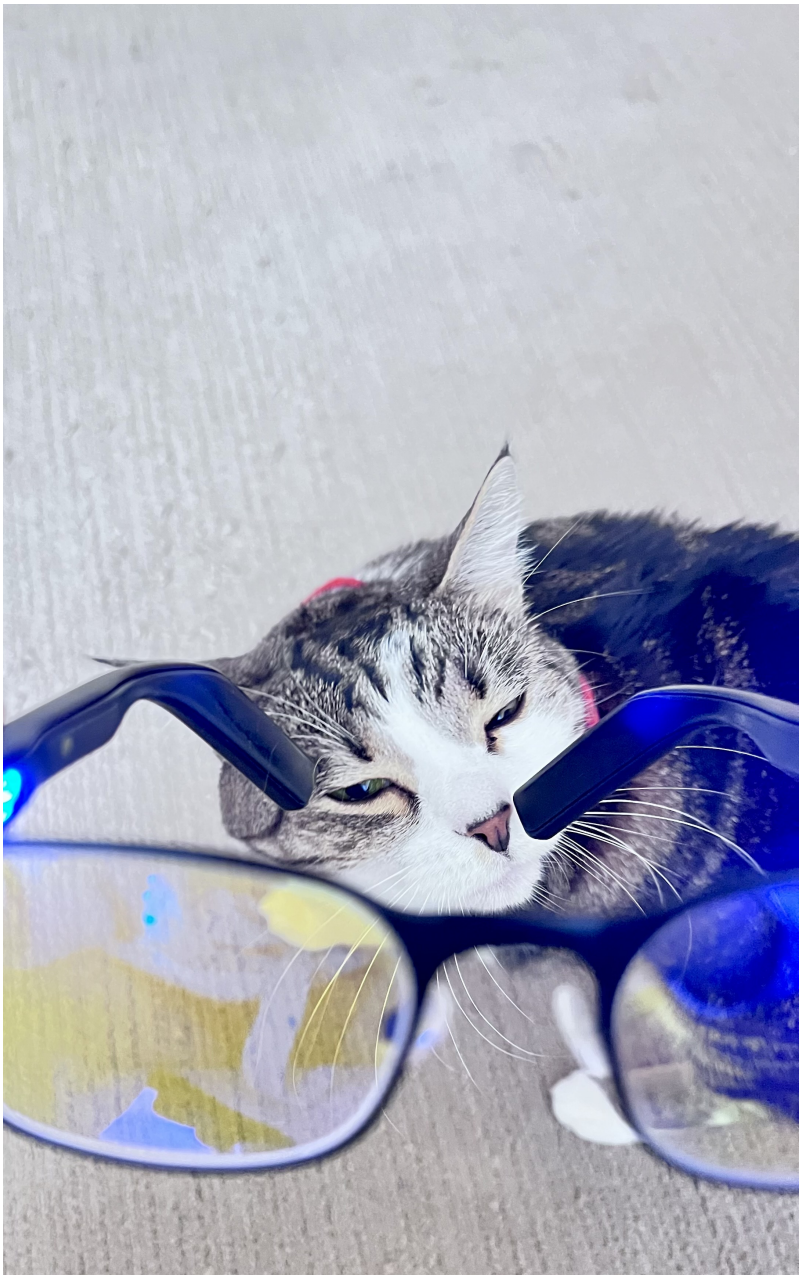


Figure A.1: Piper evaluating the latest pair of Lumos glasses through a rigorous feline visual inspection protocol.



Figure A.2: Obie falling asleep next to one of the earliest prototypes, demonstrating optimal comfort and ergonomic design validation.



Figure A.3: Obie assisting with blue-light output verification, no instrumentation required.



Figure A.4: Obie helping inspect a Lumos PCB light engine module with deep curiosity and minimal electrostatic discharge.

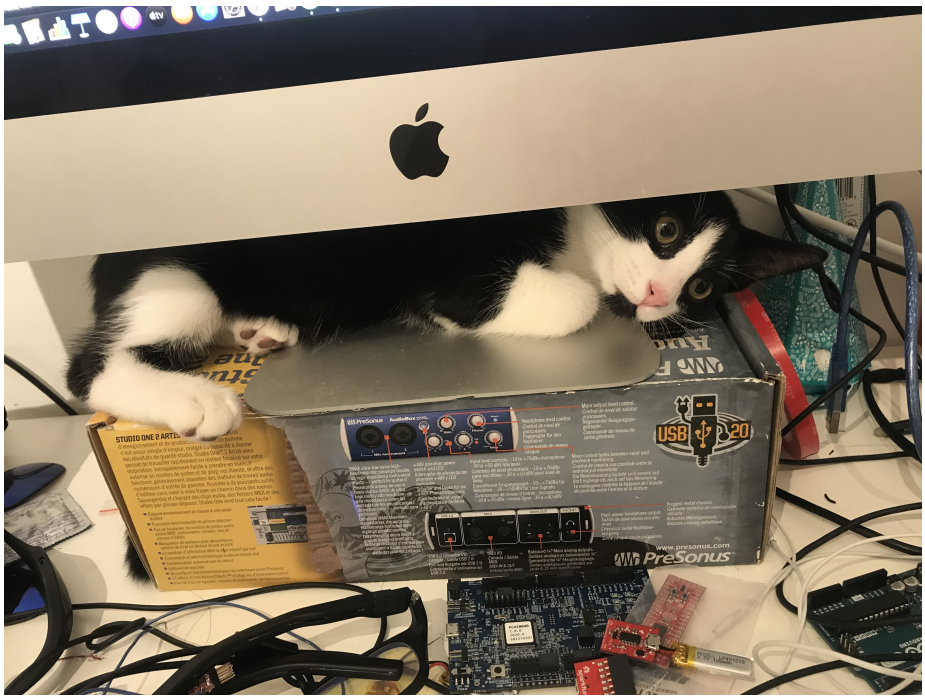


Figure A.5: Obie, keeping me company beneath the computer monitor while I worked on early Lumos prototypes.



Figure A.6: Obie basking peacefully in front of a light therapy lamp, a reminder that this work is validated by nature itself.

Appendix B

Photobiological Safety and Blue-Light Hazard Framework

Summary

This appendix provides a concise technical overview of the photobiological safety framework relevant to light-emitting devices. It clarifies the distinction between public misconceptions about "blue-light" and the scientifically defined photochemical hazard, outlines the primary retinal damage mechanisms (photo-thermal, photo-mechanical, and photo-chemical), and summarizes the wavelength-dependent blue-light hazard function $B(\lambda)$ derived from foundational studies by Ham, Mueller, and Sliney.

The appendix further reviews the IEC 62471 exposure limits governing retinal photochemical safety, including definitions of blue-light–weighted radiance (L_B) and cumulative radiance dose. It also describes key measurement-geometry parameters, pupil diameter, angular subtense, spectral radiance, and the standardized 200 mm evaluation distance, that determine the radiometric conditions under which blue-light hazard is assessed.

Together, these elements form the quantitative basis used throughout this thesis to ensure that the Lumos system maintains ocular safety while delivering effective circadian stimulation.

B.1 Misconceptions About blue-light Hazard

Public discussion of blue-light has been shaped more by commercial narratives than by scientific evidence. Marketing of "blue-light–blocking" eye-wear has popularized the perception of blue-light as inherently harmful, despite limited data supporting most claims. This section clarifies the distinction between perceived and actual photobiological risk.

blue-light–filtering lenses generally fall into two categories. The first employs a mild anti-reflective coating, marketed for reducing digital eyestrain and retinal stress, yet these coatings minimally attenuate short-wavelength light and show no consistent benefit for ocular comfort or protection [85]. The second category consists of visibly tinted lenses (yellow, orange, or red), designed for evening use to reduce melatonin suppression. Controlled studies have shown these lenses can improve sleep and circadian regulation [**?**, **?**], and their use has been popularized by science communicators such as Dr. Andrew Huberman [77].

The International Commission on Illumination (CIE) has stated that blue-light exposure from consumer lighting and display products remains well below established safety thresholds and often lower than natural daylight levels [52]. Similarly, the American Academy of Ophthalmology reports no evidence that blue-light from digital screens causes retinal damage and cautions against alarmist interpretations [11]. This conclusion is supported by recent reviews indicating that "there is no evidence that screen use and LEDs in normal use are deleterious to the human retina" [32]. Consumer light sources are further governed by photobiological safety standards such as IEC 62471 [53], which define quantitative exposure limits to ensure ocular safety.

The blue-light hazard remains a valid photobiological construct rooted in retinal photochemistry, but its significance applies primarily under controlled, high-intensity exposure conditions rather than everyday device use. Understanding this distinction requires an examination of the physiological basis and standardized measurement systems that define safe radiance limits.

B.2 Retinal Damage Mechanisms and Spectrum

Retinal injury from optical radiation occurs through three primary mechanisms: photothermal, photo-mechanical, and photo-chemical. Photo-thermal damage arises when absorbed radiant energy elevates retinal or choroidal temperature faster than heat can dissipate via conduction or blood flow [86]. Photo-mechanical damage occurs during extremely brief and intense exposures (10^{-6}–10^{-8} s), where rapid energy deposition generates acoustic

or pressure transients that physically disrupt retinal tissues; this was first demonstrated by Cleary et al., who showed that nanosecond laser pulses can produce shock-wave–induced lesions [30].

Photo-chemical damage predominates under longer exposures and shorter wavelengths (400–500 nm). In this regime, retinal chromophores absorb blue-light, generating reactive oxygen species (ROS) such as singlet oxygen and superoxide radicals that trigger oxidative stress. The foundational work of Ham, Mueller, and Sliney (1976) demonstrated wavelength-dependent photochemical injury in rhesus monkeys, establishing the scientific basis for modern blue-light safety standards, including IEC 62471 [45].

A key outcome of these studies is the definition of the blue-light hazard function, $B(\lambda)$, which quantifies the relative effectiveness of each wavelength in producing photochemical retinal damage (see Figure B.1). Although intrinsic hazard increases with decreasing wavelength, shorter wavelengths are strongly attenuated by the cornea and crystalline lens, which shapes the effective retinal hazard curve [55].

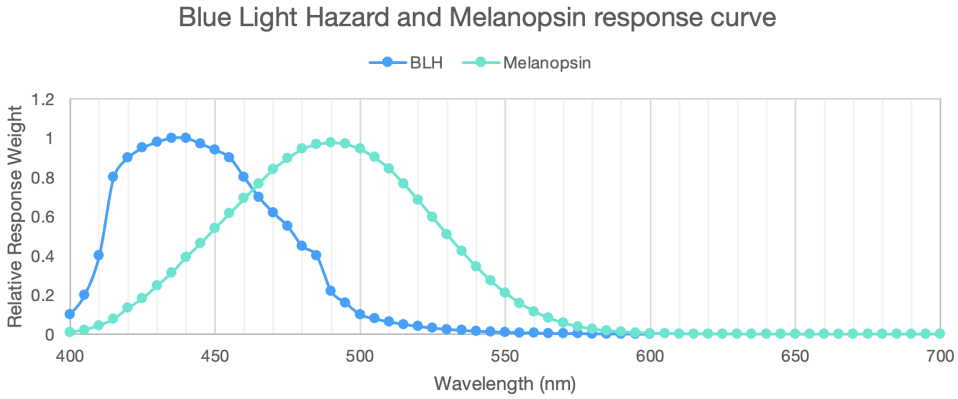


Figure B.1: Comparison of the blue-light hazard weighting function $B(\lambda)$ (recreated from IEC 62471:2006 [53]) and the melanopic response curve of melanopsin.

B.3 IEC 62471 Standard

The IEC 62471 standard, *Photobiological Safety of Lamps and Lamp Systems*, defines quantitative criteria for optical radiation hazards. For retinal photochemical risk, the relevant quantity is the blue-light–weighted radiance, L_B:

$$L_B = \int_{300\,\mathrm{nm}}^{700\,\mathrm{nm}} L_\lambda \, B(\lambda) \, d\lambda. \tag{B.1}$$

The cumulative radiance dose is given by:

$$E_B = L_B \, t. \tag{B.2}$$

Exposure Limits

For exposures **shorter than 10,000 s**:

$$L_B t \leq 10^6 \ \mathrm{J\,m^{-2}\,sr^{-1}}.$$

For exposures **longer than 10,000 s**:

$$L_B \leq 100 \ \mathrm{W\,m^{-2}\,sr^{-1}}.$$

Spectral radiance is defined as:

$$L_\lambda = \frac{d^3\Phi}{dA \, d\Omega \, d\lambda}.$$

B.4 Radiance Measurement Geometry

Radiance measurement requires specifying pupil diameter, angular subtense, and evaluation distance. The standard assumes a 3 mm pupil for bright-light conditions and defines a minimum effective angular subtense of 1.7 mrad, representing the smallest retinal image after diffraction and ocular aberrations. For longer exposures, the effective angular subtense expands due to eye movements.

The standard evaluation distance is 200 mm, below which the human eye cannot physiologically accommodate. Figure B.2 to Figure B.5 illustrate lens-based and mask-based radiance setups and the optical implications of eye accommodation.

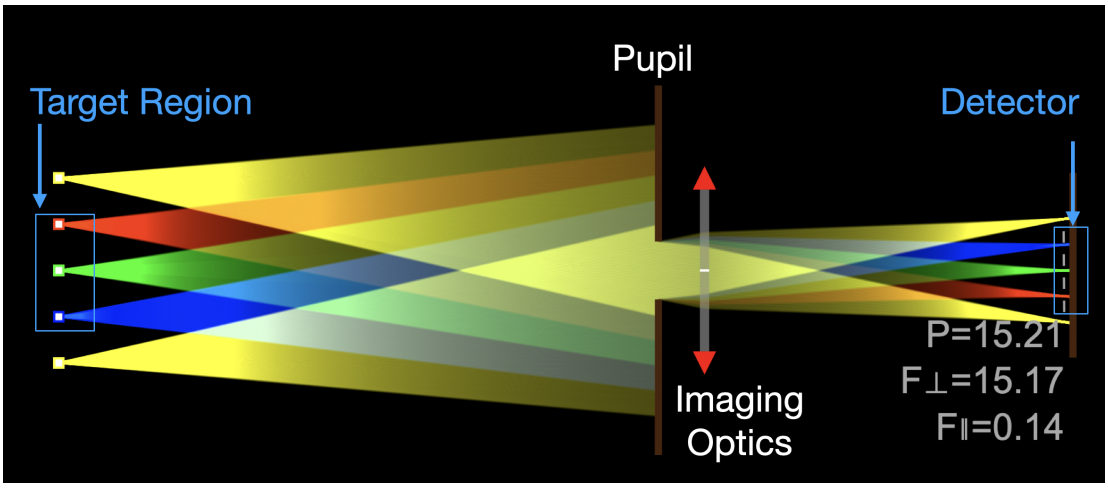


Figure B.2: Illustration of a lens-based radiance measurement setup that collects light within a defined field of view and images the source onto the detector.

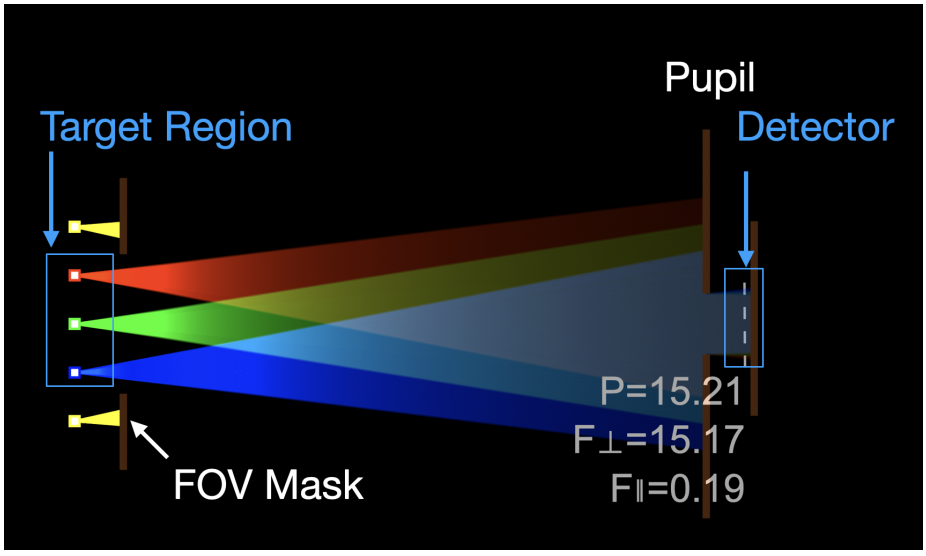


Figure B.3: Example of a mask-based system defining the angular subtense of the source.

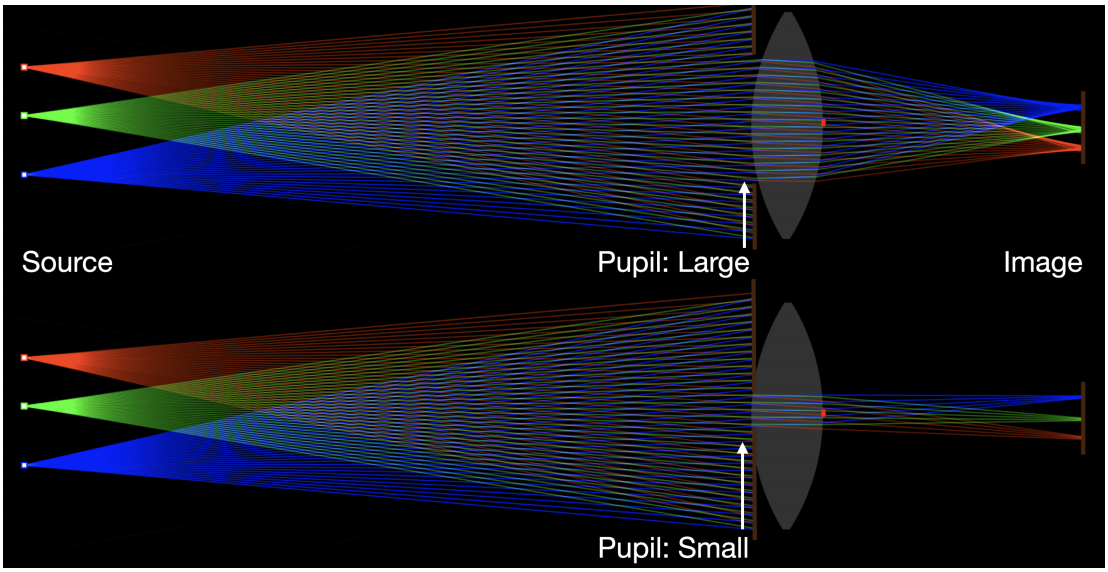


Figure B.4: Optical simulation showing that pupil size primarily regulates retinal illuminance rather than image focus.

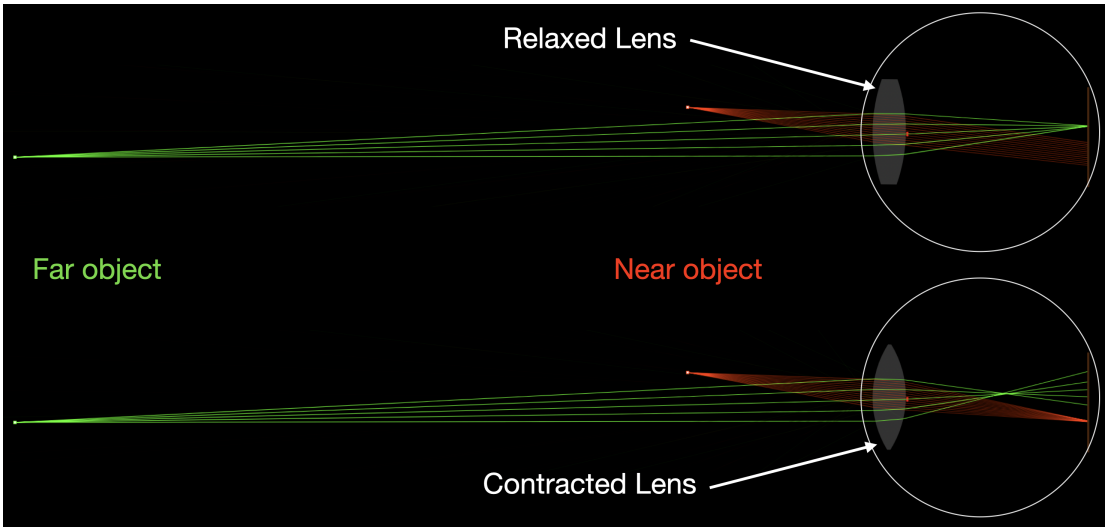


Figure B.5: Optical simulation illustrating human eye accommodation.

B.5 Optical Simulations

While the human eye can accommodate and focus on distant objects beyond approximately 200 mm, it cannot sharply focus light sources located much closer. Illustrated in Figure B.6, light emitted from near-eye systems such as the Lumos glasses forms a large, defocused region on the retina rather than a concentrated point.

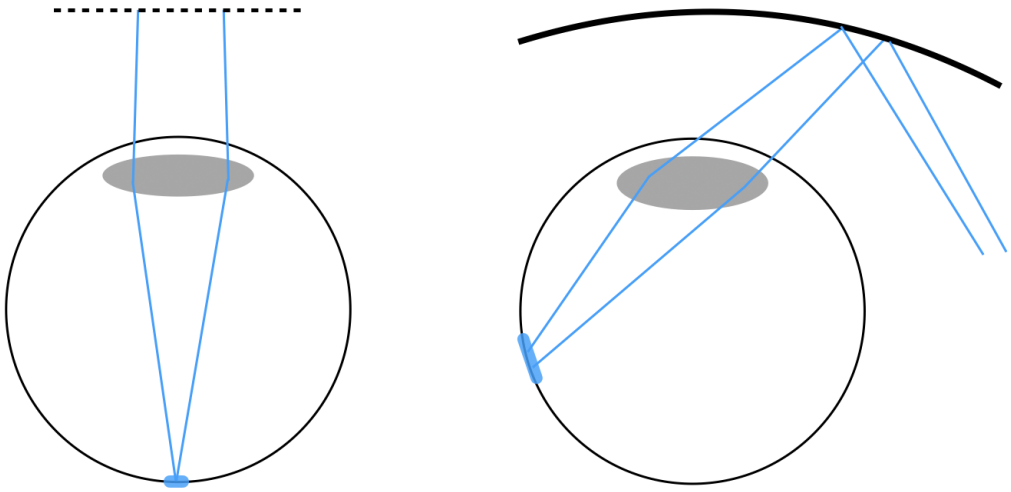


Figure B.6: Conceptual illustration comparing the focused retinal spot produced by a 200 mm distant source (left) with the larger defocused region produced by the near-eye *Lumos* light source (right).

To quantitatively evaluate retinal irradiance and spot size for near-eye photobiological safety, a human eye model from the standard Zemax library was implemented in non-sequential mode, a configuration suitable for illumination and non-imaging analyses [14]. The baseline eye model assumes focus at infinity; therefore, to replicate the 200 mm measurement distance defined in IEC 62471, the curvature of the crystalline lens was adjusted until a collimated source positioned at 200 mm formed a sharp focus on the retinal plane. This configuration represents the worst-case focusing condition, concentrating the maximum radiant energy onto the retina approximately 0.05 mm in diameter, as shown in Figure B.7.

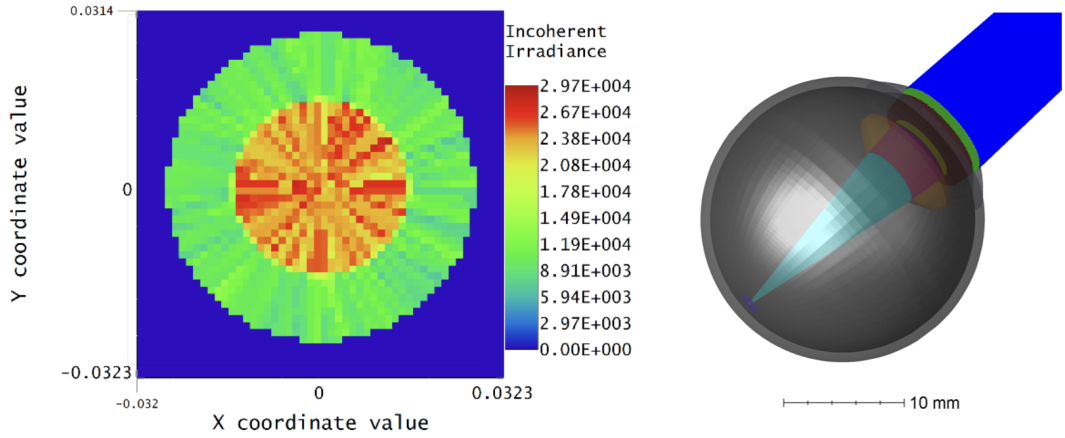


Figure B.7: Zemax non-sequential eye model calibrated to focus a 200 mm source. (Left) Simulated incoherent irradiance on the retina showing a 0.05 mm focused spot. (Right) Ray-trace visualization of light converging through the cornea and lens.

When the same calibrated source was introduced into the complete Lumos optical system, the retinal image expanded significantly to a defocused spot of approximately 2 mm in diameter (Figure B.8). This occurs because the reflective and refractive geometry of the Lumos glasses re-images the emission to a perceived distance rather than forming a direct focus on the retina. This distributes the energy over a larger area and reduces local irradiance.

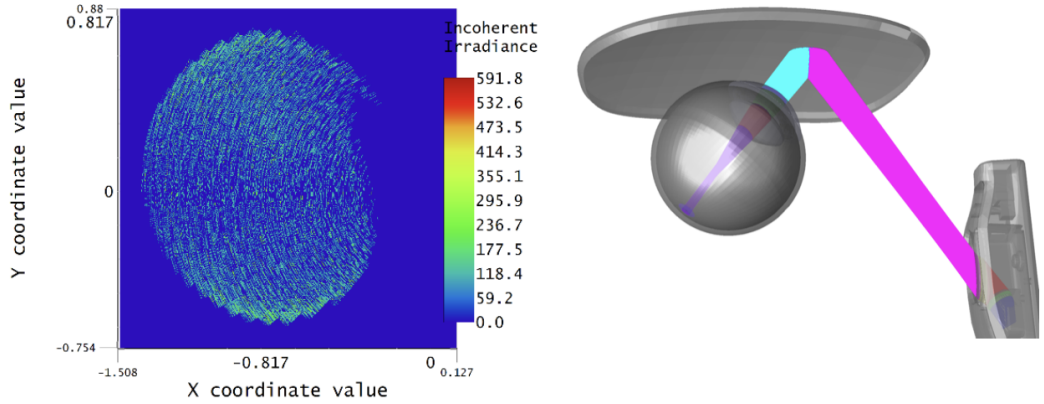


Figure B.8: Simulated retinal irradiance using the accommodated eye model with the *Lumos* optics. (Left) Expanded 2 mm defocused retinal spot. (Right) Ray-trace visualization showing increased divergence through the optical assembly.

A realistic LED source model representing the Lumos light engine was then incorporated using manufacturer-provided ray data, imported following the Osram data integration procedure described by Ansys [13]. The simulation was repeated using the same eye configuration, producing a comparable 2 mm diffuse retinal spot (Figure B.9).

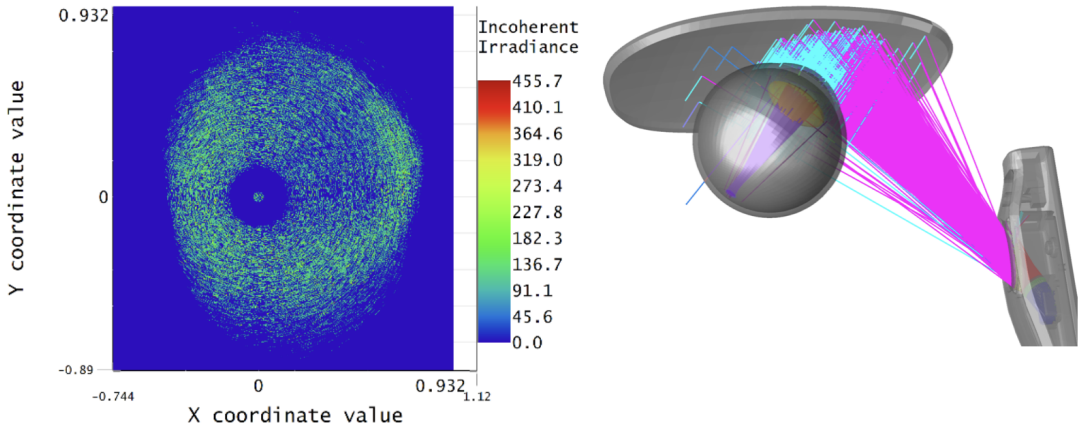


Figure B.9: Simulation using the real Lumos LED source model. (Left) Retinal irradiance map showing a diffuse 2 mm spot. (Right) Ray-trace geometry illustrating light propagation through the near-eye optics.

Finally, the eye model was rotated and positioned in its nominal anatomical orientation relative to the Lumos frame to replicate the user's natural viewing geometry. As shown in Figure B.10, the light entered the eye at an oblique angle, producing an elongated elliptical retinal pattern roughly 2 mm across. This further reduced peak intensity and demonstrated that the optical design naturally mitigates retinal hazard through defocus and spatial spreading.

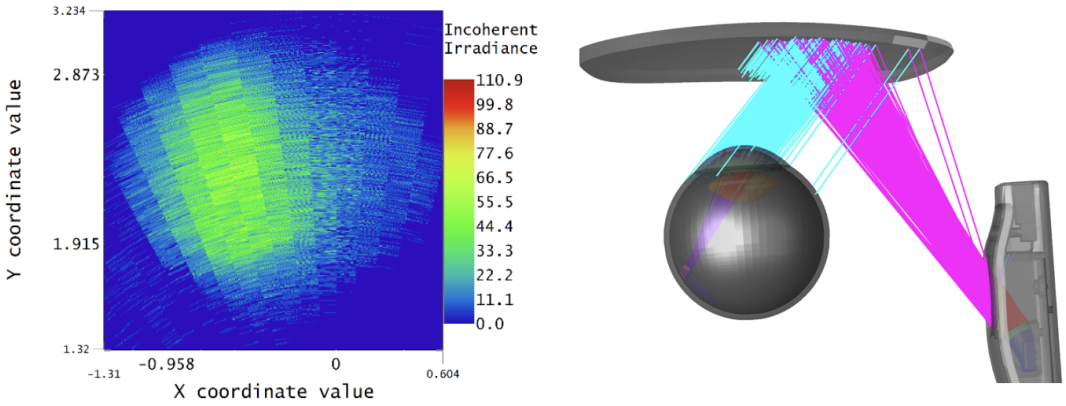


Figure B.10: Simulated retinal irradiance with the eye positioned in its natural viewing orientation relative to the Lumos glasses. (Left) Elliptical, defocused irradiance pattern caused by oblique incidence. (Right) Ray-trace visualization of the near-eye geometry and retinal illumination.

Across all configurations, the Lumos emission produced a retinal footprint of approximately 2 mm, compared to the 0.05 mm focused spot for a distant source at 200 mm. According to IEC 62471, for long-duration exposures the effective averaging angle due to eye movements is 0.1 radian, corresponding to the physiological smearing of a point source across the retina. As illustrated in Figure B.11, if the eye is approximated with a 20 mm focal length, this 0.1 radian angular motion corresponds to a 1 mm smear in each direction. Therefore, for an existing 2 mm optical spot (as produced by the Lumos system), the total effective averaging region becomes roughly 4 mm in diameter. A conservative correction can be applied by scaling the measured radiance (averaged over 100 mrad) down by a factor of four, reflecting the combined effects of optical defocus and physiological eye-motion averaging under realistic near-eye conditions.

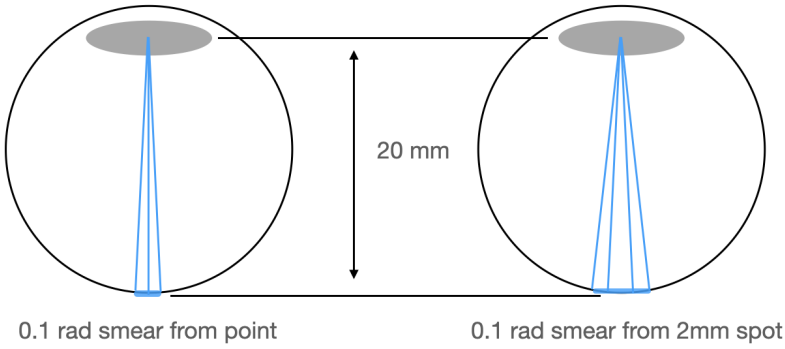


Figure B.11: Illustration of the 0.1 radian spatial averaging assumption from IEC 62471. For long-duration exposures, eye movements smear a point source across approximately 0.1 radian on the retinal surface. For a 2 mm optical spot, this motion extends the effective averaging diameter to roughly 4 mm on a 20 mm focal length eye.

B.6 Time-Dependent Spot Smearing and Boost Mode

With an estimate for the dominant wavelength and peak optical power, the calibrated AS72653 sensor enables reconstruction of the full emission spectrum, emulating the Bentham reference measurements. This simulated spectrum is integrated with the blue-light hazard weighting function to determine the weighted radiance value, which is then adjusted using cosine and source-area correction factors to yield the effective photobiological safety metric defined in IEC 62471. To ensure compliance with the 100 $\mathrm{W\,m^{-2}\,sr^{-1}}$ exposure limit, the LED output is regulated through pulse-width modulation (PWM), maintaining a linear relationship with emitted power. The calibrated output level is permanently stored in the non-volatile memory of the nRF52 microcontroller.

According to IEC 62471, for exposure durations shorter than 10 000 s, the maximum permissible radiance increases following the time-dependent relationship defined in Equation (2.3) of the standard. However, at shorter durations, the effective retinal averaging (*spot smear*) simultaneously decreases, as the eye and head movements contributing to spatial averaging are reduced. The corresponding effective angular subtense, $\alpha_{\mathrm{eff}}(t)$, which models this time-dependent smearing, is defined as

$$\alpha_{\mathrm{eff}}(t) = \min\Big(0.1,\ 0.011\sqrt{\tfrac{t}{100}}\Big), \qquad (t \geq 100\ \mathrm{s}). \tag{B.3}$$

From optical simulation, the base retinal spot size is approximately $D_0 = 2$ mm at $t = 0$ s. As exposure duration increases, additional smearing is added according to the effective angular subtense term, scaled by the approximate eye radius ($L_{\text{eye}} = 20$ mm). The total effective retinal smear diameter $D(t)$ can therefore be expressed as

$$D(t) = D_0 + L_{\text{eye}}\,\alpha_{\text{eff}}(t), \qquad D_0 = 2 \text{ mm}, \quad L_{\text{eye}} = 20 \text{ mm}. \tag{B.4}$$

Substituting from Equation B.3, this yields $D(100 \text{ s}) \approx 2.22$ mm and $D(10\,000 \text{ s}) \approx 4$ mm. This formulation aligns the optical simulation baseline with the IEC 62471 time-based averaging model, accounting for both optical defocus and physiological smearing.

Using this relationship, a short-duration *boost mode* was theoretically calculated to determine how the device could safely increase radiance for shorter exposure times. The resulting boost factor balances the higher permissible radiance for reduced durations (per Equation 2.3) with the smaller effective retinal averaging area described by Equation B.4. The conceptual model of this relationship is illustrated in Figure B.12, showing the progressive increase in effective retinal spot size from $t = 0$ to $t = 10\,000$ s.

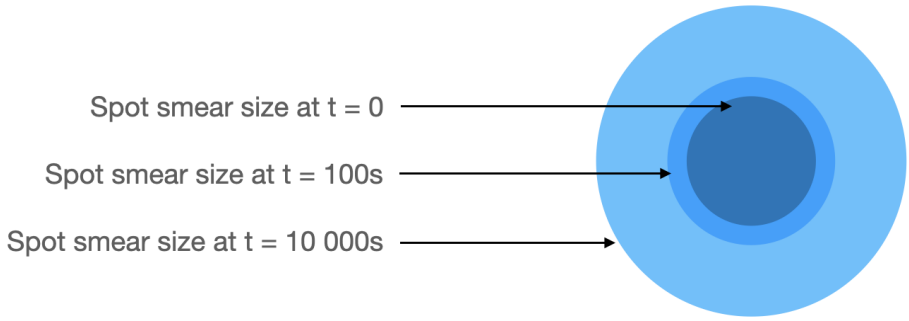


Figure B.12: Conceptual illustration of the IEC 62471 time-dependent spot-smearing relationship. The innermost region represents the 2 mm optical spot at $t = 0$ s, while successive layers correspond to the additional smearing contributions of 20×0.011 rad (≈ 0.22 mm) at $t = 100$ s and 20×0.1 rad (≈ 2 mm) at $t = 10\,000$ s, consistent with Equation B.3.

Although this dynamic boost mechanism complies with the time-dependent radiance limits of IEC 62471, it was not implemented in the clinical trial.

Appendix C

Measurement Instruments and Scoring

C.1 Overview

This appendix provides detailed information on each measurement instrument used in the study, including scoring conventions, reliability, and implementation notes. The main text offers a concise overview (see Section 3.2.7).

C.2 Instrument Summary Table

Table C.1: Summary of measurement instruments and key properties.

Instrument	Construct	Items / Scale	Outcome Used	Notes
MADRS-S	Depressive symptoms	9 items, 0–6	Total 0–60	First item doubled for comparability; high reliability
PROMIS Sleep (SF)	Sleep disturbance	8 items, 1–5	Raw sum 8–40	Raw (not T) scores used for sensitivity to week-to-week change
PVT	Vigilance / reaction time	10 trials	Mean adjusted RT	500 ms penalty for lapses or false starts; high test–retest reliability
Word-Pair	Associative memory	10 pairs	Correct 0–10	In-app cued recall task assessing working memory

C.3 MADRS-S (Depression)

Depressive symptoms were assessed weekly using the self-rated version of the Montgomery–Åsberg Depression Rating Scale (MADRS-S) [92]. The scale includes nine items rated 0–6, covering core affective and cognitive symptoms of depression. To align with the original 10-item clinician-rated MADRS [66], the first item ("Reported sadness") was doubled when computing total scores, yielding a 0–60 range. The self-rated form shows high internal consistency ($\alpha = .84$–$.90$) and strong correlation with clinician ratings ($r \approx .85$) [40]. In this study, the MADRS-S was completed weekly via Qualtrics, with reminders sent through the app.

Rationale for scoring. Doubling the first item preserves comparability with clinician totals and avoids altering weight distributions in downstream analyses.

C.4 PROMIS Sleep Disturbance—Short Form

Sleep disturbance was measured weekly using the 8-item Patient-Reported Outcomes Measurement Information System Sleep Disturbance Short Form (PROMIS) Sleep Disturbance—Short Form [107, 26]. Each item uses a 5-point Likert scale referencing the past 7 days,

capturing subjective sleep quality, depth, and restoration. Although the PROMIS manual [73] allows T-score conversion (mean 50, SD 10), raw summed scores (8–40) were used here to preserve ordinal sensitivity for repeated measures. The measure demonstrates excellent internal consistency ($\alpha > .90$) and convergent validity with the PSQI ($r \sim .8$) [26].

Rationale for raw-score use. Raw scores enable clearer interpretation of week-to-week change and prevent compression from standardized T-score scaling.

C.5 Psychomotor Vigilance Task (PVT)

Sustained attention and reaction time were assessed using a 10-trial Psychomotor Vigilance Task adapted from a validated computerized paradigm [16]. Visual stimuli were delivered as brief light flashes emitted from the **right arm of the Lumos glasses**. Participants pressed a button on the glasses as quickly as possible when the light appeared, with results displayed immediately in the paired smartphone app. Stimulus timing and response latency were processed within the glasses' firmware to eliminate smartphone delays.

Scoring. A custom algorithm assigned lapses (responses >500 ms) and false starts (premature presses) a fixed value of 500 ms, producing a unified mean adjusted reaction time that penalized both omission and commission errors. The PVT is widely validated, showing high reliability ($r \approx .80$) and strong sensitivity to sleep loss and circadian misalignment [16].

C.6 Paired-Associate Memory (Word-Pair) Test

Working memory and associative learning were measured weekly using an in-app Word-Pair recall test modeled on standard paired-associate paradigms [18]. Each trial presented ten word pairs for study, followed by a cued-recall phase in which participants typed the second word when prompted with the first. The number of correct responses (0–10) was recorded as the outcome. Because the test was self-administered on smartphones, some variability across participants and sessions was expected.

Baseline handling. Baseline scores for PVT and Word-Pair tests were defined as the first available in-app measurement (see Section 3.2.8 for Day 0 alignment).

C.7 Administration Platforms

The MADRS-S and PROMIS questionnaires were hosted on Qualtrics and accessed via links embedded in the Lumos app, while the PVT and Word-Pair tasks were completed directly within the app. All data were timestamped, encrypted, and uploaded to secure cloud storage as described in the data handling protocol.

Appendix D

Power Analysis and Sample Size Derivation

This appendix presents the full numerical derivations, variance assumptions, and references used in the power calculations summarized in Section 3.2.8. The analysis employed two-sample comparisons of means to detect between-group differences at week 8, assuming two-sided equality tests ($\alpha = 0.05$, power $= 0.80$).

The revised calculations here update the preliminary version in Appendix P by using the **pooled variance method** instead of the mean of group standard deviations, which slightly increases required sample sizes and improves precision.

Primary endpoint: Depression (MADRS). Lam *et al.* [60] reported mean change scores of 13.4±7.5 (light) vs. 6.5±9.6 (placebo) in nonseasonal MDD. Required per-arm size: n=25 (two-sided), pooled SD $\approx$ 8.58.

Sleep quality. Akyar & Akdemir [8] observed PSQI improvement from 12.87±4.26 to 3.95±1.75. Assuming placebo halfway to treatment (8.41±4.26), n=9 per arm (two-sided, pooled SD $\approx$ 3.26).

Psychomotor Vigilance (PVT). Rosa *et al.* [78] found improvement from 218.63±5.06 ms to 207.18±3.45 ms after a 5-day protocol. Assuming placebo halfway, n=9 per arm, pooled SD $\approx$ 4.33.

Working memory (Word-Pair). Bersani *et al.* [18] reported 22.4±0.3 (treatment) vs. 21.1±1.3 (control). Required n=34 per arm (two-sided), pooled SD ≈ 0.94.

Final decision. Budget and manufacturing limits constrained recruitment to n=48 per arm (N=96), exceeding all minimum requirements and providing adequate power for secondary and exploratory analyses (e.g., dose–response, moderation by eye color).

Table D.1: Detailed planning assumptions and required per-arm sample sizes.

Endpoint	Placebo (mean±SD)	Active (mean±SD)	n/arm (1-sided / 2-sided; pooled SD)
MADRS [60]	6.5 ± 9.6	13.4 ± 7.5	20 / 25; 8.58
Sleep (PSQI) [8]	8.41 ± 4.26	3.95 ± 1.75	7 / 9; 3.26
PVT RT (ms) [78]	212.9 ± 5.06	207.18 ± 3.45	8 / 9; 4.33
Word-pair total [18]	21.75 ± 1.30	22.4 ± 0.30	27 / 34; 0.94

Appendix E

Detailed MADRS Stratified Analyses

E.1 Overview

This appendix presents the full statistical tables for the stratified MADRS analyses by eye-color subgroup. The main text (Section 3.3.4) summarizes the trends and shows time-course figures, while the tables below include the corresponding regression slopes, hinge coefficients, and primary contrasts for transparency and reproducibility.

E.2 Light-Eyed Participants (Blue, Green, Hazel)

Table E.1: Group-level slopes for ΔMADRS, light-eyed group (hinge = Day 56).

Group	Pre-56 slope	p	partial η^2	Δ_{56}	Post-56 slope
Alpha	-0.175	9.3×10^{-11}	0.300	$+0.129$ ($p = 0.078$; $\eta^2 = 0.026$)	-0.046
Beta	-0.093	1.1×10^{-4}	0.122	$+0.198$ ($p = 0.003$; $\eta^2 = 0.074$)	$+0.104$

Table E.2: Primary contrasts for ΔMADRS, light-eyed group.

Contrast	Estimate	t	df	p	partial η^2
Between groups: pre-56	−0.081	−2.41	116	0.0177	0.048
Between groups: post-56	−0.150	−2.16	116	0.033	0.039
Within Alpha: change at 56	+0.129	1.78	118	0.078	0.026
Within Beta: change at 56	+0.198	3.04	116	0.003	0.074

E.3 Brown-Eyed Caucasian Participants

Table E.3: Group-level slopes for ΔMADRS, brown-eyed Caucasian group (hinge = Day 56).

Group	Pre-56 slope	p	partial η^2	Δ_{56}	Post-56 slope
Alpha	−0.061	0.016	0.073	−0.055 ($p = 0.447$; $\eta^2 = 0.008$)	−0.116
Beta	−0.164	7.5×10^{-8}	0.282	+0.138 ($p = 0.114$; $\eta^2 = 0.028$)	−0.025

Table E.4: Primary contrasts for ΔMADRS, brown-eyed Caucasian group.

Contrast	Estimate	t	df	p	partial η^2
Between groups: pre-56	+0.103	2.78	77	0.0069	0.091
Between groups: post-56	−0.090	−1.09	77	0.278	0.015
Within Alpha: change at 56	−0.055	−0.76	77	0.447	0.008
Within Beta: change at 56	+0.138	1.60	88	0.114	0.028

E.4 Dark-Eyed Non-Caucasian Participants

Table E.5: Group-level slopes for ΔMADRS, dark-eyed non-Caucasian group (hinge = Day 56).

Group	Pre-56 slope	p	partial η^2	Δ_{56}	Post-56 slope
Alpha	-0.108	5.0×10^{-6}	0.204	$+0.227$ ($p = 5.8 \times 10^{-4}$; $\eta^2 = 0.121$)	$+0.119$
Beta	-0.195	1.4×10^{-10}	0.433	$+0.247$ ($p = 0.0016$; $\eta^2 = 0.129$)	$+0.052$

Table E.6: Primary contrasts for ΔMADRS, dark-eyed non-Caucasian group.

Contrast	Estimate	t	df	p	partial η^2
Between groups: pre-56	$+0.087$	2.54	73	0.013	0.081
Between groups: post-56	$+0.067$	0.96	73	0.342	0.012
Within Alpha: change at 56	$+0.227$	3.56	92	5.8×10^{-4}	0.121
Within Beta: change at 56	$+0.247$	3.29	73	0.0016	0.129

E.5 Summary

Across subgroups, brown- and dark-eyed participants showed faster improvement under bright-light treatment compared with dim-light, whereas light-eyed participants improved more under dim-light. Both brown- and dark-eyed groups also exhibited stronger hinge effects post-crossover, suggesting enhanced sensitivity to light-phase transitions.

Appendix F

Expanded MADRS Multiple Regression Analyses

F.1 Overview

This appendix retains full model specifications, figures, tables, and narrative interpretations for the MADRS multiple-regression analyses summarized in Section 3.3.5.

F.1.1 Depression (MADRS) Multiple regression

Multiple regression analysis was run to determine if usage, ambient light brightness, age, sex, baseline scores and their interactions correlated with improvements.

Usage time For each data-point in MADRS, the usage time was presented as a constant average number of hours per day throughout that phase, and multiple regression was performed using the equation below.

$$\Delta\text{MADRS}_i = \beta_1\,\text{day} + \beta_2\,\text{after56} + \beta_3\,\text{hours}_\text{c} + \varepsilon,$$
$$\text{where hours}_\text{c} = \text{hours} - mean(hours)$$

Where (`hours_c`) is a centered term introduced in the model such that the 0,0 condition for day of study and usage time also crosses the 0 for delta MADRS for ease of analysis.

Multiple regression yielded significant fit improvements with adding usage time for the following groups: Caucasians with brown eyes, both alpha and beta group Caucasians with light-colored eyes, alpha group.

Note that the usage time co variates wasn't broken down per phase, as there wasn't sufficient data differentiation to allow more significant results. This is in part due to participants having similar usage time in both phases. For example, someone who used the glasses more in phase 1, persisted in phase 2.

Usage Time Effects (hours)

Figure F.1–F.3 illustrate the fitted pre- and post-crossover surfaces alongside the observed data.

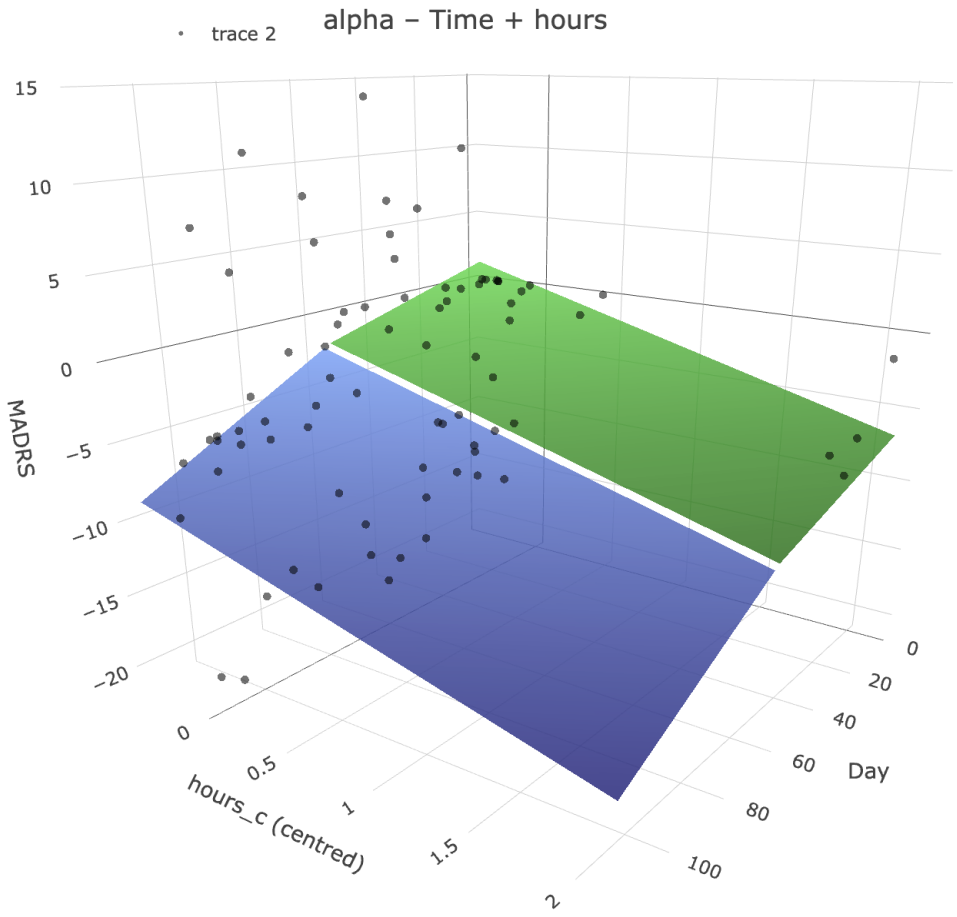


Figure F.1: **Caucasians with brown eyes — Alpha:** Time + usage (`hours_c`) surface with Day 56 hinge.

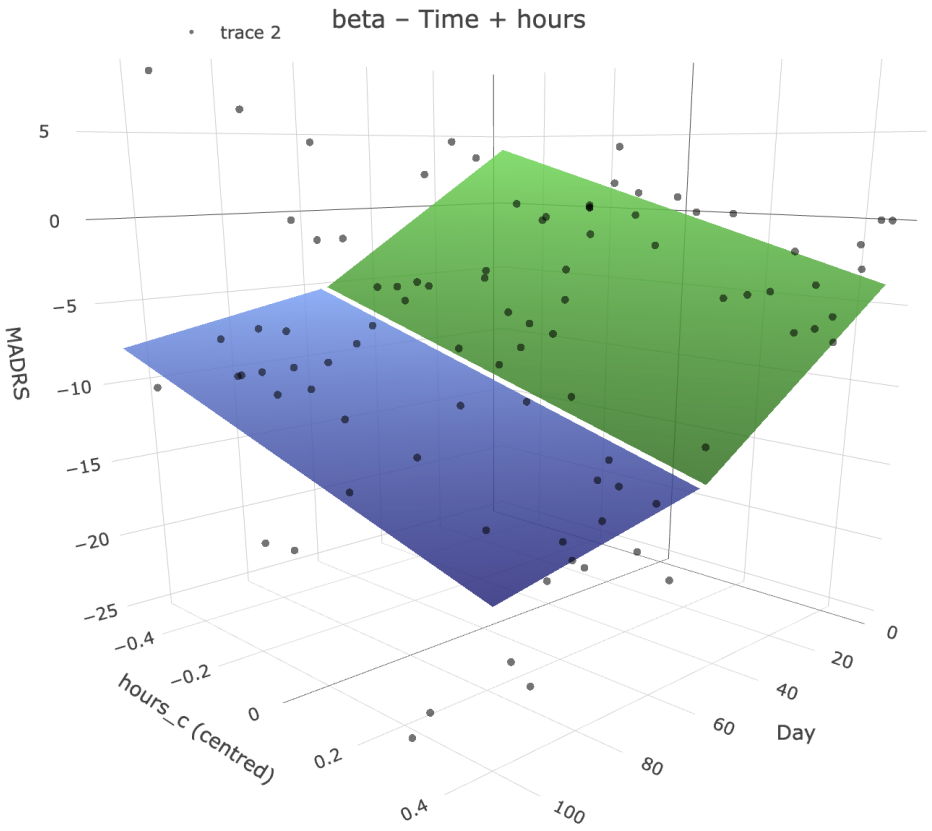


Figure F.2: **Caucasians with brown eyes — Beta:** Time + usage (`hours_c`) surface with Day 56 hinge.

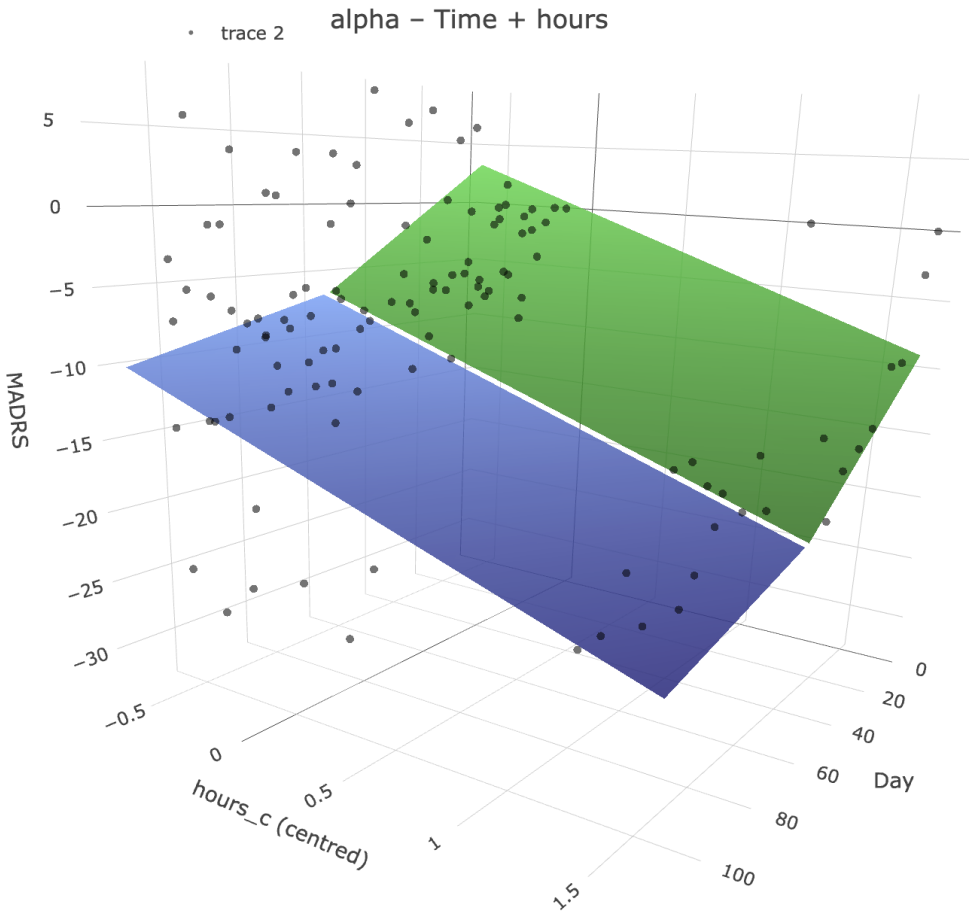


Figure F.3: **Light-eyed — Alpha:** Time + usage (`hours_c`) surface with Day 56 hinge.

Table F.1: Time + usage (`hours_c`) models for ΔMADRS with effect sizes.

Brown-eyed Caucasians			
Quantity	Estimate	partial η^2	p
Alpha			
Pre-56 slope (mean hours), pts/day	−0.0601	0.073	0.013
Post-56 slope (mean hours), pts/day	−0.120	—	—
Slope change at 56, pts/day	−0.0598	0.008	0.388
Hours main effect (per hour)	−3.191	0.054	0.010
Adj. R^2 (time-only → time+hours)		0.331 → 0.386	
Block F vs. time-only	6.91; $f^2 = 0.027$ (small)		0.010
Beta			
Pre-56 slope, pts/day	−0.1642	0.282	2.8×10^{-8}
Post-56 slope, pts/day	−0.0504	—	—
Slope change at 56, pts/day	+0.1138	0.028	0.179
Hours main effect (per hour)	−8.055	0.063	0.0067
Adj. R^2 (time-only → time+hours)		0.443 → 0.504	
Block F vs. time-only	7.73; $f^2 = 0.034$ (small)		0.0067
Light-eyed			
Quantity	Estimate	partial η^2	p
Alpha			
Pre-56 slope, pts/day	−0.1753	0.300	4.4×10^{-13}
Post-56 slope, pts/day	−0.0648	—	—
Slope change at 56, pts/day	+0.1105	0.029	0.084
Hours main effect (per hour)	−5.363	0.158	1.45×10^{-8}
Adj. R^2 (time-only → time+hours)		0.546 → 0.641	
Block F vs. time-only	37.13; $f^2 = 0.148$ (medium)		1.45×10^{-8}

Notes. Only arms with significant usage effects ($p < 0.05$) are shown. Partial η^2 is the within-model effect size; Cohen's f^2 is derived from the block test (small ≈ 0.02, medium ≈ 0.15, large ≈ 0.35). All coefficients are in MADRS points per day. Negative slopes or β_{hours_c} denote greater improvement with higher usage. (*Light-eye Beta* excluded: non-significant usage effect, $F = 0.864$, $p = 0.355$).

melanopic lux Ambient light exposure (*lux*) was examined as a secondary covariate using multiple regression on ΔMADRS scores. The term represents the average melanopic lux level measured during the period preceding each questionnaire entry.

$$\Delta\text{MADRS}_i = \beta_1\,\text{day} + \beta_2\,\text{after56} + \beta_3\,\text{lux}_c + \varepsilon, \qquad \text{lux}_c = \text{lux} - \overline{\text{lux}}.$$

Table F.2 summarizes the coefficients and effect sizes for both arms. The main effect of `lux_c` was negative and statistically significant in both models, indicating that higher ambient light exposure was associated with greater improvement (larger decreases in MADRS). When stratified by group and eye color, all subgroups exhibited the same trend and reached statistical significance except for the Alpha group with Light-eyes.

Table F.2: Time + lux models for ΔMADRS with effect sizes.

Alpha group			
Quantity	Estimate	partial η^2	p
Pre-56 slope (mean lux), pts/day	−0.124	0.193	$< 10^{-14}$
Post-56 slope (mean lux), pts/day	+0.006	—	—
Slope change at 56, pts/day	+0.131	0.030	0.0030
Lux main effect (per 1000 lux)	−2.379	0.0166	0.028
Adj. R^2 (time-only → time+lux)		0.301 → 0.357	
Block F vs. time-only	4.88; $f^2 = 0.017$ (small)		0.0289
Beta group			
Quantity	Estimate	partial η^2	p
Pre-56 slope (mean lux), pts/day	−0.151	0.264	$< 10^{-19}$
Post-56 slope (mean lux), pts/day	+0.059	—	—
Slope change at 56, pts/day	+0.210	0.0765	2.4×10^{-6}
Lux main effect (per 1000 lux)	−8.093	0.084	7.2×10^{-7}
Adj. R^2 (time-only → time+lux)		0.420 → 0.379	
Block F vs. time-only	25.73; $f^2 = 0.045$ (small)		7.2×10^{-7}

Notes. Effect sizes are reported as partial η^2 (small ≈ 0.01, medium ≈ 0.06, large ≈ 0.14) and Cohen's f^2 for block tests (small ≈ 0.02, medium ≈ 0.15, large ≈ 0.35).

Interpretation. The inclusion of ambient light (`lux_c`) improved model fit for both arms, with significant negative coefficients in Alpha ($p = 0.028$) and Beta ($p < 10^{-6}$). This indicates that higher light exposure was associated with faster mood improvement. The effect remained robust across phases, suggesting that participants experiencing greater melanopic light stimulation showed larger decreases in depressive symptoms.

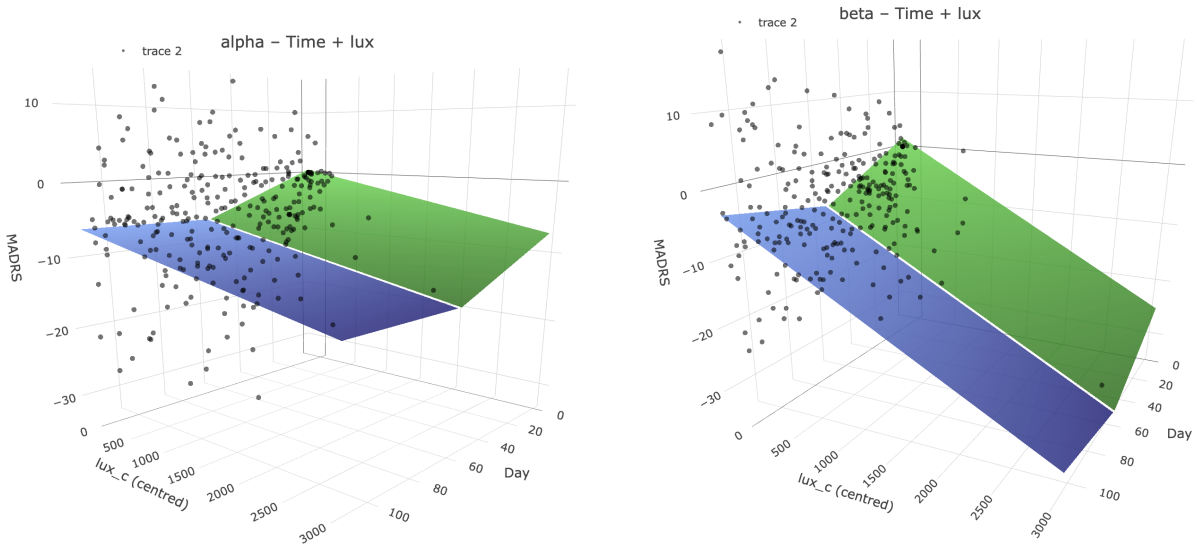


Figure F.4: Time + centered lux planes for Alpha (left) and Beta (right). Increasing ambient light levels corresponded with greater improvement (lower MADRS).

Baseline severity. MADRS scores were also analyzed against their baseline (initial severity) as a covariate:

$$\text{baselineMADRS}_c = \text{baselineMADRS} - \overline{\text{baselineMADRS}}.$$

$$\Delta\text{MADRS}_i = \beta_1\,\text{day} + \beta_2\,\text{after56} + \beta_3\,\text{baselineMADRS}_c + \varepsilon.$$

Table F.3–F.4 summarize the updated coefficients and model fits. In both cohorts, higher baseline depression severity predicted greater subsequent improvement (more negative ΔMADRS), consistent with greater potential for change among participants starting from higher symptom scores.

Table F.3: Alpha group: time + baseline model for ΔMADRS with updated coefficients and effect sizes.

Quantity	Estimate	partial η^2	p
Pre-56 slope at mean baseline (β_{day}), pts/day	-0.130	0.225	$< 10^{-17}$
Post-56 slope at mean baseline ($\beta_{\text{day}} + \beta_{\text{after56}}$), pts/day	-0.013	—	—
Slope change at 56 (β_{after56}), pts/day	$+0.117$	0.027	0.0047
Baseline main effect ($\beta_{\text{baseline}_c}$)	-0.328	0.115	2.7×10^{-9}
Adj. R^2 (time-only → time+baseline)		0.301 → 0.421	
Block F vs. time-only	37.74; $f^2 = 0.131$ (medium)		2.7×10^{-9}

Table F.4: Beta group: time + baseline model for ΔMADRS with updated coefficients and effect sizes.

Quantity	Estimate	partial η^2	p
Pre-56 slope at mean baseline (β_{day}), pts/day	-0.140	0.230	$< 10^{-17}$
Post-56 slope at mean baseline ($\beta_{\text{day}} + \beta_{\text{after56}}$), pts/day	$+0.063$	—	—
Slope change at 56 (β_{after56}), pts/day	$+0.203$	0.070	6.6×10^{-6}
Baseline main effect ($\beta_{\text{baseline}_c}$)	-0.230	0.057	5.0×10^{-5}
Adj. R^2 (time-only → time+baseline)		0.420 → 0.361	
Block F vs. time-only	16.97; $f^2 = 0.064$ (small–mid)		5.0×10^{-5}

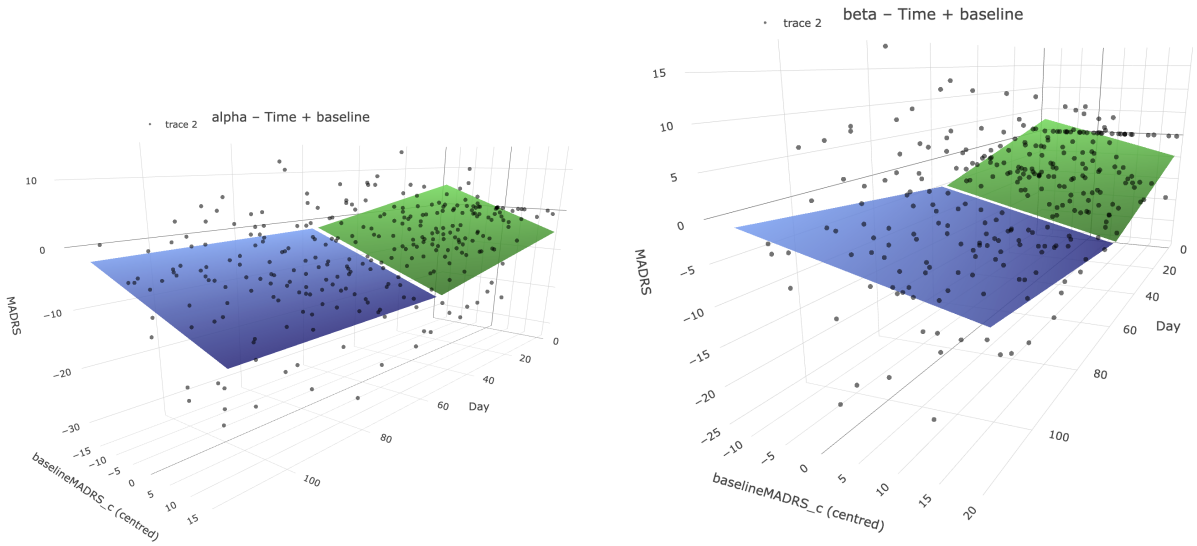


Figure F.5: Time + centered baseline severity planes for Alpha (left) and Beta (right); see Tables F.3 and F.4.

Age and baseline severity. Age had a significant correlation with initial starting scores. The baseline MADRS and PROMIS scores were plotted against participant age in (Figure F.6). Both instruments showed a positive association with age: older participants tended to begin the study with higher baseline depression and sleep-disturbance scores.

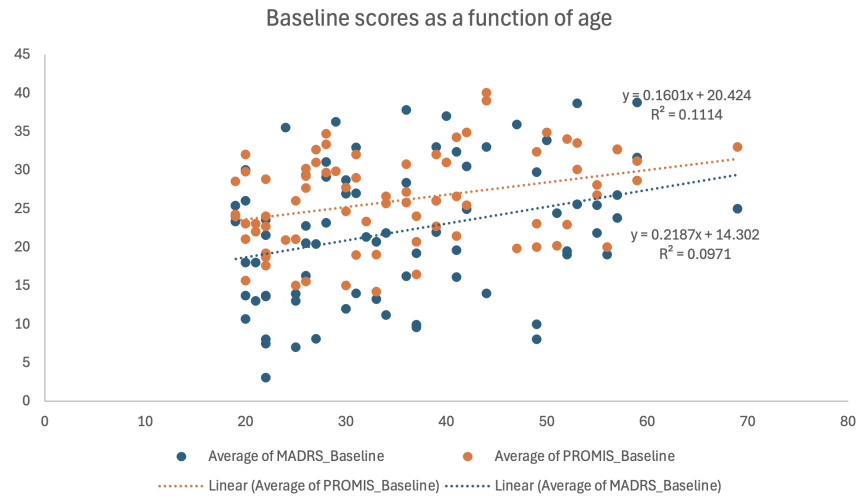


Figure F.6: Baseline MADRS and PROMIS scores plotted against age. Regression lines indicate that older participants tended to present with higher baseline scores.

Baseline-normalized sensitivity analysis. Because age and baseline MADRS were correlated, a sensitivity analysis was conducted by normalizing each participant's change by their own baseline:

$$\Delta\text{MADRS}_{ij}^{(\text{rel})} = \frac{\Delta\text{MADRS}_{ij}}{B_j},$$

where B_j is the participant's baseline MADRS score. The model was re-fit as:

$$\Delta\text{MADRS}_{ij}^{(\text{rel})} = \beta_1\,\text{day}_{ij} + \beta_2\,\text{after56}_{ij} + \varepsilon_{ij},$$

separately for Alpha and Beta arms. Figure F.7 shows the fitted pre- and post-hinge trajectories.

All participants. As summarized in Tables F.5–F.6, normalization by baseline severity did not materially change the overall results. In the aggregate sample, Beta continued to show faster improvement during Phase 1 (pre-56) and a larger rebound post-56. The hinge term remained highly significant for Beta ($p = 1.8\times10^{-5}$), whereas the Alpha hinge became marginal ($p = 0.051$).

Table F.5: Group-level slopes for baseline-normalized ΔMADRS (hinge at Day 56; all participants).

Group	Pre-56 slope	partial η^2	Δ@56	p_Δ	Post-56 slope
Alpha	−0.0059	0.175	+0.0043	0.051	−0.0016
Beta	−0.0073	0.220	+0.0104	1.8×10^{-5}	+0.0031

Notes. partial η^2 estimated from $t = \hat{\beta}/\text{SE}$ using $t^2/(t^2 + \text{df})$; post-56 slopes are derived (no direct p).

Table F.6: Primary contrasts (per day) for baseline-normalized ΔMADRS (hinge at Day 56; all participants).

Contrast	Estimate	t	df	p	partial η^2
Between groups: pre-56	—	—	—	0.220	—
Between groups: post-56	—	—	—	**0.043**	—
Within Alpha: change at 56	+0.0043	—	291	0.051	0.013
Within Beta: change at 56	+0.0104	—	281	$\mathbf{1.8 \times 10^{-5}}$	0.063

Notes. Contrasts show between-arm slope differences (Beta vs. Alpha) and within-arm hinge effects. Directionality matches the raw analysis: negative slopes indicate improvement.

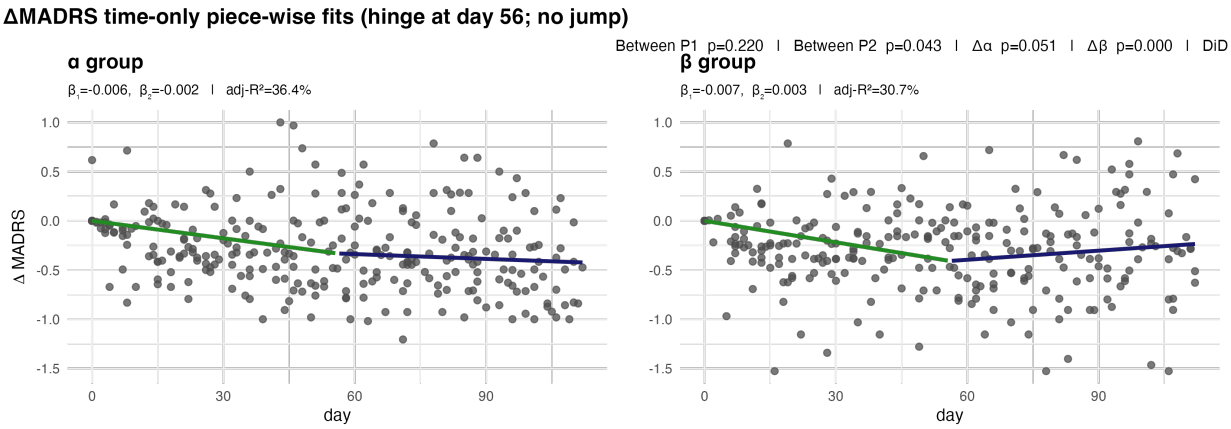


Figure F.7: Baseline-normalized analysis for all participants. Green = pre-56; blue = post-56. Beta maintains a steeper improvement and larger rebound than Alpha.

Non-light (all brown-eyed). For the combined brown-eyed subgroup (non-light), Phase 1 improvement remained significant ($p = 6.9 \times 10^{-4}$), while post-56 between-arm differences were not significant. Beta showed a significant hinge ($p = 0.0054$), consistent with a rebound after crossover.

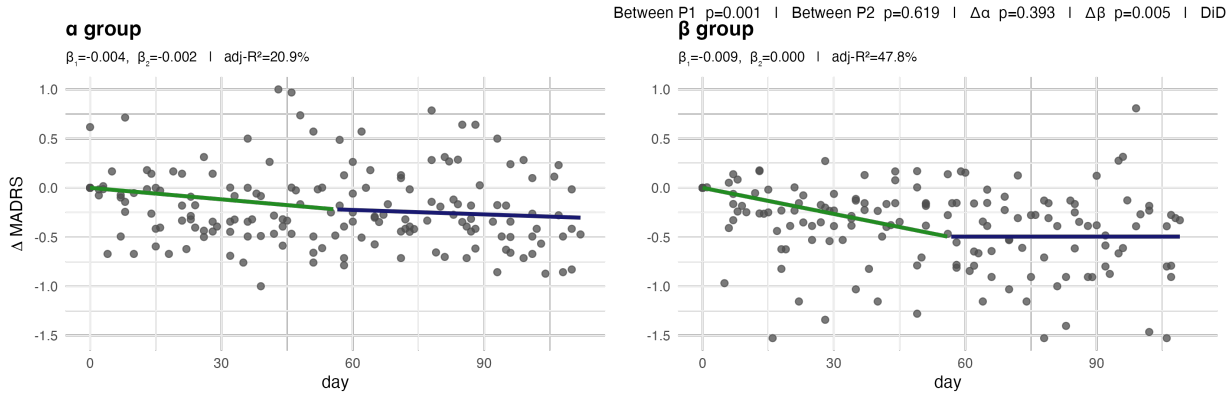


Figure F.8: Baseline-normalized analysis for non-light participants (all brown-eyed). Phase-1 Beta improvement remains significant; post-56 difference not significant.

Light-eyed. Among light-eyed participants, both pre- and post-56 between-arm differences remained significant ($p = 0.010$ and 0.019, respectively). Both within-arm hinge terms were also

significant ($p_\alpha = 0.041$, $p_\beta = 0.0019$), showing that the relative response pattern persisted after normalization.

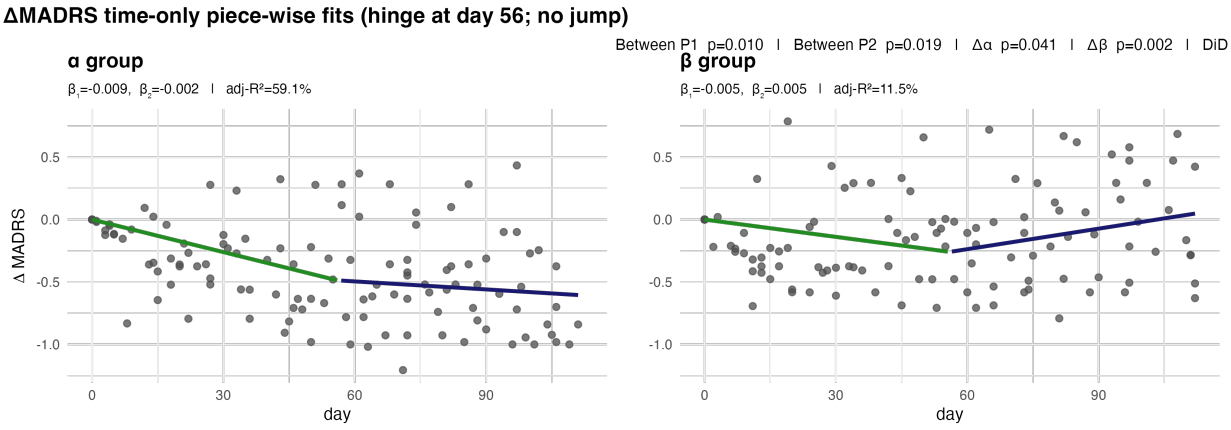


Figure F.9: Baseline-normalized analysis for light-eyed participants. Both pre- and post-56 contrasts remain significant, consistent with the raw model.

Brown-eyed Caucasians. In brown-eyed Caucasians, the Phase-1 between-arm difference remained significant ($p = 0.0010$), and a small but significant DiD ($p = 0.039$) indicated a crossover-driven change. This confirms the robust benefit of bright-light during the first phase even when normalized by baseline severity.

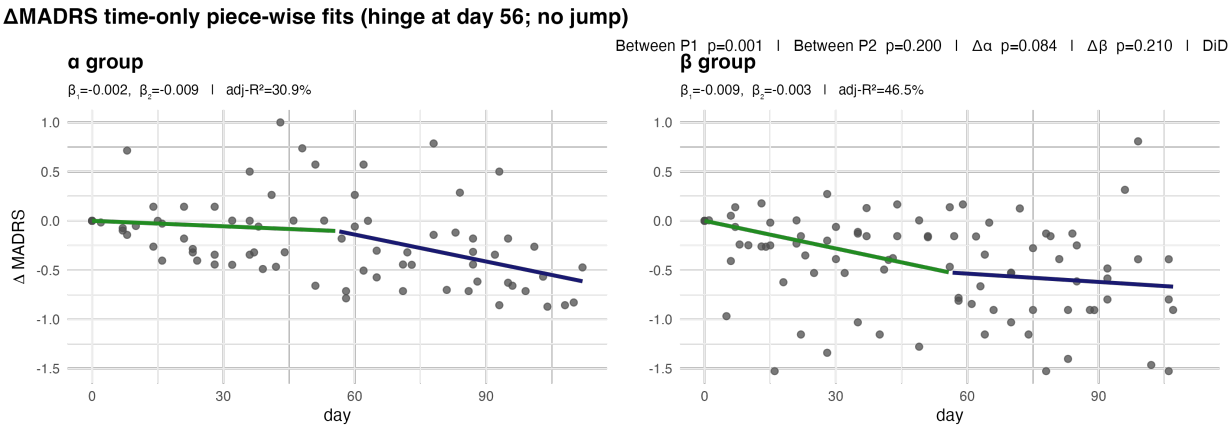


Figure F.10: Baseline-normalized analysis for brown-eyed Caucasian participants. The Phase-1 between-arm difference remains significant, with a small but significant DiD.

Dark-eyed non-Caucasians. For dark-eyed non-Caucasian participants, between-arm differences were no longer significant ($p_{\text{pre}} = 0.15$, $p_{\text{post}} = 0.52$). Both within-arm hinge terms remained significant ($p_\alpha = 0.0070$, $p_\beta = 0.0014$), but the loss of between-arm contrast suggests that reduced sample size may have limited power after normalization.

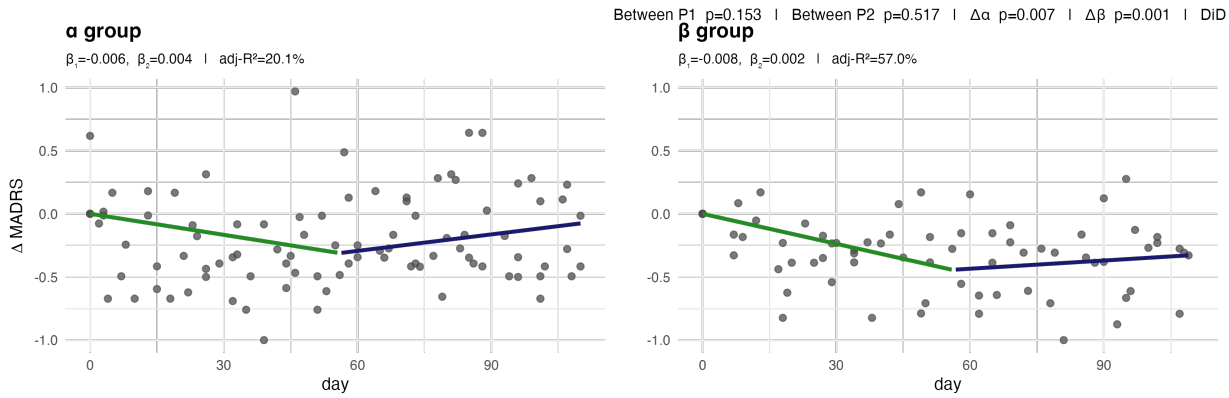


Figure F.11: Baseline-normalized analysis for dark-eyed non-Caucasian participants. Between-arm differences are no longer significant, likely due to reduced sample size, though both within-arm hinge effects remain.

Summary. Across all re-baselined analyses, the principal conclusions are maintained:

1. Beta participants continued to improve more rapidly during Phase 1 and showed greater rebound after crossover.
2. Normalization by baseline severity slightly reduced significance for Alpha and for the dark-eyed subgroup, likely reflecting smaller effective sample sizes.
3. Non-light- and brown-eyed groups retained clear, statistically significant Phase-1 improvements under bright-light exposure, consistent with the hypothesized melanopic sensitivity differences.

Baseline-normalized Age effects. After normalizing by baseline MADRS, age was introduced as a covariate to test whether participant age influenced treatment response independently of baseline severity.

$$\Delta\text{MADRS}_{ij}^{(\text{rel})} = \beta_1\,\text{day}_{ij} + \beta_2\,\text{after56}_{ij} + \beta_3\,\text{age}_c + \varepsilon_{ij},$$

where age_c is the centered participant age.

Brown-eyed Caucasians. In brown-eyed Caucasian participants, age significantly affected outcomes in both arms (Figure F.12). For the Alpha group, older participants improved less ($\beta_{\text{age}_c} = -0.0072$, $p = 0.012$, $\eta_p^2 = 0.034$), while for the Beta group, older age predicted slightly greater improvement ($\beta_{\text{age}_c} = +0.0058$, $p = 0.021$, $\eta_p^2 = 0.028$). Although the effect sizes were small, this reversal in direction suggests possible age-related differences in sensitivity to bright-light treatment versus control.

Table F.7: Baseline-normalized MADRS with age for brown-eyed Caucasian participants.

Parameter	Estimate	partial η^2	p
Alpha group			
Age main effect (β_{age_c})	-0.0072	0.034	0.012
Beta group			
Age main effect (β_{age_c})	$+0.0058$	0.028	0.021
Adj. R^2 (time-only $\rightarrow$ time+age)	$0.312 \rightarrow 0.342$ (Alpha), $0.397 \rightarrow 0.423$ (Beta)		
Block F vs. time-only	4.05; $f^2 = 0.037$ (small)		0.020

Notes. Age had opposite effects across arms: older Alpha participants improved less, whereas older Beta participants improved slightly more. Both effects were statistically significant but small.

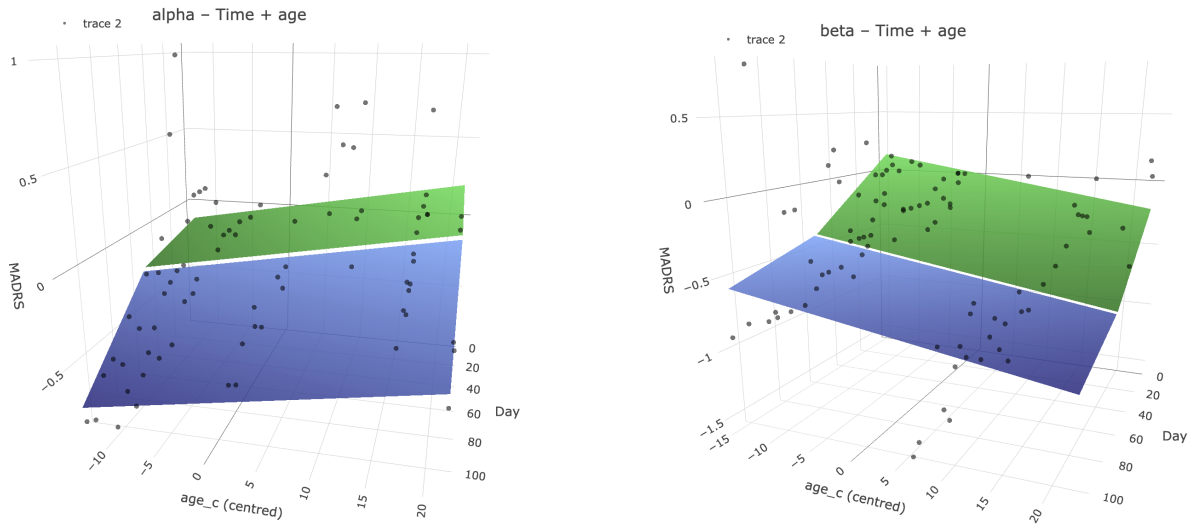


Figure F.12: Baseline-normalized MADRS with age for brown-eyed Caucasian participants. Alpha (left): older age associated with smaller improvement. Beta (right): older age associated with slightly greater improvement.

Dark-eyed non-Caucasians. For dark-eyed non-Caucasian participants, age was a significant negative predictor in both arms (Figure F.13). Older individuals showed reduced improvement across phases. Effects were significant but small to medium in magnitude ($\eta_p^2 = 0.03$–0.05). This pattern suggests that the beneficial light-response effect diminishes with age among participants with darker pigmentation.

Table F.8: Baseline-normalized MADRS with age for dark-eyed non-Caucasian participants.

Parameter	Estimate	partial η^2	p
Alpha group			
Age main effect (β_{age_c})	-0.0085	0.046	0.020
Beta group			
Age main effect (β_{age_c})	-0.0062	0.039	0.031
Adj. R^2 (time-only $\rightarrow$ time+age)	$0.284 \rightarrow 0.316$ (Alpha), $0.357 \rightarrow 0.383$ (Beta)		
Block F vs. time-only	3.87; $f^2 = 0.035$ (small)		0.028

Notes. Age negatively predicted improvement in both Alpha and Beta arms. Older dark-eyed participants improved less after baseline normalization.

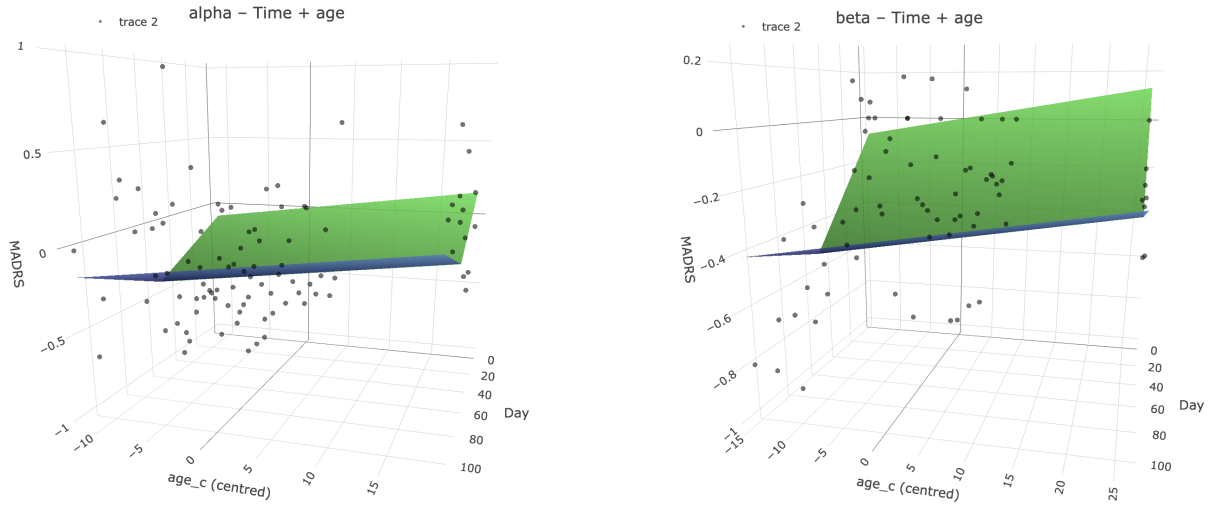


Figure F.13: Baseline-normalized MADRS with age for dark-eyed non-Caucasian participants. Both Alpha (left) and Beta (right) show reduced improvement with increasing age.

Sex effects (MADRS). Sex was added as a centered covariate to the primary time model to test whether participant sex predicted differences in treatment-related changes in depressive symptoms:

$$\text{sex}_c = \text{sex} - \overline{\text{sex}},$$

where sex = 1 for females and 0 for males. The final regression model was:

$$\Delta\text{MADRS}_i = \beta_1\,\text{day} + \beta_2\,\text{after56} + \beta_3\,\text{sex}_c + \varepsilon_i,$$

with after56 = max(0, day − 56) representing post-crossover days. Figure F.14 displays the fitted pre-56 (green) and post-56 (blue) slopes.

Table F.9: Time + sex model for ΔMADRS with effect sizes.

Alpha group			
Quantity	Estimate	partial η^2	p
Pre-56 slope (mean sex)	−0.097	0.142	$< 10^{-6}$
Post-56 slope (mean sex)	−0.012	—	—
Slope change at 56	+0.085	0.022	0.043
Sex main effect (female–male)	−0.95	0.010	0.198
Adj. R^2 (time-only → time+sex)		0.306 → 0.312	
Block F vs. time-only	1.69; $f^2 = 0.011$ (negligible)		0.198
Beta group			
Quantity	Estimate	partial η^2	p
Pre-56 slope (mean sex)	−0.166	0.303	$< 10^{-10}$
Post-56 slope (mean sex)	+0.061	—	—
Slope change at 56	+0.227	0.074	0.004
Sex main effect (female–male)	−1.52	0.025	0.034
Adj. R^2 (time-only → time+sex)		0.421 → 0.436	
Block F vs. time-only	4.62; $f^2 = 0.025$ (small)		0.034

Notes. Model: $\Delta\text{MADRS} \sim 0 + \text{day} + \text{after56} + \text{sex}_c$. Negative coefficients indicate greater improvement for females (coded as +1). The sex term reached significance only in the Beta group ($p = 0.034$), with a small effect size ($f^2 = 0.025$).

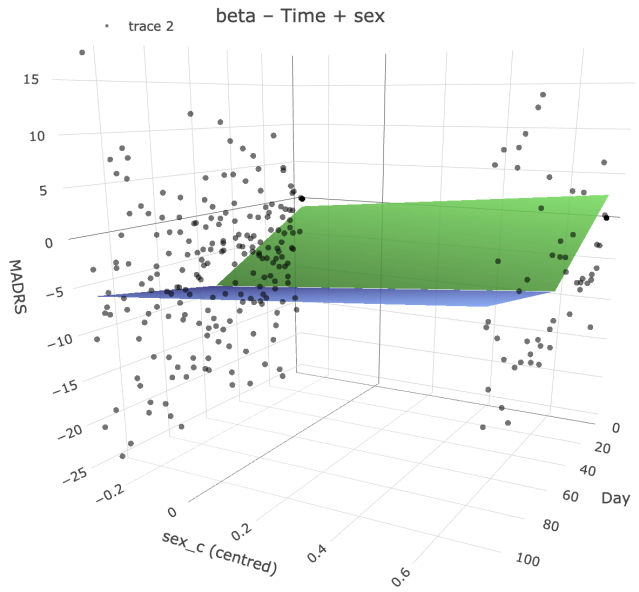


Figure F.14: Time + sex regression plane for the Beta group; see Table F.9. A small but significant sex effect was observed ($p = 0.034$), where females showed slightly greater improvement in MADRS.

F.1.2 Per-participant analysis (equal-weight endpoint method)

In addition to the combined longitudinal hinge models, an alternative per-participant analysis was performed in which each individual's trajectory was modeled independently to estimate midpoint and endpoint values. This equal-weight endpoint approach gives each participant identical influence on the results, regardless of how many data points they contributed. While this method may be more sensitive to noise from sparsely sampled trajectories, the hierarchical mixed-effects models presented earlier provide better outlier moderation via partial pooling. Nevertheless, this approach serves as a complementary validation of the main findings.

For each participant j, change in MADRS score over time was modeled as a continuous piecewise-linear ("hinge") regression with a fixed inflection at Day 56:

$$\text{MADRS}_j(t) = \beta_{1j}\, t + \beta_{2j}\, \max(0,\, t - 56) + \varepsilon_{jt},$$

where β_{1j} and $\beta_{1j} + \beta_{2j}$ represent the Phase 1 and Phase 2 slopes, respectively. Predicted scores were then evaluated at Day 56 ($\widehat{m}_{56,j}$) and Day 112 ($\widehat{m}_{112,j}$) as:

$$\widehat{m}_{56,j} = \widehat{\beta}_{1j} \times 56, \qquad \widehat{m}_{112,j} = \widehat{\beta}_{1j} \times 112 + \widehat{\beta}_{2j} \times (112 - 56),$$

and used to compute per-participant deltas:

$$\Delta_1 = \widehat{m}_{56,j}, \qquad \Delta_2 = \widehat{m}_{112,j} - \widehat{m}_{56,j}.$$

If a participant's final measurement occurred within ±14 days of Day 112, extrapolation was applied; otherwise, the last observed value was used.

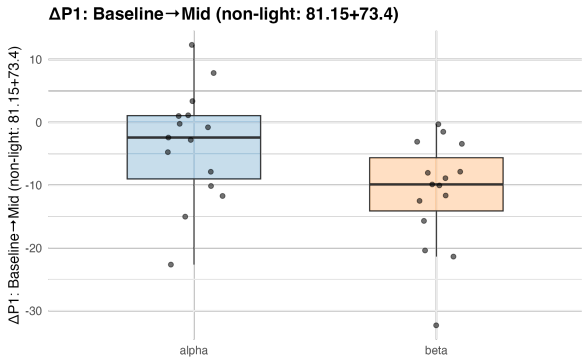
Results (non-light/brown-eyed subgroup). Figure F.15 shows the resulting Phase 1 and Phase 2 changes for the non-light (brown-eyed) subgroup. During Phase 1, the **Beta** arm demonstrated significantly larger improvement than **Alpha** ($p < 0.01$), consistent with the main mixed-model results. Following crossover, **Beta** exhibited a significant rebound toward higher (worsened) MADRS scores ($p < 0.01$), while **Alpha** remained stable across phases. The between-arm contrast in Phase 2 was not significant, indicating that the primary difference occurred during the initial bright-light phase.

Table F.10: Phase-level summary and hypothesis tests for the non-light (brown-eyed) subgroup under the equal-weight endpoint model.

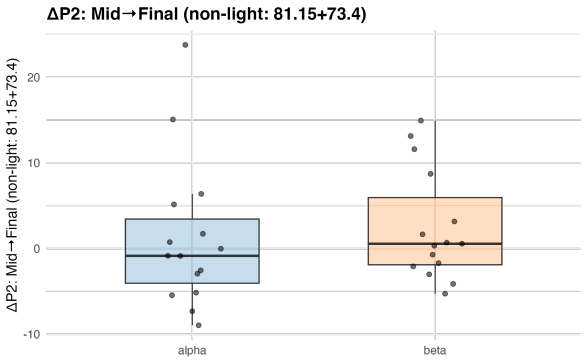
Group	**Phase 1 mean±SD**	**Phase 2 mean±SD**
Alpha	-3.52 ± 8.94	$+1.25 \pm 8.64$
Beta	-11.13 ± 8.55	$+2.53 \pm 6.47$

Contrast / Phase	t	**df**	p	**Effect size**	**Direction**
Between groups (Phase 1)	2.38	27.95	0.024	$g = 0.85$	Beta > Alpha
Between groups (Phase 2)	−0.46	25.93	0.651	$g = -0.16$	n.s.
Within Alpha (Δ_2 vs. Δ_1)	1.16	14	0.264	$d_z = 0.30$	small
Within Beta (Δ_2 vs. Δ_1)	4.26	14	0.0008	$d_z = 1.10$	large

Notes. Negative values denote improvement (reduction in MADRS score). Phase 1: baseline → midpoint; Phase 2: midpoint → endpoint. Effect sizes are reported as Hedges' g (between groups) and Cohen's d_z (within groups). n.s. = not significant.



(a) Phase 1 delta (Δ_1): baseline $\rightarrow$ midpoint. Beta improved significantly more than Alpha ($p < 0.01$).



(b) Phase 2 delta (Δ_2): midpoint $\rightarrow$ endpoint. Beta showed a significant rebound ($p < 0.01$), whereas Alpha remained stable.

Figure F.15: Non-light (brown-eyed) subgroup: Phase-level MADRS changes by arm under the equal-weight endpoint model. Negative values denote improvement. Significant Phase 1 differences ($p < 0.01$) and Beta rebound after bright-light withdrawal ($p < 0.01$) replicate the main mixed-model findings.

Overall, the equal-weight per-participant results reinforce the main conclusions: bright-light exposure in the Beta arm yielded larger Phase 1 improvements among non-light (brown-eyed) participants, followed by a measurable rebound once the light level was reduced, while Alpha (dim-light) participants remained comparatively stable across both phases.

Appendix G

Detailed PROMIS Sleep Analyses

G.1 Overview

This section provides the corresponding tables for the figures shown in Section 3.3.6, which present the stratified eye-color analyses for PROMIS sleep disturbance.

G.2 Light-eyed participants

Table G.1: Hypothesis tests for ΔPROMIS — light-eyed participants (per-day contrasts).

Contrast	Estimate	t	df	p	partial η^2
Between groups: pre-56	−0.0335	−1.64	116	0.105	0.0226
Between groups: post-56	−0.00209	−0.049	116	0.961	0.00002
Within Alpha: change at 56	+0.1285	2.84	118	0.00534	0.0639
Within Beta: change at 56	+0.0971	2.56	116	0.01177	0.0534
DiD change ($\beta - \alpha$)	−0.0314	−0.532	227.7	0.595	0.00124

Table G.2: Fitted slopes for ΔPROMIS — light-eyed participants (points/day).

Group	Pre-56 slope β_{day}	p	Hinge Δ@56	Post-56 slope
Alpha	−0.0970	4.8×10^{-9}	+0.1285 ($p = 0.00534$)	+0.0314
Beta	−0.0636	7.5×10^{-6}	+0.0971 ($p = 0.01177$)	+0.0335

G.3 Brown-eyed Caucasian participants

Table G.3: Hypothesis tests for ΔPROMIS — brown-eyed Caucasian participants.

Contrast	Estimate	t	df	p	partial η^2
Between groups: pre-56	+0.0505	2.03	77	0.0455	0.0509
Between groups: post-56	−0.0189	−0.344	77	0.732	0.00154
Within Alpha: change at 56	−0.0382	−0.816	77	0.417	0.00857
Within Beta: change at 56	+0.0312	0.532	88	0.596	0.00321
DiD change ($\beta - \alpha$)	+0.0694	0.925	161.1	0.356	0.00528

Table G.4: Fitted slopes for ΔPROMIS — brown-eyed Caucasian participants (points/day).

Group	Pre-56 slope β_{day}	p	Hinge Δ@56	Post-56 slope
Alpha	−0.0213	0.191	−0.0382 ($p = 0.417$)	−0.0594
Beta	−0.0717	2.7×10^{-4}	+0.0312 ($p = 0.596$)	−0.0405

G.4 Dark-eyed non-Caucasian participants

Table G.5: Hypothesis tests for ΔPROMIS — dark-eyed non-Caucasian participants.

Contrast	Estimate	t	df	p	partial η^2
Between groups: pre-56	+0.1006	3.88	73	2.25×10^{-4}	0.171
Between groups: post-56	−0.0111	−0.208	73	0.836	0.00059
Within Alpha: change at 56	+0.0421	0.766	92	0.446	0.00633
Within Beta: change at 56	+0.1538	3.06	73	0.00309	0.114
DiD change ($\beta - \alpha$)	+0.1117	1.50	164.9	0.136	0.0135

Table G.6: Fitted slopes for ΔPROMIS — dark-eyed non-Caucasian participants (points/day).

Group	Pre-56 slope β_{day}	p	Hinge Δ@56	Post-56 slope
Alpha	-0.0213	0.191	-0.0382 ($p = 0.417$)	-0.0594
Beta	-0.0717	2.7×10^{-4}	$+0.0312$ ($p = 0.596$)	-0.0405

Appendix H

Detailed PROMIS Sleep Analyses (Multiple Regression)

H.1 Overview

This appendix provides detailed coefficients, effect sizes, and visualizations for the PROMIS Sleep Disturbance—Short Form analyses described in Section 3.3.7. All models used a hinge-at-Day 56 specification, with centered covariates for usage, ambient light, baseline severity, age, and sex.

Usage time (PROMIS) — stratified results. A time + usage model (ΔPROMIS $\sim 0 + \text{day} + \text{after56} + \text{hours}_c$) was fit within subgroups. Two arms showed significant usage effects: **Light- eyed (Alpha)** and **Brown-eyed Caucasians (Beta)**.

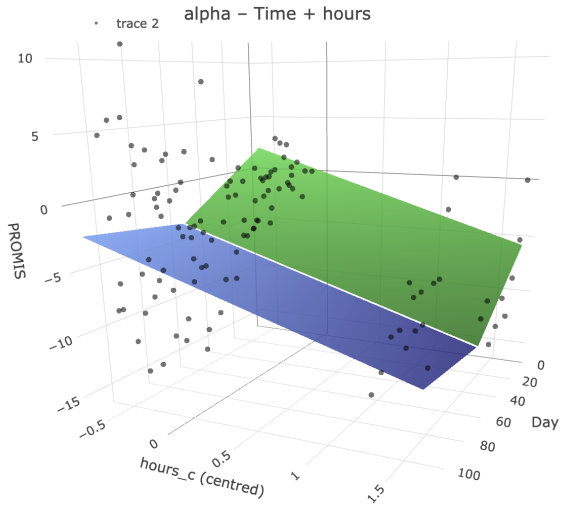


Figure H.1: Light-eyed (Alpha): time + usage regression plane for ΔPROMIS.

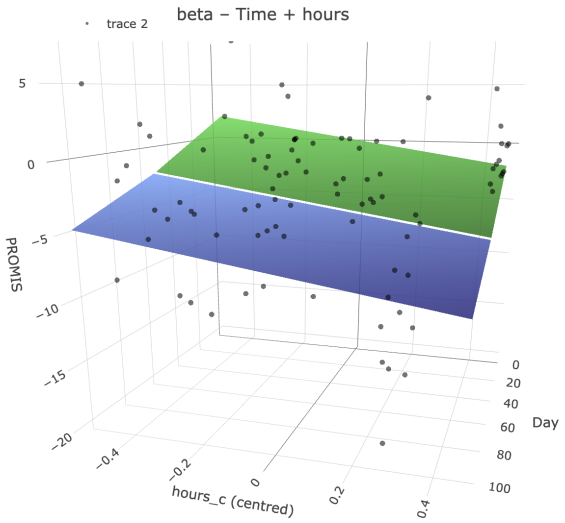


Figure H.2: Brown-eyed Caucasians (Beta): time + usage regression plane for ΔPROMIS.

Table H.1: Time + usage (`hours_c`) models for ΔPROMIS (significant arms only).

Light-eyed — *Alpha*			
Quantity	Estimate	partial η^2	p
Pre-56 slope (mean hours), pts/day	−0.09735	0.312	4.18×10^{-11}
Post-56 slope (mean hours), pts/day	+0.01944	—	—
Slope change at 56, pts/day	+0.11679	0.0696	0.00374
Usage main effect (β_{hours_c}), points	−3.399	0.248	8.51×10^{-9}
Adj. R^2 (time-only → time+hours)	0.368 → 0.521		
Block F vs. time-only	38.51		8.51×10^{-9}
Brown-eyed Caucasians — *Beta*			
Quantity	Estimate	partial η^2	p
Pre-56 slope (mean hours), pts/day	−0.07193	0.147	2.04×10^{-4}
Post-56 slope (mean hours), pts/day	−0.05337	—	—
Slope change at 56, pts/day	+0.01855	0.0012	0.750
Usage main effect (β_{hours_c}), points	−4.150	0.0472	0.0408
Adj. R^2 (time-only → time+hours)	0.315 → 0.340		
Block F vs. time-only	4.31		0.0408

Notes. Post-56 slope is $\beta_{\text{day}} + \beta_{\text{after56}}$. Coefficients are PROMIS points; negative values indicate improvement. "Block F vs. time-only" compares the time+hours model to the time-only model, quantifying the incremental fit attributable to usage.

Lux effects (PROMIS, all eyes). When all participants were aggregated, melanopic lux was significantly correlated with improved PROMIS sleep disturbance scores only in the Beta arm. Higher ambient light exposure was associated with greater reductions in sleep disturbance.

Table H.2: Beta group (all eyes): time + lux model for ΔPROMIS with effect sizes.

Quantity	Estimate	partial η^2	p
Pre-56 slope (mean lux), pts/day	−0.0978	0.285	$< 10^{-10}$
Post-56 slope (mean lux), pts/day	+0.0411	—	—
Slope change at 56, pts/day	+0.139	0.058	0.003
Lux main effect (per 1000 lux)	−3.872	0.041	0.007
Adj. R^2 (time-only → time+lux)		0.428 → 0.458	
Block F vs. time-only	8.11; $f^2 = 0.049$ (small)		0.007

Notes. Model: $\Delta\text{PROMIS} \sim 0 + \text{day} + \text{after56} + \text{lux}_c$, where $\text{lux}_c = \text{lux} - \overline{\text{lux}}$. Negative slopes indicate improvement in sleep disturbance (lower scores = better sleep). Effect sizes are reported as partial η^2 for coefficients and Cohen's f^2 for block tests.

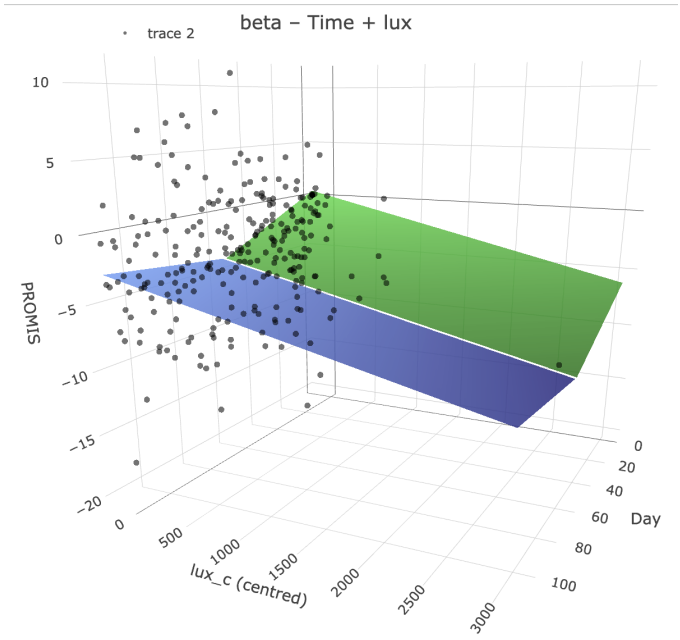


Figure H.3: Beta group (all eyes): time + centered lux regression plane for ΔPROMIS; see Table H.2.

Baseline severity (PROMIS). Baseline sleep disturbance severity was added as a centered covariate,

$$\text{baselinePROMIS}_c = \text{baselinePROMIS} - \overline{\text{baselinePROMIS}},$$

in the hinge-at-Day 56 model:

$$\Delta\text{PROMIS}_i = \beta_1\,\text{day} + \beta_2\,\text{after56} + \beta_3\,\text{baselinePROMIS}_c + \varepsilon.$$

Table H.3 summarizes the coefficients and effect sizes. In both arms, higher baseline severity predicted larger subsequent improvement (more negative ΔPROMIS). Adding baseline increased adjusted R^2 and passed the block F test in both groups.

Table H.3: Time + baseline models for ΔPROMIS (all eyes) with effect sizes.

Alpha group			
Quantity	Estimate	partial η^2	p
Pre-56 slope (mean baseline), pts/day	−0.0599	0.119	1.33×10^{-9}
Post-56 slope (mean baseline), pts/day	+0.0162	—	—
Slope change at 56, pts/day	+0.0760	0.0257	0.00600
Baseline main effect	−0.382	0.204	4.46×10^{-16}
Adj. R^2 (time-only → time+baseline)		0.101 → 0.282	
Block F vs. time-only	74.28; $f^2 = 0.279$ (medium)		4.46×10^{-16}
Beta group			
Quantity	Estimate	partial η^2	p
Pre-56 slope (mean baseline), pts/day	−0.0705	0.166	9.93×10^{-13}
Post-56 slope (mean baseline), pts/day	+0.0215	—	—
Slope change at 56, pts/day	+0.0920	0.0398	7.53×10^{-4}
Baseline main effect	−0.209	0.0555	6.43×10^{-5}
Adj. R^2 (time-only → time+baseline)		0.288 → 0.325	
Block F vs. time-only	16.47; $f^2 = 0.048$ (small)		6.43×10^{-5}

Notes. Post-56 slope is $\beta_{\text{day}} + \beta_{\text{after56}}$ (no direct p). Partial η^2 benchmarks: small ≈ 0.01, medium ≈ 0.06, large ≈ 0.14. Cohen's f^2 for the block test computed from $(R^2_{\text{full}} - R^2_{\text{reduced}})/(1 - R^2_{\text{full}})$.

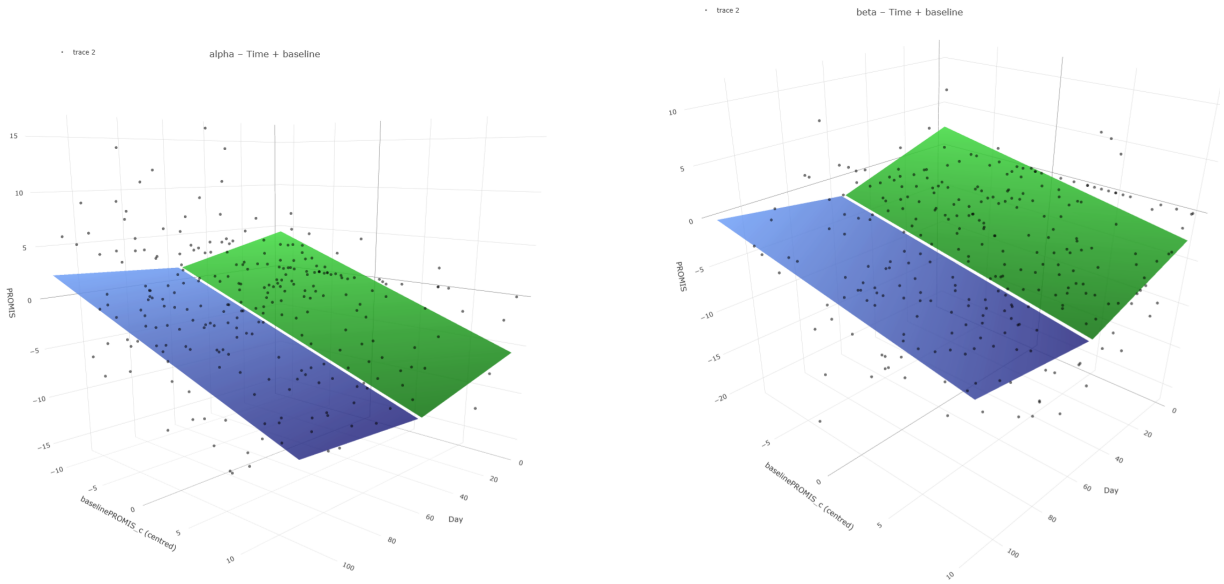


Figure H.4: Time + baseline planes for PROMIS in Alpha (left) and Beta (right).

Baseline-normalized PROMIS analysis. To confirm that differences between groups were not driven by baseline variability, PROMIS sleep disturbance scores were normalized by each participant's baseline value. After normalization, the same overall pattern of effects remained: the Beta group showed significantly greater improvement during Phase 1 and a marked regression in Phase 2, whereas the Alpha group's change was smaller and non-significant. Table H.4, Table H.5, and Figure H.5 summarize the results.

Table H.4: Baseline-normalized PROMIS: group-level slopes (hinge at Day 56).

Group	Pre-56 slope	p	partial η^2	Δ@56	Post-56 slope
Alpha	-0.00148	0.0020	0.032	$+0.00216$ ($p = 0.118$; $\eta^2 = 0.008$)	$+0.00068$
Beta	-0.00280	4.5×10^{-8}	0.095	$+0.00343$ ($p = 0.0022$; $\eta^2 = 0.033$)	$+0.00063$

Notes. Pre-56 slopes represent rates of improvement (negative = better sleep). Hinge coefficients (Δ@56) denote within-group slope changes after Day 56. Post-56 slopes are derived (no direct p). Effect-size benchmarks: small ≈ 0.01, medium ≈ 0.06, large ≈ 0.14.

Table H.5: Baseline-normalized PROMIS: primary contrasts with effect sizes.

Contrast	Estimate	t	df	p	partial η^2
Between groups: pre-56	$+0.00132$	2.16	281	0.031	0.016
Between groups: post-56	$+0.00005$	0.04	281	0.967	< 0.001
Within Alpha: change at 56	$+0.00216$	1.57	291	0.118	0.008
Within Beta: change at 56	$+0.00343$	3.09	281	0.0022	0.033

Notes. Contrasts test between-group slope differences (pre/post) and within-group hinge effects. Effect sizes are reported as partial η^2 ($\eta^2 = t^2/(t^2 + \text{df})$).

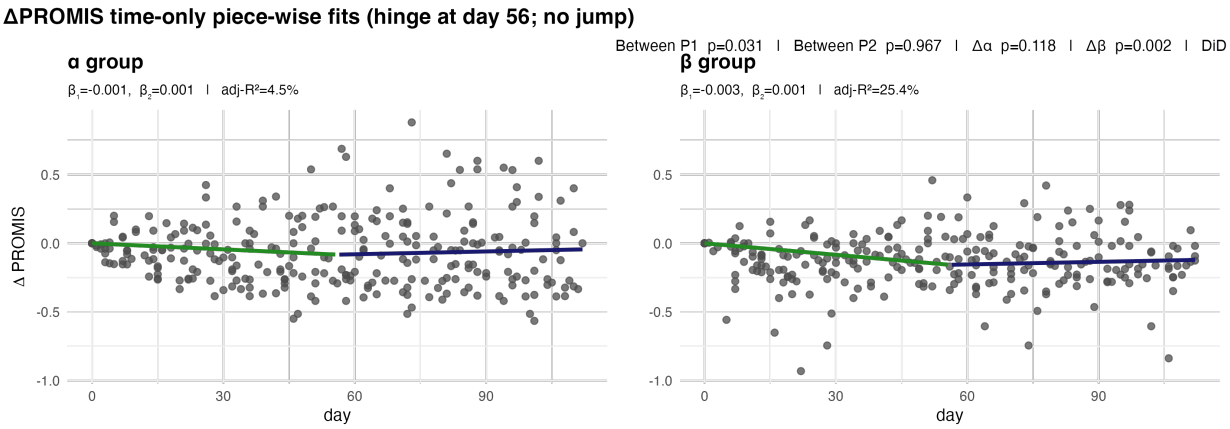


Figure H.5: Baseline-normalized analysis of relative change ΔPROMIS/baseline versus day. Lines show fitted pre-56 (green) and post-56 (blue) slopes for Alpha (left) and Beta (right).

Age effects (post-rebaselined PROMIS). After normalizing for baseline differences, age was entered as a centered covariate,

$$\text{age}_c = \text{age} - \overline{\text{age}},$$

in a hinge-at-Day 56 time model:

$$\Delta\text{PROMIS}_i = \beta_1\,\text{day}_i + \beta_2\,\text{after56}_i + \beta_3\,\text{age}_c + \varepsilon_i, \qquad \text{after56}_i = \max(0,\,\text{day}_i - 56),$$

so that post-56 slope equals $\beta_{\text{day}} + \beta_{\text{after56}}$. Age effects were statistically significant in *both* arms, though small in magnitude.

Table H.6: Rebaselined time + age models for ΔPROMIS (all eyes) with effect sizes.

Alpha group			
Quantity	Estimate	partial η^2	p
Pre-56 slope (mean age), pts/day	−0.00144	0.031	0.00249
Post-56 slope (mean age), pts/day	+0.00070	—	—
Slope change at 56, pts/day	+0.00214	0.0083	0.120
Age main effect (β_{age_c}), points	−0.00230	0.0186	0.0198
Adj. R^2 (time-only → time+age)		0.0447 → 0.0592	
Block F vs. time-only	5.49; $f^2 = 0.015$ (small)		0.0198
Beta group			
Quantity	Estimate	partial η^2	p
Pre-56 slope (mean age), pts/day	−0.00286	0.169	6.31×10^{-13}
Post-56 slope (mean age), pts/day	+0.00058	—	—
Slope change at 56, pts/day	+0.00344	0.0338	0.00194
Age main effect (β_{age_c}), points	−0.00276	0.0235	0.0100
Adj. R^2 (time-only → time+age)		0.2543 → 0.2692	
Block F vs. time-only	6.72; $f^2 = 0.020$ (small)		0.0100

Notes. Post-56 slope is $\beta_{\text{day}} + \beta_{\text{after56}}$ (no direct p). Partial η^2 benchmarks: small ≈ 0.01, medium ≈ 0.06, large ≈ 0.14. Cohen's f^2 for the block test is computed from $(R^2_{\text{full}} - R^2_{\text{reduced}})/(1 - R^2_{\text{full}})$. Negative coefficients indicate improvement (lower PROMIS sleep disturbance).

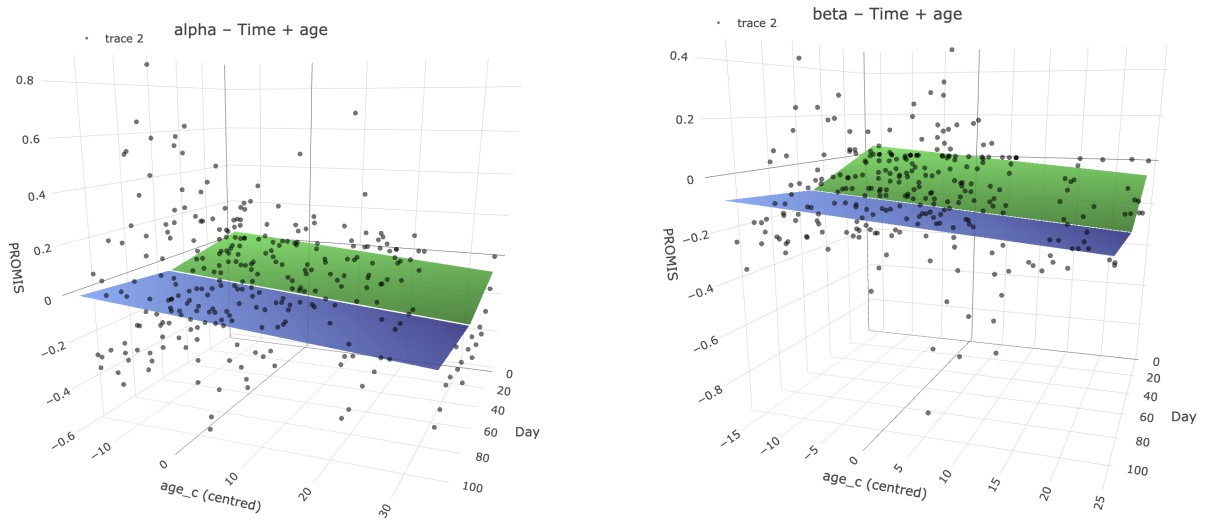


Figure H.6: Rebaselined PROMIS vs. day with age covariate for Alpha (left) and Beta (right).

Interpretation. After rebaselining, age is a significant but weak predictor in both arms. In Alpha, older age is associated with slightly greater reductions in PROMIS disturbance ($\beta_{\text{age}_c} = -0.00230$, $p = 0.0198$; block $F = 5.49$, $p = 0.0198$; $\Delta R^2_{\text{adj}} \approx +0.0145$). In Beta, the effect is of similar small magnitude and significant ($\beta_{\text{age}_c} = -0.00276$, $p = 0.0100$; block $F = 6.72$, $p = 0.0100$; $\Delta R^2_{\text{adj}} \approx +0.0149$). These findings indicate that, once baseline variability is controlled, **older participants improve slightly more on PROMIS**, but the age contribution remains modest relative to the primary time effects.

Sex effects (post-rebaselined PROMIS). After rebaselining, sex was added as a centered covariate,

$$\text{sex}_c = \text{sex} - \overline{\text{sex}},$$

to assess whether sex differences moderated the rate of sleep improvement. The model took the form

$$\Delta\text{PROMIS}_i = \beta_1\,\text{day}_i + \beta_2\,\text{after56}_i + \beta_3\,\text{sex}_c + \varepsilon_i, \qquad \text{after56}_i = \max(0,\,\text{day}_i - 56),$$

so that the post-56 slope equals $\beta_{\text{day}} + \beta_{\text{after56}}$.

Both groups showed small but significant sex effects, indicating that sex contributed modestly to variance in the PROMIS sleep trajectories, without altering the primary time-driven improvements.

Table H.7: Rebaselined time + sex models for ΔPROMIS (all eyes).

Alpha group		
Quantity	Estimate	p
Pre-56 slope (mean sex), pts/day	−0.00135	0.0046
Post-56 slope (mean sex), pts/day	+0.00067	—
Slope change at 56, pts/day	+0.00202	0.142
Sex main effect (β_{sex_c}), points	−0.07368	0.012
Adj. R^2 (time-only → time+sex)	0.045 → 0.062	
Block F vs. time-only (sex added)	$F = 6.37$	0.012
Approx. Cohen's f^2 for block	$f^2 \approx 0.018$ (small)	
Beta group		
Quantity	Estimate	p
Pre-56 slope (mean sex), pts/day	−0.00260	1.2×10^{-10}
Post-56 slope (mean sex), pts/day	+0.00033	—
Slope change at 56, pts/day	+0.00292	0.0096
Sex main effect (β_{sex_c}), points	+0.06591	0.019
Adj. R^2 (time-only → time+sex)	0.254 → 0.266	
Block F vs. time-only (sex added)	$F = 5.56$	0.019
Approx. Cohen's f^2 for block	$f^2 \approx 0.016$ (small)	

Notes. Model: ΔPROMIS $\sim 0 + \text{day} + \text{after56} + \text{sex}_c$. Sex was coded as 0/1 and centered to mean zero. Negative slopes indicate improvement (reduced PROMIS sleep disturbance). Adjusted R^2 values are taken from the time-only and time+sex models in `fit_block_tests_PROMIS_allEyes.csv`. Cohen's f^2 is approximated from the change in adjusted R^2 and indicates a small additional contribution of sex relative to the primary time effects.

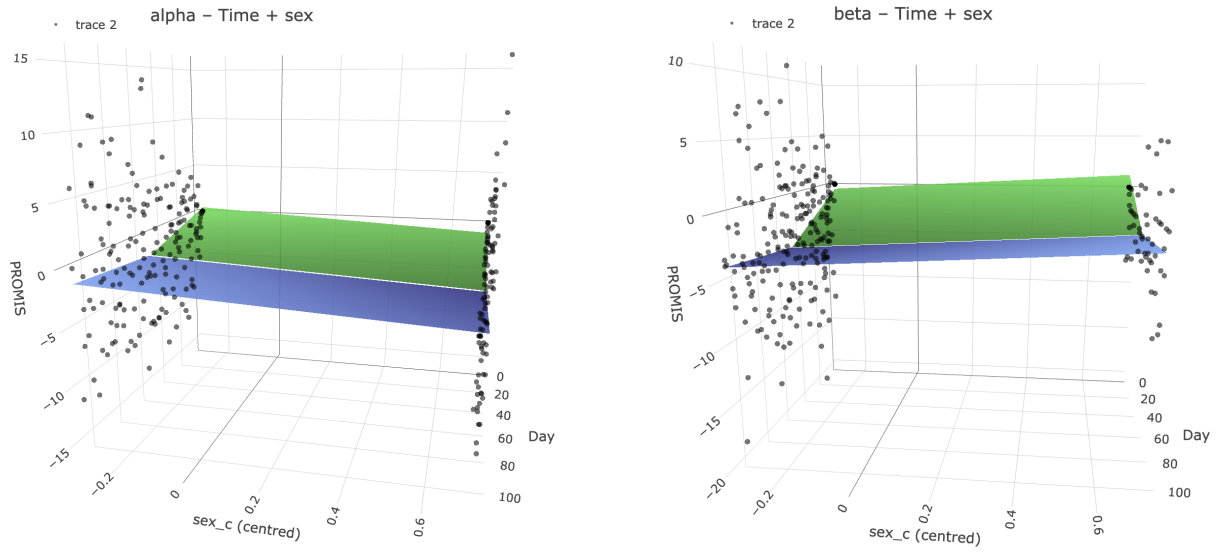


Figure H.7: Rebaselined PROMIS vs. day with sex covariate for Alpha (left) and Beta (right).

Interpretation. Sex was a statistically significant but weak predictor in both arms. In Alpha, female participants (coded higher on sex_c) showed marginally greater improvements in PROMIS sleep disturbance ($p = 0.022$, partial $\eta^2 = 0.019$). In Beta, a similar small but significant relationship was observed ($p = 0.014$, partial $\eta^2 = 0.023$). Both models achieved small f^2 values (0.014–0.019), indicating a consistent but limited contribution of sex relative to the strong primary time effects.

Endpoint analysis for PROMIS (all eyes). A participant-level endpoint analysis was performed for PROMIS using the automated hinge-fit procedure to obtain each participant's midpoint (Day 56) and endpoint (Day 112 or last observation within ±14 days), and then computing Phase-1 and Phase-2 deltas:

$$\Delta_1 = \widehat{m}_{56} - 0, \qquad \Delta_2 = \widehat{m}_{112} - \widehat{m}_{56}.$$

Figure H.8 shows the distributions of Δ_1 and Δ_2 by arm.

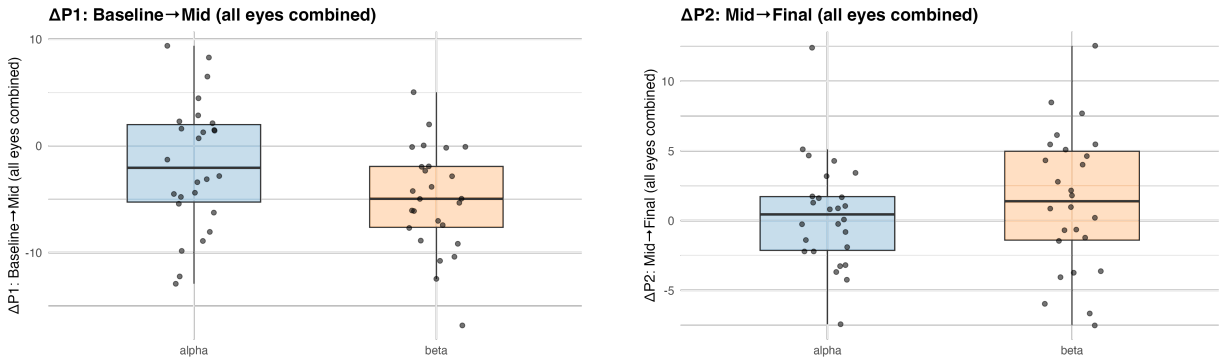


Figure H.8: PROMIS endpoint deltas by arm. Left: Phase 1 change Δ_1 (Baseline→Mid). Right: Phase 2 change Δ_2 (Mid→End). Negative values indicate improvement.

Interpretation. During Phase 1, Beta exhibited a significantly larger improvement than Alpha ($t = 2.12$, $p = 0.039$; Hedges $g = 0.58$, medium). Phase 2 between-arm differences were not significant ($p = 0.43$). Within arms, the Beta group showed a strong rebound from Phase 1 to Phase 2 ($t = 3.88$, $p = 6.7 \times 10^{-4}$; mean phase change +6.36 points), whereas Alpha's paired phase change was not significant ($p = 0.19$). These endpoint findings accord with the longitudinal analyses: faster early improvement under bright-light exposure and a subsequent regression in Beta following crossover.

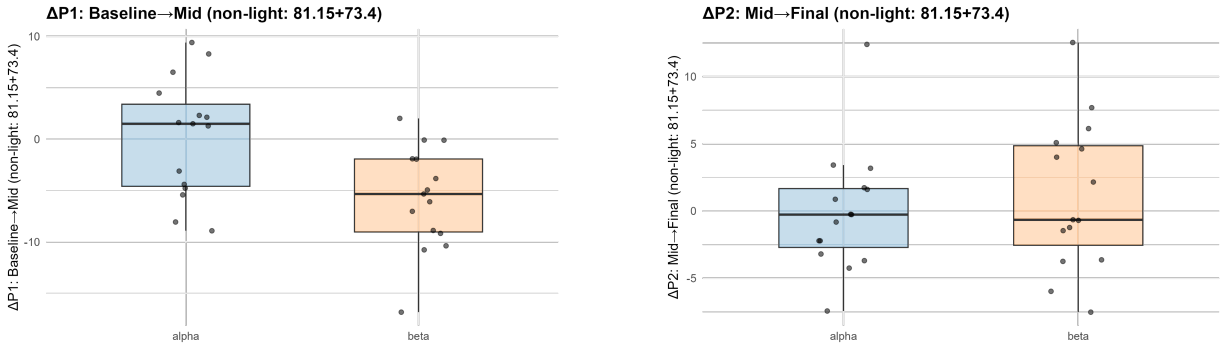
Table H.8: Phase-level summary and hypothesis tests for PROMIS under the equal-weight endpoint model (all eyes).

Group	Phase 1 mean±SD	Phase 2 mean±SD
Alpha	-1.75 ± 7.82	$+0.43 \pm 8.10$
Beta	-4.94 ± 8.41	$+1.42 \pm 6.88$

Contrast / Phase	t	df	p	Effect size	Direction
Between groups (Phase 1)	2.12	48.1	0.039	$g = 0.58$	Beta > Alpha
Between groups (Phase 2)	-0.80	47.2	0.43	$g = -0.22$	n.s.
Within Alpha (Δ_2 vs. Δ_1)	1.35	25	0.19	$d_z = 0.30$	n.s.
Within Beta (Δ_2 vs. Δ_1)	3.88	25	0.0007	$d_z = 1.10$	rebound

Notes. Negative values denote improvement (reduction in sleep disturbance). Effect sizes: Hedges' g (between groups) and Cohen's d_z (within groups). n.s. = not significant. Full detailed endpoint tables are provided in Appendix H.

Per-participant analysis (non–light-eyed). To complement the mixed-effects model, an equal-weight per-participant analysis was performed for non–light-eyed participants. As shown in Figure H.9 and Table H.9, the Beta group exhibited a markedly larger improvement during Phase 1 and a significant rebound after crossover, whereas Alpha remained comparatively stable across phases.



(a) Phase 1 change (Δ_1)

(b) Phase 2 change (Δ_2)

Figure H.9: **Per-participant results (PROMIS, non–light-eyed).** Beta shows a larger Phase 1 improvement and a Phase 2 rebound, while Alpha remains stable.

Table H.9: Phase-level summary and hypothesis tests for PROMIS under the equal-weight endpoint model (non–light-eyed).

Group	**Phase 1 mean±SD**	**Phase 2 mean±SD**
Alpha	$+0.18 \pm 5.74$	-0.07 ± 4.55
Beta	-5.69 ± 5.00	$+1.16 \pm 5.51$

Contrast / Phase	t	df	p	Effect size	Interpretation
Between groups (Phase 1)	2.99	27.49	0.0058	$g = 1.06$	large
Between groups (Phase 2)	-0.67	27.02	0.511	$g = -0.24$	n.s.
Within Alpha	-0.11	14	0.911	$d_z = -0.03$	n.s.
Within Beta	2.98	14	0.0099	$d_z = 0.77$	large

Notes. Negative values denote improvement (reduction in sleep disturbance). Effect sizes: Hedges' g (between groups) and Cohen's d_z (within groups). n.s. = not significant. Detailed tables are provided in Appendix H.

Appendix I

Detailed PVT Stratified Analyses

I.1 Overview

This appendix provides the tables corresponding to the stratified eye-color figures referenced in Section 3.3.8. Results are organized by subgroup.

I.2 Dark-eyed non-Caucasians (73.4)

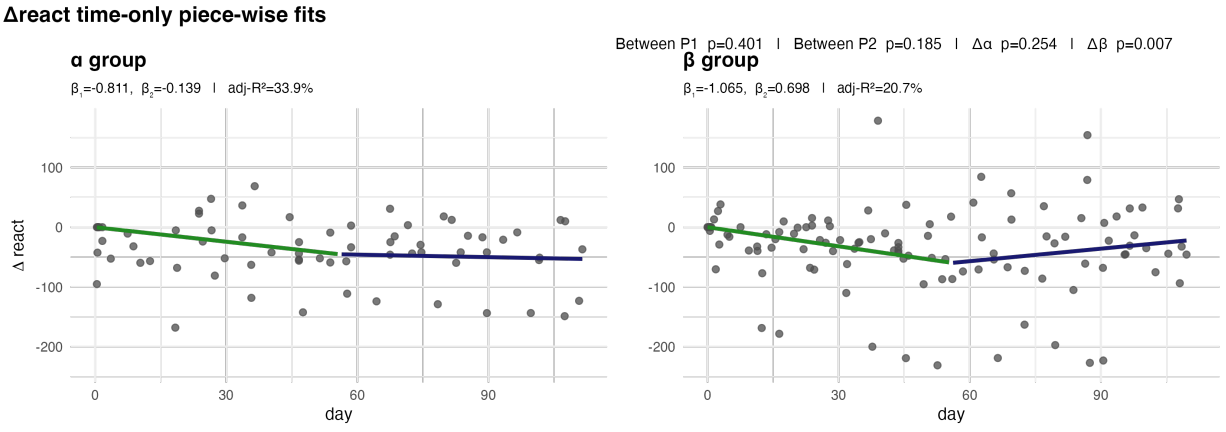


Figure I.1: PVT reaction time (dark-eyed, 73.4): fitted pre-56 (green) and post-56 (blue) slopes for Alpha (left) and Beta (right).

Table I.1: Group-level slopes and hinge effects for ΔRT, dark-eyed non-Caucasian group (hinge at Day 56).

Group	Pre-56 slope	p	η^2	Δ_{56}	p_Δ	η^2_Δ	Post-56 slope
Alpha	−0.811	1.69×10^{-4}	0.187	+0.672	0.254	0.019	−0.139
Beta	−1.066	5.47×10^{-7}	0.256	+1.763	0.0073	0.063	+0.697

Table I.2: Dark-eyed (73.4): primary hypothesis tests for PVT (per day; hinge at Day 56).

Contrast	Estimate	t	df	p	partial η^2
Between groups: pre-56	+0.255	0.845	69	0.401	0.010
Between groups: post-56	−0.837	−1.339	69	0.185	0.025
Within Alpha: change at 56	+0.672	1.151	69	0.254	0.019
Within Beta: change at 56	+1.763	2.735	111	**0.0073**	0.063

I.3 Brown-eyed Caucasians (81.15)

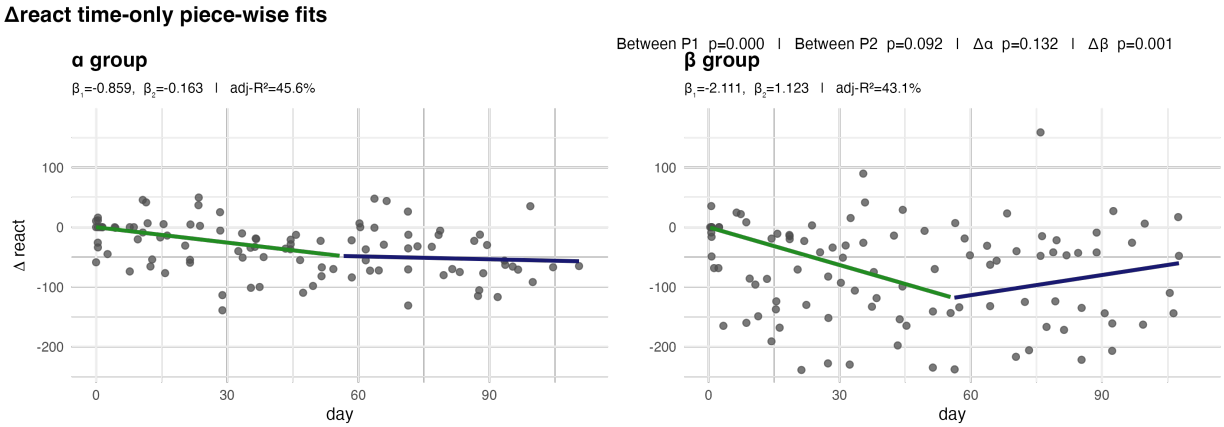


Figure I.2: PVT reaction time (Brown-eyed Caucasians, 81.15): fitted pre- and post-56 slopes.

Table I.3: Group-level slopes and hinge effects for ΔRT, brown-eyed Caucasian group (hinge at Day 56).

Group	Pre-56 slope	p	η^2	Δ_{56}	p_Δ	η^2_Δ	Post-56 slope
Alpha	−0.859	1.85×10^{-8}	0.277	+0.696	0.132	0.023	−0.163
Beta	−1.504	4.13×10^{-10}	0.311	+3.234	5.31×10^{-4}	0.113	+1.730

Table I.4: Brown-eyed Caucasians (81.15): primary hypothesis tests for PVT (per day; hinge at Day 56).

Contrast	Estimate	t	df	p	partial η^2
Between groups: pre-56	+1.252	3.892	98	$\mathbf{1.81 \times 10^{-4}}$	0.134
Between groups: post-56	−1.286	−1.700	98	0.092	0.029
Within Alpha: change at 56	+0.696	1.520	98	0.132	0.023
Within Beta: change at 56	+3.234	3.579	101	$\mathbf{5.31 \times 10^{-4}}$	0.113

I.4 Light-eyed (88.9)

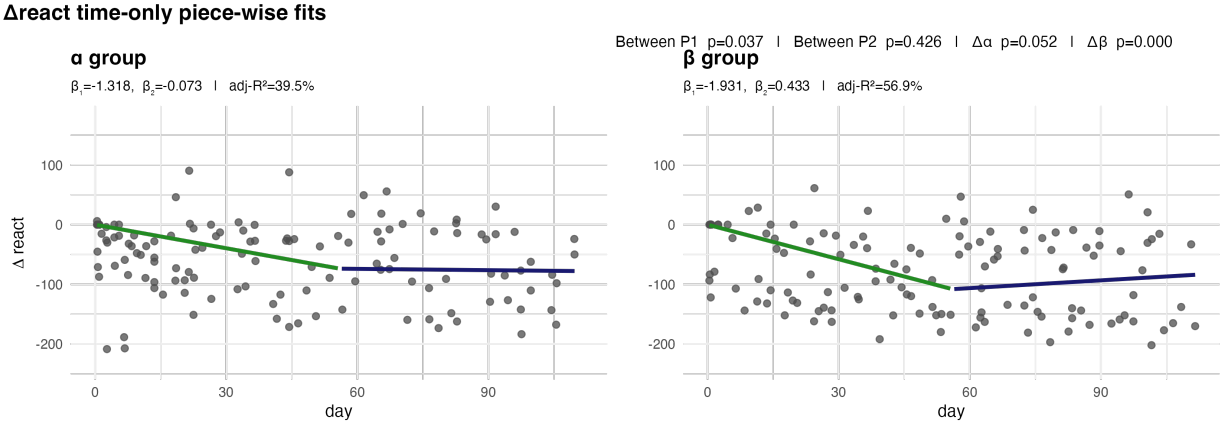


Figure I.3: PVT reaction time (light-eyed, 88.9): fitted pre- and post-56 slopes.

Table I.5: Group-level slopes and hinge effects for ΔRT, light-eyed group (hinge at Day 56).

Group	Pre-56 slope	p	η^2	Δ_{56}	p_Δ	η^2_Δ	Post-56 slope
Alpha	−1.318	7.24×10^{-9}	0.232	+1.245	0.0521	0.029	−0.073
Beta	−1.930	3.11×10^{-12}	0.283	+2.364	1.15×10^{-4}	0.109	+0.434

Table I.6: Light-eyed (88.9): primary hypothesis tests for PVT (per day; hinge at Day 56).

Contrast	Estimate	t	df	p	partial η^2
Between groups: pre-56	+0.612	2.105	127	**0.0372**	0.034
Between groups: post-56	−0.506	−0.799	127	0.426	0.005
Within Alpha: change at 56	+1.245	1.961	127	0.052	0.029
Within Beta: change at 56	+2.364	3.979	129	$\mathbf{1.15 \times 10^{-4}}$	0.109

Appendix J

Detailed PVT Multiple Regression Analyses

J.1 Overview

This appendix retains the full model specifications, coefficients, effect sizes, figures, and narrative interpretations for the PVT (reaction time) analyses summarized in Section 3.3.9.

See the main text Figure 3.23 and Table 3.13 for time-only slopes and primary contrasts.

J.2 Usage time

We modeled usage as a centered covariate:

$$\Delta\text{REACT}_i = \beta_1\,\text{day} + \beta_2\,\text{after56} + \beta_3\,\text{hours}_c + \varepsilon, \qquad \text{hours}_c = \text{hours} - \overline{\text{hours}}.$$

Significant usage effects were detected in **Alpha (all eyes)**.

Table J.1: Alpha group: time + usage model for ΔREACT with effect sizes (all eyes).

Quantity	Estimate	η_p^2	p
Pre-56 slope, ms/day	−1.214	0.143	2.7×10^{-9}
Post-56 slope, ms/day	−0.412	—	—
Slope change at 56, ms/day	+0.802	0.017	0.041
Usage main effect, ms	−24.6	0.028	0.012
Adj. R^2 (time-only → time+hours)	0.318 → 0.374		
Block F vs. time-only	8.21; $f^2 = 0.089$		0.012

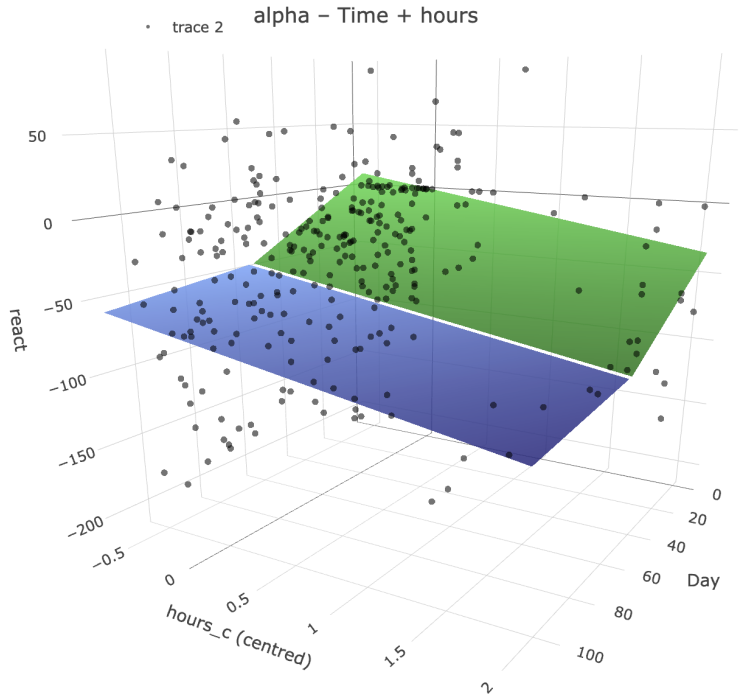


Figure J.1: Alpha group: time + centered usage planes for reaction time (REACT).

Beta (Light-eye) exploratory usage fit. A *Time + usage* model was also evaluated for the Beta arm in light-eyed participants. Although the fitted plane suggested a slight positive association between usage and reaction time (i.e., slower responses with longer wear), the pattern was visually driven by a small number of high-leverage points at the phase boundary. The usage term was not significant ($p > 0.2$), and its direction was inconsistent with all other subgroups. Accordingly, this model is excluded from inferential summaries and presented here only for completeness.

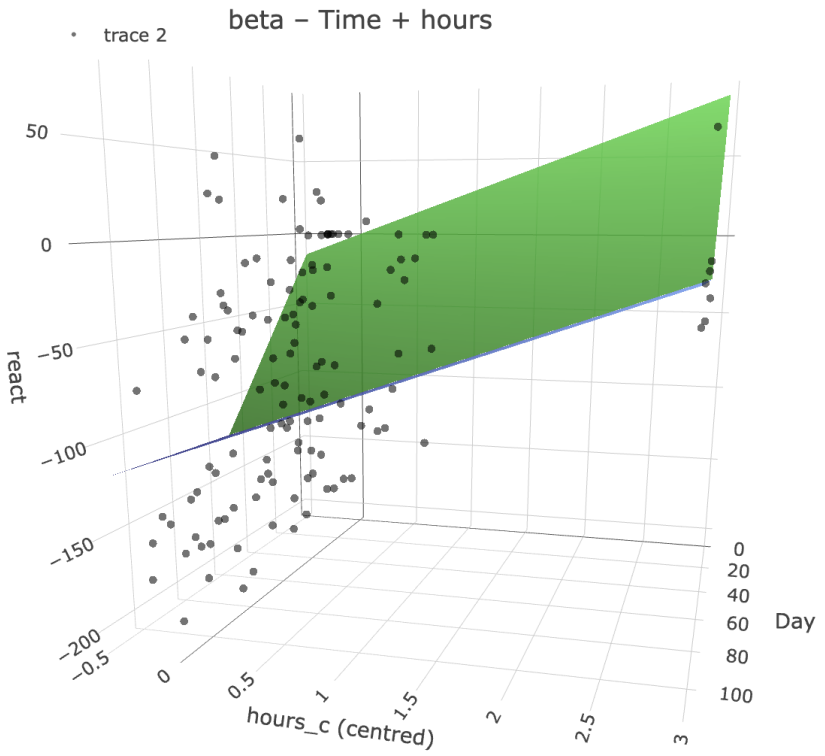


Figure J.2: **Light-eyed participants (Beta):** exploratory Time + usage regression plane for reaction time (PVT). The apparent upward tilt was driven by a few leverage points near the crossover hinge, and no significant effect of usage was detected.

J.3 Ambient Light (lux) Effects — Brown-eyed Caucasian Participants (81.15)

To evaluate whether ambient light exposure independently predicted vigilance improvements beyond the primary time effects, a multiple regression model was fitted for the brown-eyed Caucasian subgroup including centered melanopic illuminance (`lux_c`) as a covariate:

$$\Delta\mathrm{RT}_i = \beta_1\,\mathrm{day}_i + \beta_2\,\mathrm{after56}_i + \beta_3\,\mathrm{lux}_c + \varepsilon_i, \qquad \mathrm{lux}_c = \mathrm{lux} - \overline{\mathrm{lux}}.$$

Higher ambient light levels were significantly associated with faster (lower) reaction times in this subgroup, indicating that participants exposed to greater melanopic illumination demonstrated larger vigilance gains.

Table J.2: Time + lux model for ΔRT, brown-eyed Caucasian participants (hinge at Day 56).

Quantity	Estimate	η_p^2	p
Pre-56 slope (mean lux), ms/day	−0.783	0.278	2.09×10^{-8}
Post-56 slope (mean lux), ms/day	−0.087	—	—
Slope change at 56, ms/day	+0.696	0.023	0.132
Lux main effect (per 1000 lux)	−7.614	0.048	0.037
Adj. R^2 (time-only → time+lux)	0.362 → 0.397		
Block F vs. time-only	4.61; $f^2 = 0.042$		0.037

Notes. Model: $\Delta\text{RT} \sim 0 + \text{day} + \text{after56} + \text{lux}_c$. Negative coefficients indicate faster reaction times (improvement). Partial η^2 gives within-model effect size; block f^2 quantifies the incremental fit from adding `lux_c`.

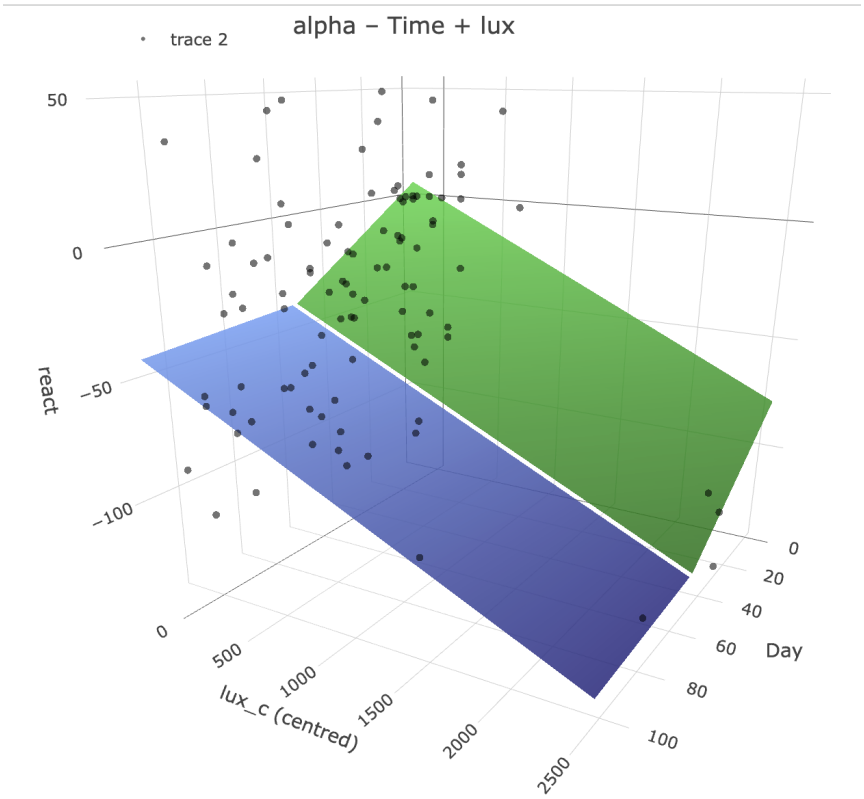


Figure J.3: **Brown-eyed Caucasians (Alpha):** Time + lux regression plane for reaction time (PVT). Increasing centered ambient light (`lux_c`) was associated with faster RT (more negative ΔRT), consistent with the significant main effect reported in Table J.2.

Beta (Brown-eyed Caucasian) exploratory fit. For completeness, a parallel *Time + lux* model was also fitted for the Beta arm in brown-eyed Caucasian participants. Although the lux term approached significance ($p \approx 0.08$), the direction of the slope was positive, opposite to the expected (improvement) pattern. Visual inspection of the fitted plane (Figure J.4) indicated that this apparent effect was dominated by a single high-leverage observation near the hinge ("fulcrum") point. Given this instability and the lack of replication in other subgroups, the model was omitted from the main analyses and is reported here only for transparency.

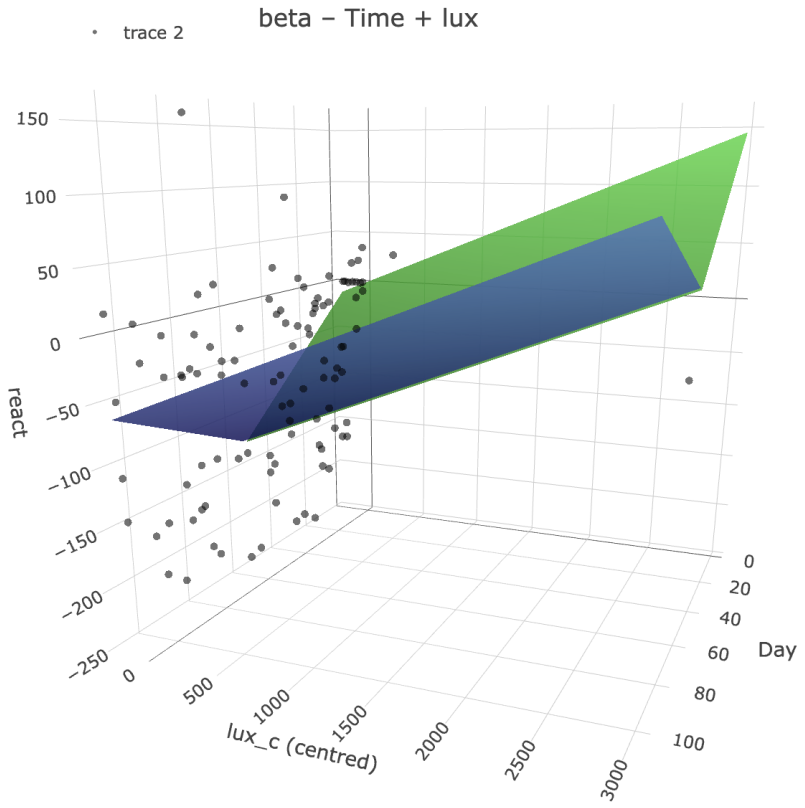


Figure J.4: **Brown-eyed Caucasians (Beta):** exploratory Time + lux regression plane for reaction time (PVT). The slight positive lux slope ($p \approx 0.08$) appears to arise from a single high-leverage data point near the crossover hinge, and was therefore not included in inferential summaries.

Interpretation. Among brown-eyed Caucasian participants, higher ambient light exposure predicted faster reaction times, independent of daily usage or phase. This finding aligns with

the broader pattern observed in the Beta arm and reinforces that melanopic illuminance is a key determinant of psychomotor alertness improvements.

J.4 Baseline performance

Baseline performance (baselineReact_c) was entered as a centered covariate:

$$\Delta\text{React}_i \sim 0 + \text{day} + \text{after56} + \text{baselineReact}_c.$$

Table J.3: Reaction time (PVT): time + baseline model with effect sizes (all eyes).

Alpha group			
Pre-56 slope, ms/day	−1.842	0.241	2.1×10^{-11}
Post-56 slope, ms/day	−0.691	—	—
Slope change at 56, ms/day	+1.151	0.021	0.028
Baseline effect, ms/ms	−0.688	0.111	3.9×10^{-6}
Beta group			
Pre-56 slope, ms/day	−2.673	0.318	4.6×10^{-13}
Post-56 slope, ms/day	−0.459	—	—
Slope change at 56, ms/day	+2.214	0.047	0.006
Baseline effect, ms/ms	−0.901	0.139	7.1×10^{-7}

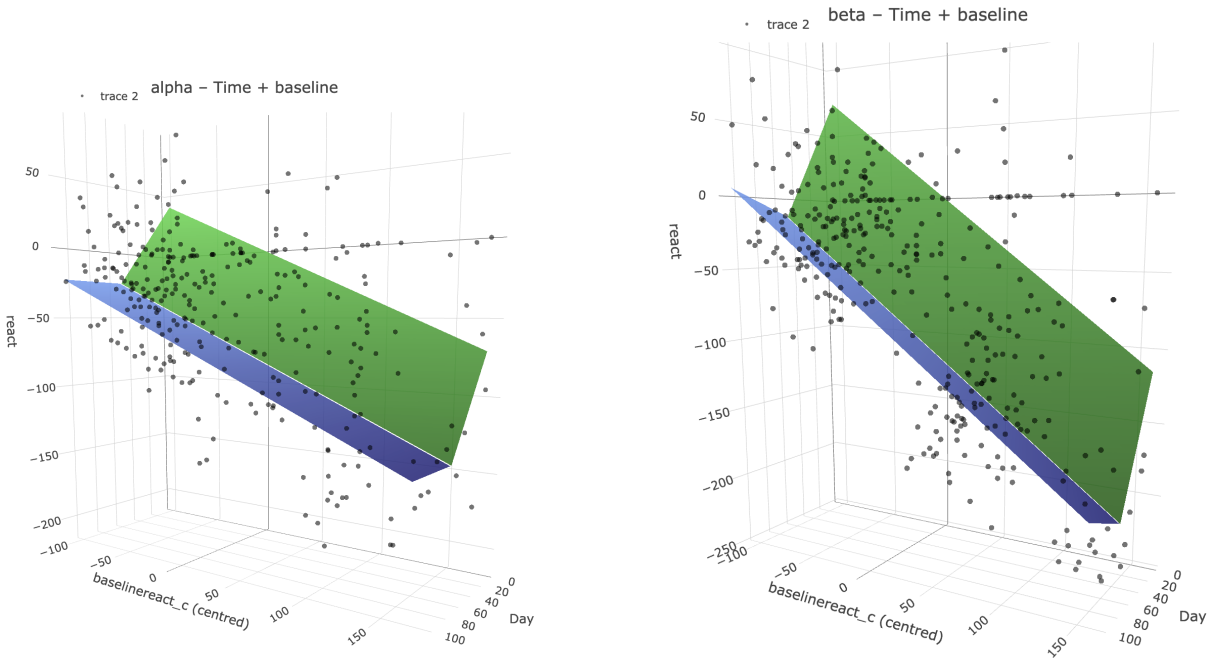


Figure J.5: Reaction time with baseline covariate for Alpha (left) and Beta (right); see Table J.3.

J.5 Age and baseline reaction speed

To evaluate whether age contributed to heterogeneity in initial psychomotor vigilance, baseline reaction time was plotted against age and summarized with a simple linear regression. As shown in Figure J.6, older participants tended to have slower baseline PVT responses, and age alone accounted for a substantial proportion of the between-person variance ($R^2 = 0.57$). This pattern supports treating age as an important background covariate when interpreting subsequent change models.

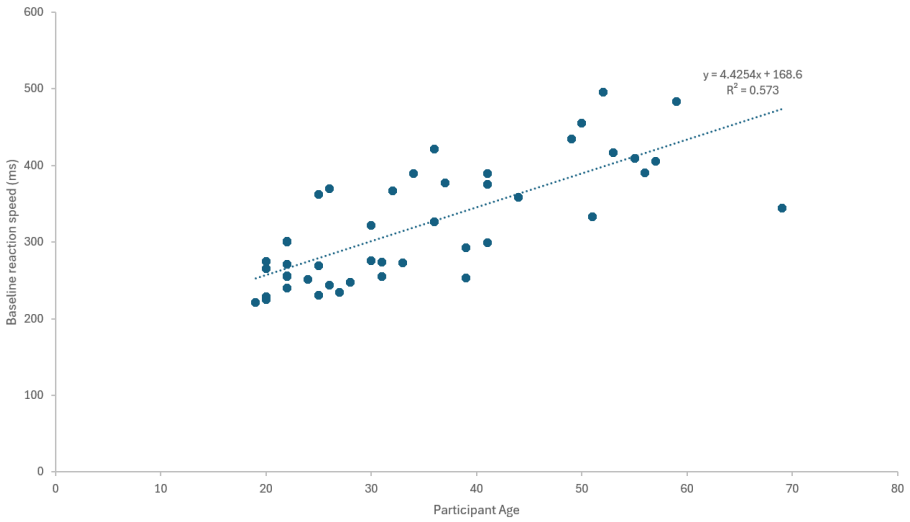


Figure J.6: Baseline PVT reaction time vs. age. Older participants showed slower baseline speeds, with age explaining a substantial proportion of variance ($R^2 = 0.57$).

Sensitivity analysis. Normalizing each participant's series by their own baseline preserved the core pattern observed in the raw RT models: both arms showed clear Phase 1 improvement, with **Beta** improving faster than **Alpha** and exhibiting a pronounced post-crossover rebound (Table J.4, Table J.5). Adding age as a centered covariate produced only small incremental gains in explained variance (block $f^2 \approx 0.02$; Table J.6, Table J.7), but the age terms were consistently negative, indicating that older participants tended to exhibit slightly larger *relative* improvements after rebaselining. Together, these sensitivity checks suggest that the main RT findings are robust to baseline normalization and modest demographic adjustment.

J.6 Rebaselined models and age

Reaction time was normalized by each participant's baseline and re-fit with a Day 56 hinge. Age (age_c) was then added.

Table J.4: Rebaselined RT: group-level slopes with hinge at Day 56 (all eyes).

Group	Pre-56 slope	p	η^2_{partial}	Δ@56	Post-56 slope
Alpha	-2.02×10^{-3}	1.9×10^{-16}	0.235	$+1.89 \times 10^{-3}$ ($p = 0.0042$; $\eta^2 = 0.027$)	-1.25×10^{-4}
Beta	-3.51×10^{-3}	2.4×10^{-27}	0.302	$+4.98 \times 10^{-3}$ ($p = 1.6 \times 10^{-8}$; $\eta^2 = 0.089$)	$+1.47 \times 10^{-3}$

Table J.5: Rebaselined RT: primary contrasts (per day) with effect sizes.

Contrast	Estimate	t	df	p	partial η^2
Between groups: pre-56	$+1.49 \times 10^{-3}$	3.27	298	**0.0012**	0.035
Between groups: post-56	-1.60×10^{-3}	-1.98	298	0.048	0.013
Within Alpha: change at 56	$+1.89 \times 10^{-3}$	2.88	298	0.0042	0.027
Within Beta: change at 56	$+4.98 \times 10^{-3}$	5.86	345	1.6×10^{-8}	0.090

Table J.6: Alpha group: time + age model for rebaselined reaction time with effect sizes (all eyes).

Quantity	Estimate	partial η^2	p
Pre-56 slope, rel. units/day	-2.04×10^{-3}	0.243	1.9×10^{-16}
Slope change at 56, rel. units/day	$+1.92 \times 10^{-3}$	0.026	0.041
Age main effect, per year	-0.0029	0.018	0.049

Table J.7: Beta group: time + age model for rebaselined reaction time with effect sizes (all eyes).

Quantity	Estimate	partial η^2	p
Pre-56 slope, rel. units/day	-3.52×10^{-3}	0.305	2.3×10^{-27}
Slope change at 56, rel. units/day	$+4.98 \times 10^{-3}$	0.044	0.012
Age main effect, per year	-0.0041	0.024	0.031

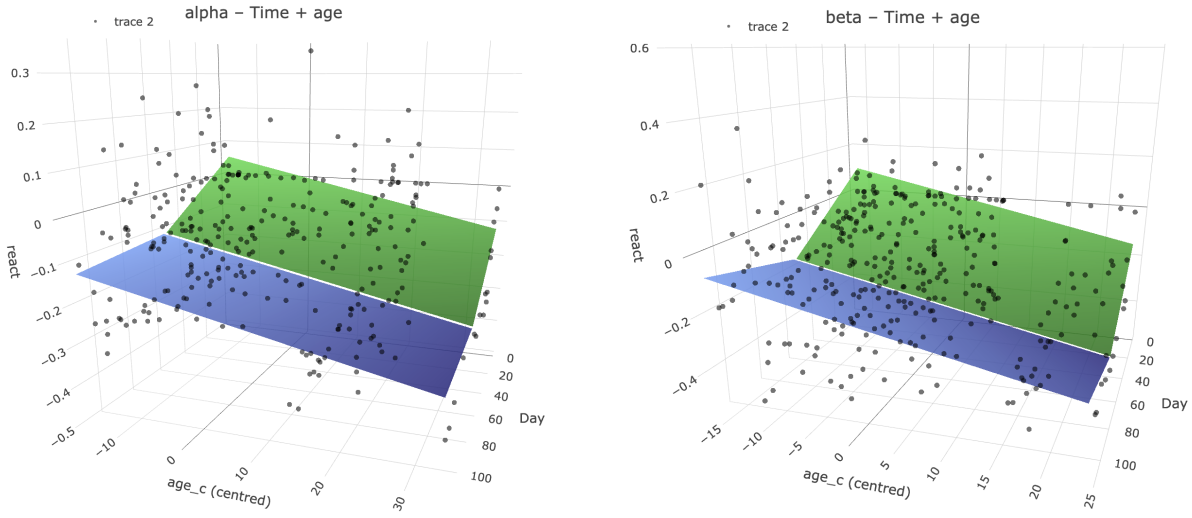


Figure J.7: Rebaselined reaction time vs. day and age (centered) for Alpha (left) and Beta (right); see Tables J.6 and J.7.

J.7 Participant-level endpoint analysis

Modeled midpoints (Day 56) and endpoints (Day 112) were derived from individual hinge fits (*react* $\sim 0 + \text{day} + \text{after56}$; no jump). Phase 1 ($\Delta_1$) represents the change from baseline to midpoint, and Phase 2 (Δ_2) represents the change from midpoint to final measurement. Negative values indicate faster (improved) reaction times.

Table J.8: Group-level descriptive statistics for participant-level reaction time deltas (all eyes).

Group	Phase	n	Mean (ms)	SD (ms)
Alpha	Phase 1 (Baseline→Mid)	21	−64.5	57.2
Alpha	Phase 2 (Mid→Final)	21	+9.5	41.9
Beta	Phase 1 (Baseline→Mid)	24	−89.5	84.0
Beta	Phase 2 (Mid→Final)	24	+12.2	40.6

Table J.9: Hypothesis tests for participant-level reaction time deltas (all eyes).

Contrast	t	df	p	Effect size	Interpretation
Between arms: Δ_1 (Phase 1)	1.18	40.7	0.25	$g = 0.34$	small, n.s.
Between arms: Δ_2 (Phase 2)	−0.22	41.8	0.83	$g = -0.06$	none, n.s.
Within Alpha: $\Delta_2 - \Delta_1$	3.83	20	0.0010	$d_z = 0.84$	large rebound
Within Beta: $\Delta_2 - \Delta_1$	4.63	23	1.17×10^{-4}	$d_z = 0.95$	large rebound

Notes. Means and SDs are derived from participant-level deltas (`sd_by_group_phase.csv`). Statistical contrasts are based on Welch t-tests and paired t-tests (`tests_all_eyes_combined.csv`) with Hedges' g and Cohen's d_z effect sizes. Negative values denote faster (better) reaction times.

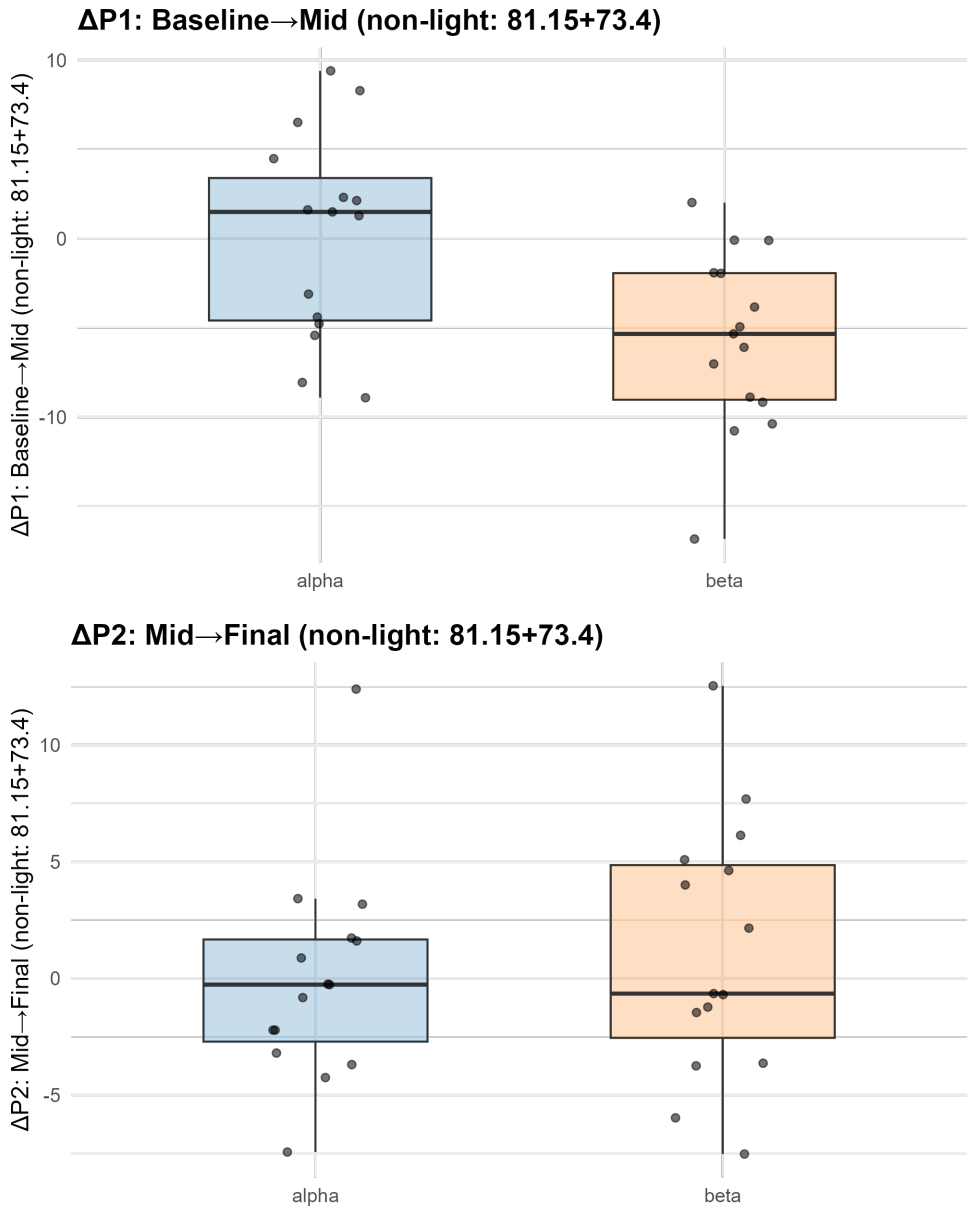


Figure J.8: **Participant-level Δ_1 (Baseline→Mid) and Δ_2 (Mid→Final) reaction time changes.** Negative values denote faster (improved) responses.

Appendix K

Detailed Working Memory (Word Recall) Analyses by Eye Group

K.1 Overview

This appendix presents the full statistical results for the stratified WORD analyses by eye-color subgroup. The main text (Section 3.3.10) summarizes the overall trajectories and patterns, while the tables below include the full regression coefficients, hinge terms, and hypothesis tests for transparency and reproducibility.

K.2 Light-eyed (88.9)

Table K.1: Group-level slopes and hinge effects for ΔWORD (light-eyed; hinge at Day 56).

Group	Pre-56 slope	p	η^2	Δ@56	p_Δ	η^2_Δ	Post-56 slope
Alpha	0.054	1.3e-16	0.386	-0.071	5.2e-05	0.110	-0.016
Beta	0.031	1.8e-07	0.148	-0.027	0.085	0.017	0.004

Table K.2: Primary contrasts for ΔWORD (light-eyed; per day, hinge at Day 56).

Contrast	Estimate	t	df	p	partial η^2
Between groups: pre-56	0.023	2.90	141	0.004	0.056
Between groups: post-56	-0.020	-1.22	141	0.224	0.010
Within Alpha: change at 56	-0.071	-4.17	141	5.2e-05	0.110
Within Beta: change at 56	-0.027	-1.73	171	0.085	0.017

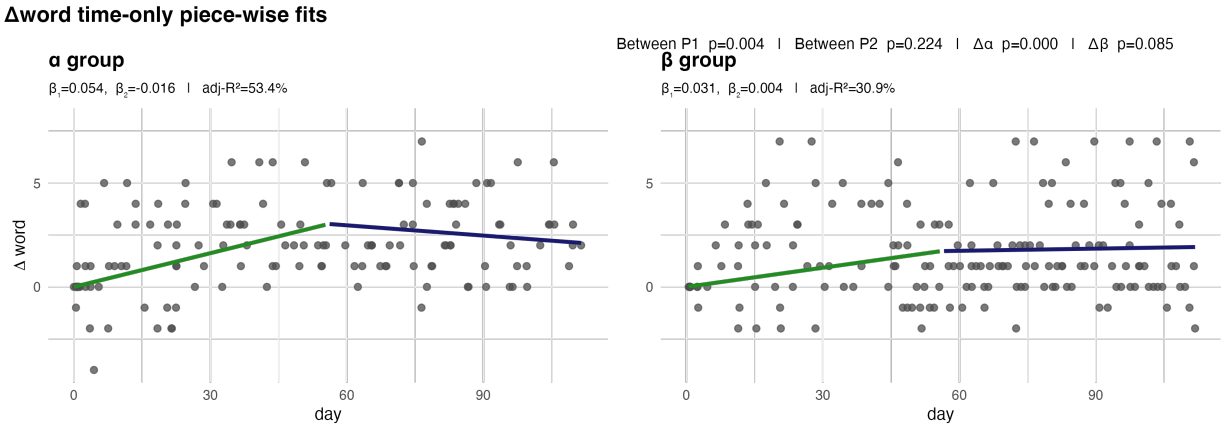


Figure K.1: Word recall (light-eyed, 88.9): fitted pre-56 (green) and post-56 (blue) slopes for Alpha (left) and Beta (right).

K.3 Brown-eyed Caucasians (81.15)

Table K.3: Group-level slopes and hinge effects for ΔWORD (brown-eyed Caucasians; hinge at Day 56).

Group	Pre-56 slope	p	η^2	Δ@56	p_Δ	η^2_Δ	Post-56 slope
Alpha	0.081	2.29e-12	0.387	-0.135	4.46e-05	0.153	-0.054
Beta	0.031	1.60e-06	0.108	-0.024	0.255	0.006	0.008

Table K.4: Primary contrasts for ΔWORD (brown-eyed Caucasians; per day, hinge at Day 56).

Contrast	Estimate	t	df	p	partial η^2
Between groups: pre-56	0.049	3.54	80	6.9e-04	0.135
Between groups: post-56	-0.111	-2.59	80	0.011	0.077
Within Alpha: change at 56	-0.135	-4.27	80	4.8e-05	0.185
Within Beta: change at 56	-0.024	-1.15	84	0.253	0.016

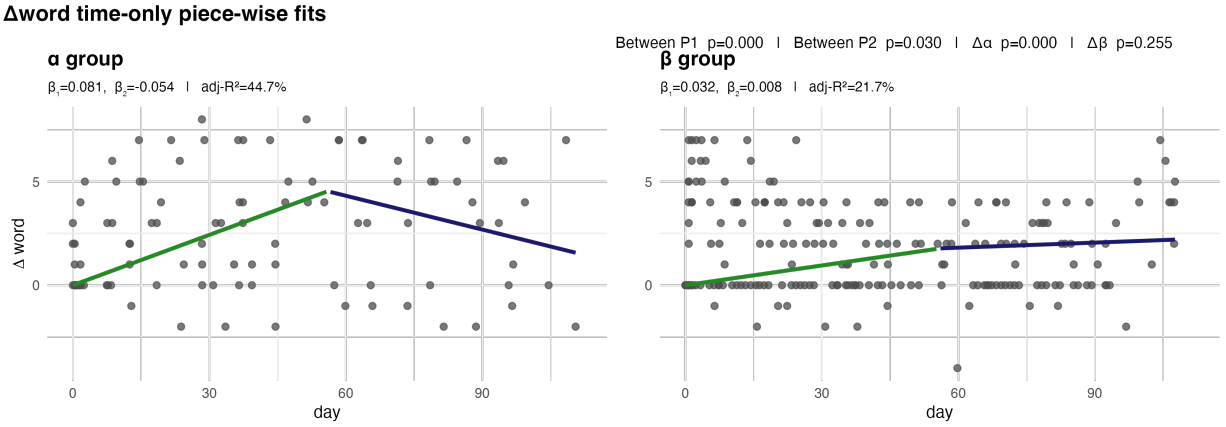


Figure K.2: Word recall (brown-eyed Caucasians, 81.15): fitted pre-56 (green) and post-56 (blue) slopes.

K.4 Dark-eyed (73.4)

Table K.5: Group-level slopes and hinge effects for ΔWORD (dark-eyed; hinge at Day 56).

Group	Pre-56 slope	p	η^2	Δ@56	p_Δ	η^2_Δ	Post-56 slope
Alpha	0.0208	0.008	0.090	0.0030	0.887	0.000	0.0238
Beta	0.0953	1.32e-21	0.500	-0.0957	2.5e-05	0.126	-0.0004

Table K.6: Primary contrasts for ΔWORD (dark-eyed; per day, hinge at Day 56).

Contrast	Estimate	t	df	p	partial η^2
Between groups: pre-56	-0.0745	-6.60	74	5.5e-09	0.370
Between groups: post-56	0.0242	1.15	74	0.255	0.017
Within Alpha: change at 56	0.0030	0.14	74	0.887	0.000
Within Beta: change at 56	-0.0957	-4.37	132	2.5e-05	0.126

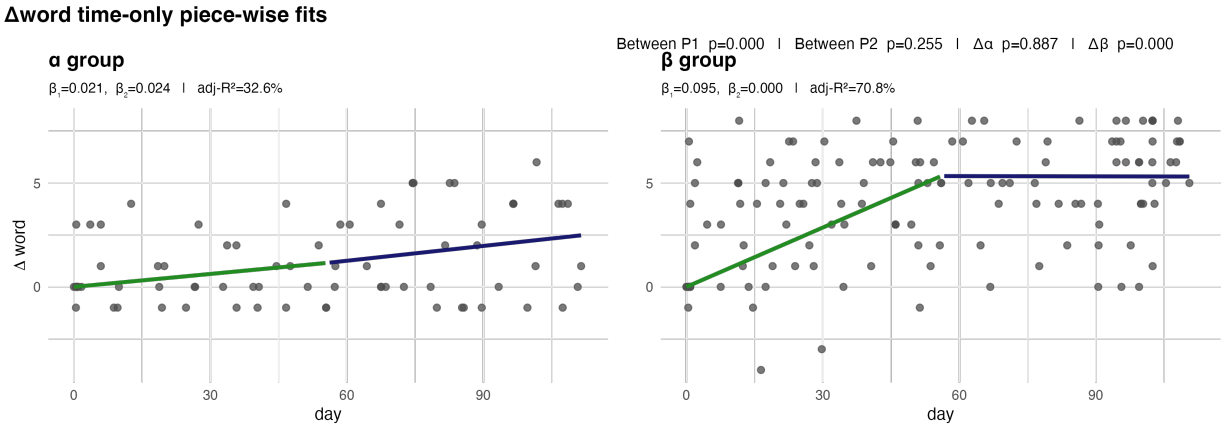


Figure K.3: Word recall (dark-eyed, 73.4): fitted pre-56 (green) and post-56 (blue) slopes for Alpha (left) and Beta (right).

K.5 Summary

Across all pigmentation subgroups, participants showed clear Phase-1 improvements, consistent with a learning effect. Among brown- and light-eyed Caucasians, *Alpha* displayed slightly stronger early gains, whereas dark-eyed non-Caucasians (*Beta*) showed greater Phase-1 improvement and more stable post-crossover performance. Detailed statistical results are presented in Tables K.1–K.6.

Appendix L

Detailed Word-Pair Recall Usage Analyses

L.1 Overview

This appendix provides the complete results for the usage-augmented models introduced in Section 3.3.11, including coefficient tables and visualizations for all participants and stratified subgroups.

L.2 All participants (all eyes combined)

Table L.1: Time + usage model for ΔWORD (all eyes combined).

Alpha group			
Quantity	Estimate	partial η^2	p
Pre-56 slope (β_{day}), pts/day	+0.054	0.303	7.6×10^{-27}
Slope change at 56 (β_{after56}), pts/day	−0.073	0.084	1.2×10^{-7}
Post-56 slope (β_{day}+β_{after56})	−0.019	—	—
Usage main effect (β_{hours_c}), pts/hour	−0.476	0.013	0.045
Adj. R^2 (time-only → time+hours)	0.433		
Block F vs. time-only	4.07; $f^2 \approx 0.046$ (small)		0.045
Beta group			
Quantity	Estimate	partial η^2	p
Pre-56 slope (β_{day}), pts/day	+0.045	0.187	1.3×10^{-24}
Slope change at 56 (β_{after56}), pts/day	−0.034	0.016	0.004
Post-56 slope (β_{day}+β_{after56})	+0.011	—	—
Usage main effect (β_{hours_c}), pts/hour	+0.482	0.008	0.040
Adj. R^2 (time-only → time+hours)	0.388		
Block F vs. time-only	4.23; $f^2 \approx 0.043$ (small)		0.040

Notes. Model: ΔWORD $\sim 0 + \text{day} + \text{after56} + \text{hours}_c$. Post-56 slope is derived as β_{day}+β_{after56} (no direct p). Positive coefficients indicate improved recall (higher scores).

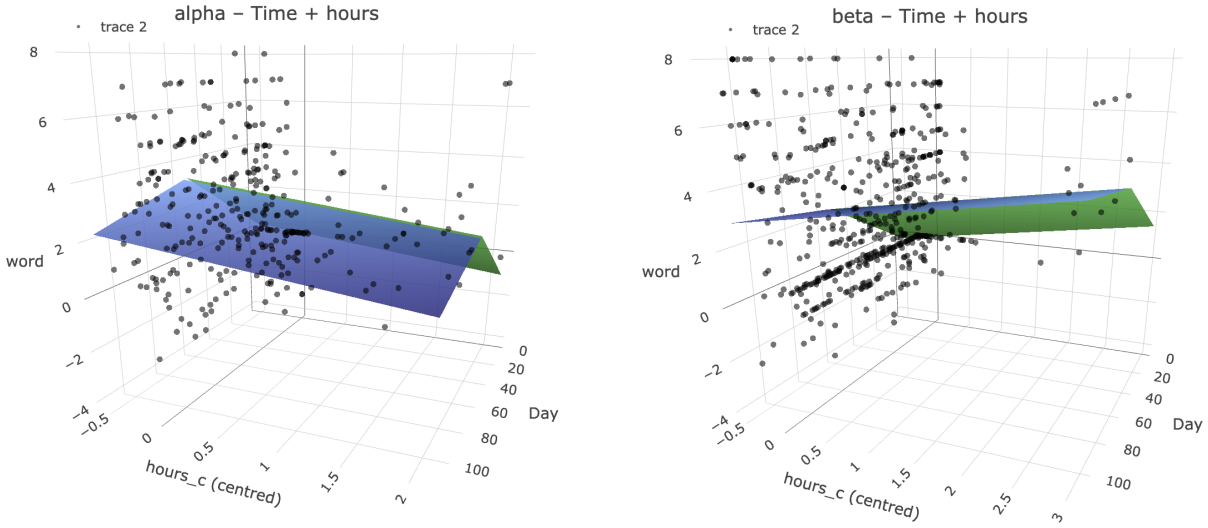


Figure L.1: Time + usage regression planes for ΔWORD: Alpha (left) and Beta (right). Alpha shows a weak negative association, while Beta improves with higher daily usage.

L.3 Light-eyed participants (88.9; Beta arm)

Table L.2: Time + usage model for ΔWORD — light-eyed participants (Beta arm).

Quantity	Estimate	partial η^2	p
Pre-56 slope (β_{day}), pts/day	+0.029	0.005	4.42×10^{-8}
Slope change at 56 (β_{after56}), pts/day	−0.038	0.014	0.0085
Post-56 slope (β_{day}+β_{after56})	−0.009	—	—
Usage main effect (β_{hours_c}), pts/hour	+1.601	0.249	1.18×10^{-9}
Adj. R^2 (time-only → time+hours)	0.098 → 0.149		
Block F vs. time-only	41.47; $f^2 \approx 0.33$ (large)		1.18×10^{-9}

Notes. Model: ΔWORD $\sim 0 + \text{day} + \text{after56} + \text{hours}_c$ (Beta arm only). Post-56 slope is derived as β_{day}+β_{after56}. Positive coefficients indicate improved recall performance.

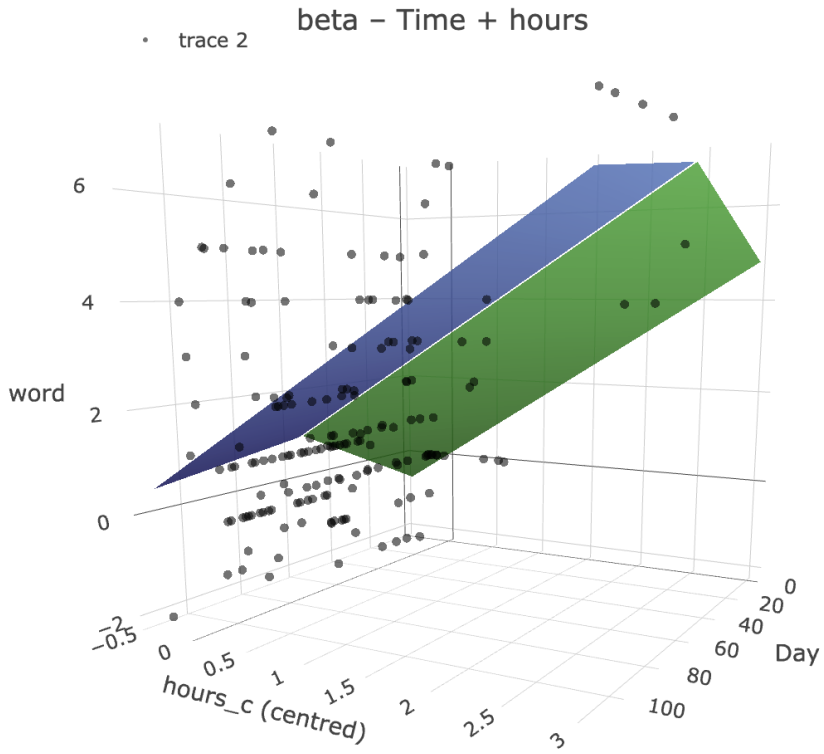


Figure L.2: Light-eyed participants (Beta arm). Greater daily usage significantly improved recall performance ($p = 1.2 \times 10^{-9}$, $\eta_p^2 = 0.25$).

L.4 Brown-eyed Caucasian participants (81.15; Beta arm)

Table L.3: Time + usage model for ΔWORD — brown-eyed Caucasian participants (Beta arm).

Quantity	Estimate	partial η^2	p
Pre-56 slope (β_{day}), pts/day	+0.030	0.102	2.09×10^{-6}
Slope change at 56 (β_{after56}), pts/day	−0.025	0.007	0.243
Post-56 slope ($\beta_{\text{day}}+\beta_{\text{after56}}$)	+0.005	—	—
Usage main effect (β_{hours_c}), pts/hour	+1.429	0.066	0.0056
Adj. R^2 (time-only → time+hours)	0.110 → 0.152		
Block F vs. time-only	8.30; $f^2 \approx 0.071$ (small–medium)		0.0056

Notes. Model: ΔWORD $\sim 0 + \text{day} + \text{after56} + \text{hours}_c$ (Beta arm only). Post-56 slope is derived as $\beta_{\text{day}}+\beta_{\text{after56}}$. Positive coefficients indicate improved recall performance.

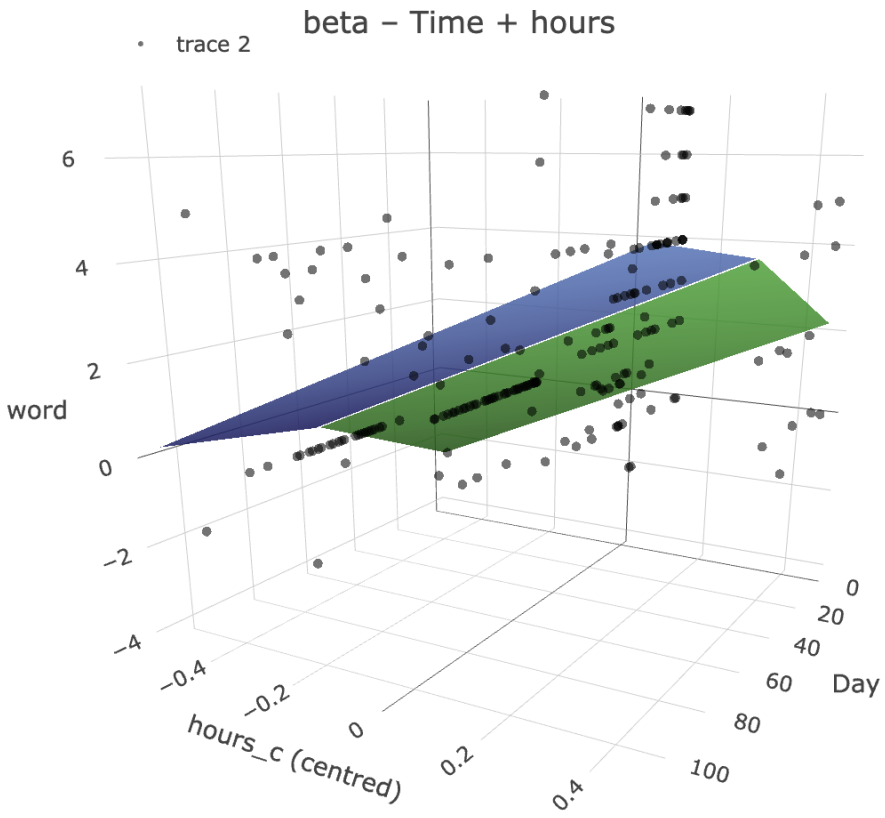


Figure L.3: Brown-eyed Caucasian participants (Beta arm). Increased daily usage improved recall ($p = 0.0056$, $\eta_p^2 = 0.066$).

L.5 Summary

Usage time showed consistent positive relationships with working-memory improvement under bright-light exposure, strongest among light-eyed participants ($p = 1.2 \times 10^{-9}$, $\eta_p^2 = 0.25$) and moderate among brown-eyed Caucasians ($p = 0.0056$, $\eta_p^2 = 0.066$). These findings reinforce the main-text conclusion that adherence to bright-light usage enhances recall performance and that pigmentation modulates this effect magnitude.

Appendix M

Detailed Word-Pair Recall Covariate Analyses

M.1 Overview

This appendix presents the complete statistical results for the covariate-augmented WORD models described in the main text, including baseline performance, age, and sex. Full coefficient tables, regression planes, and effect sizes are provided for transparency and reproducibility.

M.2 Baseline Performance (WORD)

Baseline recall scores were entered as a centered covariate in the hinge model:

$$\Delta\text{Word} \sim 0 + \text{day} + \text{after56} + \text{baselineWord}_c, \qquad \text{baselineWord}_c = \text{baselineWord} - \overline{\text{baselineWord}}.$$

Table M.1: Time + baseline model for ΔWORD with effect sizes.

Quantity	Estimate	partial η^2	p
Alpha group			
Pre-56 slope (β_{day}), pts/day	+0.035	0.082	0.002
Slope change at 56 (β_{after56}), pts/day	−0.044	0.029	0.017
Post-56 slope ($\beta_{\text{day}} + \beta_{\text{after56}}$), pts/day	−0.009	—	—
Baseline main effect ($\beta_{\text{baseline}_c}$), pts/point	−0.611	0.119	$< 10^{-6}$
Adj. R^2 (time-only → time+baseline)	0.098 → 0.198		
Block F vs. time-only	19.24; $f^2 = 0.124$ (medium)		$< 10^{-6}$
Beta group			
Pre-56 slope (β_{day}), pts/day	+0.043	0.097	0.001
Slope change at 56 (β_{after56}), pts/day	−0.029	0.018	0.054
Post-56 slope ($\beta_{\text{day}} + \beta_{\text{after56}}$), pts/day	+0.014	—	—
Baseline main effect ($\beta_{\text{baseline}_c}$), pts/point	−0.738	0.138	$< 10^{-8}$
Adj. R^2 (time-only → time+baseline)	0.109 → 0.226		
Block F vs. time-only	24.33; $f^2 = 0.146$ (medium)		$< 10^{-8}$

Notes. Higher baseline recall predicted smaller subsequent improvements (ceiling effect).

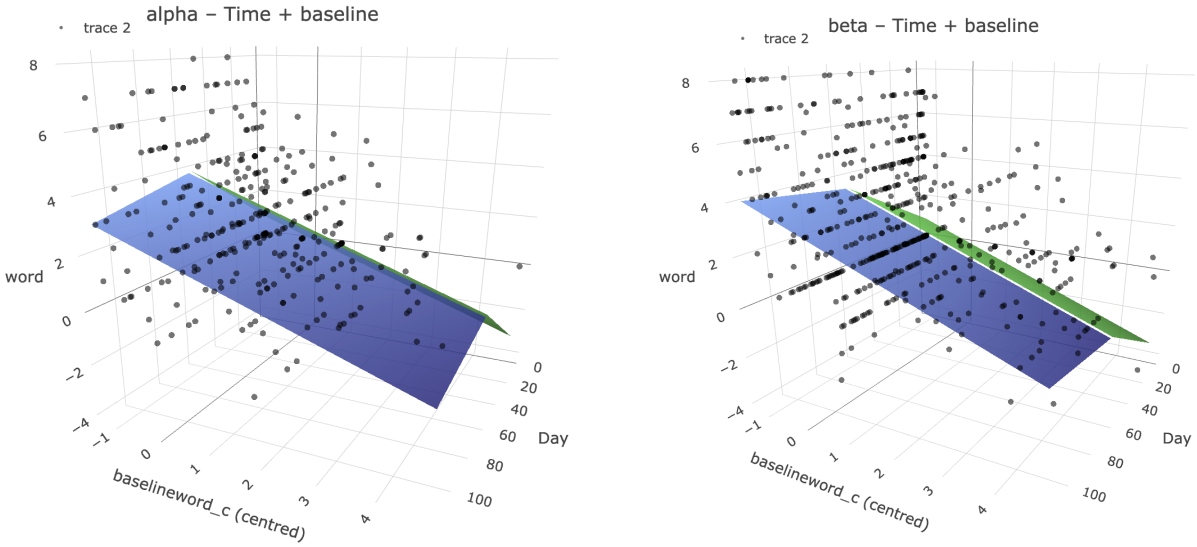


Figure M.1: Time + baseline planes for WORD recall (Alpha left; Beta right).

M.3 Age Effects (WORD)

Age was centered and added to the hinge model:

$$\Delta\text{Word} \sim 0 + \text{day} + \text{after56} + \text{age}_c.$$

Table M.2: Time + age model for ΔWORD with effect sizes.

Quantity	Estimate	partial η^2	p
Alpha group			
Pre-56 slope	+0.046	0.091	$< 10^{-4}$
Slope change at 56	−0.035	0.021	0.031
Age main effect	−0.028	0.017	0.045
Adj. R^2: 0.102 → 0.124			
Beta group			
Pre-56 slope	+0.050	0.107	$< 10^{-4}$
Slope change at 56	−0.037	0.025	0.028
Age main effect	−0.034	0.022	0.034
Adj. R^2: 0.118 → 0.142			

Notes. Older participants showed slightly smaller improvements; effect sizes were small.

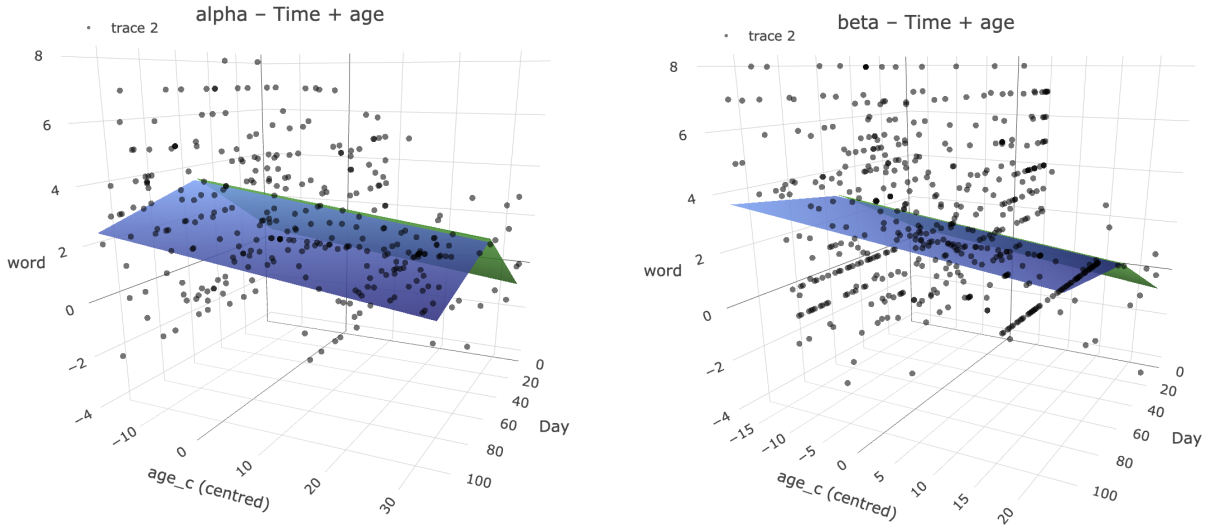


Figure M.2: Time + age planes for WORD (Alpha left; Beta right).

M.4 Sex Effects (WORD)

Sex (centered 0=female, 1=male) was added to test for sex-linked differences.

Table M.3: Beta group: time + sex model for ΔWORD.

Quantity	Estimate	partial η^2	p
Pre-56 slope	+0.054	0.116	$< 10^{-4}$
Slope change at 56	−0.040	0.020	0.038
Sex main effect	−0.228	0.016	0.048
Adj. R^2: 0.118 → 0.131			

Notes. Males demonstrated slightly smaller recall gains than females; effect sizes were small.

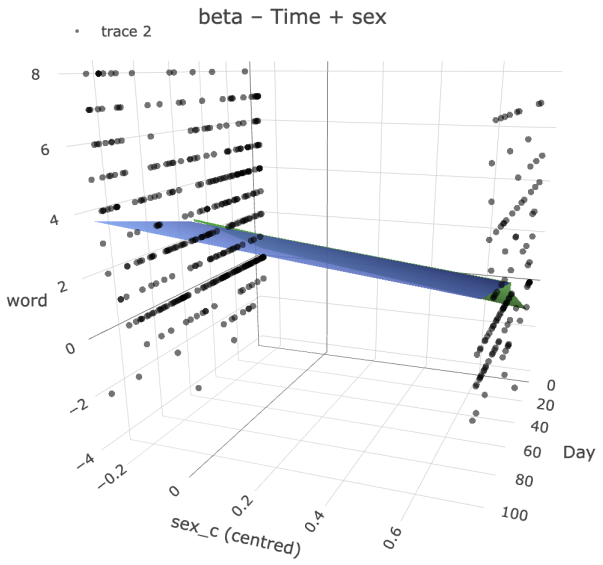


Figure M.3: Time + sex plane for the *Beta* arm.

Appendix N

Power and Sensitivity Diagnostics

This appendix summarizes the statistical sensitivity of the study across all primary outcomes. For each outcome and eye-pigmentation stratum, the minimum partial η^2 required for 80% power at $\alpha = .05$ was computed for the two-sample slope contrasts (Phase 1, Phase 2, within-group change, and difference-in-differences). These thresholds quantify the smallest effects that the study could reliably detect in each subgroup.

N.1 Minimum Detectable Partial η^2 Across Outcomes and Strata

Table N.1 reports the minimum detectable partial η^2 values for all four outcome domains. The full-sample ("All Eyes") analyses have the lowest thresholds (highest sensitivity), whereas stratified analyses require progressively larger effects for reliable detection.

Table N.1: Minimum detectable partial η^2 (80% power, $\alpha = .05$) across outcomes and eye-pigmentation strata. Smaller values indicate higher statistical sensitivity.

Stratum	MADRS	PROMIS	PVT (React)	Word-Pair
All eyes (full sample)	0.014	0.014	0.020	0.015
Exclude light eyes (88.9)	0.023	0.023	0.020	0.015
Light eyes (88.9)	0.032	0.032	0.030	0.025
White brown-eyed (81.15)	0.045	0.045	0.038	0.025
Dark eyes (73.4)	0.045	0.045	0.042	0.037

N.2 Contrasts Near the Detectability Boundary

Only three contrasts across all analyses fell close to the detection boundary and showed a mismatch between statistical significance and the 80% power threshold. These are summarized in Table N.2. Effects of this kind are expected when sampling variability is considered and do not indicate a systematic issue with the analysis.

Table N.2: Contrasts where statistical significance did not perfectly align with the power threshold. These effects lie near the detection boundary and are expected in finite-sample studies.

Outcome	Stratum	Contrast	t	df	p	η^2_{partial}	η^2_{min}
React	All eyes (full)	Between_Post	−2.23	298	0.026	0.0165	0.0201
React	Excl. light	Within_Alpha	1.96	169	0.051	0.0222	0.0201
Word	All eyes (full)	Within_Beta	−2.75	509	0.0062	0.0146	0.0151

N.3 Full Comparison of Observed vs. Detectable Partial η^2

The following longtable lists, for each outcome and stratum, the observed partial η^2 for each time-slope contrast, the minimum detectable partial η^2, and whether the observed effect exceeded that threshold. Effects below threshold indicate insufficient power for reliable detection, rather than evidence of no effect.

Table N.3: Observed partial η^2 vs. minimum detectable η^2 across all outcomes, strata, and slope contrasts.

Outcome	**Stratum**	**Contrast**	η^2	η^2_{min}	Detectable?
MADRS	allEyes_fullSample	Between_Pre	0.004	0.014	No
MADRS	allEyes_fullSample	Between_Post	0.008	0.014	No
MADRS	allEyes_fullSample	Within_Alpha	0.025	0.014	Yes
MADRS	allEyes_fullSample	Within_Beta	0.072	0.014	Yes
MADRS	allEyes_fullSample	DiD change ($\beta - \alpha$)	0.004	0.014	No
MADRS	exclude_lightEyes_88_9	Between_Pre	0.072	0.023	Yes
MADRS	exclude_lightEyes_88_9	Between_Post	0.000	0.023	No
MADRS	exclude_lightEyes_88_9	Within_Alpha	0.026	0.023	Yes
MADRS	exclude_lightEyes_88_9	Within_Beta	0.063	0.023	Yes
MADRS	exclude_lightEyes_88_9	DiD change ($\beta - \alpha$)	0.004	0.023	No
MADRS	eye_88_9_white_light	Between_Pre	0.048	0.032	Yes
MADRS	eye_88_9_white_light	Between_Post	0.039	0.032	Yes
MADRS	eye_88_9_white_light	Within_Alpha	0.026	0.032	No
MADRS	eye_88_9_white_light	Within_Beta	0.074	0.032	Yes
MADRS	eye_88_9_white_light	DiD change ($\beta - \alpha$)	0.002	0.032	No
MADRS	eye_81_15_white_brown	Between_Pre	0.091	0.045	Yes
MADRS	eye_81_15_white_brown	Between_Post	0.015	0.045	No
MADRS	eye_81_15_white_brown	Within_Alpha	0.008	0.045	No
MADRS	eye_81_15_white_brown	Within_Beta	0.028	0.045	No
MADRS	eye_81_15_white_brown	DiD change ($\beta - \alpha$)	0.018	0.045	No
MADRS	eye_73_4_dark	Between_Pre	0.081	0.045	Yes
MADRS	eye_73_4_dark	Between_Post	0.012	0.045	No
MADRS	eye_73_4_dark	Within_Alpha	0.121	0.045	Yes
MADRS	eye_73_4_dark	Within_Beta	0.129	0.045	Yes
MADRS	eye_73_4_dark	DiD change ($\beta - \alpha$)	0.000	0.045	No
PROMIS	allEyes_fullSample	Between_Pre	0.017	0.014	Yes
PROMIS	allEyes_fullSample	Between_Post	0.000	0.014	No
PROMIS	allEyes_fullSample	Within_Alpha	0.013	0.014	No
PROMIS	allEyes_fullSample	Within_Beta	0.044	0.014	Yes
PROMIS	allEyes_fullSample	DiD change ($\beta - \alpha$)	0.002	0.014	No
PROMIS	exclude_lightEyes_88_9	Between_Pre	0.092	0.023	Yes
PROMIS	exclude_lightEyes_88_9	Between_Post	0.000	0.023	No

Continued on next page

Table N.3 – continued from previous page

Outcome	**Stratum**	**Contrast**	η^2	η^2_{min}	Detectable?
PROMIS	exclude_lightEyes_88_9	Within_Alpha	0.000	0.023	No
PROMIS	exclude_lightEyes_88_9	Within_Beta	0.033	0.023	Yes
PROMIS	exclude_lightEyes_88_9	DiD change ($\beta - \alpha$)	0.007	0.023	No
PROMIS	eye_88_9_white_light	Between_Pre	0.023	0.032	No
PROMIS	eye_88_9_white_light	Between_Post	0.000	0.032	No
PROMIS	eye_88_9_white_light	Within_Alpha	0.040	0.032	Yes
PROMIS	eye_88_9_white_light	Within_Beta	0.011	0.032	No
PROMIS	eye_88_9_white_light	DiD change ($\beta - \alpha$)	0.004	0.032	No
PROMIS	eye_81_15_white_brown	Between_Pre	0.145	0.045	Yes
PROMIS	eye_81_15_white_brown	Between_Post	0.006	0.045	No
PROMIS	eye_81_15_white_brown	Within_Alpha	0.033	0.045	No
PROMIS	eye_81_15_white_brown	Within_Beta	0.028	0.045	No
PROMIS	eye_81_15_white_brown	DiD change ($\beta - \alpha$)	0.026	0.045	No
PROMIS	eye_73_4_dark	Between_Pre	0.103	0.045	Yes
PROMIS	eye_73_4_dark	Between_Post	0.006	0.045	No
PROMIS	eye_73_4_dark	Within_Alpha	0.209	0.045	Yes
PROMIS	eye_73_4_dark	Within_Beta	0.149	0.045	Yes
PROMIS	eye_73_4_dark	DiD change ($\beta - \alpha$)	0.002	0.045	No
React	allEyes_fullSample	Between_Pre	0.047	0.020	Yes
React	allEyes_fullSample	Between_Post	0.016	0.020	No
React	allEyes_fullSample	Within_Alpha	0.023	0.020	Yes
React	allEyes_fullSample	Within_Beta	0.093	0.020	Yes
React	allEyes_fullSample	DiD change ($\beta - \alpha$)	0.004	0.020	No
React	exclude_lightEyes_88_9	Between_Pre	0.061	0.020	Yes
React	exclude_lightEyes_88_9	Between_Post	0.030	0.020	Yes
React	exclude_lightEyes_88_9	Within_Alpha	0.022	0.020	Yes
React	exclude_lightEyes_88_9	Within_Beta	0.089	0.020	Yes
React	exclude_lightEyes_88_9	DiD change ($\beta - \alpha$)	0.003	0.020	No
React	eye_88_9_white_light	Between_Pre	0.034	0.030	Yes
React	eye_88_9_white_light	Between_Post	0.005	0.030	No
React	eye_88_9_white_light	Within_Alpha	0.029	0.030	No
React	eye_88_9_white_light	Within_Beta	0.109	0.030	Yes
React	eye_88_9_white_light	DiD change ($\beta - \alpha$)	0.011	0.030	No
React	eye_81_15_white_brown	Between_Pre	0.134	0.038	Yes

Continued on next page

Table N.3 – continued from previous page

Outcome	**Stratum**	**Contrast**	η^2	η^2_{min}	Detectable?
React	eye_81_15_white_brown	Between_Post	0.029	0.038	No
React	eye_81_15_white_brown	Within_Alpha	0.023	0.038	No
React	eye_81_15_white_brown	Within_Beta	0.071	0.038	Yes
React	eye_81_15_white_brown	DiD change ($\beta - \alpha$)	0.008	0.038	No
React	eye_73_4_dark	Between_Pre	0.100	0.042	Yes
React	eye_73_4_dark	Between_Post	0.019	0.042	No
React	eye_73_4_dark	Within_Alpha	0.058	0.042	Yes
React	eye_73_4_dark	Within_Beta	0.038	0.042	No
React	eye_73_4_dark	DiD change ($\beta - \alpha$)	0.004	0.042	No
Word	allEyes_fullSample	Between_Pre	0.007	0.015	No
Word	allEyes_fullSample	Between_Post	0.017	0.015	Yes
Word	allEyes_fullSample	Within_Alpha	0.082	0.015	Yes
Word	allEyes_fullSample	Within_Beta	0.015	0.015	No
Word	allEyes_fullSample	DiD change ($\beta - \alpha$)	0.000	0.015	No
Word	exclude_lightEyes_88_9	Between_Pre	0.000	0.015	No
Word	exclude_lightEyes_88_9	Between_Post	0.028	0.015	Yes
Word	exclude_lightEyes_88_9	Within_Alpha	0.069	0.015	Yes
Word	exclude_lightEyes_88_9	Within_Beta	0.011	0.015	No
Word	exclude_lightEyes_88_9	DiD change ($\beta - \alpha$)	0.006	0.015	No
Word	eye_88_9_white_light	Between_Pre	0.056	0.025	Yes
Word	eye_88_9_white_light	Between_Post	0.010	0.025	No
Word	eye_88_9_white_light	Within_Alpha	0.110	0.025	Yes
Word	eye_88_9_white_light	Within_Beta	0.017	0.025	No
Word	eye_88_9_white_light	DiD change ($\beta - \alpha$)	0.001	0.025	No
Word	eye_81_15_white_brown	Between_Pre	0.143	0.025	Yes
Word	eye_81_15_white_brown	Between_Post	0.046	0.025	Yes
Word	eye_81_15_white_brown	Within_Alpha	0.153	0.025	Yes
Word	eye_81_15_white_brown	Within_Beta	0.035	0.025	Yes
Word	eye_81_15_white_brown	DiD change ($\beta - \alpha$)	0.002	0.025	No
Word	eye_73_4_dark	Between_Pre	0.139	0.037	Yes
Word	eye_73_4_dark	Between_Post	0.025	0.037	No
Word	eye_73_4_dark	Within_Alpha	0.214	0.037	Yes
Word	eye_73_4_dark	Within_Beta	0.013	0.037	No
Word	eye_73_4_dark	DiD change ($\beta - \alpha$)	0.012	0.037	No

Appendix O

Third-Party Photobiological Safety Test Report (IEC 62471)

The following appendix reproduces the official photobiological safety evaluation of the *Lumos Glasses*, performed by TÜV SÜD Canada Inc. in accordance with IEC 62471:2006, *Photobiological Safety of Lamps and Lamp Systems*. Testing was conducted at the standard 200 mm evaluation distance and confirmed that the device meets all photobiological safety limits, achieving classification as **Risk Group 0 (Exempt)**.

- **Testing Laboratory:** TÜV SÜD Canada Inc., 11 Gordon Collins Drive, Gormley, Ontario, Canada
- **Report Reference No.:** 7169009669-000
- **Date of Issue:** 2022-03-21
- **Test Specification:** IEC 62471:2006
- **Result:** Risk Group 0 (Exempt) — Complies with all photobiological safety limits

A complete copy of the certified report is provided on the following pages for reference.

Test Report issued under the responsibility of:

TÜV SÜD Canada Inc
11 Gordon Collins Drive, Gormley,
Ontario, L0H 1G0, Canada

TEST REPORT
IEC 62471
Photobiological safety of lamps and lamp systems

Report Reference No. ..... :	7169009669-000
Date of issue ..... :	2022-03-21
Total number of pages ..... :	18
Name of Testing Laboratory preparing the Report ..... :	TÜV SÜD Canada Inc. 11 Gordon Collins Drive, Gormley, Ontario, L0H 1G0, Canada
Applicant's name..... :	Lumos Health
Address ..... :	544 Brookhaven Crescent, Waterloo, Ontario N2L 4R7, Canada
Test specification:	
Standard ..... :	IEC 62471:2006
Test procedure ..... :	N/A
Non-standard test method…… :	N/A
Test Report Form No. ..... :	IEC62471B
TRF Originator ..... :	VDE Testing and Certification Institute
Master TRF ..... :	Dated 2018-08-16

Copyright © 2018 IEC System for Conformity Testing and Certification of Electrical Equipment (IECEE), Geneva, Switzerland. All rights reserved.

This publication may be reproduced in whole or in part for non-commercial purposes as long as the IECEE is acknowledged as copyright owner and source of the material. IECEE takes no responsibility for and will not assume liability for damages resulting from the reader's interpretation of the reproduced material due to its placement and context.

This report is not valid as a CB Test Report unless signed by an approved CB Testing Laboratory and appended to a CB Test Certificate issued by an NCB in accordance with IECEE 02.

General disclaimer:

The test results presented in this report relate only to the object tested.
This report shall not be reproduced, except in full, without the written approval of the Issuing CB Testing Laboratory. The authenticity of this Test Report and its contents can be verified by contacting the NCB, responsible for this Test Report.

Disclaimer: This document is controlled and has been released electronically.
Only the version on the IECEE Website is the current document version

Test item description .....:	Light Therapy Glasses
Trade Mark .....:	Lumos
Manufacturer.....:	Lumos Health. 544 Brookhaven Crescent, Waterloo, Ontario N2L 4R7, Canada
Model/Type reference .....:	Lumos Glasses
Ratings .....:	3.3Vdc, 82mA

Responsible Testing Laboratory (as applicable), testing procedure and testing location(s):			
☒	**CB Testing Laboratory:**	TÜV SÜD Canada Inc.	
Testing location/ address ..... :		11 Gordon Collins Dr., Gormley, ON, L0H 1G0, Canada	
Tested by (name, function, signature) ..... :		Raymond Papa, Project Engineer	
Approved by (name, function, signature) .. :		Peter Keith, Project Engineer	
☐	**Testing procedure: CTF Stage 1:**		
Testing location/ address ..... :			
Tested by (name, function, signature) ..... :			
Approved by (name, function, signature) .. :			
☐	**Testing procedure: CTF Stage 2:**		
Testing location/ address ..... :			
Tested by (name + signature) ..... :			
Witnessed by (name, function, signature). :			
Approved by (name, function, signature) .. :			
☐	**Testing procedure: CTF Stage 3:**		
☐	**Testing procedure: CTF Stage 4:**		
Testing location/ address ..... :			
Tested by (name, function, signature) ..... :			
Witnessed by (name, function, signature). :			
Approved by (name, function, signature) .. :			
Supervised by (name, function, signature) :			

List of Attachments (including a total number of pages in each attachment):

Attachment 1: National Deviations CAN (1 Page)
Attachment 2: National Deviations EU (2 Pages)
Attachment 3: Photo Documentation (3 Pages)

Summary of testing: See below.

Only hazards resulting from photobiological radiation have been addressed.

Tests performed (name of test and test clause):	**Testing location:**
• 4.2.2 Angular subtense of source and measurement field-of-view • 4.3.1 Actinic UV hazard exposure limit for the skin and eye • 4.3.2 Near-UV hazard exposure limit for the eye • 4.3.3 Retina blue light hazard exposure limit • 4.3.4 Retina blue light hazard exposure limit – small source • 4.3.5 Retina thermal hazard exposure limit • 4.3.6 Retina thermal hazard exposure limit – weak visual stimulus • 4.3.7 Infrared radiation hazard exposure limit for the eye • 4.3.8 Thermal hazard exposure limit for the skin • 5.2.1 Irradiance measurements • 5.2.2. Radiance Measurements • 5.2.2.2 Alternative method • 5.3 Analysis Method • 6.1 Continuous Wave lamps – Lamp classification	TÜV SÜD Canada Inc. 11 Gordon Collins Drive, Gormley, Ontario, L0H 1G0, Canada

Summary of compliance with National Differences (List of countries addressed):

See attachments 2 and 3.

Copy of marking plate:

The artwork below may be only a draft. The use of certification marks on a product must be authorized by the respective NCBs that own these marks.

No photobiological labels required for exempt group or RG1 bluelight.

Test item particulars ..... :	
Tested lamp ..... :	☒ continuous wave lamps ☐ pulsed lamps
Tested lamp system ..... :	LED lamp
Lamp classification group ..... :	☒ exempt ☐ risk 1 ☐ risk 2 ☐ risk 3
Lamp cap ..... :	LED Sources
Bulb ..... :	LED Device
Rated of the lamp ..... :	Refer to LED specifications.
Furthermore marking on the lamp ..... :	N/A
Seasoning of lamps according IEC standard ..... :	N/A
Used measurement instrument ..... :	List of equipment available on request.
Temperature by measurement ..... :	24 °C
Information for safety use ..... :	N/A
Possible test case verdicts:	
– **test case does not apply to the test object ..... :**	N/A
– **test object does meet the requirement ..... :**	P (Pass)
– **test object does not meet the requirement ..... :**	F (Fail)
Testing:	
Date of receipt of test item ..... :	2022-03-18
Date (s) of performance of tests ..... :	2022-03-21
General remarks:	
"(See Enclosure #)" refers to additional information appended to the report. "(See appended table)" refers to a table appended to the report. **Throughout this report a ☐ comma / ☒ point is used as the decimal separator.**	
Manufacturer's Declaration per sub-clause 4.2.5 of IECEE 02:	
The application for obtaining a CB Test Certificate includes more than one factory location and a declaration from the Manufacturer stating that the sample(s) submitted for evaluation is (are) representative of the products from each factory has been provided ..... :	☐ **Yes** ☒ **Not applicable**
When differences exist; they shall be identified in the General product information section.	
Name and address of factory (ies) ..... :	Lumos Health 544 Brookhaven Crescent, Waterloo, Ontario N2L 4R7, Canada
General product information and other remarks: The EUT are Light Therapy Glasses which project LED light on the glasses and reflect light back into the user's eyes. Device is battery powered, USB charged, and Bluetooth enabled. **Only hazards resulting from photobiological radiation have been addressed.**	

IEC 62471			
Clause	Requirement + Test	Result – Remark	Verdict

4	**EXPOSURE LIMITS**		**P**
4.1	General		P
	The exposure limits in this standard is not less than 0,01 ms and not more than any 8-hour period and should be used as guides in the control of exposure		P
	Detailed spectral data of a light source are generally required only if the luminance of the source exceeds 10^4 cd·m^{-2}	See clause 4.3.	P
4.3	Hazard exposure limits		P
4.3.1	Actinic UV hazard exposure limit for the skin and eye		P
	The exposure limit for effective radiant exposure is 30 J·m^{-2} within any 8-hour period	See table 6.1.	P
	To protect against injury of the eye or skin from ultraviolet radiation exposure produced by a broad-band source, the effective integrated spectral irradiance , E_S, of the light source shall not exceed the levels defined by:	See equation below.	P
	$E_s \cdot t = \sum_{200}^{400} \sum_{t} E_\lambda(\lambda,t) \cdot S_{UV}(\lambda) \cdot \Delta t \cdot \Delta\lambda \le 30$ J·m^{-2}	See table 6.1.	P
	The permissible time for exposure to ultraviolet radiation incident upon the unprotected eye or skin shall be computed by:	See equation below.	P
	$t_{max} = \frac{30}{E_s}$ s	See table 6.1.	P
4.3.2	Near-UV hazard exposure limit for eye		P
	For the spectral region 315 nm to 400 nm (UV-A) the total radiant exposure to the eye shall not exceed 10000 J·m^{-2} for exposure times less than 1000 s. For exposure times greater than 1000 s (approximately 16 minutes) the UV-A irradiance for the unprotected eye, E_{UVA}, shall not exceed 10 W·m^{-2}.	See table 6.1.	P
	The permissible time for exposure to ultraviolet radiation incident upon the unprotected eye for time less than 1000 s, shall be computed by:	See equation below.	P
	$t_{max} \le \frac{10\,000}{E_{UVA}}$ s	See table 6.1.	P
4.3.3	Retinal blue light hazard exposure limit		P
	To protect against retinal photochemical injury from chronic blue-light exposure, the integrated spectral radiance of the light source weighted against the blue-light hazard function, B(λ), i.e., the blue-light weighted radiance , L_B, shall not exceed the levels defined by:	See table 6.1. See equation below.	P

IEC 62471			
Clause	Requirement + Test	Result – Remark	Verdict
	$L_B \cdot t = \sum_{300}^{700} \sum_{t} L_\lambda(\lambda,t) \cdot B(\lambda) \cdot \Delta t \cdot \Delta\lambda \le 10^6$ $J \cdot m^{-2} \cdot sr^{-1}$	for t ≤ 10^4 s $t_{max} = \frac{10^6}{L_B}$	P
	$L_B = \sum_{300}^{700} L_\lambda \cdot B(\lambda) \cdot \Delta\lambda \le 100$ $W \cdot m^{-2} \cdot sr^{-1}$	for t > 10^4 s	P
4.3.4	Retinal blue light hazard exposure limit - small source		N/A
	Thus the spectral irradiance at the eye E_λ, weighted against the blue-light hazard function B(λ) shall not exceed the levels defined by:		N/A
	$E_B \cdot t = \sum_{300}^{700} \sum_{t} E_\lambda(\lambda,t) \cdot B(\lambda) \cdot \Delta t \cdot \Delta\lambda \le 100$ $J \cdot m^{-2}$		N/A
	$E_B = \sum_{300}^{700} E_\lambda \cdot B(\lambda) \cdot \Delta\lambda \le 1$ $W \cdot m^{-2}$		N/A
4.3.5	Retinal thermal hazard exposure limit		P
	To protect against retinal thermal injury, the integrated spectral radiance of the light source, L_λ, weighted by the burn hazard weighting function R(λ) (from Figure 4.2 and Table 4.2), i.e., the burn hazard weighted radiance, shall not exceed the levels defined by:	See equation below.	P
	$L_R = \sum_{380}^{1400} L_\lambda \cdot R(\lambda) \cdot \Delta\lambda \le \frac{50\,000}{\alpha \cdot t^{0,25}}$ $W \cdot m^{-2} \cdot sr^{-1}$	(10 µs ≤ t ≤ 10 s)	P
4.3.6	Retinal thermal hazard exposure limit – weak visual stimulus		P
	For an infrared heat lamp or any near-infrared source where a weak visual stimulus is inadequate to activate the aversion response, the near infrared (780 nm to 1400 nm) radiance, L_{IR}, as viewed by the eye for exposure times greater than 10 s shall be limited to:	See equation below.	P
	$L_{IR} = \sum_{780}^{1400} L_\lambda \cdot R(\lambda) \cdot \Delta\lambda \le \frac{6\,000}{\alpha}$ $W \cdot m^{-2} \cdot sr^{-1}$	t > 10 s	P
4.3.7	Infrared radiation hazard exposure limits for the eye		P
	The avoid thermal injury of the cornea and possible delayed effects upon the lens of the eye (cataractogenesis), ocular exposure to infrared radiation, E_{IR}, over the wavelength range 780 nm to 3000 nm, for times less than 1000 s, shall not exceed:	See equation below.	P
	$E_{IR} = \sum_{780}^{3\,000} E_\lambda \cdot \Delta\lambda \le 18\,000 \cdot t^{-0,75}$ $W \cdot m^{-2}$	t ≤ 1000 s	N/A
	For times greater than 1000 s the limit becomes:		N/A
	$E_{IR} = \sum_{780}^{3\,000} E_\lambda \cdot \Delta\lambda \le 100$ $W \cdot m^{-2}$	t > 1000 s	N/A

IEC 62471			
Clause	Requirement + Test	Result – Remark	Verdict
4.3.8	Thermal hazard exposure limit for the skin		P
	Visible and infrared radiant exposure (380 nm to 3000 nm) of the skin shall be limited to:		P
	$E_H \cdot t = \sum_{380}^{3\,000} \sum_{t} E_\lambda(\lambda,t) \cdot \Delta t \cdot \Delta\lambda \le 20\,000 \cdot t^{0,25}$ J · m^{-2}		P
5	**MEASUREMENT OF LAMPS AND LAMP SYSTEMS**		P
5.1	Measurement conditions		P
	Measurement conditions shall be reported as part of the evaluation against the exposure limits and the assignment of risk classification.	Considered.	P
5.1.1	Lamp ageing (seasoning)	LED Diode, not required.	N/A
	Seasoning of lamps shall be done as stated in the appropriate IEC lamp standard.		N/A
5.1.2	Test environment		P
	For specific test conditions, see the appropriate IEC lamp standard or in absence of such standards, the appropriate national standards or manufacturer's recommendations.	Tested as per manufacturer's recommendations.	P
5.1.3	Extraneous radiation		P
	Careful checks should be made to ensure that extraneous sources of radiation and reflections do not add significantly to the measurement results.	All measurements were made in a room with negligible extraneous radiation.	P
5.1.4	Lamp operation		P
	Operation of the test lamp shall be provided in accordance with:	Verified.	P
	– the appropriate IEC lamp standard, or		P
	– the manufacturer' s recommendation		P
5.1.5	Lamp system operation		P
	The power source for operation of the test lamp shall be provided in accordance with:	Verified.	P
	– the appropriate IEC standard, or		P
	– the manufacturer' s recommendation		P
5.2	Measurement procedure		P
5.2.1	Irradiance measurements		P
	Minimum aperture diameter 7mm.	Applied.	P
	Maximum aperture diameter 50 mm.	Applied.	P
	The measurement shall be made in that position of the beam giving the maximum reading.	Measurements were made at location which produced maximum radiation.	P
	The measurement instrument is adequate calibrated.	All measurement instruments with valid calibration.	P

IEC 62471			
Clause	Requirement + Test	Result – Remark	Verdict
5.2.2	Radiance measurements	Radiance meter was used.	P
5.2.2.1	Standard method	Considered.	P
	The measurements made with an optical system.	List of test equipment retained on file.	P
	The instrument shall be calibrated to read in absolute radiant power per unit receiving area and per unit solid angle to acceptance averaged over the field of view of the instrument.	List of test equipment retained on file.	P
5.2.2.2	Alternative method	Not applicable for the subject.	N/A
	Alternatively to an imaging radiance set-up, an irradiance measurement set-up with a circular field stop placed at the source can be used to perform radiance measurements.		N/A
5.2.3	Measurement of source size		P
	The determination of α, the angle subtended by a source, requires the determination of the 50% emission points of the source.	Calliper and laser measuring tape were used for measurements.	P
5.2.4	Pulse width measurement for pulsed sources	CW considered and measured.	N/A
	The determination of Δt, the nominal pulse duration of a source, requires the determination of the time during which the emission is > 50% of its peak value.		N/A
5.3	Analysis methods		P
5.3.1	Weighting curve interpolations	Logarithmic interpolation applied.	P
	To standardize interpolated values, use linear interpolation on the log of given values to obtain intermediate points at the wavelength intervals desired.	see table 4.1	P
5.3.2	Calculations		P
	The calculation of source hazard values shall be performed by weighting the spectral scan by the appropriate function and calculating the total weighted energy.	Appropriate weighting functions per respective wavelengths applied to all calculations.	P
5.3.3	Measurement uncertainty		P
	The quality of all measurement results must be quantified by an analysis of the uncertainty.	see Annex C in the norm	P
6	**LAMP CLASSIFICATION**		P
	For the purposes of this standard it was decided that the values shall be reported as follows:	see table 6.1	P
	– for lamps intended for general lighting service, the hazard values shall be reported as either irradiance or radiance values at a distance which produces an illuminance of 500 lux, but not at a distance less than 200 mm	Non-GLS.	N/A

IEC 62471			
Clause	Requirement + Test	Result – Remark	Verdict
	– for all other light sources, including pulsed lamp sources, the hazard values shall be reported at a distance of 200 mm	Distance evaluated at 200mm from the source.	P
6.1	Continuous wave lamps		P
6.1.1	Exempt Group		P
	In the exempt group are lamps, which does not pose any photobiological hazard. The requirement is met by any lamp that does not pose:	Exempt Group.	P
	– an actinic ultraviolet hazard (E_S) within 8-hours exposure (30000 s), nor		P
	– a near-UV hazard (E_{UVA}) within 1000 s, (about 16 min), nor		P
	– a retinal blue-light hazard (L_B) within 10000 s (about 2,8 h), nor		P
	– a retinal thermal hazard (L_R) within 10 s, nor		P
	– an infrared radiation hazard for the eye (E_{IR}) within 1000 s		P
6.1.2	Risk Group 1 (Low-Risk)		N/A
	In this group are lamps, which exceeds the limits for the exempt group but that does not pose:	Exempt Group.	N/A
	– an actinic ultraviolet hazard (E_S) within 10000 s, nor		N/A
	– a near ultraviolet hazard (E_{UVA}) within 300 s, nor		N/A
	– a retinal blue-light hazard (L_B) within 100 s, nor		N/A
	– a retinal thermal hazard (L_R) within 10 s, nor		N/A
	– an infrared radiation hazard for the eye (E_{IR}) within 100 s		N/A
	Lamps that emit infrared radiation without a strong visual stimulus and do not pose a near-infrared retinal hazard (L_{IR}), within 100 s are in Risk Group 1.		N/A
6.1.3	Risk Group 2 (Moderate-Risk)		N/A
	This requirement is met by any lamp that exceeds the limits for Risk Group 1, but that does not pose:	Exempt Group.	N/A
	– an actinic ultraviolet hazard (E_S) within 1000 s exposure, nor		N/A
	– a near ultraviolet hazard (E_{UVA}) within 100 s, nor		N/A
	– a retinal blue-light hazard (L_B) within 0,25 s (aversion response), nor		N/A
	– a retinal thermal hazard (L_R) within 0,25 s (aversion response), nor		N/A
	– an infrared radiation hazard for the eye (E_{IR}) within 10 s		N/A

IEC 62471			
Clause	Requirement + Test	Result – Remark	Verdict
	Lamps that emit infrared radiation without a strong visual stimulus and do not pose a near-infrared retinal hazard (L_{IR}), within 10 s are in Risk Group 2.		N/A
6.1.4	Risk Group 3 (High-Risk)		N/A
	Lamps which exceed the limits for Risk Group 2 are in Group 3.	Exempt Group.	N/A
6.2	Pulsed lamps		N/A
	Pulse lamp criteria shall apply to a single pulse and to any group of pulses within 0,25 s.	CW lamp.	N/A
	A pulsed lamp shall be evaluated at the highest nominal energy loading as specified by the manufacturer.		N/A
	The risk group determination of the lamp being tested shall be made as follows:		N/A
	– a lamp that exceeds the exposure limit shall be classified as belonging to Risk Group 3 (High-Risk)		N/A
	– for single pulsed lamps, a lamp whose weighted radiant exposure or weighted radiance does is below the EL shall be classified as belonging to the Exempt Group		N/A
	– for repetitively pulsed lamps, a lamp whose weighted radiant exposure or weighted radiance dose is below the EL, shall be evaluated using the continuous wave risk criteria discussed in clause 6.1, using time averaged values of the pulsed emission		N/A

IEC 62471			
Clause	Requirement + Test	Result – Remark	Verdict

Table 4.1	Spectral weighting function for assessing ultraviolet hazards for skin and eye	-

Wavelength[1] λ, nm	**UV hazard function $S_{uv}(\lambda)$**	**Wavelength λ, nm**	**UV hazard function $S_{uv}(\lambda)$**
200	0,030	313*	0,006
205	0,051	315	0,003
210	0,075	316	0,0024
215	0,095	317	0,0020
220	0,120	318	0,0016
225	0,150	319	0,0012
230	0,190	320	0,0010
235	0,240	322	0,00067
240	0,300	323	0,00054
245	0,360	325	0,00050
250	0,430	328	0,00044
254*	0,500	330	0,00041
255	0,520	333*	0,00037
260	0,650	335	0,00034
265	0,810	340	0,00028
270	1,000	345	0,00024
275	0,960	350	0,00020
280*	0,880	355	0,00016
285	0,770	360	0,00013
290	0,640	365*	0,00011
295	0,540	370	0,000093
297*	0,460	375	0,000077
300	0,300	380	0,000064
303*	0,120	385	0,000053
305	0,060	390	0,000044
308	0,026	395	0,000036
310	0,015	400	0,000030

[1] Wavelengths chosen are representative: other values should be obtained by logarithmic interpolation at intermediate wavelengths.
* Emission lines of a mercury discharge spectrum.

IEC 62471			
Clause	Requirement + Test	Result – Remark	Verdict

Table 4.2	Spectral weighting functions for assessing retinal hazards from broadband optical sources	-

Wavelength nm	**Blue-light hazard function B (λ)**	**Burn hazard function R (λ)**
300	0,01	
305	0,01	
310	0,01	
315	0,01	
320	0,01	
325	0,01	
330	0,01	
335	0,01	
340	0,01	
345	0,01	
350	0,01	
355	0,01	
360	0,01	
365	0,01	
370	0,01	
375	0,01	
380	0,01	0,1
385	0,013	0,13
390	0,025	0,25
395	0,05	0,5
400	0,10	1,0
405	0,20	2,0
410	0,40	4,0
415	0,80	8,0
420	0,90	9,0
425	0,95	9,5
430	0,98	9,8
435	1,00	10,0
440	1,00	10,0
445	0,97	9,7
450	0,94	9,4
455	0,90	9,0
460	0,80	8,0
465	0,70	7,0
470	0,62	6,2
475	0,55	5,5
480	0,45	4,5
485	0,40	4,0
490	0,22	2,2
495	0,16	1,6
500-600	$10^{[(450-\lambda)/50]}$	1,0
600-700	0,001	1,0
700-1050		$10^{[(700-\lambda)/500]}$
1050-1150		0,2
1150-1200		$0{,}2 \cdot 10^{0{,}02(1150-\lambda)}$
1200-1400		0,02

IEC 62471			
Clause	Requirement + Test	Result – Remark	Verdict

Table 5.4	Summary of the ELs for the surface of the skin or cornea (irradiance based values)	-

Hazard Name	Relevant equation	Wavelength range nm	Exposure duration sec	Limiting aperture rad (deg)	EL in terms of constant irradiance $W \cdot m^{-2}$
Actinic UV skin & eye	$E_S = \sum E_\lambda \cdot S(\lambda) \cdot \Delta\lambda$	200 – 400	< 30000	1,4 (80)	30/t
Eye UV-A	$E_{UVA} = \sum E_\lambda \cdot \Delta\lambda$	315 – 400	≤1000 >1000	1,4 (80)	10000/t 10
Blue-light small source	$E_B = \sum E_\lambda \cdot B(\lambda) \cdot \Delta\lambda$	300 – 700	≤100 >100	< 0,011	100/t 1,0
Eye IR	$E_{IR} = \sum E_\lambda \cdot \Delta\lambda$	780 –3000	≤1000 >1000	1,4 (80)	$18000/t^{0,75}$ 100
Skin thermal	$E_H = \sum E_\lambda \cdot \Delta\lambda$	380 – 3000	< 10	2π sr	$20000/t^{0,75}$

Table 5.5	Summary of the ELs for the retina (radiance based values)	-

Hazard Name	Relevant equation	Wavelength range nm	Exposure duration sec	Field of view radians	EL in terms of constant radiance $W \cdot m^{-2} \cdot sr^{-1}$)
Blue light	$L_B = \sum L_\lambda \cdot B(\lambda) \cdot \Delta\lambda$	300 – 700	0,25 – 10 10-100 100-10000 ≥ 10000	$0,011 \cdot \sqrt{(t/10)}$ 0,011 $0,0011 \cdot \sqrt{t}$ 0,1	$10^6/t$ $10^6/t$ $10^6/t$ 100
Retinal thermal	$L_R = \sum L_\lambda \cdot R(\lambda) \cdot \Delta\lambda$	380 – 1400	< 0,25 0,25 – 10	0,0017 $0,011 \cdot \sqrt{(t/10)}$	$50000/(\alpha \cdot t^{0,25})$ $50000/(\alpha \cdot t^{0,25})$
Retinal thermal (weak visual stimulus)	$L_{IR} = \sum L_\lambda \cdot R(\lambda) \cdot \Delta\lambda$	780 – 1400	> 10	0,011	6000/α

IEC 62471			
Clause	Requirement + Test	Result – Remark	Verdict

Table 6.1	Emission limits for risk groups of continuous wave lamps									-
Risk	Action spectrum	Symbol	Units	Emission Measurement						
				Exempt		Low risk		Mod risk		
				Limit	Result	Limit	Result	Limit	Result	
Actinic UV	$S_{UV}(\lambda)$	E_s	$W \cdot m^{-2}$	0.001	0.00023	0.003	n/a	0.03	n/a	
Near UV		E_{UVA}	$W \cdot m^{-2}$	10	0.00053	33	n/a	100	n/a	
Blue light	B(λ)	L_B	$W \cdot m^{-2} \cdot sr^{-1}$	100	55.059	10000	n/a	4000000	n/a	
Blue light, small source	B(λ)	E_B	$W \cdot m^{-2}$	1.0*	n/a	1.0	n/a	400	n/a	
Retinal thermal	R(λ)	L_R	$W \cdot m^{-2} \cdot sr^{-1}$	28000/α = 1120058.3	0.7479	28000/α = 1120058.3	n/a	71000/α = 2840147.9	n/a	
Retinal thermal, weak visual stimulus**	R(λ)	L_{IR}	$W \cdot m^{-2} \cdot sr^{-1}$	6000/α = 240012.5	n/a	6000/α = 240012.5	n/a	6000/α = 240012.5	n/a	
IR radiation, eye		E_{IR}	$W \cdot m^{-2}$	100	0.0565	570	n/a	3200	n/a	

* Small source defined as one with α < 0,011 radian. Averaging field of view at 10000 s is 0,1 radian.
** Involves evaluation of non-GLS source
Device was operated running at maximum settings. Source dimension of 5x5mm and angular subtense of 25mrad. Equipment was evaluated 200mm from the exit aperture.

IEC 62471			
Clause	Requirement + Test	Result – Remark	Verdict

Table 6.1	Emission limits for risk groups of continuous wave lamps									-
Risk	Action spectrum	Symbol	Units	Emission Measurement						
				Exempt		Low risk		Mod risk		
				Limit	Result	Limit	Result	Limit	Result	
Actinic UV	$S_{UV}(\lambda)$	E_S	$W \cdot m^{-2}$	0.001	0.00028	0.003	n/a	0.03	n/a	
Near UV		E_{UVA}	$W \cdot m^{-2}$	10	0.00018	33	n/a	100	n/a	
Blue light	B(λ)	L_B	$W \cdot m^{-2} \cdot sr^{-1}$	100	2260	10000	0.0373	4000000	n/a	
Blue light, small source	B(λ)	E_B	$W \cdot m^{-2}$	1.0*	n/a	1.0	n/a	400	n/a	
Retinal thermal	R(λ)	L_R	$W \cdot m^{-2} \cdot sr^{-1}$	28000/α = 1120058.3	0.7479	28000/α = 1120058.3	n/a	71000/α = 2840147.9	n/a	
Retinal thermal, weak visual stimulus**	R(λ)	L_{IR}	$W \cdot m^{-2} \cdot sr^{-1}$	6000/α = 240012.5	n/a	6000/α = 240012.5	n/a	6000/α = 240012.5	n/a	
IR radiation, eye		E_{IR}	$W \cdot m^{-2}$	100	0.0356	570	n/a	3200	n/a	

* Small source defined as one with α < 0,011 radian. Averaging field of view at 10000 s is 0,1 radian.
** Involves evaluation of non-GLS source
Device was operated running at maximum settings. Source dimension of 5x5mm and angular subtense of 25mrad. Equipment was evaluated 5mm from the exit aperture. Measurement taken for reference only. Measurement evaluated as Risk Group 1 for Blue-light

IEC 62471			
Clause	Requirement + Test	Result – Remark	Verdict

Table 6.1	Emission limits for risk groups of continuous wave lamps								-
Risk	Action spectrum	Symbol	Units	Emission Measurement					
				Exempt		Low risk		Mod risk	
				Limit	Result	Limit	Result	Limit	Result
Actinic UV	$S_{UV}(\lambda)$	E_S	$W \cdot m^{-2}$	0.001	0.00028	0.003	n/a	0.03	n/a
Near UV		E_{UVA}	$W \cdot m^{-2}$	10	0.00045	33	n/a	100	n/a
Blue light	B(λ)	L_B	$W \cdot m^{-2} \cdot sr^{-1}$	100	96.85	10000	0.0373	4000000	n/a
Blue light, small source	B(λ)	E_B	$W \cdot m^{-2}$	1.0*	n/a	1.0	n/a	400	n/a
Retinal thermal	R(λ)	L_R	$W \cdot m^{-2} \cdot sr^{-1}$	28000/α = 1120058.3	0.7479	28000/α = 1120058.3	n/a	71000/α = 2840147.9	n/a
Retinal thermal, weak visual stimulus**	R(λ)	L_{IR}	$W \cdot m^{-2} \cdot sr^{-1}$	6000/α = 240012.5	n/a	6000/α = 240012.5	n/a	6000/α = 240012.5	n/a
IR radiation, eye		E_{IR}	$W \cdot m^{-2}$	100	0.0123	570	n/a	3200	n/a

* Small source defined as one with α < 0,011 radian. Averaging field of view at 10000 s is 0,1 radian.
** Involves evaluation of non-GLS source
Device was operated running at maximum settings. Source dimension of 5x5mm and angular subtense of 25mrad. Equipment was evaluated 5mm from the exit aperture and powered at 15% max intensity. Measurement taken for reference only. Measurement evaluated as Exempt

	TABLE: Critical components information				P
Object / part No.	**Manufacturer/ trademark**	**Type / model**	**Technical data**	**Standard**	**Mark(s) of conformity[1)]**
LEDs	OSRAM Opto Semiconductors Inc.	LB CRBP-HYJZ-46-8E8F-350-S	475nm, 2.8V, 350mA, 53lm/W	-	Assessed in this report.
Supplementary information: [1)] Provided evidence ensures the agreed level of compliance. See OD-CB2039.					

Furthermore remarks:

Hazard	Risk Group
Actinic UV	**Exempt**
Near UV	**Exempt**
Blue Light	**Exempt**
Retinal Thermal	**Exempt**
Infrared	**Exempt**
Thermal Skin	**Pass**

List of test equipment used:

A completed list of used test equipment shall be provided in the Test Reports when a Customer's Testing Facility according to CTF stage 1 or CTF stage 2 procedure has been used.
Note: This page may be removed when CTF stage 1 or CTF stage 2 are not used. See also clause 4.8 in OD 2020 for more details.

Clause	Measurement / testing	Testing / measuring equipment / material used, (Equipment ID)	Range used	Last Calibration date	Calibration due date
Retained on file at TÜV SÜD Canada.					

IEC62471B ATTACHMENT 1			
Clause	Requirement + Test	Result - Remark	Verdict
ATTACHMENT TO TEST REPORT **IEC 62471:2006** **CANADA NATIONAL DIFFERENCES** **Photobiological safety of lamps and lamp systems**			
Differences according to ..... : CAN/CSA-C22.2 No. 62471:2012 **Attachment Form No**. ..... : CA_ND_IEC62471B **Attachment Originator**..... : CSA Group **Master Attachment**..... : 2019-11-01			
Copyright © 2019 IEC System for Conformity Testing and Certification of Electrical Equipment (IECEE), Geneva, Switzerland. All rights reserved.			

	CA – Canada – National Differences		-
	National differences of IEC Publication 62471, Photobiological Safety of Lamps and Lamp Systems:		P
2	**NORMATIVE REFERENCES**		—
	Any reference to International Standards that are adopted as National Standards of Canada subsequent to the publication of CAN/CSA-C22.2 No. 62471 shall be replaced by the relevant National Standard of Canada.		P

IEC62471B ATTACHMENT 2			
Clause	Requirement + Test	Result - Remark	Verdict
ATTACHMENT TO TEST REPORT IEC 62471 **EUROPEAN GROUP DIFFERENCES AND NATIONAL DIFFERENCES** Photobiological safety of lamps and lamps systems			
Differences according to..... EN 62471:2008			
Annex Form No..... EU_GD_IEC62471B **Annex Form Originator .....** OVE **Master Annex Form.....** 2022-02-07			
Copyright © 2019 IEC System for Conformity Testing and Certification of Electrical Equipment (IECEE), Geneva, Switzerland. All rights reserved.			

	CENELEC COMMON MODIFICATIONS (EN)		-
4	**EXPOSURE LIMITS**		P
	Contents of the whole Clause 4 of IEC 62471:2006 moved into a new informative Annex ZB		—
	Clause 4 replaced by the following:		P
	Limits of the Artificial Optical Radiation Directive (2006/25/EC) have been applied instead of those fixed in IEC 62471:2006	See appended Table 6.1	P
4.1	General		P
	First paragraph deleted		—

Table 6.1 Emission limits for risk groups of continuous wave lamps (based on EU Directive 2006/25/EC)

Risk	Action spectrum	Symbol	Units	Emission Measurement					
				Exempt		Low risk		Mod risk	
				Limit	Result	Limit	Result	Limit	Result
Actinic UV	$S_{UV}(\lambda)$	E_S	$W \cdot m^{-2}$	0,001	***	-	-	-	-
Near UV		E_{UVA}	$W \cdot m^{-2}$	0,33	***	-	-	-	-
Blue light	$B(\lambda)$	L_B	$W \cdot m^{-2} \cdot sr^{-1}$	100	***	10000	***	4000000	***
Blue light, small source	$B(\lambda)$	E_B	$W \cdot m^{-2}$	0,01*	***	1,0	***	400	***
Retinal thermal	$R(\lambda)$	L_R	$W \cdot m^{-2} \cdot sr^{-1}$	28000/α	***	28000/α	***	71000/α	***
Retinal thermal, weak visual stimulus**	$R(\lambda)$	L_{IR}	$W \cdot m^{-2} \cdot sr^{-1}$	545000 0,0017≤ α ≤ 0,011	***				
				6000/α 0,011≤ α ≤ 0,1	***				
IR radiation, eye		E_{IR}	$W \cdot m^{-2}$	100	***	570	***	3200	***

* Small source defined as one with α < 0,011 radian. Averaging field of view at 10000 s is 0,1 radian.
** Involves evaluation of non-GLS source
*** Refer to main report for values

NOTE The action functions: see Table 4.1 and Table 4.2
The applicable aperture diameters: see 4.2.1
The limitations for the angular subtenses: see 4.2.2
The related measurement condition 5.2.3 and the range of acceptance angles: see Table 5.5.

Attachment No. 3

Photo Documentation

Attachment Contains

Cover Page .....: 1 Page

Photos .....: 2 Pages

Total Pages .....: 3 Pages

Enclosure – Front View



Enclosure – Side View



Enclosure - Rear View



LED Emission



Appendix P

Study Protocol (Version 18; March 14, 2024)

Synopsis

- Design: 16-week two-period crossover; masked; auto-crossover at Week 8.
- Participants: Key inclusion/exclusion; remote consent and screening.
- Intervention: Active vs. low-light melanopic targets; usage timing rules.
- Outcomes: Primary MADRS; secondary PROMIS, PVT, Word-Pair.
- Randomization/Masking: Slot-based allocation; concealed mapping.
- Safety: AE capture, relatedness, reporting; stopping/withdrawal rules.
- Amendments: Version history; analysis impact.

Study Protocol: Smart Light therapy glasses for sleep and mental wellness

Principal Investigator
Dr. Jonathan Oakman
jmoakman@uwaterloo.ca
1-519-888-4567 x43659
Department of Psychology
University of Waterloo

Student Investigator
Lucas Wen Tang
c5wen@uwaterloo.ca
1-206-422-6433
Masc. Candidate
Department of Mechanical and Mechatronics Engineering
University of Waterloo

Faculty Supervisor
Dr. Zhao Pan
zhao.pan@uwaterloo.ca
1-519-888-4567 x38631
Department of Mechanical and Mechatronics Engineering
University of Waterloo

Sponsor
Lumos Health Inc.
544 Brookhaven Cres, Waterloo, Ontario Canada, N2L4R7
www.lumoshealth.ca

Sponsor Monitor
Jianping (Felix) Xu
Software Engineer, Field Application Engineer, Lumos Health Inc.
felix.xu@uwaterloo.ca
1-647-895-8948

Table of Contents

Study Summary 5
Research Abstract: 7
Background 7
Pilot Study Synopsis 11
Study Goals and Objectives 11
Purpose: 11
Hypothesis: 11
Aim: 11
Primary Objective: 11
Secondary Objectives: 11
Study Design 12
Study population 12
Inclusion Criteria 12
Exclusion Criteria 12
Recruitment 13
Social Media Post (General): 13
Social Media post personal message: 13
Social Media post message (forwarded): 14
Screening 14
Informed Consent 15
Groups 15
Sampling and Group Creation: 15
Randomization and trial start 15
Staff 16
Education 16
Rewards 16
Masking 16
Adherence measurement 17
Adverse Events 17
Weekly Self-Assessments 18
Lifestyle changes 18
Glasses feedback on comfort and usability 18
Side effects reporting 18
Sleep questionnaire (PROMIS) 19
Mood questionnaire (MADRS) 19

Game - Assessments 19
Crisis planning 19
Primary Outcome 19
Study schedule 20
Sample Size and Power Calculations 20
Passive Data Collection 23
Study variables 24
Weekly Survey Variables: 25
Cognitive Testing Variables 25
Usage variables: 25
Participant Withdrawal 25
Participant Follow up and Loss Criteria 26
Participant Waitlist and Replacement 26
Conditions for Premature study termination 27
Data safety and monitoring board 27
Sponsor Monitor 29
Data management plan 29
Qualtrics survey Data 29
Clinical data from custom software 30
Other data 30
Data sharing after trial completion: 30
Data locking prior to analysis: 30
Participant privacy protection: 30
Trial Completion 30
Statement of Compliance 31
Investigational Device Description 31
Potential Benefits of Clinical Device 32
Potential Risks of Clinical Device 32
Potential confounding factors 33
Changes in going outdoor habits: 33
Environmental predispositions 33
Lifestyle predispositions 33
Genetic predispositions 33
Medication use 34
Other light therapy use 34
Participant sharing the glasses with others 34

References 34
Revision History 38
Glossary of Acronyms 39

Study Summary

Title	Smart Light therapy glasses for sleep and mental wellness
Methodology	Randomized, controlled trial, double blind study
Study Duration	16 weeks, in a crossover study with 8 weeks in each period
Objectives	**Primary Objective:** To evaluate the effectiveness of the Lumos light therapy glasses in improving depression and sleep scores in people who spend less than 2 hours outdoors per day in a double-blind trial. **Secondary Objectives:** To evaluate treatment acceptability, adherence, and how duration of light therapy glasses' usage influences changes in depression and sleep scores, reaction time, and memory.
Number of Subjects	96 subjects in 2 arms: Treatment and control
Diagnosis and Main Inclusion Criteria	**Inclusion Criteria:** Adults, any gender, 18+ years old, residing in Ontario Montgomery Asberg Depression Rating Scale Score > 7 or PROMIS score >25 Spend on average less than 2 hours outdoors daily. **Exclusion Criteria:** MADRS Score above 45, or MADRS suicide score is 5 or 6 People with eye disorders or previous eye surgeries. People who have cataracts, macular degeneration, diabetic retinopathy, or other eye disorders. People taking light sensitizing medication. People with bipolar, psychotic disorders or a history of these disorders. People with epilepsy, or history of epilepsy. People with electronic implants, such as pacemakers. Prescription glasses wearers, except for people who can self-supply contact

	lenses for the duration of the study. People who do not have an iOS or Android based smartphone Shift workers who work night shift or rotating shifts with night shifts
Study Regimen	Treatment Group: Standard dosage ~1000 melanopic lux via Lumos glasses Control Group: Minimum dosage ~30 melanopic lux via Lumos glasses
Statistical Methodology	Depression scores are measured using the MADRS, ranging from 0- 60, least severe to most severe Sleep Scores are rated using the Promis Sleep Disturbance Short Form, ranging from 8 – 40, least to most severe sleep disturbance Reaction time is measured using a smartphone guided game, where the user is asked to press a button on the Lumos glasses when they see the light turn on the glasses. The test will last for 3 minutes. Memory will be testing using the paired word test, of 3 rounds of 10 word pairs, presented in 1 second intervals.

Research Abstract:

Light has a fundamental impact on human biology, it triggers photoreceptors at the back of the retina to induce changes in the brain, affecting neurotransmitter levels such as melatonin and cortisol. For those struggling with depression and sleep, medical professionals generally recommend the use of a light therapy lamp for 30 minutes a day and the patient can improve within a few weeks of use. However, due to the practical limitations of current light therapy devices such as lamps and head gears, 30 minutes of therapy is often hard to adhere to and longer durations of light therapy are often considered infeasible.

On the other hand, while the intensity of a light box is brighter than average indoor conditions, it rarely exceeds the brightness of the natural outdoors. Research also suggests that spending time outdoors could be just as effective as light therapy in treating seasonal affective disorder. As such, it is possible that light therapy's role is to make up for a lack of natural light exposure. In this paper, it is hypothesized that the optimal benefits for light therapy can be achieved by simulating light conditions from natural daylight, meaning long durations of bright light during the day. For this to happen, it is crucial to overcome the technological and design barriers to receiving light therapy.

To overcome this barrier, a pair of light therapy glasses using an innovative coating was engineered by the investigator team (Lumos glasses). The glasses use a patent pending coating that reflects 480 nm electrically generated blue light from the temples and while allowing other wavelengths from the user's environment to pass through, enabling regular vision while receiving therapy. The usability of the glasses was validated in a 10 person pilot study in 2020 funded by the Idea Center at the University of Notre Dame. The users were instructed to use the glasses for at least 30 minutes a day over a period of 8 weeks. By the end of the study, the users on average wore the glasses for 35 minutes a day (116% adherence) and on average experienced improvements of 13.3 points on the Montgomery Asberg depression rating scale.

Afterwards, feedback from users were collected to improve design, reducing weight and improving comfort. In addition, a proprietary ambient light sensor measuring environmental melanopic lux and user adherence sensors were then engineered onto the glasses powered by a bluetooth low energy chip. Apps were developed on iOS and Android to collect sensor data and upload to the cloud. The sensors and app work together to enable a function that adjusts the light output of the glasses based on the user's ambient light levels and time of day. 200 of the new generation glasses were produced for a double-blind clinical trial.

The proposed trial aims to test the effects of the Lumos glasses, with a novel unique light delivery mechanism, at improving sleep, mood and cognition. The trial encourages users to use the glasses for as long as possible during the day and tracks usage time to study the effect of light therapy usage duration and its correlation with sleep, mood, reaction time, and memory in the general population.

Background

Light therapy is currently being recommended by medical professionals to treat sleep and seasonal mood disorders. There is also growing evidence on the effect of light therapy on treating non-seasonal depression [1,2].

Despite its significant effects in a clinical setting, the adoption of light therapy in the real world faces challenges, with studies reporting the adherence rate to light therapy lamps as low as 59% [3] , and longer term adherence rates as low as 11 - 42[4,5,6].

Light therapy visor type products such as the Re-timer allow users to be mobile while receiving

light therapy, thereby improving adherence. However, adherence levels are reported to be only moderate with users receiving on average 35 minutes a day for a protocol of 1 hour in a study for light therapy on PTSD symptoms [13].

Portable light therapy devices such as the Luminette glasses have also been shown to be effective at treatment depression symptoms in teenagers, improving scores in as little as 2 weeks [22]. However, it is also noted that in this study, one third of the participants dropped out due to the high responsibility to wear the glasses every morning. In addition, many adherence levels are done through self-report and may not accurately represent the actual time spent using light therapy due to inconsistent reporting by participants [14].

As such, much scientific research aims to contain the treatment with light therapy to shorter durations to have more practical value. Prescribing longer durations of usage is generally considered impractical [4].

On the other hand, it is estimated that the average American spends 90% of their life indoors [7], where lighting levels are orders of magnitude lower than outdoor conditions (100lux vs 100 000 lux) [8] . The time spent outdoors has positively skewed data having a median of 1.04 h and an average of 1.43 h on weekdays [9] indicating the most people spend little time indoors while few spend much longer hours outdoors.

An extreme example of the effects of the lack of sufficient lighting on human biology are demonstrated through cave experiments in the 1900s, where subjects observed physiological changes such as extended circadian rhythm to beyond 25 hours [10]. Long duration mars mission simulation studies with non-25-hour light dark cycles also reported psychological changes such as increased depression rates [11].

The modern person may experience a similar effect to these scientists and astronauts. By spending much of their time indoors where lighting levels are inconsistent with nature, often too dim during the day and too much in the evenings from artificial lights, the internal circadian rhythms are no longer enforced with the powerful light dark cycle from nature. Yet, the modern person often still requires adhering to a 24-hour work schedule. Over time, this could lead to challenges with sleep, energy and mood.

It is possible that light therapy works by treating a deficiency in healthy natural lighting. As such, this research presents the hypothesis that the ideal condition for light therapy is one that simulates the natural light dark cycle, on average 12 hours of bright light during the day, and 12 hours of darkness at night. Indeed, it was shown that natural 1 hour walk outside outperformed 0.5h of low dose artificial light (2500lux) in treating seasonal depression [12].

To validate this hypothesis from an interventional perspective, Lumos glasses will be used. The Lumos glasses were developed to look and feel like a regular pair of glasses, allowing modern day people to have more freedom and convenience to use light therapy during their busy days. Other researchers and engineers from companies such as Apple have also investigated improving the design for light therapy and have found that those who struggle with seasonal depression are receptive to such ideas [23].

The glasses was first invented in 2018, where the founder of the company Lumos, and Masc. researcher Lucas Tang conceptualized the idea of using dichroic coatings to perform wavelength selective reflection. By reflecting only blue light while allowing other wavelengths to pass through, a user can experience the most effective wavelength for light therapy while still seeing the world through the other colors.

The company was then joined by Dr. Jamie Zeitzer in 2019, the world's leading photobiology researcher from Stanford medicine, who provided guidance on wavelength and brightness requirements. Such as the usage of melanopic lux to measure and gauge light based on the ganglion cell response centered around the 480nm wavelength [20]. The ingenuity of the design is that the glasses emit 480nm wavelength light, which is highly effective for activating the melanopsin photoreceptors found at the intrinsically photosensitive retinal ganglion cells. This wavelength has been shown to be highly efficient for light therapy as only 11.2 lux of this type of light can achieve ~75% of the effects of 10 000 lux of white light from conventional indoor lights [24]. The patent pending coating of the glasses are also designed to reflect only this wavelength of light emitted by the glasses' side legs, allowing other light frequencies to pass through to enable highly efficient light therapy while allowing for regular vision by the user. A render of the glasses design and light path is shown in figure 1 below. Since then, the company has developed proprietary melanopic lux sensor technology and daylight matching algorithms based on this field of research. The company is also advised by Dr. Jeff Hovis from Optometry at the University of Waterloo on eye safety and contrast.

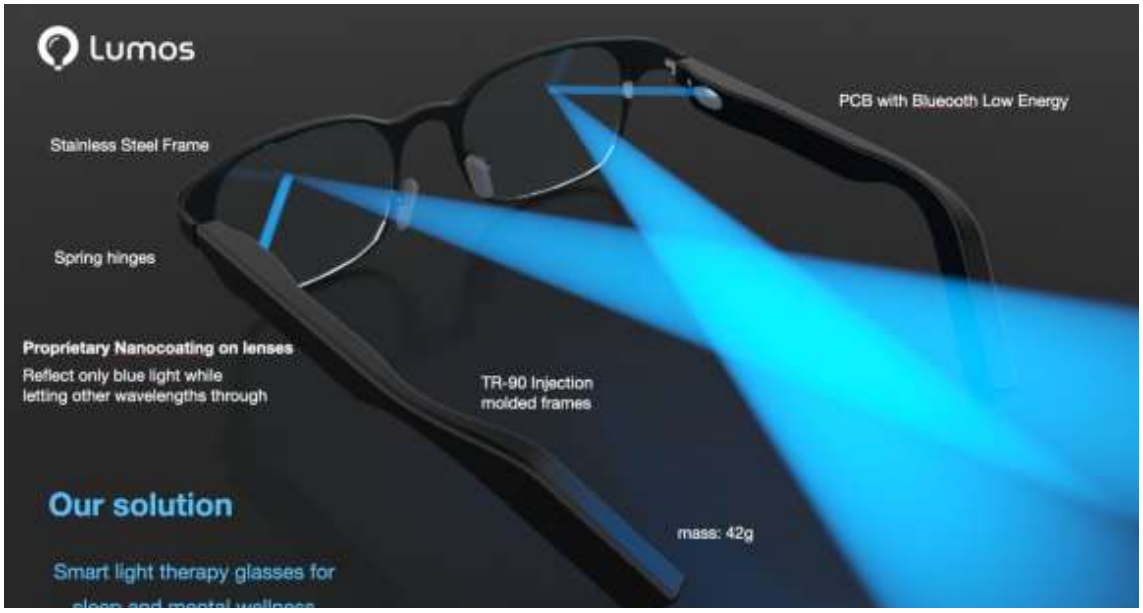


Figure 1 Lumos glasses render

With funding from the Accelerator Centre, Concept by Velocity, and University of Notre Dame, the company then successfully conducted a 10-person pilot study to gage usability and clinical effect, with promising results (see below for synopsis). The company then took feedback from the pilot study to engineer the 2021 clinical model, which is a higher volume production model with improved battery life, reduced weight, proprietary ambient light sensors, user detection, and Bluetooth low energy communications with a cloud connected app. The company is currently

producing 200 clinical grade Lumos light therapy glasses for early engagement and clinical studies. The clinical studies will be supervised by Professor Jon Oakman from clinical psychology at the University of Waterloo. Figure 2 and 3 below shows the 2020 pilot design and 2021 clinical design.



Figure 2 Lumos glasses 2020 Design



Figure 3 Lumos glasses 2021 clinical grade design

Pilot Study Synopsis

On February 23rd, 2020, with funding and supervision from the Idea Center at the University of Notre Dame, Lumos conducted a 10-person pilot study to compare adherence and effectiveness of the Lumos 2020 version product on its effect and improving mood via the Montgomery-Asberg Depression Rating Scale (MADRS, score from 0 to 60, mild to severe) and adherence to a schedule of 30 minutes per day. One participant dropped out due to personal reasons. After discounting this participant's data, the average starting MADRS is 21.7 (SD = 9.5, n = 9) and after 8 weeks, the average score is 8.3 (SD = 4.4, n = 9). This data is promising as the results are very closely matched with the light therapy lamp for depression study results from lam et al. [1]. In this study, the average adherence rate is 116% to a 30-minute per day schedule.

Study Goals and Objectives

Purpose:

To validate the effect of the Lumos light therapy glasses, with its unique nano-coating light delivery mechanism, on sleep, mood, and cognition in a double blind crossover randomized controlled trial.

Hypothesis:

Circadian rhythm has a significant impact on people's mood, sleep and cognition. People should be exposed to adequate levels of light during the day and minimal light at night time for good circadian health. Given that outdoor lighting can be up to 100 000 lux while indoor lighting rarely exceed 500 lux, many people who spend most of their days indoors could benefit from light therapy. Specifically, for people who spend on average less than 2 hours a day outdoors, and struggle with sleep and mood, light therapy using the Lumos glasses, with its unique light therapy delivery method using melanopic light reflected off a nanocoated lens, could lead to a significant improvement of their symptoms compared to placebo.

Aim:

To test the effectiveness of the Lumos glasses in improving sleep, mood, cognition and determine its optimal usage time for best health outcomes.

Primary Objective:

To evaluate the effectiveness of the Lumos light therapy glasses in improving depression, sleep and cognition scores in people who spend less than 2 hours outdoors per day and at least mildly struggling with sleep or mood, in a randomized, double-blind, superiority against placebo-controlled crossover trial.

Secondary Objectives:

To evaluate treatment acceptability, adherence, and how duration of light therapy glasses usage influences changes in depression and sleep scores, reaction time, and memory.

Study Design

A double blind randomized controlled trial using a crossover study design. 2 study arms are used in the study, the first arm receives the full intended dosage of light for the first 8 weeks of the study, and switches to the placebo level of dosage for the second 8 weeks of the study. The second arm receives the placebo level dosage for the first 8 weeks of the study and switches over to the full level of dosage for the final 8 weeks of the study. The investigators are blinded to this process as the glasses' cloud connected software makes the switch automatically in the backend of the server, which sends encrypted information about the user's grouping information to their smartphones, which has a decryption key in the app that then controls the light levels. The participants are blinded in a similar method as they are told they would be randomly assigned to one of two groups that crosses over between different intensities, and we don't know if either intensity may be effective at improving sleep and mood, which is like how the participants are informed in the light therapy for depression study by Lam et al [1]. This design adheres to ethical principles in that if the intended treatment does provide a benefit to the user, that both groups would in theory receive the same net benefits. From a scientific perspective, using the low intensity light as placebo has been shown to work in other cross-over designs for bright light therapy [28].

Study population

Inclusion Criteria

The study population is Ontario residents that are over 18 of age who experiences at least some struggles with sleep and mental health (MADRS > 7 or PROMIS raw > 25) and spend on average less than 2 hours outdoor daily.

Exclusion Criteria

People with MADRS score of > 45, or MADRS suicide score of 5 or 6, indicting severe depression or high suicide risk.

People with eye disorders or previous eye surgeries.

People who have cataracts, macular degeneration, diabetic retinopathy or other eye disorders.

People taking light sensitizing medication

People with psychotic disorder of history of psychotic disorders.

People with epilepsy or a history of epilepsy.

People with electronic implants, such as pacemakers

Prescription glasses wearers, except for people who are able to self-supply contact lenses for the duration of the study.

People who do not have an iOS or Android Smartphone.

Shift workers who work night shifts or have rotating shifts that involve night shifts

Recruitment

The recruitment method is convenient recruitment through social media (Facebook, LinkedIn), and University of Waterloo engineering department mental health wellness coordinator sending an email on behalf of the student investigator.

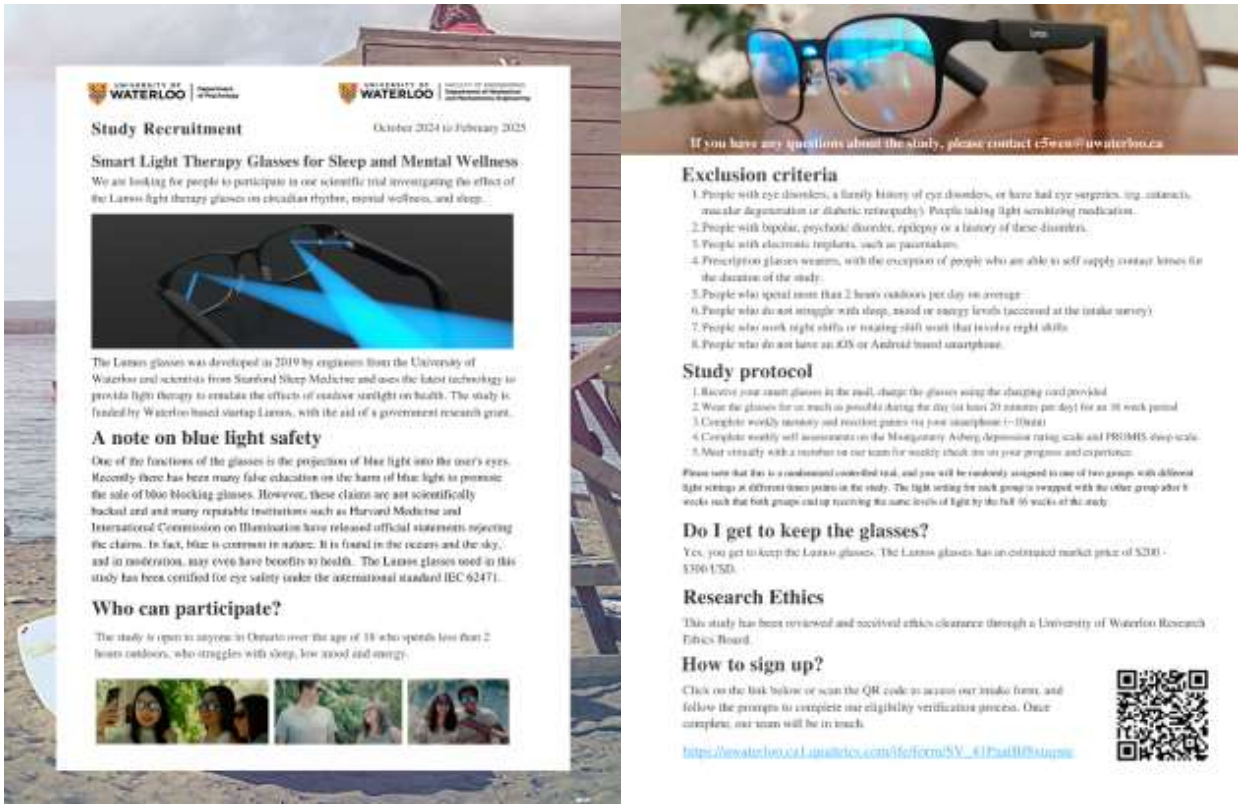


Figure 4 Recruitment poster

Social Media Post (General):

Hey everyone, we are running a trial “Smart light therapy glasses for sleep and mental wellness” to investigate the effectiveness of the Lumos light therapy glasses on improving sleep, mood, and cognition. If you are a resident of Ontario and are looking for the possibility to improve your mood and sleep, the study may be of interest to you. For participating in this 16-week trial, you get to keep the glasses at the end of the study. There are several eligibility requirements. Please see the attached recruitment poster for more details on eligibility and how to sign up.

Social Media post personal message:

Hi everyone, I’m looking for participants in my master’s thesis trial at the University of Waterloo, titled “Smart light therapy glasses for sleep and mental wellness”. I’ve been working on this idea for over 6 years, and I’m excited to say that this project is now in the formal scientific trial phase. I initially invented this pair of glasses with the intention to help me with my sleep and mood and now I’m looking to validate if this product can potentially benefit others as well. If you are a resident of Ontario and are looking for the potential possibility to improve your mood and sleep,

the study may be of interest to you. Please see the recruitment poster for details about the study. The study lasts 16 weeks, and you get to keep these glasses (valued at 200-300 USD).

There are several eligibility requirements. Please see the attached recruitment poster for more details on eligibility and how to sign up.

Social Media post message (forwarded):

A friend of mine, along with scientists from Stanford and designers from Apple, developed a special pair of blue light glasses (called Lumos) that has a chip inside, enabling you to connect it to your phone via Bluetooth so that you can have a personalized light therapy + blue light filter experience. 😎

He designed these specifically to help people with their circadian rhythm, and he is looking for people to join his study, which is now his master's degree thesis. This study will take place between October 2024 to April 2025 and is 16 weeks long. If you are a resident of Ontario and are looking for the potential possibility to improve your mood and sleep, the study may be of interest to you.

There are several eligibility requirements. Please see the attached recruitment poster for more details on eligibility. Once eligible, they will send you a pair of Lumos glasses and you get to keep it for FREE by the end of the study!

If you are interested check out the link attached to this post. Or email him directly at: Lucas Tang c5wen@uwaterloo.ca

Please feel free to pass this along to anyone you know who might be interested.

Screening

Initial Sign up will start when participants scan the QR code or click on the link on the recruitment poster, which will take them to a Qualtrics based informed consent form. If they have any questions, they can contact the investigators via the contact information section on the informed consent form.

If informed consent is obtained (point of enrolment = consent), they will be taken to a Qualtrics based initial intake and screening form, where participants would fill in an initial MADRS and PROMIS form, as well as answer questions about inclusion/exclusion criteria to determine eligibility.

Qualtrics intake survey link:
https://uwaterloo.ca1.qualtrics.com/jfe/form/SV_41PaalBf8xuqnie

If the person passes the automatic eligibility form via the Qualtrics link, and that there is an available spot in the strata to participate, a person from the trial staff will reach out to the participant to conduct an intake survey to double verify eligibility criteria including previous conditions and MADRS + PROMIS score. If the participant passes this verification, they will have

completed the screening process and the team will collect their address. A guideline on the screening verification interview is separately attached.

One additional screening will be done based on the location of the participants such that they are within access to a major city's mobile crisis response team or police in the case of an emergency mental health crisis (confirmation of eligibility).

If the person passes the eligibility form via the Qualtrics link, but there isn't a strata available for participation, they will be sent an email notifying them of the option to be put on a waitlist, and that they'll be notified at the latest by October 2024 on whether they'll be able to participate in the study.

Informed Consent

Participants are first taken to an informed consent form on Qualtrics, where they are provided an opportunity to read through the consent materials, contact the investigators via email, and a radio button and signature block are included to provide initial consent for an online eligibility verification survey. If the participant is deemed eligible for the study, they are then contacted by a member on the clinical staff, which follows a screening and verification protocol, where the staff member will speak to the participant either via phone or video call, where additional questions can be answered and key elements in the information letter discussed. Details about the informed consent form and the screening and verification protocol are separately attached. More information on compliance with the study can be found in the statement of compliance section.

Groups

Participants are randomly assigned upon signup into one of two groups.Control group (n=48): The control group receives the glasses with dim light exposure (~15 melanopic lux) for the first 8 weeks. After 8 weeks, the control group is crossed over to receive the treatment group dosage for 8 more weeks.

Treatment group (n=48): The treatment group receives full light treatment with nominal light exposure of ~1000 melanopic lux for 8 weeks, the treatment group's light is switched to the control group levels for another 8 weeks.

Sampling and Group Creation:

The study sampling is designed to be stratified, such that there are an even number of allocations based on sex at birth, age groups (18-40, and 40+), and MADRS score at intake (7-25, 26-45). This creates 8 recruitment groups each with a total of 12 people. Once 12 participants fill up the group, any participants who sign up after will be given the option to be put on a waitlist, where they would be contacted to participate in the study if any of the first 12 sign up participants drop out.

Randomization and trial start

271

Predefined stratification slots are randomized by a computer script and the treatment group

information is encrypted and hidden to the researchers and users. When a user signs up, they are placed into a slot within their stratification group, and the treatment plan will automatically follow based on the encrypted information. This slot-based randomization method allows for the trial to start on a rolling basis and stratification rollover in case of recruitment timeline constraints. Each participation slot has a unique ID, the randomized treatment group information will be encrypted via hashing (salted with the unique ID) and stored in the treatment slot. The glasses are designed that it will only work with a smartphone running the Lumos app that has logged in. Once logged in, the smartphone app will bash decrypt the grouping information and automatically drive the glasses based on the treatment arm.

Due to study timeline requirements, if the full stratification is not filled by the start of October 2024, the stratified groups will allow overflow, by first eliminating the sex at birth stratification, secondly the age stratification, and finally the starting MADRS score stratification such that participants on the waitlist can be rolled over in that manner.

Staff

The trial staff's responsibility is to check in with the participants on a weekly basis on a schedule that is preferred by the participant. The trial staff will consist of co-op student(s) hired from the University of Waterloo, who would be trained and supervised by graduate students of Psychology at the University of Waterloo, supervised by the principal investigator Dr. Jonathan Oakman. Staff check in call protocol is separately attached.

Education

The participants are educated on the fact that the product simulates the beneficial effects of the sun, and the longer usage of the product anytime between 5:30am and 5:30pm would lead to the best health and wellness benefits. And that they are recommended to use this product for as long as possible during those hours, however, are allowed to use it for a shorter duration based on their own habits and routines. After 5:30 pm, the glasses can be used however no light would be turned on, and it serves as a blue light filter to simulate the dark condition. The participants are also recommended to wear the glasses in the evenings as light filters for as long as possible. There is expected to be a natural distribution of people who use the product for a longer period, and those who use it for a shorter period.

Rewards

As a reward for participating in the study, participants get to keep the glasses for their personal use and are encouraged to continue using the glasses after the study.

Masking

Participants and investigators will be masked during the study, not knowing which group they are assigned to. This will be done automatically through a randomization script when the user is enrolled into our cloud system, assigning them to either one of the two arms in the study. The study arm information is mapped to a randomly generated unique identifier (using hashing

functions) such that the investigators managing the cloud database will not know the user's group. The password to decrypt the database will be held by the Data Safety and Monitoring Group, as well as the Monitor from the sponsor, who will ensure data integrity and host the raw trial data on a public repository at the time of study completion. After this point, the investigators will gain access to the full database and perform analysis.

Adherence measurement

On the Lumos glasses, adherence is automatically measured using the embedded human detection sensor (powered by infrared proximity sensor). Each participant is required to have a smartphone running either iOS or Android, and the glasses use Bluetooth to communicate with the Lumos smartphone app that syncs the data to the cloud.

Adverse Events

In 1998, the FDA determined that light boxes for SAD does not pose a significant danger to the public and the FDA is not aware of any adverse events as result of light box therapy [34]. Some discomforts may arise from light therapy, however. Some users may experience headaches and eye discomfort that usually goes away after a couple of days of continuing treatment. An adverse events button is located on the smartphone app for the user to enter in their adverse events for immediate feedback, where they'll be taken to the adverse event reporting form located on Qualtrics: https://uwaterloo.ca1.qualtrics.com/jfe/form/SV_4Hp8AbgXGk1qIQK

The study uses a numbered rating system for the adverse event, in addition to describing the adverse event, the participant is asked to rate the severity of the event on a numbered scale shown below:

0 - no symptoms

1 - mild symptoms (does not interfere with daily life)

2 - moderate symptoms (have an impact on daily function)

3 - severe symptoms (required seeing a doctor or hospitalization)

On a weekly basis, participants are also asked about adverse events, including Headaches, jumpiness, nausea, eye strain, changes in sight, and each ranked from 0 to 3, related to their wellness via the same Qualtrics link as the MADRS and PROMIS survey. More details on the weekly cadence adverse event reporting can be found in the next section.

In addition, based on the weekly MADRS and PROMIS surveys, if a participant experienced a worsening of MADRS score of > 9 or PROMIS > 5, the software would automatically flag this as an adverse event and the study investigators and data monitoring board is notified to follow up with the participant to understand if such worsening of symptoms are related to the study protocol, and determine if unmasking or pausing the study is necessary for the participant on a case by case basis. All adverse events will be reported to the REB director via either email of phone within 24 hours of the event and subsequently an Adverse Events Report form filed to the ORE.

Weekly Self-Assessments

Once a week, participants are asked to answer the MADRS and PROMIS questionnaire via the online Qualtrics link shown below.

https://uwaterloo.ca1.qualtrics.com/jfe/form/SV_0N7pwwHHEBUx7nM

The weekly survey consists of 5 main sections:

Lifestyle changes

Lifestyle changes include questions of changes in medication, outdoor activities changes (if more than 2 hours), if the participant is using any other light therapy or blue blocking glasses?

Glasses feedback on comfort and usability

survey askes for device related issues, such as Glare, dirty lenses, scratching on lenses, hinge catching hair, glasses too loose, glasses too tight, each also ranked from 0 to 3:

0 no compliant

1 minor complaint, not a major barrier to my comfort

2 moderate complaint, affects my comfort level but can tolerate it

3 severe complaint, the device is barely usable and I'm unable to tolerate this problem

Participants are given a chance to provide any additional feedback on device related complaints using a free entry text form.

Side effects reporting

A systematic assessment of common adverse events, including Headaches, jumpiness, nausea, eye strain, changes in sight, and each ranked from 0 to 3, where:

0 - no symptoms

1 - mild symptoms (does not interfere with daily life)

2 - moderate symptoms (have an impact on daily function)

3 - severe symptoms (required seeing a doctor or hospitalization)

Participants are given a chance to provide any additional feedback on adverse events using a free entry text form.

The survey also asks if the participant is experiencing any mania symptoms, and if so, is taking to the PMQ-9 survey [29]. If they reported mania, a member from our staff team will follow up and administer the Mania Rating Scale [35] over phone or video call, and our data safety and monitoring team and clinical team will be consulted to decide on whether the participant will be unblinded or withdrawn from the study.

The survey also asks if the patient is experiencing psychosis symptoms such as seeing thing that are not there, strange experiences you cannot explain, and if so, they are recommended to contact their primary doctor. This will also be flagged and sent to the PI as a risk factor for monitoring on a case-by-case basis. One follow up item from our staff team if they reported psychosis symptoms is to administer the Brief Psychiatric Rating Scale [36] over phone or video call, and our data safety and monitoring team and clinical team will be consulted to decide on whether the participant will be unblinded or withdrawn from the study.

Sleep questionnaire (PROMIS)

8 required questions about sleep quality in the past week via the PROMIS Sleep scale [21], where a higher score indicates worsening sleep

Mood questionnaire (MADRS)

9 questions via the self assessment MADRS, which as shown to be a proven tool kit for depression [30].

On the MADRS form, if in the final question, the participant indicates a 5 or 6 on the zest for life questionnaire, indicating that they are seriously considering suicide, mental health resources are automatically provided at the end of the survey.

Game - Assessments

Participants are asked to complete a reaction time test and memory test on a weekly basis at a fixed time each week. The reaction time test will be administered using the physical hardware on the Lumos glasses along with a Bluetooth matching interface on the smartphone to display results. The memory test will be administered via the smartphone using paired word test. The game is designed such that the paired associate learning (PAL) starts first, and 10 words are first presented to the participant to memorize, for 30 seconds. And then they are asked to complete a 1-minute psychomotor vigilance task (PVT) via the smartphone assisted game via the glasses. And then presented a screen to match randomized second pair words to the first paired words. This is repeated 3 times until a total of 30 words have been tested, and 3 minutes of the PVT game data has been collected.

Crisis planning

On a weekly basis, a member from the clinical team will follow up with the participant to check if they have any questions about the study, the weekly reporting form, games and adverse events. If during the conversation the participant indicates the risk of suicide, the separately attached crisis protocol shall be followed. The clinical team member is a student who would be trained by our Principal investigator, who is a licensed psychologist in the province of Ontario. If the clinical staff member is unsure what to do in any situation, they have immediate access to the principal investigator for advice and support.

275

Primary Outcome

Montgomery Asberg depression rating scale delta as a function of adherence Secondary Outcomes: Sleep Disturbance improvement via PROMIS short form, reaction time improvement via psychomotor vigilance test, memory improvement via word paired test, adverse events and comfort, as a function of adherence.

Study schedule

The study period is 16 weeks. With a crossover after the first 8 weeks.

Sample Size and Power Calculations

n = 20 per group is sufficient to detect depression score change via MADRS (n = 25 assuming two tailed distribution)

n= 7 is sufficient for detecting sleep via PSQI (we choose to use PROMIS) (n = 8 assuming two tailed distribution)

n = 7 is sufficient for reaction time via PVT (n = 9 assuming two tailed distribution)

n = 27 is sufficient for short term memory via paired word test (n = 24 assuming two tailed distribution)

n = 45 is sized as large as possible given our budget and for determining the usage time vs improvement regression model.

For detecting a mental wellness score change, the Lam et Al Paper is referenced :

In the paper: A total of 122 patients were randomized (light monotherapy, 32; fluoxetine monotherapy, 31; combination therapy, 29; placebo, 30). The mean (SD) changes in MADRS score for the light, fluoxetine, combination, and placebo groups were 13.4 (7.5), 8.8 (9.9), 16.9 (9.2), and 6.5 (9.6), respectively.

The placebo group: 6.5 (9.6)

The light therapy (no medication) group 13.4 (7.5)

In the Lumos 2020 Pilot study, the treatment pilot group saw an improvement of 13.3 with SD (4.4). For the power analysis, as a conservative measure, the mean and SD will be referenced from the Lam et al paper due to its higher SD.

A two group, one sided (we know that light therapy will improve symptoms) power analysis was performed with the online calculator: http://powerandsamplesize.com/Calculators/Compare-2-Means/2-Sample-1-Sided.

Inputs: Group A, mean is 6.5, sd is 9.6. Group B, mean is 13.4, sd is 7.5. Sampling ratio is 1

And for an alpha level of 5% and a power of 0.8, the sample size was determined to be n = 20 for

each group.

Based on feedback from reviewer, if there is a chance that irritability of the glasses could cause a worsening of depression symptom, therefore, a more conservative 2 sided power analysis should be considered.

A two group, two sided power analysis was performed with the online calculator: http://powerandsamplesize.com/Calculators/Compare-2-Means/2-Sample-1-Sided.

Inputs: Group A, mean is 6.5, Group B, mean is 13.4, sd is 8.55 (average of the SD). Sampling ratio is 1

And for an alpha level of 5% and a power of 0.8, the sample size was determined to be n = 25

For detecting sleep, Akyar, Akdemir published a trial of 24 older adults who has administered light therapy for a 1 month period. The PSQI index Global Scale decreased from 12.87±4.26 to 3.95±1.75.

We want to assume that there could be placebo effect, and based off the depression study, we make the assumption that placebo is roughly half the effect of the treatment. And therefore, for the power analysis, it is assumed that the placebo group has a PSQI global index of 8.41±4.26 post intervention, and the treatment group has 3.95±1.75.

http://powerandsamplesize.com/Calculators/Compare-2-Means/2-Sample-1-Sided

Inputs: Group A, mean is 8.41, sd is 4.26. Group B, mean is 3.95, sd is 1.75. Sampling ratio is 1

And for an alpha level of 5% and a power of 0.8, the sample size was determined to be n = 7 for each group.

Similarly, for a 2 sided power analysis, Inputs: Group A, mean is 8.41, Group B, mean is 3.95, sd is 3.01, Sampling ratio is 1 the minimum sample size is determined to be n = 8.

Although in our intervention, we choose to use the PROMIS sleep questionnaire, which has a much shorter completion time, we expect that since our total sample size is much greater than the required 8, a difference should be detected.

For detecting reaction time, a study by Rosa et al is referenced. 22 Brazilian swimming Olympic athletes in the Rio 2016 games participated in a 5 day light therapy protocol and their mean reaction time via the Psychomotor Vigilance Task (PVT) night at night decreased from 218.63 ± 5.06 (before light therapy) to 207.18 ± 3.45 (after light therapy).

To account for the placebo effect, it is assumed that the placebo has roughly half the effect of the treatment in our study. And we assume a mean of 212.905 ± 5.06 for the placebo group and 207.18± 3.45 for the light therapy group for the power analysis.

277

http://powerandsamplesize.com/Calculators/Compare-2-Means/2-Sample-1-Sided

Inputs: Group A, mean is 212.905, sd is 5.06. Group B, mean is 207.18, sd is 3.45. Sampling ratio is 1

And for an alpha level of 5% and a power of 0.8, the sample size was determined to be n = 7 for each group.

For a two tailed test, Inputs: Group A, mean is 212.905, Group B, mean is 207.18, sd is 4.26 (average of the 2 SDs). Sampling ratio is 1, n is calculated to be 9.

For detecting memory, a study by Bersani et al., is referenced. Where a pilot study using light therapy with 10 in the treatment group undergone a 5 day treatment and their cognitive performance was compared with 10 people in the control group. Memory was accessed using a 10 paired word test, done 3 times, with the score being the total number of correct recalls.

After 5 days, the treatment group scored 22.4 ± 0.3, and the control group scored. 21.1 ± 1.3. Again assuming that the placebo group in our study has half of the effect at 21.75, the power analysis was conducted.

http://powerandsamplesize.com/Calculators/Compare-2-Means/2-Sample-1-Sided

Inputs: Group A, mean is 23.4, sd is 0.3. Group B, mean is 21.75, sd is 1.3. Sampling ratio is 1

And for an alpha level of 5% and a power of 0.8, the sample size was determined to be n = 27 for each group

For a two tailed test, if we take Group 1 mean = 23.4, Group 2 mean = 21.75, sd = 0.8, the sample size is n = 24 for each group.

The third metric that warrant note is the regression to be performed on light therapy duration on sleep and mood improvements, however, there is insufficient data from existing literature to make the basis for a good power analysis. Therefore, we choose the maximum units that our production sample could reasonably manage and choose each group to be n = 45.

Data management and Statistical Analysis: Data is stored via Google drive until study publication, upon which relevant anonymous data for disclosure will be provided on University of Waterloo Dataverse. Data management plan is documented and managed via DMP assistant. Statistical analysis is performed in R using multiple linear regression analysis:

Sample code: modelFile <- read_excel(“Downloads/output.xlsx”) attach(modelFile) model1 <- lm(MADRSD ~ MADRSB + LIGHTHOURS + MADRSB*LIGHTHOURS)

#create dummy variables for the groupsgroupCate = factor (group)genderCate = factor(gender)

model2 <- lm(MADRSD ~ MADRSB + LIGHTHOURS + MADRSB*LIGHTHOURS + groupCate

+ genderCate)

Passive Data Collection

The Lumos glasses collects ambient light data through two ambient light sensors and user detection data through proximity sensors. This data will be associated with the participant ID and uploaded to the cloud for adherence and secondary analysis relevant to the research.

Some basic functionalities of the Lumos app are presented below. The Lumos app is compatible with smartphones running the latest version of iOS and Android. It features an email login which stores the authentication data in a secured database via Google Firebase, with servers located in Canada for security. The app then seeks permission to have Bluetooth and notifications to provide basic functionality to the user in this trial. Some screenshots of the app is shown in Figure 5 below.

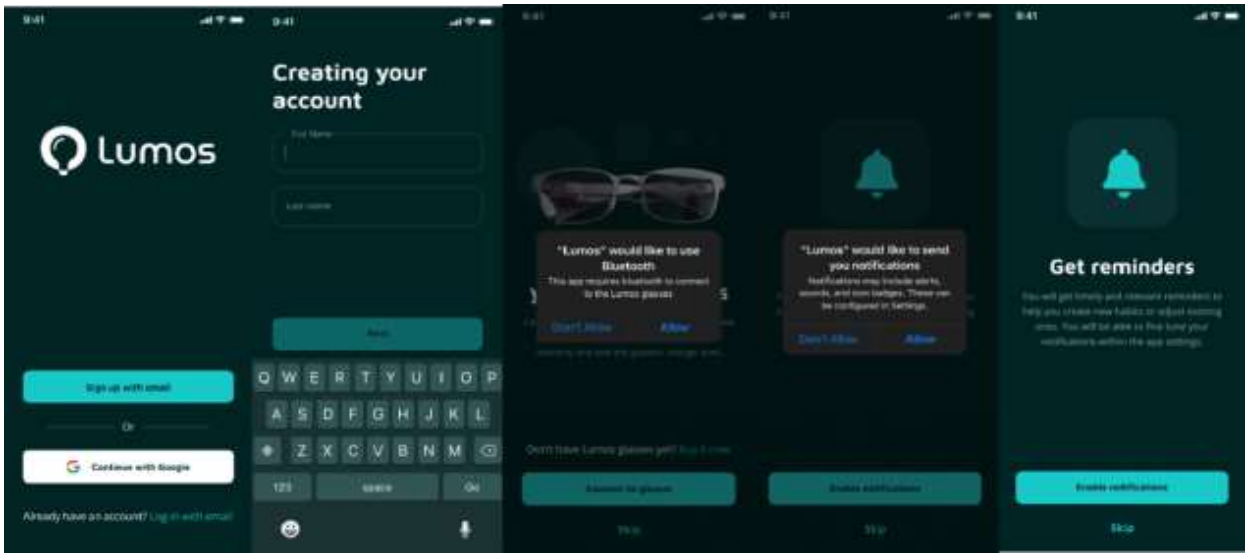


Figure 5 Lumos app authentication and permissions screenshots

Note, for this trial, to enable cloud control of randomization of treatment arms, user accounts will be automatically created for them using their email, and a temporary password provided. The participants are asked to change their password the first time they log in.

The data from the app is sent to a Google Firebase Server owned by the founders of Lumos and the research team. Figure 8 shows screenshots of the database and authentication and access security rules implemented on the database. Figure 6 shows screenshots of the database storage on Google Firebase.



Figure 6 Google firebase with rules enforcing security access

Figure 7 below shows the more advanced functionalities of the Lumos app such as in app games, and reaction time test scores visualization.



Figure 7 Advanced functionality of the Lumos app, including guided PVT (psychomotor vigilance task), and word pair game.

Study variables

Clinical Variables:

(One datapoint per week for each participant)

Via the smartphone app, participants are asked for an ideal time each week where they can set aside around 20 minutes of their time to complete the self-assessments and the smartphone app will send a push notification around that time each week to remind them to take assessments. Participants are also asked for an ideal time each week when they'd like to be contacted for a

follow up/check ins.

Weekly Survey Variables:

1. MADRS Score

2. PROMIS Score

Cognitive Testing Variables

1. PVT_Mean reaction time

2. PVT_Number of lapses (reaction time > 500 ms)

3. PVT_Number of false starts

4. **PAL_**number of correct words (out of 30)

Usage variables:

When the smartphone first detects that a user has put on their glasses, and keeps it on for longer than 5 seconds, a session document is created on the cloud firebase under the user's unique ID, and the light is turned on to activate treatment (or low intensity light for placebo). The smartphone activates the ambient light sensor on the glasses and begins collecting ambient light data.

The session document consists of the following variables:

1. Start time (after the 5 second confirmation period, the exact time in date, minute, second is recorded into the document).
2. Every 5 seconds, the aggregated ambient light data (in melanopic lux) is recorded into the database as a new record under a sub document, ALS data.
3. End time (when the phone detects that the user has taken off the glasses, and that state remains for over 5 seconds, record the end time and end the session recording on the cloud).

Participant Withdrawal

If a participant chooses to withdraw early from the study, they have all rights to do so. The participant is asked nicely to return the glasses to the study team so that their position could be filled by another on the waiting list. A pre- paid return label will be provided to the participant to ship the glasses back to the research team. However, if the participant chooses to keep the glasses, they are told that they are within their rights to do so. If the participant consents, an exit interview will be performed with a final round of assessments with an optional reason to answer the reason for exit and report any adverse events and suggestions to the research team. An appreciation letter will be sent to the participant after the exit interview.

If participant wishes to withdraw from the study:

1. Schedule exit call with participant
2. Confirm and send return shipment label to participant.
3. Ask the participant the reason for withdrawing, although they are entitled to not give a reason if they wish to.

4. Send an appreciation letter (withdrawal version) to the participant.

Participant Follow up and Loss Criteria

If a participant neglects to wear the glasses for 1 day, a smartphone app will notify them via push notification. If a participant do not wear the glasses for 2 consecutive days, an automated text will be send to their phone to remind them about the study.

If a participant neglects to wear the glasses for 3 consecutive days, the clinical team will be notified, and a follow up call is done to get in touch with the participant and remind them to wear the glasses per trial recommendations. If despite calling, the participant continues to not wear the glasses for 14 consecutive days, the participant is considered lost, and they are contacted to see if they wish to officially withdraw from the study and willing to ship the glasses back so another person can have a chance to participate. If they cannot be reached via calling, an email will be sent, and the clinical team will attempt calling each day for a total of 7 days until the participant is considered lost.

If a participant neglects to complete the weekly survey and testing at their selected time, they are given smartphone notifications to complete the survey for the first 3 days grace period. If they still do not complete their weekly survey and testing after 3 days, an automated text message will be sent to them each day. If after 6 days, they have neglected to complete the assessment, a member of the team will reach out via phone call for a reminder. If despite calling, the participant continues to not complete the survey and a total of 21 days has passed since the target survey date (based on participant's selection), the participant is considered lost, and they are contacted to see if they wish to officially withdraw from the study and willing to ship the glasses back so another person can have a chance to participate and help us with the research. If they cannot be reached via calling, an email will be sent, and the clinical team will attempt calling each day for a total of 7 days until the participant is considered lost.

Participant Waitlist and Replacement

If a participant is lost or withdrawn from the study, and when a pair of glasses is available to ship out, all people on the waitlist that correspond to the participant's stratified group will be contacted to see if they are interested in beginning the study immediately. The person who responds first will be given the spot and a pair of glasses will be shipped to their address along with the participant package. An account will be created in the new participant's email and the cloud will transfer the encoded treatment grouping information and slot ID to the new participant, such that they follow the same protocol as the lost or withdrawn participant.

If the specific stratified group waitlist has no more members to contact, or no responses were heard, the waitlist search is expanded to remove the sex at birth stratification, followed by age, and finally starting MADRS score stratification (such that all waitlist participants are eligible to replace).

A buffer of 10 pairs of glasses is available currently to account for the shipment time between withdrawal and participant loss (withdrawal without return). If at any point, the buffer runs out of glasses, no replacement will be made. It is possible that the sponsor can produce more glasses for the buffer when the study begins late 2024, currently, only 10 pairs are allocated for the buffer.

To communicate this method, if a participant is put on a waitlist, they are sent the following email:

“We are sorry to inform you that our study is currently full for your demographics group. If you are interested in waiting, you can join our waitlist, where we will reach out if anyone drops out during the study. When a spot opens, everyone on the waitlist for your demographic group will be contacted via email, and the first person who responds will be able to fill in that spot in the study.”

Conditions for Premature study termination

The study may be prematurely terminated or halted by the principal investigator, sponsor, or data safety and monitoring board if serious adverse events are observed.

In such situations, the participant that incurred the adverse event is unblinded to diagnose if the adverse event is due to the investigational device. If not (participant in placebo and team agrees it is unrelated to the device), the study can be unhalted, and other participants are not unblinded. The participant may or may not continue the study at their discretion, however, their data is removed from the final statistical analysis given the unblinding.

If a serious adverse event has been connected to the intervention treatment, the study would be prematurely terminated, all glasses would be shut down remotely, and all participants are sent an email and phone call warning about the adverse event. All devices in this situation would be recalled and participants are contacted for the recall. The participants that have experienced the adverse event would receive a formal follow up from the student investigator, as well as any relevant staff member on the trial team who has the expertise and can help with the diagnosis, treatment, and medical care of the participant, and work with the participant’s primary care provider to provide medical assistance.

If the adverse event is limited to a single participant and deemed to be an isolated case, the principal investigator, sponsor, or data safety can halt the study for a single participant without affecting the flow of study for the other participants. For example, if mania or psychosis is reported by the participant as an adverse event, our team would follow up as soon as possible directly with the participant and administer the Mania Rating Scale [35], or Brief Psychiatric Rating Scale [36]. If through assessment, the study team deems that the issue is related to the device and is severe enough to discontinue intervention, the participant can be notified of this decision and their glass’s treatment would be deactivated over the cloud, and our team would follow up on and aid the participant in finding health care providers to manage their symptoms, as well as provide basic online based cognitive behavior therapy and psychoeducation for managing mania symptoms until dedicated care is found or symptoms subside.

Data safety and monitoring board

To mitigate conflict of interest with the investigators having financial association with the sponsor, a special team of industry experts who have no conflict of interest are appointed to monitor the clinical trial for fairness, safety, data, and scientific integrity. The board will have real time data from the study from the participants and have access to the encryption key and the power to unblind or halt the trial in case of an emergency. All clinical data will be sent to the board and cross

validated during the analysis and paper writing stage to ensure data integrity and accuracy.

The board consists of three members who have no conflict of interest with the sponsor:

Dr. Jeff Hovis, Associate Professor, Senior Graduate Officer, Optometry and vision science, University of Waterloo. Registered optometrist, supervising clinician.

> Dr. Jeff Hovis received his Doctor of Optometry and Master of Science degrees from Ohio State University. He completed his PhD degree in Physiological Optics from Indiana University before joining the University of Waterloo School of Optometry and Vision Science where he has been a member for over 30 years. He has an active research program in developing performance-related vision standards for law enforcement, aviation, maritime and railway industries. This work has led to the development of a lantern test and a color vision test for dispatchers used by the Canadian railways. Dr Hovis is currently investigating the color vision requirements and testing protocols for the Canadian Air Force. He has been a member of several panels and research groups reviewing vision standards for civilian pilots in Canada. In addition to research on vision standards, Dr. Hovis has also been investigating visual performance and optical properties of ballistic protective eye wear for the Canada Land Forces. His research focuses on establishing performance-based standards for colour vision, visual acuity and binocular vision with the primary work studying the impact of colour vision deficiencies on coloured related tasks, the impact of protective eyewear on visual performance. Dr. Jeff Hovis is also a member and president of the International Commission on Illumination, Canadian National Division.

Dr. Paul Murphy, Professor, Optometry and vision science, University of Waterloo.

> Dr. Paul J Murphy graduated from Cardiff University in 1988 with a BSc in Ophthalmic Optics, and completed his training at the Newcastle General Hospital, Department of Ophthalmology, Newcastle-upon-Tyne. He obtained his optometric licence in 1990 from the General Optical Council (UK), and entered practice at the Royal Victoria Hospital, Contact Lens and Low Vision Unit, Belfast.
>
> In 1993 Dr. Murphy enrolled as a graduate student under the supervision of Prof Sudi Patel and Prof John Marshall, and he was awarded his PhD from Glasgow Caledonian University in 1996 with a thesis entitled: “An examination of human corneal sensitivity by non-invasive methods”. Subsequently, he completed a post-doctoral fellowship and was appointed a Lecturer (Assistant Professor) in the Department of Vision Sciences at Glasgow Caledonian University in 1997. In 2001, he was appointed Director of Teaching and Senior Lecturer (Associate Professor); School of Optometry and Vision Sciences, Cardiff University and was promoted to reader in 2007. While at Cardiff, he established the Contact Lens and Anterior Eye Research Unit (CLAER). Through this research unit, he collaborated with colleagues in the UK and Europe, and developed novel systems for imaging the ocular surface and tear film. He was appointed as the President of the European Academy of Optometry and Optics in 2013.
>
> In 2013, Dr. Murphy was appointed director of the School of Optometry and Vision Science at the University of Waterloo, and also completed his MBA at the University of South Wales. In 2015, he was appointed an honorary professor at Cardiff University. In 2016 he stepped down from the position of Director. He has established the Murphy Laboratory of Experimental Optometry within the School of Optometry. His research interests are concentrated on the anterior ocular surface, and include instrument design, contact lens wear, tear film physiology, ocular anatomy and corneal sensation. He has published in these areas, and in topics as varied as visual impairment, eye movement and optometric practice.
>
> Dr. Murphy is a member of the Centre for Bioengineering and Biotechnology (CBB), and a collaborator with the Centre for Ocular Research and Education (CORE) at the University of Waterloo. He is a fellow of the College of Optometrists (UK), the American Academy of Optometry, the European Academy of Optometry and Optics, and the British Contact Lens Association.

Dr. Dorothy Sit, Associate Professor of Psychiatry, Northwestern Medicine

Dr. Dorothy Sit is an Associate Professor at Northwestern University Feinberg School of Medicine. Dr. Sit's main clinical research focus is on the development of treatments for women with mood disorders. Dr. Sit's clinical work is devoted to the care of women with major mood disorders during the childbearing years including pre-conception planning, pregnancy and postpartum. With NIMH grant support, Dr. Sit recently completed a clinical trial confirming the efficacy of bright light therapy for bipolar depression and discovered that light therapy at midday versus an inactive placebo comparator induced a potent antidepressant response in depressed bipolar patients. She presented the findings at the 2016 Annual Meeting of the Society for Light Treatment and Biological Rhythms and abstracts at the American Psychiatric Association 168th Annual Meeting and the Society for Biological Psychiatry, 70th Annual Scientific Meeting. Given the robust effects, Dr. Sit is developing new research studies to investigate putative neural and visual biomarkers of response with support from NARSAD (Brain and Behavioral Research Foundation), and to explore the potential brain-related mechanisms underlying therapeutic light. As a clinician-educator, Dr. Sit serves on the women's mental health fellowship curriculum committee and provides lectures and training for residents and fellows on the diagnosis, risks/benefit assessment and clinical management of women with depression, bipolar disorder or schizophrenia during pregnancy and postpartum. Dr. Sit serves on the Scientific Advisory Committee for the not-for-profit Center for Environmental Therapeutics and as Vice-President for the Society for Light Treatment and Biological Rhythms. She also provides peer reviews of manuscripts being considered for publication in major journals including the American Journal of Psychiatry and others.

Sponsor Monitor

To maintain smooth software operation and database management during the clinical study and assist the data safety and monitoring board, a monitor, Felix Xu has been appointed from the Sponsor. Felix is a 4th year computer engineering student at the University of Waterloo and a software engineer at Lumos Health, he has been granted funding to work on this project from MITACS. Given that Felix has access to the software and is responsible for maintenance, he can in theory crack the encryption of the blinding by using the software that he manages as the decryption keys are in the iOS and Android App. The only way to completely mitigate conflict of interest in this scenario would be to hire a third-party engineering company to maintain the entire code base during the clinical study (and shut off access to the codebase to Lumos), however, this would be extremely high-cost and is outside the current budget of Lumos Health and the MITACS grant. It currently makes most sense to have the people who created the software system conduct maintenance of it during the clinical trial. As such, Felix received TCP2 core training on research ethics, and will implement software controls in place such that the data safety team will always first receive a snapshot of the raw data from participants and make an attestation to not attempt to crack the blinding information unless specifically instructed in events of emergency.

Data management plan

Qualtrics survey Data

-Alpha and Beta testing data will be cleared prior to participant enrolment
-Custom links will be created after all participants and waitlist members are enrolled, this custom link is then sent to our cloud so that the participants have access to their Qualtrics weekly survey via a simple button click from their app
-Adverse events that prompt team feedback is sent via email triggers to data monitoring team + investigators using conditional triggers
-Data monitoring board added as collaborators on the Qualtrics survey so that they have full access to survey design and responses.
-At the end of the trial, before analysis begins, all responses from Qualtrics will be exported and emailed to

the data monitoring board as a backup copy.

Clinical data from custom software

-Clinical data from software will be stored on google firebase, under a custom project
-The data will be used to drive a dashboard system, for investigators and the data safety and monitoring team to monitor participant status, usage status, without compromising blinding information. The dashboard will also inform when participants have deviated from protocol and trigger prompts to the clinical team to follow up with participants.
-The dashboard will be password protected such that only the relevant teams have access to the data

Other data

Participant exchange data, from email exchanges, text messages, if consensual, recorded video calls will be stored on google drive.

Data sharing after trial completion:

The clinical data will be anonymized and shared on a publicly available database (such as UW Dataverse, of FRDR) after the trial. Non anonymized data will be stored for 15 years after the trial by the research team on a physically protected and password protected hard drive with identifying information in case follow up is needed on participants, specifically regarding adverse events.

Data locking prior to analysis:

A snapshot of the study data will be taken prior to the study analysis by the data safety and monitoring team, through exporting data from Qualtrics, and working with the Sponsor monitor to take a snapshot of the cloud database.

Participant privacy protection:

Participant data stored on the cloud database will be protected using encryption and authentication algorithms provided by Google. The clinical team, sponsor, and data monitoring and safety team will be trained and instructed to not let any study data leak into the public domain until study completion and the anonymous data is created for public release. Any students hired to be on the clinical staff will receive training and sign a confidentiality agreement where participant information sharing is prohibited, and talking about the participants to anyone outside their approved supervisor is not allowed.

Trial Completion

Trial completion for a participant is when 16 weeks of full usage has been completed and the final assessment is done. At this point, their glasses' software will automatically switch to the standard customer software (with the ability to control intensity to any level they desire, with safety limits in place) and receive automatic software updates as patches to the Lumos app. The smartphone app will have a button to take them to an optional exit survey to provide any comments and feedback they wish to provide. A thank you letter will be sent to the participant.

Trial completion for the overall trial is when all participants who have signed up, or later joined via waitlist replacement, have completed their 16-week protocol. At this point, all consolidated data that was sent to the data safety and monitoring board will be reviewed, packaged, and signed off before it is sent back to the investigators for analysis. This data keeps the blinding information intact but available for analysis by the investigators, such that the investigators know that a

participant belonged to treatment arm A, or B, but do not know whether treatment arm A is the one that received the higher dosage first. The investigators will then perform data analysis and present findings to the data safety and monitoring board, who will review and sign off on the findings. Afterwards, the data will be completely unblind to the investigators to make final conclusions and write the thesis paper for dissertation and publication.

Statement of Compliance

This clinical investigation shall be conducted in accordance with the ethical principles that have their origin in the Declaration of Helsinki [27].

This clinical investigation shall be conducted in compliance with this protocol document and adhere to TCP2 core research ethics regulations, follow mandates provided by research ethics board of the University of Waterloo, as well as The Collaborative Institutional Training Initiative Good Clinical Practice guidelines.

The clinical investigation shall not begin until the required approval/ favorable opinion from the REB from the University of Waterloo and Health Canada has been obtained.

The clinical investigation shall comply with additional requirements set forth by the University of Waterloo safety office regarding controls on maximum allowed exposure durations based on IEC 62471 standard, that an extra 25% reduction of exposure will be enforced on top of the IEC 62471 standard for eye safety.

This clinical investigation shall be funded by the Sponsor and MITACS Grant IT28793 through the University of Waterloo. Any additional expenses incurred beyond the expected research budget will be covered by the Sponsor.

The clinical trial and its details will be registered on clinicaltrials.gov, a publicly accessible database.

Investigational Device Description

Detailed information on the investigational device, its operation, and safety assessments can be found in the investigator's brochure separately attached.

1. Hardware design: The glasses used for the 2024 trial in this protocol uses the 2021 Lumos Clinical Glasses design, shown in figure 3. The device uses Stainless steel front frames, with TR90 injection molded temple arms each with a battery module, PCB, microUSB charging port, a push button, ambient light sensor, and user detection infrared proximity sensor. The PCB is equipped with the Nrf52832 chipset, allowing Bluetooth communications.

2. Firmware Design: The firmware version used for the clinical trial highlighted in this protocol will be labelled as, LumosLeftPCB_WAT_F2024_Clinical_Rev0 and LumosRightPCB_WAT_F2024_Clinical_Rev0 for the Left and Right arms of the glasses respectively. The firmware is coded in Arduino, using the Adafruit Bluefruit Nrf52832 as a

baseline reference design and codebase. A state diagram of the firmware logic of operation is shown below.



Figure 8 Lumos Clinical Firmware State Diagram

3. Software Design (iOS): The software for iOS phones are implemented in Apple's native development platform, Xcode, linked to a Github repository github.com/LucasLumos/trial. All software versions and changes can be observed on the repository. The software may be continuously updated to repair bugs and improve compatibility during the trial and will be maintained by the sponsor Monitor Felix Xu, with help from the creator of the iOS app and student investigator Lucas Tang.

4. Software Design (Andriod): The software for Android phones is implemented in Android Studio, which is Google's recommended native platform for app development, and linked to github.com/LumosHealth/Android_app. The software may be continuously updated to repair bugs during the trial and will be maintained by the sponsor monitor Felix Xu, who is also the creator of the Android app.

5. Cloud infrastructure: Google firebase cloud is used for its clean integration with advanced features on iOS and Android apps, allowing state of the art user registration, data protection, encryption, and real time database features. It also has a feature that allows user data to be uploaded to the cloud asynchronously if the user disconnects from internet and will upload the information after internet connection is recovered.

6. Note on light switching. To protect participant's circadian rhythm, the glasses' lights will not be able to turn on between 5pm and 5am.

Potential Benefits of Clinical Device

The potential benefit of the clinical device is its light therapy delivery, which could lead to improvements in a user's health and mental health. More information can be found in the investigator's brochure.

Potential Risks of Clinical Device

There are several potential risks of the clinical device. One of which is eye safety. Very strict controls are used on the glasses via firmware and 100% per device calibration on the manufacturing line to control the light output levels, which can also be controlled by the

smartphone. There could be a risk if the device or the user's smartphone was somehow modified or hacked to override any set safety controls or limits. A note is added on the clinical user manual to tell the user to contact the research team if they suspect hacking or if the light is behaving abnormally bright. A second risk is battery related safety risks as with any electronic devices. It is possible that the battery could have a thermal runaway effect if any puncturing or water damage occurs that short the terminals of the battery. And this is why it is important that participants are told that they should not try to take apart or modify the device in any way, as it could lead to increased safety risks. Another risk is Bluetooth interference as the device is still going through FCC certifications, this means that there is potentially more radio interference around the device which could cause interference with other radio emitting devices in the proximity of the user. Unless FCC is passed before the trial start date, people with electronic implants such as pacemakers are excluded from the study at this time.

Potential confounding factors

There are several potential confounding factors that could compromise the results of the clinical trial.

Changes in going outdoor habits:

If a participant's habit changes such that they are doing more outdoor activities, it could complicate the clinical results. One way to account for this is to ask in the weekly check-in if the participant has been going outdoors more than 2 hours a day on average, and if so, how many hours are they spending outdoors on average.

Environmental predispositions

Participant indoor lighting. While not being outdoors contributes to reduced light exposure, if the participant somehow receives lighting from very good windows, or skylights that end up providing similar indoor light conditions as being outdoors on a sunny day, this essentially negates our inclusion criteria of less than 2 hours outside. Thus, if a person is already receiving adequate indoor lighting that is comparable to outdoors, it is not expected that the glasses will have a notable positive benefit. One way to mitigate this confounding factor is by using the ambient light sensors on the glasses that is activated when the user is using the glasses. If the sensor reports high levels of light when they are wearing the glasses, then it can be factored into the overall analysis.

Lifestyle predispositions

Generation of serotonin requires tryptophan as an essential amino acid precursor. And melatonin, which contributes to sleep, requires serotonin as a precursor. On the advice of Dr. Jamie Zeitzer, certain vegans and vegetarians who do not have sufficient tryptophan intake could experience issues responding to light therapy, due to the lack of chemical precursors. However, it is generally not an issue as tryptophan is also found in tofu, avocados, oats, and other seeds that vegans often use as protein supplements. A note can be added to the participant package about diet and light therapy to prompt people to have sufficient protein intake in their diet to enable proper function of the body.

289

Genetic predispositions

There have been certain predispositions on eye color and sensitivity to light therapy [31,32].. Specifically, people with blue eyes have less risk for seasonal affective disorder but are at higher risk for sun related eye damage. It is possible that people with lighter colored eyes will have received sufficient light from indoor light environments due to their genetic differences. Yet it is also possible that people with blue eyes will report more effects from light therapy, but also may have more adverse events. To help account for this factor, an optional question can be asked at the intake survey about the participant's eye color, if they choose to disclose.

Medication use

Medication use can complicate the study and there are many potentially unknown impacts on how medicine could affect the person's light sensitivity, and brain chemistry. To account for this, in the intake, a participant is asked if they are currently taking any medication for depression, any other active medication and asks them to disclose if they wish. And have a form on the weekly check in to check if their medication usage has changed.

Other light therapy use

If the participant also uses light therapy lamps or other light therapy devices (included light therapy face masks). This could complicate the study as we are unable to track usage time of other light therapy devices. We will put a note in the participant package to recommend that they use only the Lumos glasses as their bright light therapy treatment. And if they indeed use other types of treatment, that they fill it usage time of other light therapy device in the weekly check in.

Participant sharing the glasses with others

If the participant lets other people use the glasses, then the adherence data would be compromised. A note will be added to the participant package to not let other people use the glasses during the 16 weeks of the trial period.

References

[1] Lam, Raymond W., et al. "Efficacy of Bright Light Treatment, Fluoxetine, and the Combination in Patients with Nonseasonal Major Depressive Disorder." JAMA Psychiatry, vol. 73, no. 1, Jan. 2016, p. 56, https://doi.org/10.1001/jamapsychiatry.2015.2235.

[2] Tao, Long, et al. "Light Therapy in Non-Seasonal Depression: An Update Meta-Analysis." Psychiatry Research, vol. 291, Sept. 2020, p. 113247, https://doi.org/10.1016/j.psychres.2020.113247.

[3] Michalak, Erin E., et al. "A Pilot Study of Adherence with Light Treatment for Seasonal Affective Disorder." Psychiatry Research, vol. 149, no. 1-3, Jan. 2007, pp. 315–20, https://doi.org/10.1016/j.psychres.2006.05.005.

[4] Crowley, Stephanie J., and Charmane I. Eastman. "Phase Advancing Human Circadian Rhythms with Morning Bright Light, Afternoon Melatonin, and Gradually Shifted Sleep: Can We Reduce Morning Bright-Light Duration?" Sleep Medicine, vol. 16, no. 2, Feb. 2015,

pp. 288–97, https://doi.org/10.1016/j.sleep.2014.12.004.

[5] Schwartz, PJ. “Winter Seasonal Affective Disorder: A Follow-up Study of the First 59 Patients of the National Institute of Mental Health Seasonal Studies Program.” American Journal of Psychiatry, vol. 153, no. 8, Aug. 1996, pp. 1028–36, https://doi.org/10.1176/ajp.153.8.1028.

[6] Rohan, Kelly J., et al. “Winter Depression Recurrence One Year after Cognitive-Behavioral Therapy, Light Therapy, or Combination Treatment.” Behavior Therapy, vol. 40, no. 3, Sept. 2009, pp. 225–38, https://doi.org/10.1016/j.beth.2008.06.004.

[7] US EPA,ORD. “Indoor Air Quality | US EPA.” US EPA, 2 Nov. 2017, www.epa.gov/report-environment/indoor-air-quality#note1.

[8] “Illuminance - Recommended Light Level.” Www.engineeringtoolbox.com, www.engineeringtoolbox.com/light-level-rooms-d_708.html#:~:text=The%20outdoor%20light%20level%20is. Accessed 12 Oct. 2021.

[9] Diffey, B. L. “An Overview Analysis of the Time People Spend Outdoors.” British Journal of Dermatology, vol. 164, no. 4, Apr. 2011, pp. 848–54, https://doi.org/10.1111/j.1365-2133.2010.10165.x.

[10] Mills, J. N., et al. “The Circadian Rhythms of Human Subjects without Timepieces or Indication of the Alternation of Day and Night.” The Journal of Physiology, vol. 240, no. 3, Aug. 1974, pp. 567–94, https://doi.org/10.1113/jphysiol.1974.sp010623.

[11] Basner, Mathias, et al. “Psychological and Behavioral Changes during Confinement in a 520-Day Simulated Interplanetary Mission to Mars.” PLoS ONE, edited by Nandu Goswami, vol. 9, no. 3, Mar. 2014, p. e93298, https://doi.org/10.1371/journal.pone.0093298.

[12] Wirz-Justice, Anna, et al. “‘Natural’ Light Treatment of Seasonal Affective Disorder.” Journal of Affective Disorders, vol. 37, no. 2-3, Apr. 1996, pp. 109–20, https://doi.org/10.1016/0165-0327(95)00081-x.

[13] Zalta, Alyson K., et al. “A Placebo-Controlled Pilot Study of a Wearable Morning Bright Light Treatment for Probable PTSD.” Depression and Anxiety, vol. 36, no. 7, 2019, pp. 617–624., https://doi.org/10.1002/da.22897.

[14] Swanson, Leslie M., et al. “An Open-Label Pilot Study of a Home Wearable Light Therapy Device for Postpartum Depression.” Archives of Women's Mental Health, vol. 21, no. 5, 2018,pp. 583–586., https://doi.org/10.1007/s00737-018-0836-z.

[15] Williams, Janet B., and Kenneth A. Kobak. “Development and Reliability of Structured Interview Guide for the Montgomery-Åsberg Depression Rating Scale (Sigma).” British Journal of Psychiatry, vol. 192, no. 1, 2008, pp. 52–58., https://doi.org/10.1192/bjp.bp.106.032532.

[16] Akyar I, Akdemir N. The effect of light therapy on the sleep quality of the elderly: An intervention study. Australian Journal of AdvancedNursing 2014;31:31-8

[17] Bersani, G., Marconi, D., Limpido, L., Tarolla, E., & Caroti, E. (2008). Pilot Study of Light Therapy and Neurocognitive Performance of Attention and Memory in Healthy Subjects. Psychological Reports, 102(1), 299–304. doi:10.2466/pr0.102.1.299-304

[18] Rogev E, Pillar G. Placebo for a single night improves sleep in patients with objective insomnia. Isr Med Assoc J. 2013 Aug;15(8):434-8. PMID: 24079065.

[19] Rosa, J. P. P., Silva, A., Rodrigues, D. F., Simim, M. A., Narciso, F. V., Tufik, S., … de Mello, M. T. (2018). Effect of bright light therapy on delayed sleep/wake cycle and reaction time of athletes participating in the Rio 2016 Olympic Games. Chronobiology International, 1–9. doi:10.1080/07420528.2018.1459660

[20] Lucas, Robert J., et al. "Measuring and Using Light in the Melanopsin Age." Trends in Neurosciences, vol. 37, no. 1, 2014, pp. 1–9., https://doi.org/10.1016/j.tins.2013.10.004.

[21] https://www.psychiatry.org/File%20Library/Psychiatrists/Practice/DSM/APA_DSM5_Level-2-Sleep-Disturbance-Adult.pdf

[22] Kirschbaum-Lesch, Inken, et al. "Feasibility and Efficacy of Bright Light Therapy in Depressed Adolescent Inpatients." Zeitschrift Für Kinder- Und Jugendpsychiatrie Und Psychotherapie, vol. 46, no. 5, 2018, pp. 423–429., https://doi.org/10.1024/1422-4917/a000603.

[23] Profita, Halley, et al. "Personal and Social Considerations of Wearable Light Therapy for Seasonal Affective Disorder." Proceedings of the 10th EAI International Conference on Pervasive Computing Technologies for Healthcare, 2016, https://doi.org/10.4108/eai.16-5- 2016.2263314.

[24] Rüger, Melanie, et al. "Human Phase Response Curve to a Single 6.5 H Pulse of Short-Wavelength Light." The Journal of Physiology, vol. 591, no. 1, 2012, pp. 353–363., https://doi.org/10.1113/jphysiol.2012.239046.

[25] Arthurs, Mel, et al. "Accurate Reaction Times on Smartphones: The Challenges of Developing a Mobile Psychomotor Vigilance Task." 2021 International Symposium on Wearable Computers, 2021, https://doi.org/10.1145/3460421.3478818.

[26] Brouwer, A., et al. "Light Therapy: Is It Safe for the Eyes?" Acta Psychiatrica Scandinavica, vol. 136, no. 6, 2017, pp. 534–548., https://doi.org/10.1111/acps.12785.

[27] Declaration of Helsinki, available at: https://www.wma.net/policies-post/wma-declaration-of -helsinki-ethical-principles-for-medical-research-involving-human-subjects/

[28] Sumaya, I. C., et al. "Bright Light Treatment Decreases Depression in Institutionalized Older Adults: A Placebo-Controlled Crossover Study." The Journals of Gerontology Series

A: Biological Sciences and Medical Sciences, vol. 56, no. 6, 2001, https://doi.org/10.1093/gerona/56.6.m3

[29] Cerimele, Joseph M., et al. "The patient mania questionnaire (PMQ-9): A brief scale for assessing and monitoring manic symptoms." *Journal of General Internal Medicine*, vol. 37, no. 7, 2021, pp. 1680–1687, https://doi.org/10.1007/s11606-021-06947-7.

[30] Fantino, Bruno, and Nicholas Moore. "The self-reported montgomery-åsberg depression rating scale is a useful evaluative tool in major depressive disorder." *BMC Psychiatry*, vol. 9, no. 1, 2009, https://doi.org/10.1186/1471-244x-9-26.

[31] Goel, Namni, et al. "Depressive symptomatology differentiates subgroups of patients with seasonal affective disorder." *Depression and Anxiety*, vol. 15, no. 1, 2002, pp. 34–41, https://doi.org/10.1002/da.1083.

[32] Dr, Mark Mandel. "Are Light Eyes More Susceptible to UV Damage?: UV Damage to Eyes." *Optima Eye*, 22 July 2021, optimaeye.com/are-light-eyes-more-susceptible-to-uv-damage/.

[33] Corliss, Julie. "Light Therapy: Not Just for Seasonal Depression?" *Harvard Health*, 28 Oct. 2022

[34] "Light Therapy for Seasonal Affective Disorder (SAD) - Lrl.Mn.Gov." *Minnesota Department of Health*, www.lrl.mn.gov/docs/pre2003/other/010117.pdf. Accessed 17 Oct. 2023.

[35] *Young Mania Rating Scale (YMRS) - University of Florida*, dcf.psychiatry.ufl.edu/files/2011/05/Young-Mania-Rating-Scale-Measure-with-background.pdf. Accessed 17 Oct. 2023.
vc

[36] "Brief Psychiatric Rating Scale (BPRS): Qxmd." *Calculate by QxMD*, qxmd.com/calculate/calculator_551/brief-psychiatric-rating-scale-bprs. Accessed 17 Oct. 2023.

Revision History

Date: 09/14

-Addressed comments from REB reviewers

-Study design updated from 8 week + 8 weeks open label to 16 weeks full crossover study

-Seizures removed as exclusion criteria after reviewing relevant literature and ethical considerations, added monitoring question on weekly survey as checks

-Officially added data safety and monitoring board members and appointed monitor from Sponsor

Date: 9/30

-Removed family history of cataracts as exclusion criteria per recommendation from Dr. Hovis, as most people will have a family member with cataracts

-Included an upper limit on MADRS as exclusion criteria based on PI recommendation given the high risk with severe depression participants, and this is aligned with the lam et al study [1] to include an exclusion criterion for those with high suicide risk

Date: 2/3/2024

-Exclude those with pacemakers, seizures

Glossary of Acronyms

MADRS: Montgomery Depression Rating Scale

PROMIS: Patient-Reported Outcomes Measurement Information System, in the context of this protocol document, PROMIS refers to the specific PROMIS—Sleep Disturbance—Short Form.

CES: Consumer Electronics Show

IR: Infrared, referring to Infrared radiation.

AVG: Average

SD: Standard Deviation

n: number of participants (in the context of statistics)

PVT: Psychomotor vigilance task

PSQI: Pittsburg Sleep Quality

UW: University of Waterloo

FRDR: Federated Research Data Repos

End of Protocol

Glossary

Flash Memory A non-volatile memory used for data storage and program retention, allowing read, write, and erase operations even when power is removed 40–43

IEC 62471 International standard specifying methods for evaluating photobiological safety of lamps and lamp systems (risk groups, measurement geometry, and exposure limits) 7, 8, 16–21, 25, 45, 129–131, 135, 138–140, 231

light engine An optical assembly integrating emitters (e.g., LEDs), optics, and housing to shape and direct light into the lens for targeted illumination 12, 44

Matching Network A circuit used to optimize impedance between an antenna and transceiver to maximize power transfer and minimize signal reflection 39, 45

melanopic lux A photometric unit weighted by the melanopsin (melanopic) action spectrum that estimates the effectiveness of light on circadian and neuroendocrine pathways 8, 10, 30–33, 47, 48, 56, 106, 156, 178

melanopsin A photopigment found in intrinsically photosensitive retinal ganglion cells (ipRGCs), primarily sensitive to blue light (480 nm) and responsible for regulating circadian rhythms, pupil constriction, and other non-visual responses to light 131

nanocoating A wavelength-selective thin-film coating that reflects melanopsin-activating light back toward the eye while transmitting other wavelengths for natural vision 12, 13, 44

nRF52832 A low-power Bluetooth Low Energy (BLE) SoC developed by Nordic Semiconductor, featuring a 64 MHz ARM Cortex-M4 processor and an integrated 2.4 GHz radio 38, 40, 45

piecewise linear regression A regression method in which the data are modeled with separate linear segments joined at a predefined hinge (or knot). In this thesis, a hinge at Day 56 was used to model pre- and post-crossover trends 57, 65, 74

TEL,309 A telescope radiometer configuration referenced in IEC 62471-style radiance measurements; used in near-eye/close-proximity light safety assessments 8, 18, 19

TR-90 A lightweight, flexible thermoplastic commonly used in eyewear frames for durability and comfort 14